



National Library  
of Canada

Bibliothèque nationale  
du Canada

CANADIAN THESES  
ON MICROFICHE

THÈSES CANADIENNES  
SUR MICROFICHE

(65)

0-318-17527-3

65436

NAME OF AUTHOR/NOM DE L'AUTEUR David W. Evans

TITLE OF THESIS/TITRE DE LA THÈSE "Photophysics of the Phenlnaphthalens and Binaphthyls:  
Evidence for Conformers"

UNIVERSITY/UNIVERSITÉ McMaster

DEGREE FOR WHICH THESIS WAS PRESENTED/  
GRADE POUR LEQUEL CETTE THÈSE FUT PRÉSENTÉE Ph.D.

YEAR THIS DEGREE CONFERRED/ANNÉE D'OBTENTION DE CE DEGRÉ 1983

NAME OF SUPERVISOR/NOM DU DIRECTEUR DE THÈSE Dr. J.D. Laposa

Permission is hereby granted to the NATIONAL LIBRARY OF  
CANADA to microfilm this thesis and to lend or sell copies  
of the film.

*L'autorisation est, par la présente, accordée à la BIBLIOTHI-  
QUE NATIONALE DU CANADA de microfilmer cette thèse  
de prêter ou de vendre des exemplaires du film.*

The author reserves other publication rights, and neither the  
thesis nor extensive extracts from it may be printed or other-  
wise reproduced without the author's written permission.

*L'auteur se réserve les autres droits de publication; ni  
thèse ni de longs extraits de celle-ci ne doivent être imprimés  
ou autrement reproduits sans l'autorisation écrite de l'auteur.*

DATED/DATE June 29, 1983. SIGNED/SIGNÉ David W. Evans

PERMANENT ADDRESS/RÉSIDENCE FIXE 250 St George St., Apt. 903  
Toronto, Ont.  
M5R 3L8

PHOTOPHYSICS OF THE PHENYLNAPHTHALENES  
AND BINAPHTHYLS: EVIDENCE FOR CONFORMERS

By

DAVID WILLIAM EVANS, B.Sc.

A Thesis

Submitted to the School of Graduate Studies  
in Partial Fulfillment of the Requirements

for the Degree

Doctor of Philosophy

McMaster University



April, 1983

9

PHOTOPHYSICS OF THE PHENYLNAPHTHALENES  
AND BINAPHTHYLS

DOCTOR OF PHILOSOPHY (1983)

McMASTER UNIVERSITY  
Hamilton, Ontario

TITLE: Photophysics of the Phenyl-naphthalenes and Binaphthyls:  
Evidence for Conformers

AUTHOR: David William Evans, B.Sc. (Trent University)

SUPERVISOR: Dr. J.D. Laposa

NUMBER OF PAGES: xviii, 294

### Abstract

The simple biaryls 1- and 2- phenylnaphthalene, 1,1'-, 1,2'- and 2,2'-binaphthyl may, in principle, exist as distinct molecular conformers differing chiefly in their rotational configuration about the interannular bond. The steady-state fluorescence and fluorescence decay spectroscopy of these molecules in dilute solution has been examined for evidence of such single bond rotational conformers.

While the fluorescence of 1-phenylnaphthalene originates from essentially a unique molecular conformation in fluid solution or in rigid organic glasses at 77K, singlet decay measurements of 2-phenylnaphthalene at 295K and 77K indicate the presence of at least two emissive components. This is confirmed by the emission spectroscopy at low temperature and by the effect of selective oxygen quenching on the room temperature fluorescence. In a polycrystalline matrix of methylcyclohexane at 77K the 2-phenylnaphthalene molecule appears constrained to a single, more planar conformation.

Of the binaphthyls only the 2,2'-isomer exhibits complex fluorescence behaviour in the fluid hydrocarbon solvents, the spectrum showing a distinct excitation wavelength dependence while the fluorescence decay can be best analyzed as the sum of long and short lived exponential decays. Molecular oxygen was used to enhance these spectroscopic differences, differentially quenching the longer lived conformer of 2,2'-binaphthyl. The Shpol'skii (polycrystalline)

emission spectrum of this compound at 77K indicated the presence of ~~two~~ spectroscopically distinct conformers different from those seen in fluid media and separated by  $\sim 525 \text{ cm}^{-1}$  in their fluorescence origins. 1,1'- and 1,2'-binaphthyl, while giving no evidence of conformeric fluorescence at 295K did give a biexponential fluorescence decay in organic glasses at 77K.

These studies suggest that relatively stable single bond conformers may be more ubiquitous than is generally supposed. Where these conformers differ spectroscopically the techniques of fluorescence emission and decay spectroscopy may be successfully applied in conjunction with the selective quenching technique.

#### ACKNOWLEDGEMENTS

I wish to thank my research supervisor, Dr. J.D. Laposa for his invaluable advice and guidance, offered so unstintingly during the course of this work.

A large debt of gratitude is owing to Dr. A.J. Yarwood for his willingness to impart his experimental expertise and for so freely giving of his time.

To Dave Condirston, my thanks for his friendship and collaboration; it did much to ease the early years.

I am grateful to the Department of Chemistry for their financial support during my stay at McMaster.

My thanks to Dr. Brian McCarry for his fruitful advice on matters preparative and chromatographic, but especially for his lasting friendship.

I am indebted to Kerstin Stockman for her skill and perseverance in typing this thesis.

Finally, my lasting gratitude to my parents for their patient support.

## TABLE OF CONTENTS

	Page
CHAPTER 1	
INTRODUCTION	1
1.1 General	1
1.2 Previous Spectroscopic and Photophysical Work on Conformers	3
1.3 Conformers in the Biaryl Systems and the Aims of This Present Work	6
CHAPTER 2	
THEORY AND BACKGROUND	12
2.1 The Wave Equation	12
2.2 Spectroscopic Transitions	12
2.3 The Theory of Electronic Spectra	13
2.4 Fate of Absorbed Energy	16
2.5 Fluorescence Quantum Yields	21
2.6 Fluorescence Excitation	23
2.7 Singlet Decay Times	24
2.8 Fluorescence Decay Kinetics of Multicomponent Systems	32
2.9 Polycrystalline Matrices and the Shpol'skii Effect	42
2.10 Oxygen Quenching of Fluorescence	44
CHAPTER 3	
EXPERIMENTAL	47
3.1 Solutes	47
3.2 Solvents	49



3.3	Purification of Solutes	50
3.4	Fluorescence Emission and Fluorescence Excitation Spectra	53
3.5	Absorption Spectra	59
3.6	Determination of Relative Fluorescence Quantum Yields	59
3.7	Measurement of Singlet Lifetimes	64
CHAPTER 4	PHOTOPHYSICS OF THE PHENYLNAPHTHALENES	78
4.1	Photophysics of 1-Phenylnaphthalene	78
4.1.1	Fluorescence Emission and Excitation Spectroscopy	78
4.1.2	Fluorescence Quantum Yield Measurements	84
4.1.3	Fluorescence Decay Measurements	84
4.1.4	Analysis and Discussion of the Photophysics of 1-Phenylnaphthalene	86
4.2	Photophysics of 2-Phenylnaphthalene	93
4.2.1	Fluorescence Emission and Excitation Spectroscopy	93
4.2.1a	Fluorescence in Fluid and Glassy Media	93
4.2.1b	Fluorescence in Polycrystalline (Shpol'skii) Matrices	103
4.2.2	Fluorescence Quantum Yield Measurements	111
4.2.3	Fluorescence Decay Measurements	112
4.2.4	Analysis and Discussion of the Photophysics of 2-Phenylnaphthalene	118

CHAPTER 5	PHOTOPHYSICS OF THE BINAPHTHYLS	126
5.1	Photophysics of 1,1'-Binaphthyl	126
5.1.1	Fluorescence Emission and Excitation Spectroscopy	126
5.1.2	Fluorescence Quantum Yield Measurements	132
5.1.3	Fluorescence Decay Measurements	133
5.1.4	Analysis and Discussion of the Photophysics of 1,1'-Binaphthyl	138
5.2	Photophysics of 1,2'-Binaphthyl	151
5.2.1	Fluorescence Emission and Excitation Spectroscopy	151
5.2.2	Fluorescence Quantum Yield Measurements	155
5.2.3	Fluorescence Decay Measurements	156
5.2.4	Analysis and Discussion of the Photophysics of 1,2'-Binaphthyl	158
5.3	Photophysics of 2,2'-Binaphthyl	163
5.3.1	Fluorescence Emission and Excitation Spectroscopy	163
5.3.1a	Fluorescence Spectroscopy at Room Temperature	163
5.3.1b	Fluorescence Spectroscopy in Organic Glasses at 77K	169
5.3.1c	Fluorescence in Polycrystalline (Shpol'skii) Matrices	179
5.3.1d	Oxygen Quenching of the Steady-State Fluorescence of 2,2'-Binaphthyl at Room Temperature	191
5.3.2	Fluorescence Quantum Yield Measurements	194

5.3.3	Fluorescence Decay Measurements	196
5.3.4	Analysis and Discussion of the Photophysics of 2,2'-Binaphthyl	234
CHAPTER 6	SUMMARY	247
APPENDIX I	ROOM TEMPERATURE ABSORPTION SPECTRA OF 1- AND 2-PHENYLNAPHTHALENE; 1,1'-, 1,2'- and 2,2'- BINAPHTHYL AND 1,2,7,8-DIBENZOFUORENE	253
APPENDIX II	TESTING OF THE DECONVOLUTION PROCEDURES	259
APPENDIX III	FLUORESCENCE DECAY CURVES OF 2,2'-BINAPHTHYL	276
APPENDIX IV	FLUORESCENCE SPECTROSCOPY AND PHOTOPHYSICS OF 1,2,7,8-DIBENZOFUORENE	278
BIBLIOGRAPHY		282

# LIST OF TABLES

		Page
Table 3.1	Singlet Decay Times of Some Standard Substances	74
Table 4.1	Fluorescence Emission Bands of $10^{-4}$ - $10^{-5}$ M 1-Phenylanthracene in 3MP or Isopentane Glass at 77K	80
Table 4.2	Relative Fluorescence Quantum Yields of 1-Phenylanthracene	84
Table 4.3	Fluorescence Lifetimes of 1-Phenylanthracene in Dilute Solution Fitted to a Monoexponential Decay	85
Table 4.4	Radiative Lifetimes and Rate Constants for 1-Phenylanthracene	86
Table 4.5	Vibrational Frequencies from the Fluorescence Spectrum of $10^{-4}$ M 2-Phenylanthracene in Polycrystalline Methylcyclohexane at 77K	106
Table 4.6	Relative Fluorescence Quantum Yields of 2-Phenylanthracene	112
Table 4.7	Fluorescence Lifetimes of the Long-Lived Component of 2-Phenylanthracene in Dilute Solution	116
Table 4.8	Radiative Lifetimes and Radiative and Nonradiative Rate Constants for the Long- Lived Component in 2-Phenylanthracene	118
Table 5.1	Vibrational Structure in the Fluorescence Spectrum of 1,1'-Binaphthyl and Naphthalene at 77K	129
Table 5.2	Relative Fluorescence Quantum Yields for 1,1'-Binaphthyl	132
Table 5.4	Fluorescence Decay Parameters of 1,1'- Binaphthyl in Dilute Glassy Solution at 77K	136

Table 5.5	Radiative Lifetimes and Radiative and Non-radiative Rate Constants for 1,1'-Binaphthyl at 295K	147
Table 5.6	Relative Fluorescence Quantum Yields for 1,2'-Binaphthyl	156
Table 5.7	Fluorescence Lifetimes of 1,2'-Binaphthyl in Dilute Solution at 295K Fitted to a Mono-exponential Decay Law	156
Table 5.8	Comparison of Mono- and Biexponential Fit of Fluorescence Lifetime Data for 1,2'-Binaphthyl in 3MP at 77K	157
Table 5.9	Radiative Lifetimes and Radiative and Non-radiative Rate Constants for 1,2'-Binaphthyl at 295K	
Table 5.10	Emission Wavelengths of 2,2'-Binaphthyl in Alkane Solvents at 295K and 77K	173
Table 5.11	Emission Wavelengths of 2,2'-Binaphthyl in Absolute Ethanol at 295K and 77K	176
Table 5.12	Excitation Wavelengths of 2,2'-Binaphthyl in Absolute Ethanol and Isopentane at 77K	177
Table 5.13	Frequencies from the Fluorescence Spectrum of 2,2'-Binaphthyl-h <sub>14</sub> and -d <sub>14</sub> in Polycrystalline Methylcyclohexane at 77K	183
Table 5.14	Vibrational Subsystems in the Fluorescence Emission Spectrum of 2,2'-Binaphthyl-h <sub>14</sub> in Polycrystalline Methylcyclohexane at 77K	187
Table 5.15	Vibrational Subsystems in the Fluorescence Emission Spectrum of 2,2'-Binaphthyl-d <sub>14</sub> in Polycrystalline Methylcyclohexane at 77K	188
Table 5.16	Relative Fluorescence Quantum Yields of 2,2'-Binaphthyl in Cyclohexane as a Function of Excitation Wavelength at 295K	195
Table 5.17	Relative Fluorescence Quantum Yields of 2,2'-Binaphthyl in 2-Methylpentane at 295K and 77K as a Function of Excitation Wavelength	195

Table 5.18	Fluorescence Decay of 2,2'-Binaphthyl in Cyclohexane at 295K Fit to a Biexponential. Decay Model: Comparison of N <sub>2</sub> and D <sub>2</sub> Filled Excitation Sources	197
Table 5.19	Comparison of Mono- and Biexponential Fitting of Decay Data for 2,2'-Binaphthyl in Cyclohexane at 295K	200
Table 5.20	Fluorescence Decay Parameters for 2,2'-Binaphthyl-h <sub>14</sub> in Cyclohexane at 295K; $\lambda_F = 340$ nm	210
Table 5.21	Fractional Excited State Populations and Absorbances for Conformers of 2,2'-Binaphthyl in Cyclohexane at 295K	214
Table 5.22	Fluorescence Decay Parameters for 2,2'-Binaphthyl-d <sub>14</sub> in Cyclohexane at 295K; $\lambda_F = 340$ nm	223
Table 5.23	Lifetimes and Ratios of Preexponential Factors for Fluorescence Decay of 2,2'-Binaphthyl-d <sub>14</sub> in Cyclohexane at 295K as a Function of Emission Wavelength: $\lambda_A = 315.9$ nm	225
Table 5.24	Fluorescence Decay Parameters for 2,2'-Binaphthyl-h <sub>14</sub> in 3-Methylpentane at 295K and 77K	226
Table 5.25	Fluorescence Decay Parameters for 2,2'-Binaphthyl-h <sub>14</sub> in Ethanol at 295K and 77K	227
Table 5.26	Fluorescence Decay Parameters for 2,2'-Binaphthyl-h <sub>14</sub> in Isopentane at 295K and 77K	228
Table 5.27	Refractive Index Correction Applied to Observed Lifetimes for 2,2'-Binaphthyl at 295K	230
Table II.1	Deconvolution of Noisy Synthetic Data for Biexponential Decay Law	262
Table II.2	Results of Deconvolution of Biexponential Decay Generated by Addition of Real, Mono-exponential Fluorescence Decay Curves in MCA Trial I	269

Table II.3	Results of Deconvolution of Biexponential Decay Generated by Addition of Real, Mono-exponential Fluorescence Decay Curves in MCA Trial II	270
Table II.4	Fluorescence Decay of a Cyclohexane Solution of 9,10-Diphenylanthracene and 1,2-Benzanthracene at 295K as Fit to a Biexponential Decay Law	274
Table IV.1	Radiative Lifetimes and Radiative and Non-radiative Rate Constants for First Excited Singlet State of 1,2,7,8-Dibenzofluorene at 295K	281

## LIST OF FIGURES

		Page
Figure 1.1	Single Bond Rotational Conformers of the 1,3-Butadienes	4
Figure 1.2	Single Bond Rotational Conformers of 2-Vinylnanthracene	5
Figure 1.3	General Structure of the trans-1,2-Diaryl-ethylenes	6
Figure 1.4	Qualitative View of the Steric Hindrance in Coplanar s-cis and s-trans 1,1'-Binaphthyl	7
Figure 1.5	Qualitative View of the Steric Hindrance in Coplanar s-cis and s-trans 2,2'-Binaphthyl	8
Figure 2.1	Jablonski Diagram Showing the Principal Photo-physical Processes in Complex Molecules	19
Figure 2.2	Multicomponent Fluorescence Decay Schemes	32
Figure 3.1	Apparatus for Emission Experiments - Block Diagram	54
Figure 3.2	Evacuatable Fluorescence Cell	56
Figure 3.3	Block Diagram of Lifetime Apparatus	65
Figure 3.4	Lifetime System Optics in Double Monochromator Configuration	66
Figure 3.5	Low Pressure Flash Lamp Design	67
Figure 4.1	Fluorescence Emission and Excitation Spectra of 1-Phenylnaphthalene in Alkane Solvents at 295K and 77K	79
Figure 4.2	Temperature Independent Intersystem Crossing and Thermally Activated Intersystem Crossing	90
Figure 4.3	Jablonski Diagram for Photophysics of 1-Phenylnaphthalene in 3MP at 77K	92



Figure 4.4	Qualitative Potential Energy Scheme for Two Lowest Singlet States of 2-Phenyl-naphthalene	94
Figure 4.5	Fluorescence Excitation Spectra at 295K and 77K and Fluorescence Emission Spectrum at 295K of $5 \times 10^{-5} \text{M}$ 2-Phenyl-naphthalene in 3-Methylpentane	96
Figure 4.6	Fluorescence Emission Spectrum of $5 \times 10^{-5} \text{M}$ 2-Phenyl-naphthalene in 3-Methylpentane at 77K as Function of Excitation Wavelength	97
Figure 4.7	Fluorescence Emission Spectrum of $10^{-4} \text{M}$ 2-Phenyl-naphthalene in Air-Saturated 3-Methylpentane at 295K as a Function of Excitation Wavelength	101
Figure 4.8	Uncorrected Fluorescence Emission Spectrum of $10^{-4} \text{M}$ 2-Phenyl-naphthalene in Polycrystalline Methylcyclohexane at 77K	104
Figure 4.9	Observed and Fitted Monoexponential Fluorescence Decay Curves for $10^{-4} \text{M}$ 2-Phenyl-naphthalene in Cyclohexane at 295K Showing Presence of Short-Lived Component	113
Figure 4.10	Excitation Wavelength Dependence of Observed 2-Phenyl-naphthalene Fluorescence Decay in 3MP at 295K	115
Figure 4.11	Steric Interactions of Nonbonded Hydrogens in 1- and 2-Phenyl-naphthalene	120
Figure 4.12	Proposed Singlet State Potential Energy Diagram for 2-Phenyl-naphthalene in 3MP at 77K	122
Figure 4.13	Potential Energy Diagram of Ground and Two Lowest Excited Singlet States of Trans-Stilbene	125
Figure 5.1	Fluorescence Emission and Excitation Spectra of Dilute Solutions of 1,1'-Binaphthyl at 295K and 77K	127
Figure 5.2	Qualitative View of Steric Restrictions for s-cis vs s-trans Racemization of 1,1'-Binaphthyl	139
Figure 5.3	Potential Energy as a Function of Dihedral Angle for the Electronic Ground State of 1,1'-Binaphthyl	140

Figure 5.4	Potential Energy of First Excited Singlet State of 1,1'-Binaphthyl	142
Figure 5.5	Potential Energy of $S_0$ and $S_1$ for 1,1'-Binaphthyl	143
Figure 5.6	Fluorescence Emission and Excitation Spectra of $10^{-5}$ 1,2'-Binaphthyl in Isopentane at 295K and 77K	152
Figure 5.7	Qualitative View of Steric Restrictions for s-cis Vs s-trans Conformers of 1,2'-Binaphthyl	154
Figure 5.8	Proposed Potential Energy Diagram for Ground and First Excited Singlet States of 1,2'-Binaphthyl	161
Figure 5.9	Fluorescence Emission Spectra of 2,2'-Binaphthyl-h <sub>14</sub> in Cyclohexane at 295K as a Function of Excitation Wavelength	164
Figure 5.10	Fluorescence Emission Spectra of 2,2'-Binaphthyl-h <sub>14</sub> in Isopentane at 295K as a Function of Excitation Wavelength	166
Figure 5.11	Fluorescence Emission Spectra of 2,2'-Binaphthyl in Ethanol at 295K as a Function of Excitation Wavelength	168
Figure 5.12	Fluorescence Emission Spectra of 2,2'-Binaphthyl in Isopentane at 77K as a Function of Excitation Wavelength	170
Figure 5.13	Fluorescence Excitation Spectra of 2,2'-Binaphthyl in Isopentane at 77K as a Function of Emission Wavelength	171
Figure 5.14	Fluorescence Emission Spectra of 2,2'-Binaphthyl in 3-Methylpentane at 77K as a Function of Excitation Wavelength	172
Figure 5.15	Fluorescence Emission and Excitation Spectra of 2,2'-Binaphthyl in Ethanol at 77K	175
Figure 5.16	Fluorescence Emission Spectra of 2,2'-Binaphthyl-h <sub>14</sub> in Polycrystalline Methylcyclohexane at 77K as a Function of Excitation Wavelength	181

Figure 5.17	Fluorescence Emission Spectra of 2,2'-Binaphthyl-d <sub>14</sub> in Polycrystalline Methylcyclohexane at 77K as a Function of Excitation Wavelength	182
Figure 5.18	Fluorescence Excitation Spectra of 2,2'-Binaphthyl-h <sub>14</sub> in Polycrystalline Methylcyclohexane at 77K as a Function of Emission Wavelength	184
Figure 5.19	Structural Formula and Numbering for 1,2,7,8-Dibenzofluorene	190
Figure 5.20	Fluorescence Emission for 2,2'-Binaphthyl in Cyclohexane at 295K: Degassed and O <sub>2</sub> Quenched	192
Figure 5.21	Relative Contribution of Species 1 and Species 2 to Total Decay Intensity	202
Figure 5.22	Fluorescence Emission of 2,2'-Binaphthyl in Cyclohexane at 295K, Area Normalized	207
Figure 5.23	Mono- and Biexponential Fitting of the Fluorescence Decay Curve for 2,2'-Binaphthyl	213
Figure 5.24	Calculated Relative Molar Absorptivities of Two Proposed Conformers of 2,2'-Binaphthyl	215
Figure 5.25	Ratios of $\alpha_1/\beta_1$ for Filtered and Monochromated Emission Decay of 2,2'-Binaphthyl Fluorescence	217
Figure 5.26	2,2'-Binaphthyl in Cyclohexane: Calculated Fluorescence Curves $F_1(\lambda_F)$ and $F_2(\lambda_F)$	219
Figure 5.27	Fluorescence of 2,2'-Binaphthyl in Cyclohexane: Species 1 Fluorescence by Calculation and Selective Quenching	220
Figure 5.28	Proposed Potential Energy Diagram for Ground and First Excited Singlet States of the 2,2'-Binaphthyl Conformers	241
Figure I.1	Absorption Spectrum of 1-Phenylnaphthalene	254
Figure I.2	Absorption Spectrum of 2-Phenylnaphthalene	254
Figure I.3	Absorption Spectrum of 1,1'-Binaphthyl	254
Figure I.4	Absorption Spectrum of 1,2'-Binaphthyl	254
Figure I.5	Absorption Spectrum of 2,2'-Binaphthyl	254

Figure I.1	Absorption Spectrum of 1,2,7,8-Dibenzo fluorene	254
Figure III.1a,b	Mono- and Biexponential Fitting of Decay Curves for 2,2'-Binaphthyl: $\lambda_A = 337.1$ nm; $\lambda_F = 340$ nm	277
Figure III.2a,b	Mono- and Biexponential Fitting of Decay Curves for 2,2'-Binaphthyl: $\lambda_A = 328.5$ nm; $\lambda_F = 340$ nm	277
Figure III.3a,b	Mono- and Biexponential Fitting of Decay Curves for 2,2'-Binaphthyl: $\lambda_A = 326.8$ nm; $\lambda_F = 340$ nm	277
Figure III.4a,b	Mono- and Biexponential Fitting of Decay Curves for 2,2'-Binaphthyl: $\lambda_A = 313.6$ nm; $\lambda_F = 340$ nm	277
Figure IV.1	Fluorescence Emission and Excitation Spectra of 1,2,7,8-Dibenzofluorene at 295K	279
Figure IV.2	Fluorescence Emission and Excitation Spectra of 1,2,7,8-Dibenzofluorene at 77K	280

## CHAPTER ONE

### INTRODUCTION

#### 1.1 General

Molecular spectroscopy in its broadest sense deals with the emission or absorption of electromagnetic radiation by molecules. Spectroscopy provides one of the most powerful tools for the elucidation of molecular structure and dynamics. There are several different branches of spectroscopy, depending on the amount of energy involved in the absorption or emission process. Transitions between rotational energy levels of molecules fall in the microwave region of the electromagnetic spectrum and can, for suitable molecules, yield detailed information regarding the molecular structure, particularly bond distances and angles. At higher energies one finds transitions between vibrational levels of molecules, a process studied by infrared spectroscopy and its complement, Raman (inelastic) scattering. These two techniques allow one to gain a knowledge of molecular structure and symmetry, moments of inertia and molecular force constants. Electronic spectroscopy can give qualitative or quantitative information on the structure of the ground state and various excited electronic states of molecules.

A particularly useful type of emission process is photoluminescence, that is emission of light subsequent to light absorption. Since the excitation energies employed in the absorption process usually lie in the visible or ultraviolet region of the spectrum the sample

molecules undergo electronic excitation. In addition to obtaining the time-independent emission spectra one may also follow the kinetics of the photoluminescence process, details of which are of great interest to physicists and biochemists as well as to spectroscopists. Measurement of excited state lifetimes and luminescence quantum yields permit quantitative evaluation of the processes involved in the deactivation of excited electronic states.

A widely studied class of molecules, in terms of their luminescent and photophysical processes, are aromatic compounds. Beginning with the works of Stark<sup>1</sup> and Stark and Meyer<sup>2</sup> on the luminescence of benzene and benzene derivatives near the turn of the century, aromatic hydrocarbons have been the single most intensively studied class of luminescent molecules.

Photoluminescence may be further sub-divided into those processes involving no change in the multiplicity or net spin angular momentum accompanying the transition as opposed to those radiative processes in which the spin angular momentum of the molecule does indeed change. The former process is referred to as fluorescence and since aromatic molecules generally have singlet ground states the most common type of fluorescence involves the radiative transition from the first electronically excited singlet state to the ground electronic state, denoted  $S_0 \rightarrow S_1$ . The latter process, wherein the radiative transition is attended by a change in the spin angular momentum is designated as phosphorescence. In aromatic molecules phosphorescence describes the radiative transition from the lowest lying triplet electronic state to the singlet ground state,  $S_0 \rightarrow T_1$ .

Of particular interest in this present study is the application of steady-state fluorescence emission spectroscopy and singlet decay spectroscopy to aromatic systems in which several potentially emissive excited singlet states of fluorophores are simultaneously present. A trivial case of such dual or multiple emission would involve simple combination of two or more chemically distinct species, each of which are individually fluorescent. A simple example would be to envisage mixing of solutions containing, say, phenanthrene and anthracene, each of which is characterized by its distinct absorption and fluorescence emission spectrum and singlet decay time. The binary solution, in the absence of interaction between the two fluorophores, would then be expected to exhibit absorption, emission and singlet decay properties determined by the proportion of each species present. Obviously then the fluorescence emission and decay properties and, to a lesser extent, the absorption properties may be used as criteria to distinguish the presence or absence of a second fluorescent species.

A second and more subtle source of dual or multiple fluorescence involves species which are not chemically distinct in the usual sense but which may nonetheless differ in their fluorescence properties. This category is typified by aromatic molecules which may exist in two or more nearly isoenergetic molecular conformations, differing only in their orientation about a carbon-carbon single bond.

## 1.2 Previous Spectroscopic and Photophysical Work on Conformers

Mulliken<sup>3,4</sup> was the first to point to the possible existence of discrete molecular conformers derived by rotation about a carbon-carbon single bond. In his theoretical study of butadienes he proposed two

planar rotational conformers of the 1,3-butadienes, namely

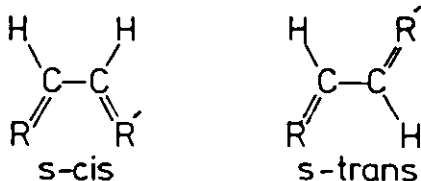


Figure 1.1

#### Single Bond Rotational Conformers of the 1,3-Butadienes

where s denotes single bond isomerism or conformerism.

Since the  $C_2-C_3$  single bond lies between adjacent carbon-carbon double bonds Mulliken argued that the actual bond order of the  $C_2-C_3$  bond was somewhat greater than that expected for a simple, isolated C-C bond and hence the barrier to rotation about the  $C_2-C_3$  bond could be expected to be intermediate between that expected for the single and double carbon-carbon bonds. Furthermore, Mulliken proposed that these s-cis and s-trans conformers may, in principle, differ spectroscopically. In favourable cases it may be hoped that the fluorescence emission and decay properties of the conformers will be sufficiently different, so that one may be able to confirm the presence of the other conformer or conformers and perhaps quantify the relative amounts of the various species.

The first published case of this s-cis - s-trans isomerism being detected spectroscopically came in 1962 when Cherkasov<sup>5</sup> reported the temperature and wavelength dependence of the emission of 2-vinyl-anthracene solutions to be explicable in terms of rotational isomerism about the conjugated single bond. The absorption spectrum of 2-vinyl-anthracene was also found to be temperature dependent, suggesting that the conformers were actually present in their ground electronic states,



prior to excitation. Continued studies by Cherkasov and coworkers<sup>6-8</sup> using time-resolved fluorescence emission spectroscopy and phase fluorometry confirmed the presence of at least two emitting species. Of particular interest were the phase fluorometry experiments<sup>7</sup>, since the temperature and emission wavelength dependence of the fluorometric phase pointed to a measureable difference in the singlet lifetimes of the conformers involved. This group proposed that two conformers were principally responsible for the observed fluorescence behaviour, the coplanar or nearly coplanar s-cis and s-trans-2-vinylnanthracenes, the latter being about 0.9 kcal/mole ( $3 \times 10^2 \text{ cm}^{-1}$ ) more stable in the ground state.

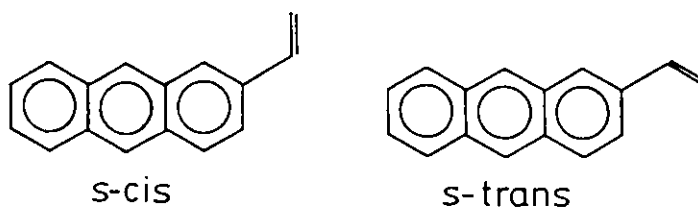


Figure 1.2

#### Single Bond Rotational Conformers of 2-Vinylnanthracene

The positional isomers 1- and 9-vinylnanthracene did not exhibit comparable conformeric emission behaviour.<sup>6</sup> For the former isomer this is likely the result of one conformer being strongly disfavoured on steric grounds, i.e., the sterically favoured conformer is totally predominant, while for the 9-vinylnanthracene symmetry considerations dictate that the two coplanar conformers be identical.

Recently a very large number of workers<sup>9-14</sup> have investigated the s-cis - s-trans conformeric emission behaviour of the trans-1,2-diarylethylenes, the most active group being that of Fischer et al.<sup>15-20</sup> The general structure of these trans-1,2-diarylethylenes is shown below, where Ar and Ar' are typically phenyl, 1- or 2-naphthyl, 2-anthryl, 3-phenanthryl, 3-pyrenyl and others.

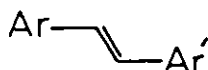


Figure 1.3

#### General Structure of the trans-1,2-diarylethylenes

Here again the conformers are derived by rotation about the nominally single bond conjugated with the olefinic and aromatic double bonds. The groups mentioned above have found evidence for the ground and excited state existence of two or more rotational conformers, as manifested by the excitation wavelength dependence of the fluorescence emission spectra and quantum yields and by the multi-exponential decay kinetics of such systems.

These investigations of the trans 1,2-diarylethylenes have naturally been extended to the aza-analogs of these compounds. Preliminary results reported for the dipyridylethylenes and styrylpyridines indicate the presence of discrete fluorescent conformers for the ortho and meta hetero-derivatives.<sup>21-23</sup>

#### 1.3 Conformers in the Biaryl Systems and the Aims of This Present Work

Although not explicitly identified with the cis-trans single

bond isomerism described by Mulliken, Hochstrasser, in 1961,<sup>24</sup> recognized the potential for single bond rotational conformerism in 1,1'-binaphthyl. The difference in the fluorescence emission of 1,1'-binaphthyl in fluid and rigid solutions was ascribed by that author to the change in emissive state ( $S_1$ ) geometry on passing from rigid to fluid media, with more extensive torsional relaxation about the  $C_1-C_1'$  bond being possible at lower viscosity. This represents a very generalized case of single bond rotational isomerism since essentially only a single ground state conformer is likely present, although this condition may be relaxed on excitation. Indeed, both possible coplanar conformers of 1,1'-binaphthyl may represent high energy forms of the molecule, the s-cis configuration being especially disfavoured on steric grounds. The situation in the 1,1'-binaphthyl ground

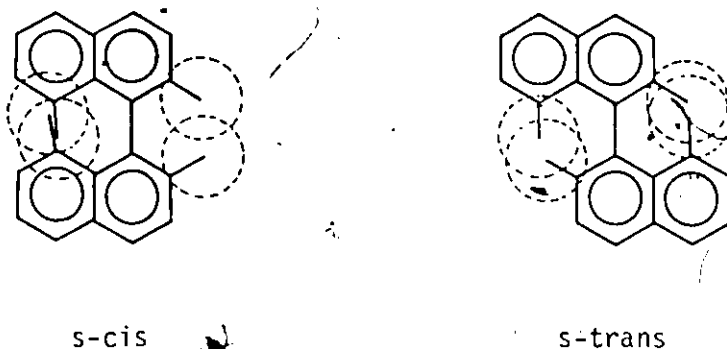


Figure 1.4

Qualitative View of Steric Hindrance in Coplanar

s-cis and s-trans 1,1'-Binaphthyl

(broken circles represent Van der Waals radii of hydrogen)

state is analogous to the explanation proposed for the lack of conformers in 1-vinylnanthracene, namely one configuration being substantially more

stable than its other rotational conformers.

In the sterically less hindered biaryl 2-phenylnaphthalene the energy differences between the conformers may be smaller, such that significant populations of different rotational conformers may coexist. Nauman and coworkers<sup>25-27</sup> attributed the excitation wavelength dependence of the 2-phenylnaphthalene fluorescence at 77K to photoselection of such conformers. Of course in this phenyl-substituted biaryl the distinction between the planar s-cis and s-trans conformers vanishes by symmetry but as Nauman suggested, the conformers need, in principle, only to differ in their interannular or dihedral angle,  $\theta$ , to be potentially distinct by spectroscopic methods. Similarly, the relatively unhindered 2,2'-binaphthyl might be expected to have several distinct stable and nearly isoenergetic rotational conformers.

A brief report in the literature<sup>28</sup> indicated that the apparently anomalous excitation wavelength dependence of the fluorescence emission of 2,2'-binaphthyl solutions might have its origin in the presence of both the coplanar s-cis and s-trans molecular conformers.

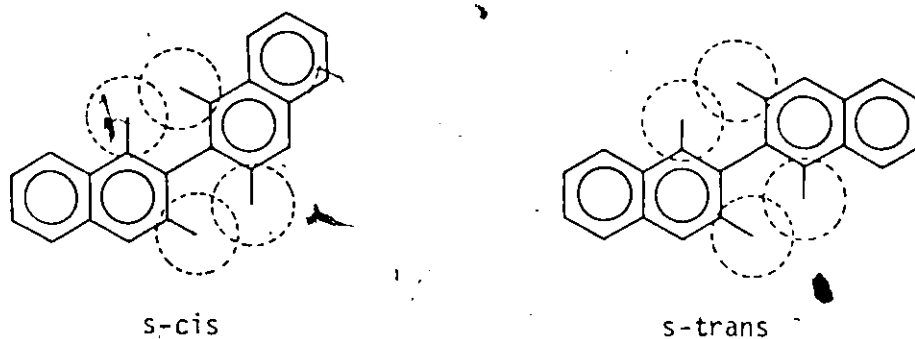


Figure 1.5

Qualitative View of Steric Hindrance in Coplanar

s-cis and s-trans 2,2'-Binaphthyl

(broken circles represent Van der Waals radii of hydrogen)

The aim of this present work is to confirm the relatively unsupported steady-state fluorescence studies on these biaryls and to extend this investigation to 1-phenylnaphthalene and 1,2'-binaphthyl for which very little is known. In addition to the steady-state evidence for conformers, i.e., excitation wavelength dependence of the emission spectra and fluorescence quantum yields and emission wavelength dependence of the excitation spectra, will be added the very powerful tool of fluorescence decay spectroscopy. This is an especially valuable supplement to the conventional forms of fluorometry since it may be possible to discriminate temporally between the fluorescence of several species having strongly overlapping absorption and emission spectra. While a single emitting species or conformer will give rise to a simple monoexponential decay of the fluorescence intensity a multi-component system will follow a multi-exponential decay scheme. Practically, the goal will be to distinguish biexponential decay behaviour from a monoexponential decay of the fluorescence intensity. Apart from the qualitative capability of discerning the number of distinct fluorophores, fluorescence decay spectroscopy, in conjunction with the steady-state emission and quantum yield measurements, permits one to evaluate many of the kinetic parameters for the photophysics of the lowest excited singlet state. In favourable cases the combination of these techniques will even permit evaluation of the relative proportions of the ground state conformers, as well as their individual fluorescence and absorption spectra.<sup>11</sup>

A qualitative picture of the ground and excited state geometries of the biaryls, with respect to torsion about the interannular bond, may

be made. By comparison of the absorption and emission spectra with those of certain model compounds one may deduce the extent of  $\pi$ -interaction between the constituent aromatic rings and hence the degree of twist between the  $\pi$ -systems of the biaryls. Specifically these model compounds are the parent compound naphthalene and a rigid, planar, methylene-bridged analog of 2,2'-binaphthyl, 1,2,7,8-dibenzofluorene. Changes or lack of them in the fluorescence emission spectra with temperature will permit some conclusions to be drawn with regard to the relative equilibrium geometries of ground and excited states of the biaryls.

The fluorescence of the five biaryls in polycrystalline organic matrices (cyclohexane, methylcyclohexane and n-alkanes) at 77K will also be examined at varying solute concentrations. The appearance of much sharper quasilinear or Shpol'skii spectra in such polycrystalline media is usually taken as evidence that the aromatic chromophore has or may assume a planar geometry.<sup>29</sup> Conversely, the non-appearance of a quasilinear spectrum may be indicative of a highly twisted nonplanar fluorophore, i.e., the dihedral angle of the aryl moieties is large. For those species found to yield Shpol'skii emission spectra the vibrational details of the electronic emission spectrum provide information on the ground state vibrational frequencies of the molecule. Such quasilinear vibronic emission spectra have frequently been used as a complement to infrared and Raman studies in assigning the types and symmetries of the normal modes of vibration of molecules in the electronic ground state.

The effect of deuterium isotope substitution on the luminescence characteristics of aromatic hydrocarbons has been of considerable interest for some time, particularly as an aid in the understanding of

nonradiative electronic transitions.<sup>30</sup> Deuteration is known to significantly affect the phosphorescence processes of aromatic molecules, increasing phosphorescence quantum yields and lifetimes<sup>31-33</sup> while the fluorescence processes are relatively unaffected.<sup>34</sup> Introduction of deuterium will be expected to alter the vibrational frequencies seen in the quasilinear spectrum, the vibrational spacing decreasing with the heavier isotope.

Deliberate introduction of an efficient singlet quencher, molecular oxygen, into fluid solutions of the biaryls can serve a useful role in discerning the presence or absence of a second fluorescent component.<sup>34</sup> Even with strongly overlapping absorption and emission spectra one may selectively quench the fluorescence of the longer lived fluorophore while leaving the shorter lived species less affected. Comparison of steady-state emission spectra for degassed and oxygenated solutions of the biaryls would then reveal alterations in the spectral distributions if more than a single fluorescent component were present, assuming the fluorescence lifetimes to be sufficiently different. In this manner oxygen quenching studies serve as a complement to the other spectroscopic techniques for distinguishing dual or multiple emission processes.

## CHAPTER TWO

### THEORY AND BACKGROUND

#### 2.1 The Wave Equation

The non-relativistic time-independent Schroedinger equation for a molecule can be expressed as the eigenvalue equation

$$\hat{H}(q,Q)\psi(q,Q) = E\psi(q,Q) \quad (2.1)$$

where  $\hat{H}$  is the Hamiltonian operator,  $\psi$  and  $E$  are the stationary state wavefunctions and energies while  $q$  and  $Q$  are the generalized set of electronic and nuclear coordinates, respectively.

#### 2.2 Spectroscopic Transitions

The wavenumber of a spectroscopic transition between two stationary states  $a$  and  $b$ , of energies  $E_a$  and  $E_b$  will be given by

$$\bar{\nu} = \frac{|E_b - E_a|}{hc} \quad (2.2)$$

where  $h$  is Planck's constant and  $c$  is the speed of light. The probability of an electronic dipole transition between these two states is proportional to the transition moment

$$\vec{R}_{ab} = \langle \psi_b | \vec{M} | \psi_a \rangle \quad (2.3)$$

where  $\psi_a$  and  $\psi_b$  are the stationary state wavefunctions of the two states involved and  $\vec{M}$  is the electric dipole moment.



### 2.3 The Theory of Electronic Spectra

The transition moment for an electric dipole transition between two non-degenerate vibronic states,  $\psi_{e',v'}$  and  $\psi_{e'',v''}$ , is given by

$$\vec{R}_{e',v';e'',v''} = \langle \psi_{e',v'} | \vec{M} | \psi_{e'',v''} \rangle \quad (2.4)$$

where the prime and double primes refer to upper and lower states respectively. Use of the Born-Oppenheimer Approximation<sup>35</sup> to separate the electronic and nuclear motions enables the rotationless wavefunction to be expressed as the product

$$\psi_{ev}(q,Q) = \psi_e(q,Q)\psi_v(Q) \quad (2.5)$$

where  $\psi_e$  and  $\psi_v$  are the electronic and vibrational wavefunctions respectively. Since the electronic dipole moment operator is a vector, it can be resolved as a sum of electronic and nuclear parts,

$$\vec{M} = \vec{M}_e + \vec{M}_n \quad (2.6)$$

The vibronic transition moment (Equation 2.4) then becomes

$$\begin{aligned} \vec{R}_{e',v';e'',v''} &= \langle \psi_{v'}(Q) | \langle \psi_{e'}(q,Q) | \vec{M}_e | \psi_{e''}(q,Q) \rangle | \psi_{v''}(Q) \rangle \\ &+ \langle \psi_{v'}(Q) | \vec{M}_n | \psi_{v''}(Q) \rangle \langle \psi_{e'}(q,Q) | \psi_{e''}(q,Q) \rangle. \end{aligned} \quad (2.7)$$

Since the electronic wavefunctions of the two states are orthogonal the second term in Equation 2.7 vanishes so Equation 2.7 simplifies to

$$\vec{R}_{e',v';e'',v''} = \langle \psi_{v'}(Q) | \vec{R}_{e'e''}(Q) | \psi_{v''}(Q) \rangle \quad (2.8)$$

where the pure electronic transition moment

$$\vec{R}_{e'e''}(Q) = \langle \psi_{e'}(q,Q) | \vec{M}_e | \psi_{e''}(q,Q) \rangle \quad (2.9)$$

is a function of the nuclear coordinates. The matrix element of the electronic transition moment varies only slightly with  $Q$  so the Condon approximation may be applied to remove the dependence of  $R_{e'e''}(Q)$  on the nuclear coordinates. If  $\psi_e$  is evaluated only at the equilibrium nuclear configuration of the state,  $Q_0$ , from which the transition originates Equation 2.9 becomes

$$\vec{R}_{e'e''}(Q_0) = \langle \psi_e(q, Q_0) | \vec{M}_e | \psi_{e''}(q, Q_0) \rangle \quad (2.10)$$

where  $Q_0$  is the equilibrium nuclear configuration of the initial state (the lower state for absorption and the upper state for emission). The transition moment, Equation 2.8, then simplifies to

$$\vec{R}_{e'v'e''v''} = \vec{R}_{e'e''}(Q_0) \langle \psi_{v'}(Q) | \psi_{v''}(Q) \rangle. \quad (2.11)$$

For an electronically allowed transition  $R_{e'e''}(Q_0) \neq 0$ . From group theoretical considerations this will be the case if the direct product  $\Gamma(\psi_{e'}) \times \Gamma(\psi_{e''}) \times \Gamma(\vec{M})$  is totally symmetric under the symmetry operations of the point group to which the molecule belongs for at least one of the components of the vector  $\vec{M}$ . If the transition is electronically allowed, the vibrational transitions accompanying this electronic transition (i.e., the vibrational fine structure of the electronic spectrum) will be those for which  $\langle \psi_{v'}(Q) | \psi_{v''}(Q) \rangle \neq 0$ . This integral will be non-zero if the direct product  $\Gamma(\psi_{v'}) \times \Gamma(\psi_{v''})$  contains the totally symmetric representation.

For an electronically forbidden transition  $\vec{R}_{e'e''}(Q_0)$  will be zero so within the restrictions of the Born-Oppenheimer and Condon approximations the electric dipole transition moment,  $\vec{R}_{e'v'e''v''}$ , for the vibronic

transitions would also vanish. Within these approximations there should be no mechanism of "intensity borrowing". Vibronic interactions do, however, occur because  $\psi_e$  and  $\psi_v$  are not exactly separable. This is equivalent to relaxation of the Condon approximation, since the electronic wavefunctions will truly be dependent on the nuclear coordinates.

In the Herzberg-Teller theory<sup>36</sup> of vibronic interactions this dependence on the nuclear coordinates can be expressed as a series expansion of the electronic Hamiltonian  $\hat{H}_e$  (or the electronic transition moment) in terms of the normal (nuclear) coordinates of the molecule,  $Q_i$ :

$$\hat{H}_e = (\hat{H}_e)_0 + \sum_i \left( \frac{\partial \hat{H}_e}{\partial Q_i} \right)_0 Q_i + \dots \quad (2.12)$$

where the  $Q_i$  are the nuclear coordinates of the  $i^{\text{th}}$  normal vibration relative to their equilibrium values in the vibrationless ground state and the subscript nought refers to the equilibrium nuclear configuration of the ground electronic state. The second term in the expansion, Equation 2.12, accounts for the interaction between the electronic and nuclear motions and will be zero in the Born-Oppenheimer and Condon approximations. It is assumed that there is a set of zeroth order wavefunctions,  $\psi_k^0(q, Q)$  which represent the purely electronic wavefunctions of the molecule. These wavefunctions will be solutions to the zeroth order eigenvalue equation

$$(\hat{H}_e)_0 \psi_k^0(q, Q) = E_k^0 \psi_k^0(q, Q). \quad (2.13)$$

The higher order perturbations in the electronic Hamiltonian mix into this zeroth order state  $\psi_k^0$  contributions from other states,  $\psi_j^0$  in the manner

$$\psi_k = \psi_k^0 + \sum_{k \neq j} C_{kj} \psi_j^0 \quad (2.14)$$

The coefficients,  $C_{kj}$ , are given by perturbation theory

$$C_{kj} = \frac{\langle \psi_j^0 | \hat{H}' | \psi_k^0 \rangle}{|E_k^0 - E_j^0|}, \quad j \neq k \quad (2.15)$$

where  $\hat{H}'$  is the perturbation term of the electronic Hamiltonian. For the coefficients  $C_{kj}$  to be non-zero the symmetry condition

$$\Gamma(\psi_j^0) \times \Gamma(\psi_k^0) = \Gamma(Q_i) \quad (2.16)$$

must be met. In the usual scheme of Herzberg-Teller vibronic coupling the intensity of electronically forbidden transitions arises from the interaction with non-totally symmetric vibrational modes of appropriate symmetry. Totally symmetric modes may bring intensity to otherwise weak electronically allowed transition. For naphthalene the electronic transition moment for the  $^1A_g \rightarrow ^1B_{2u}$  transition is effectively zero, owing to the nearly exact cancellation of the individual large components of the net transition moment.<sup>37</sup> Totally symmetric vibrations can relieve this restriction and bring considerable intensity to the transition. Other examples of totally symmetric vibrations contributing intensity in allowed transitions have been found for the  $S_0 - S_1$  transition of phenanthrene<sup>38,39</sup> and in azulene.<sup>40</sup> In molecules of low symmetry the symmetry selection rules are such that most transitions will be electronically allowed.

## 2.4 Fate of Absorbed Energy

At room temperature most molecules, prior to excitation, will be present in their vibrationless electronic ground states. Excitation of

these molecules can be achieved with incident light of energy greater than or equal to the difference between the vibrationless ground electronic state and the vibrationless first excited electronic state. Depending on the choice of excitation energies the excited molecule will be formed in vibrational levels of  $S_1$  or higher electronic states,  $S_2$ ,  $S_3$ , etc. The excess vibrational energy is rapidly dissipated by collisions with solvent molecules in the condensed phase. This vibrational relaxation or thermalization of the excess vibrational energy occurs with a rate constant of  $> 10^{12} \text{ s}^{-1}$ , of the same order as the rate of execution of vibrational motion in the molecule. If the initially excited electronic state is not  $S_1$  but some higher singlet state a process known as internal conversion can occur. Internal conversion is the nonradiative transition between isoenergetic states having the same multiplicity. The molecule can be envisaged as passing from a low vibrational state of the higher electronically excited state into a high vibrational state of a lower lying electronic state of the same multiplicity. From this high vibrational state further vibrational relaxation will occur.

These processes of vibrational relaxation and internal conversion will rapidly take the excited molecules to a thermally equilibrated (Boltzmann) vibrational distribution in the first excited singlet state. Unlike the higher excited singlet states, internal conversion from  $S_1$  to  $S_0$  is much slower than the competing depletion processes out of  $S_1$ , namely radiative return to the ground state or intersystem crossing to the triplet manifold. A theory of radiationless transitions has been developed by Siebrand<sup>41,42</sup> and Robinson and Frosch<sup>43,44</sup> which accounts for this observation. The transition probability for the radiationless

process is proportional to the Franck-Condon factor for the vibrational levels of the appropriate isoenergetic states. This will, in turn, be proportional to the degree of vibrational excitation in each electronic state and hence to the energy gap between these electronic states. Since the energy gap  $S_0 - S_1$  is generally much larger than the energy gap between  $S_1 - S_2$ ,  $S_2 - S_3$  etc. the difference in vibrational quantum number at the isoenergetic crossing point of  $S_1$  and  $S_0$  will be large, i.e. the crossing would have to occur from a low vibrational state of  $S_1$  into a very high vibrational state of  $S_0$ . For such transitions the Franck-Condon factors will be small and the transition probability low. The internal conversion rate  $S_1 \rightarrow S_0$  for most aromatic hydrocarbons is slow and often does not compete with the radiative rate constant of  $10^7 - 10^9 \text{ s}^{-1}$  or the rate of intersystem crossing to the triplet state,  $10^6 - 10^8 \text{ s}^{-1}$ . For these reasons fluorescence is found to occur nearly invariably from the first excited singlet state only. Historically this was formulated in two empirical statements, Vavilov's law and Kasha's rule.<sup>34</sup> Vavilov's law simply states that the fluorescence quantum efficiency or quantum yield is independent of the excitation wavelength, a natural result of the fast internal conversion from higher excited singlet states occurring with unit efficiency. Kasha's rule states that in complex molecules in condensed phases the emission will occur from the lowest excited electronic state of given multiplicity, i.e., fluorescence is from  $S_1$  while phosphorescence is from  $T_1$ . The number of molecules found to fluoresce efficiently from higher excited singlet states is small but has grown rapidly in recent years.<sup>45-50</sup>

Some of the principal photophysical processes for complex molecules

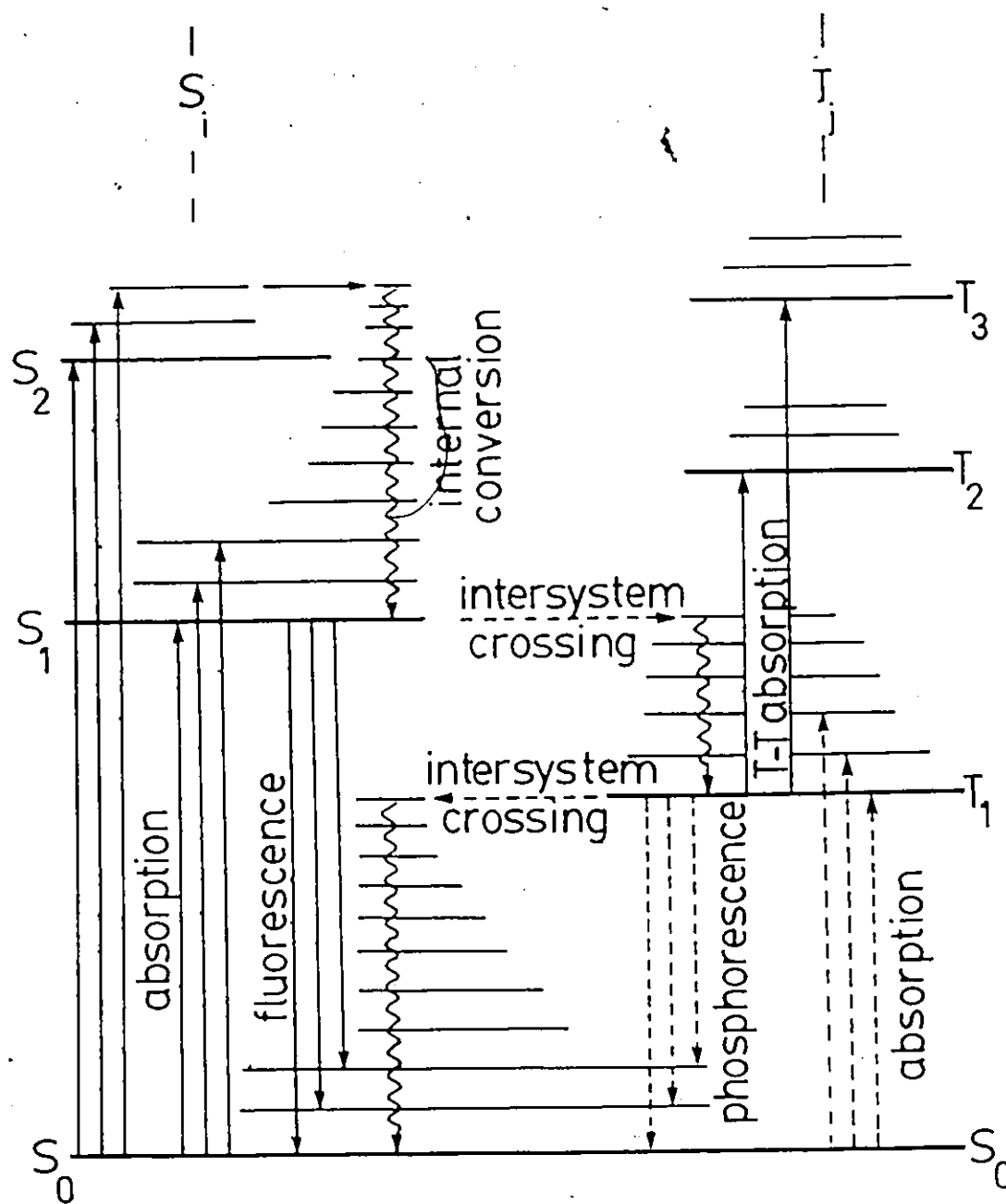


Figure 2.1

Jablonski Diagram Showing the  
Principal Photophysical Processes in Complex Molecules

are shown in the Jablonski diagram, Figure 2.1. As mentioned previously, shortly after excitation the majority of electronically excited molecules will arrive in the vibrationless state of  $S_1$ , whence they can undergo three processes: (i) fluorescence, or a radiative transition to various vibrational states of the ground electronic state, a process involving no change in the spin multiplicity; (ii) internal conversion to the  $S_0$  potential energy surface followed by vibrational relaxation within  $S_0$ , often an unimportant process for aromatic molecules; (iii) intersystem crossing, which is a radiationless passage from a singlet electronic state to an isoenergetic level in a triplet electronic state (or vice versa), followed by further vibrational relaxation and, perhaps internal conversion within the triplet manifold. After thermal equilibration in the lowest triplet state,  $T_1$ , the molecule can return to the electronic (singlet) ground state by two means: (i) isoenergetic intersystem crossing, usually to a high vibrational state of the  $S_0$  potential energy surface; (ii) a radiative transition (phosphorescence) to vibrational levels of  $S_0$ , eventually arriving back in the thermally equilibrated ground state. As a change in total spin multiplicity is required for the radiative transition  $T_1 \rightarrow S_0$  the radiative rate constant for phosphorescence is very low, usually about  $10^{-1} \text{ s}^{-1}$  for aromatic hydrocarbons.

The large  $T_1 - S_0$  energy gap also leads to slow rates of intersystem crossing  $T_1 \rightarrow S_0$ , comparable to the radiative rate constant. This leads to an intrinsically long lifetime for the lowest triplet. As bimolecular quenching processes tend to be much more efficient than any of the intrinsic unimolecular deactivation pathways for  $T_1$ , phosphorescence is rarely observed in condensed phase at ambient temperatures.



Considering a single excited singlet species  $A^*$  which is subjected to a number of first order deactivation processes (for example, fluorescence, internal conversion and  $S_1 \rightarrow T_1$  intersystem crossing), one can write the rate of disappearance of  $A^*$  as

$$\frac{-d\{A^*\}}{dt} = \sum_i k_i \{A^*\} \quad (2.17)$$

where  $k_i$  are the rate constants for the processes depleting the excited state. In integrated form this gives

$$\{A^*\} = \{A^*\}_0 \exp(-t/\tau) \quad (2.18)$$

where  $\{A^*\}_0$  is the initial excited state concentration and

$$\tau = (\sum_i k_i)^{-1} \quad (2.19)$$

The quantity  $\tau$  is known as the mean lifetime of the excited state. If  $A^*$  is a singlet species then  $\tau$  is known as the fluorescence lifetime. A description of the technique used to obtain the fluorescence lifetimes in this work is found in Sections 2.7 and 3.7.

## 2.5 Fluorescence Quantum Yields

The fluorescence quantum yield of a species is defined as that fraction of excited molecules that emit a fluorescence photon. Writing the rate equation for species  $^1A^*$  under steady illumination (photo-stationary conditions) one has

$$\frac{d(^1A^*)}{dt} = I_a - (k_f + k_{isc} + k_{ic}) (^1A^*) \quad (2.20)$$

where  $k_f$ ,  $k_{isc}$ ,  $k_{ic}$  are the rate constants for fluorescence, intersystem

crossing and internal conversion respectively;  $\{^1A^*\}_0$  is the steady rate of production of the excited singlet state  $^1A^*$  by absorption of the incident photons. Since  $\frac{d\{^1A^*\}}{dt} = 0$  under photostationary conditions and the rate of fluorescence emission is given by  $k_f\{^1A^*\}$  it follows that the fluorescence quantum yield can be written as

$$\phi_f = \frac{\text{photons emitted as fluorescence}}{\text{photons initially absorbed}} = \frac{k_f\{^1A^*\}}{\{^1A^*\}_0} \quad (2.21)$$

$$= \frac{k_f}{k_f + k_{isc} + k_{ic}} = \frac{k_f}{k_f + k_{nr}}$$

where the nonradiative rate constants have been combined as  $k_{nr}$ .

The determination of absolute fluorescence quantum yields has many attendant experimental difficulties<sup>51</sup> so the vast majority of quantum yields reported in the literature are relative, not absolute quantum yields. These relative quantum yields have been obtained through measurement of the fluorescence intensity of the compound of interest with respect to the fluorescence intensity of a reference material, the quantum yield of which is well known or at least is generally agreed upon. The number of compounds with well characterized absolute quantum yields is very small indeed.

At low solute concentrations and with the fluorescence observed at normal incidence the fluorescence quantum yield of the sample is related to the fluorescence quantum yield of the reference by

$$\phi_f^s / \phi_f^r = \frac{F_s}{F_r} \cdot \frac{I(\lambda_r)}{I(\lambda_s)} \cdot \frac{A_r(\lambda_r)}{A_s(\lambda_s)} \cdot \frac{n_s^2}{n_r^2} \quad (2.22)$$

The subscripts and superscripts s and r refer to sample and reference respectively while the quantity F is the integrated area under the

corrected fluorescence emission curve (i.e. corrected for wavelength dependence of detection response).  $I(\lambda)$  is the relative photon output of the light source at the excitation wavelength  $\lambda$ ;  $A(\lambda)$  is the absorbance of the solution at wavelength  $\lambda$  and  $n$  is the average refractive index of the solution over the fluorescence emission spectrum. This expression can be simplified by the choice of experimental conditions. In the special case where the sample and reference solutes are in the same solvent at the same temperature, have equal absorbances and are excited at a common wavelength Equation 2.22 reduced to

$$\phi_f^s / \phi_f^r = F_s / F_r \quad (2.23)$$

Furthermore, use of sample and reference solutes with overlapping emission spectra and using identical geometries and optics obviates the need to explicitly correct the fluorescence spectra, the correction factors in  $F_s$  and  $F_r$  being identical.

A comprehensive review on the measurement of fluorescence quantum yields has been given by Demas and Crosby.<sup>51</sup>

## 2.6 Fluorescence Excitation

The absolute intensity of fluorescence emission is equal to the intensity of light absorbed multiplied by the quantum efficiency or quantum yield of fluorescence,

$$F = (I_o - I_t)\phi_f = (I_o(1 - 10^{-\epsilon Cl}))\phi_f \quad (2.24)$$

where  $F$  is the total, absolute fluorescence intensity ( $\text{quanta} \cdot \text{s}^{-1}$ ),  $I_o$  and  $I_t$  are the incident and transmitted intensities of the exciting light (also in  $\text{quanta} \cdot \text{s}^{-1}$ ),  $\epsilon$  is the molar absorptivity ( $\text{litre} \cdot \text{mole}^{-1} \cdot \text{cm}^{-1}$ ),

C and l are the solute concentration ( $\text{moles} \cdot \text{litre}^{-1}$ ) and solution path length (cm) respectively, and  $\phi_f$  is the fluorescence quantum yield. The difference  $I_0 - I_t$  represents the quantum intensity of absorbed light. For weakly absorbing solutions (low C or  $\epsilon$ ) the exponent  $\epsilon Cl$  is small and Equation 2.24 simplifies to

$$F = 2.303 I_0 \epsilon Cl \phi_f \quad (2.25)$$

Hence for a solution of a single solute at fixed concentration the fluorescence intensity will be directly proportional to  $I_0 \epsilon \phi_f$ . If Vavilov's law is obeyed, i.e.,  $\phi_f$  is independent of excitation wavelength and  $I_0$  is also constant with wavelength the fluorescence intensity is proportional to the molar absorptivity  $\epsilon$ . The observed fluorescence intensity at a fixed emission wavelength should vary as  $\epsilon(\lambda_A)$  as the excitation wavelength is scanned across the absorption profile. This so-called fluorescence excitation spectrum should then closely resemble the absorption spectrum of the solute. A reasonable representation of the absorption spectrum can often be obtained even when  $I_0$  is not rigorously constant with the excitation wavelength  $\lambda_A$  or where the absorbance of the solution is fairly high.

## 2.7 Singlet Decay Times

The singlet decay times or fluorescence lifetimes in this present study were determined by the method of time-correlated single photon counting, the most widely used technique in recent years. Numerous reviews of this topic have been published.<sup>52-59</sup>

The single photon counting technique of fluorescence lifetime measurements is based on the concept that the intensity time profile of

all the photons emitted following a single pulse of excitation light can be reproduced by determining the probability distribution for emission of a single photon, as a function of time, following the single excitation pulse. Simply stated, rather than exciting a statistically large number of molecules at once then monitoring their emission over time one may equally well excite a very small number of molecules but repeat the experiment (excitation) many times. Excitation is achieved by a pulsed light source, either a laser or spark discharge lamp. This excitation pulse is detected electronically or optically, by means of the so-called "start" photomultiplier tube. This "start" pulse in turn triggers the voltage ramp of a time-to-amplitude converter or TAC. This TAC generates a voltage ramp that increases linearly with time. A second high gain photomultiplier viewing the sample emission acts as the "stop" signal source. Arrival of a fluorescence photon at this "stop" photomultiplier and subsequent production of an output signal terminates the linearly increasing voltage ramp of the TAC. The voltage amplitude of the TAC will then be proportional to the time difference between "start" and "stop" pulses. If no "stop" pulse is received by the TAC by the end of its preset voltage sweep the voltage ramp is reset and no output signal is generated. The reset or strobe time of the TAC must, of course, be shorter than the period between excitation pulses. If a valid "stop" signal is received within the voltage-time domain of the TAC a time-correlated voltage pulse will be output to the multichannel pulse height analyzer, commonly called simply a multichannel analyzer or MCA. The MCA is primarily a storage device, with discrete channels of memory or storage corresponding to discrete voltage ranges. Incoming signals from

the TAC are sorted by pulse amplitude (i.e., voltage) and allocated to the appropriate channel in the MCA. Over many excitation-decay cycles a histogram is accumulated in the MCA of "stop" events (fluorescence photons) versus voltage. Since the probability of detecting a single photon is directly proportional to the intensity of emission and the pulse amplitude or voltage is correlated to the time between excitation and emission, the resulting counts-voltage distribution will be proportional to the emission intensity versus time profile.

The initial premise of the time-correlated single photon counting method (i.e., the correspondence of the single photon emission probability distribution and the net intensity vs time profile) is predicated on the assumption that no more than one emitted photon is detected per excitation pulse. If, for example, two photons were incident on the photocathode of the "stop" photomultiplier following a single excitation pulse the photon arriving first would furnish the "stop" signal resetting the TAC voltage ramp. The second photon, arriving later, will be ignored by the TAC as it now has no corresponding "start" signal. This phenomenon is called pulse pile-up, specifically type S or statistical pile-up in Selinger's designation.<sup>53,56</sup> Pulse pile-up systematically discriminates against late arriving photons, resulting in a net intensity time distribution skewed to shorter times and lifetimes determined from such curves will be erroneously short. A second type of pulse pile-up is possible type E pile-up in Selinger's terminology.<sup>56</sup> All detection systems possess an inherent limitation in the processing time of detector, amplifier, discriminators or analyzers, usually called the dead time of the instrument. Multiple pulses arriving within this dead time are perceived only as a

single event. While all counting experiments are subject to this type of pile-up error, this can be partially corrected mathematically in the data reduction<sup>60,61</sup> or circumvented experimentally.<sup>53,56,62-64</sup> The latter way is usually more convenient. Experimentally the simplest way to reduce both types of pulse pile-up is to attenuate the emission intensity such that the average number of detected emission photons per excitation flash is small. With  $\leq 0.05$  detected photons per lamp pulse the error introduced by pulse pile-up will be negligible.<sup>65</sup>

The true fluorescence decay curve is that obtained by excitation with a delta function light source, i.e., infinitesimally narrow excitation pulse. While this situation is approached with some long-lived fluorophores generally the excitation pulse has a not inconsiderable temporal width on the time scale of the fluorescence decay. For short-lived species the observed fluorescence decay curve represents a significant distortion of the true decay profile so extraction of the true decay function from the experimentally obtained profile requires the solution of the convolution integral

$$G(t) = \int_0^t E(t')I(t - t')dt' \quad (2.26)$$

where  $G(t)$  is the observed, distorted fluorescence intensity as a function of time,  $E(t)$  is the instrumental response function or the lamp temporal profile distorted by the detection system and  $I(t)$  is the true fluorescence decay profile obtained with  $\delta$ -pulse excitation. A great many techniques have been explored to solve this convolution integral including the method of moments,<sup>66-69</sup> Laplace transforms,<sup>70,71</sup> method of exponential series,<sup>72</sup> Fourier transforms<sup>73-76</sup> and reiterative convolution.<sup>58,59,77</sup>

This last method, iterative or reiterative convolution, has proven one of the most popular and successful. One drawback of this technique is the need to assume a particular functional form of the time decay function,  $I(t)$ , although this may often be deduced from the suspected photophysical scheme. This trial decay function  $I'(t)$ , containing the appropriate adjustable parameters, is numerically integrated with the experimentally determined lamp temporal function,  $E(t)$ , to yield a trial curve  $G'(t)$  which is then compared with the experimentally obtained  $G(t)$ . The free parameters in the trial decay function  $I'(t)$  are adjusted until the best fit is obtained between the calculated and observed functions,  $G'(t)$  and  $G(t)$ . For fluorescent species in dilute solution subject to only unimolecular deactivation processes or to time-independent bimolecular quenching processes a reasonable function form to assume for  $I(t)$  is that of a sum of exponentially decaying terms, i.e.,

$$I(t) = \sum_{i=1}^n \alpha_i \exp(-t/\tau_i) \quad (2.27)$$

Specifically, the cases of  $n = 1$  or  $2$  can be handled with confidence and the goodness-of-fit criteria have been used successfully to distinguish mono- from biexponential decay kinetics.<sup>11,58,78-83</sup> Attempts to extract up to three lifetime components (i.e., six parameters) have been made by reiterative convolution techniques, with variable success.<sup>77,81,84</sup>

The trial function  $G'(t)$  and the observed decay function,  $G(t)$  are compared by a least squares method. The weighted mean variance of the fitted function will be given by<sup>53,77,85</sup>



$$S^2 = \frac{\frac{1}{v} \sum_{i=1}^N \left\{ \frac{1}{\sigma_o(i)} [y_o(i) - y_c(i)]^2 \right\}}{\frac{1}{N} \sum_{i=1}^N \frac{1}{\sigma_o(i)^2}} \quad (2.28)$$

where the subscripts o and c refer to observed and calculated (fit) values respectively;  $y(i)$  is the number of counts (i.e., intensity) in the  $i^{\text{th}}$  channel (i.e., time);  $\sigma_o(i)$  is the variance of the  $i^{\text{th}}$  channel;  $v$  is the number of degrees of freedom left after fitting  $N$  total data points to the  $n+1$  parameters; for a monoexponential decay law  $n$  will be two ( $\alpha, \tau$ ) while for a biexponential model  $n$  will be four ( $\alpha_1, \tau_2, \alpha_1, \tau_2$ ). The weighted average of the individual variances in each channel will be given by

$$\frac{\sigma_o(i)^2}{\sigma_o(i)^2} = \frac{\frac{1}{N} \sum_{i=1}^N \left( \frac{1}{\sigma_o(i)^2} \right)}{\frac{1}{N} \sum_{i=1}^N \frac{1}{\sigma_o(i)^2}} = \frac{1}{\frac{1}{N} \sum_{i=1}^N \frac{1}{\sigma_o(i)^2}} \quad (2.29)$$

Whereas the true parent variance  $\sigma^2$  is only characteristic of the parent distribution and is not characteristic of the fit, the experimentally estimated variance,  $S^2$ , is a measure of both the intrinsic distribution of the data and the goodness-of-fit. A convenient measure of the goodness-of-fit will be to compare the estimated variance  $S^2$  and the parent variance  $\sigma^2$ ,

$$\chi^2_v = \frac{\chi^2}{v} = \frac{S^2}{\sigma_o(i)^2} \quad (2.30)$$

where  $\chi^2 = \sum_{i=1}^N \left\{ \frac{1}{\sigma_o(i)^2} [y_o(i) - y_c(i)]^2 \right\}$  and where  $\chi^2_v$  is called the

reduced chi-squared.

For single photon counting, i.e., the counting of rare events, the counting error is Poisson distributed about a mean of  $y_0(i)$  in the  $i^{\text{th}}$  channel. The variance,  $\sigma_0(i)^2$ , of this Poisson distribution is simply equal to the number of counts in the  $i^{\text{th}}$  channel or interval,<sup>53,77</sup> namely

$$\sigma_0(i)^2 = y_0(i) \quad (2.31)$$

The expression for the reduced chi-squared, Equation 2.30, then reduces to

$$\chi^2_v = \frac{1}{v} \sum_{i=1}^N \left\{ \frac{[y_0(i) - y_c(i)]^2}{y_0(i)} \right\}. \quad (2.32)$$

Assuming no experimental noise or error other than the Poisson counting error one would expect that  $\chi^2_v$  should approach unity for a good fit of the trial function and the observed decay function.  $\chi^2_v \gg 1$  is indicative of a poor fit, that is the trial decay function  $I'(t)$  used to calculate  $G'(t)$  via the convolution integral is not a good model for the true decay function,  $I(t)$ . Knight and Selinger point this out explicitly: "the most complex theoretical model which can be justified by the data is that for which SSQR [sum of squares reduced =  $S^2$ ] is not statistically significantly different from SSQP [sum of squares of Poisson error =  $\sigma_0(i)^2$ ]."a,53

While reduced chi-squared values slightly less than one may occur with a reasonable, finite probability for a well fitted model too,

<sup>a</sup> Square brackets added by this author in explanation of terminology.

reduced chi-squared values much less than unity may be taken to indicate use of an overly complex model function (i.e., too many adjustable parameters) in the fitting procedure. A perfectly determined function for which no random Poisson counting noise is even allowed will give a  $\chi^2_v$  of zero.

It is occasionally difficult to distinguish between two different models yielding similar values of  $\chi^2_v$ ; for example both a mono- and a biexponential form of the true decay law may yield comparable values of the reduced chi-squared. The parameter  $\chi^2_v$  is not, in itself, sensitive to small systematic deviations between the observed and fitted curves although these systematic differences may be noticeable in a plot of the deviations themselves. For a good fit the differences between the observed and calculated functions should be randomly distributed while a nonrandom scatter of the residuals indicates some inadequacy in the fitting function. Grinvald and Steinberg<sup>77</sup> were the first to propose the use of a more objective test for the randomness of the residuals in fluorescence decay measurements, using the autocorrelation function of the weighted residuals

$$C(j) = \frac{\frac{1}{\ell} \sum_{k=1}^{\ell} R(k) R(k+j)}{\frac{1}{N} \sum_{k=1}^N R(k)^2} \quad (2.33)$$

where  $\ell = N/2$  and  $j = 1, \dots, \ell$  and  $R(k)$  is the weighted residual in the  $k^{\text{th}}$  channel and is given by

$$R(k) = \frac{1}{y_0(k)^{1/2}} \{y_0(k) - y_c(k)\} \quad (2.34)$$

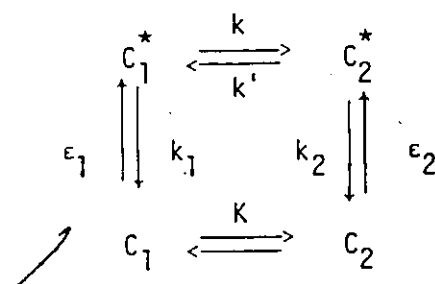
$C(1) = +1$  by definition, while for an infinitely large data set  $C(j > 1)$  would be zero. For real data sets  $C(j > 1)$  should be close to and randomly scattered about zero (usually  $|C(j > 1)| < 0.20$ ). A plot of  $C(j)$  versus  $j$  will then reveal any systematic nonrandomness in the weighted residuals. Application of the autocorrelation function to fluorescence decay data is gaining widespread acceptance.<sup>16,81,82,84</sup>

Statistical treatment of fluorescence decay data is a rapidly expanding and evolving field with several new criteria for model and parameter evaluation being recently proposed.<sup>69,84,86,87</sup>

## 2.8. Fluorescence Decay Kinetics of Multicomponent Systems

The appearance of two components in the fluorescence emission may arise in several manners: (i) excitation of two distinct ground state species followed by fluorescence from their respective excited singlet states or (ii) excitation of a single ground state species followed, in the excited state, by conformational changes leading to the production of a second, spectroscopically distinguishable species. These alternative Schemes are illustrated below.

Scheme I:



Scheme II:

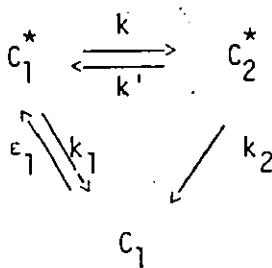


Figure 2.2

Multicomponent Fluorescence Decay Schemes

where  $k/k' = K^*$ ;  $C_1/C_2 = K$ ;  $k_1 = k_{f,1} + k_{nr,1}$ ;  $k_2 = k_{f,2} + k_{nr,2}$ ;  $\epsilon_1$  and  $\epsilon_2$  represent the excitation (absorption) steps for species 1 and 2.

The kinetics of Scheme I are similar to those encountered for intermolecular exciplex or excimer formation and emission<sup>88-90</sup> with the bimolecular rate constants in those treatments replaced by the appropriate unimolecular ones and with the additional direct excitation step  $\epsilon_2$ , for production of  $C_2^*$ .

Kinetic Scheme II is essentially that developed for intramolecular exciplex or excimer formation and deactivation, the kinetics of which have been closely examined in recent years.<sup>82,83,91,92</sup>

For Scheme I the differential rate equations following  $\delta$ -pulse excitation will be

$$\frac{d[C_1^*]}{dt} = k'[C_2^*] - (k_1 + k)[C_1^*] \quad (2.35)$$

and

$$\frac{d[C_2^*]}{dt} = k[C_1^*] - (k_2 + k')[C_2^*] \quad (2.36)$$

General solutions to these coupled differential equations have been given elsewhere<sup>88-90,93</sup> and are of the form

$$[C_1^*] = A_1 e^{-\lambda_1 t} + B_1 e^{-\lambda_2 t} \quad (2.37)$$

$$[C_2^*] = A_2 e^{-\lambda_1 t} + B_2 e^{-\lambda_2 t} \quad (2.38)$$

where  $\lambda_{1,2} = \frac{1}{2} \{ k_1 + k + k_2 + k' \pm [(k_2 + k' - k_1 - k)^2 + 4kk']^{1/2} \}$ . The four constants  $A_1, B_1, A_2, B_2$  are not independent, as seen from the initial conditions at  $t = 0$

$$A_1 + B_1 = [C_1^*]_0 \quad (2.39)$$

and

$$A_2 + B_2 = [C_2^*]_0 \quad (2.40)$$

So

$$[C_1^*] = A_1(e^{-\lambda_1 t} - e^{-\lambda_2 t}) + [C_1^*]_0 e^{-\lambda_2 t} \quad (2.41)$$

$$[C_2^*] = B_2(e^{-\lambda_2 t} - e^{-\lambda_1 t}) + [C_2^*]_0 e^{-\lambda_1 t} \quad (2.42)$$

For the initial rates one may write, from Equations 2.35 and 2.36

$$\left(\frac{d[C_1^*]}{dt}\right)_{t=0} = k'[C_2^*]_0 - (k_1 + k)[C_1^*]_0 \quad (2.43)$$

$$\left(\frac{d[C_2^*]}{dt}\right)_{t=0} = k[C_1^*]_0 - (k_2 + k')[C_2^*]_0 \quad (2.44)$$

while from Equations 2.41 and 2.42 the initial rates are

$$\left(\frac{d[C_1^*]}{dt}\right)_{t=0} = A_1(\lambda_2 - \lambda_1) - \lambda_2[C_1^*]_0 \quad (2.45)$$

$$\left(\frac{d[C_2^*]}{dt}\right)_{t=0} = B_2(\lambda_1 - \lambda_2) - \lambda_1[C_2^*]_0 \quad (2.46)$$

By equating the initial rate expressions one gets

$$A_1 = \frac{k'[C_2^*]_0 - (k_1 + k - \lambda_2)[C_1^*]_0}{\lambda_2 - \lambda_1} \quad (2.47)$$

$$B_2 = \frac{k[C_1^*]_0 - (k_2 + k' - \lambda_1)[C_2^*]_0}{\lambda_1 - \lambda_2} \quad (2.48)$$

Leaving the constants as  $A_1$  and  $B_2$  for compactness, the rates of fluorescence emission of species 1 and 2 following  $\delta$ -pulse excitation are

$$I_1(t) = k_{f,1}[C_1^*] = k_{f,1} A_1 e^{-\lambda_1 t} + ([C_1^*]_0 - A_1) e^{-\lambda_2 t} \quad (2.49)$$

$$I_2(t) = k_{f,2}[C_2^*] = k_{f,2} ([C_2^*]_0 - B_2) e^{-\lambda_1 t} + B_2 e^{-\lambda_2 t} \quad (2.50)$$

These expressions are applicable to Scheme II if  $[C_2^*]_0$  is set to zero, i.e.,  $C_2^*$  is not formed by direct excitation but only via conversion of  $C_1^*$ . This is equivalent to the intramolecular exciplex-excimer kinetics. Setting  $[C_2^*]_0 = 0$ , the intensity of species 2 subsequent to excitation is

$$I_2'(t) = k_{f,2} B_2' (e^{-\lambda_2 t} - e^{-\lambda_1 t}) \quad (2.51)$$

where

$$B_2' = k[C_1^*]_0 / (\lambda_1 - \lambda_2). \quad (2.52)$$

For  $I_1'(t)$  the functional form will be the same as Equation 2.49 with the constant  $A_1$  replaced by

$$A_1' = (\lambda_2 - k_1 - k)[C_1^*]_0 / (\lambda_2 - \lambda_1). \quad (2.53)$$

Since  $\lambda_2$  is greater than  $\lambda_1$  one has the familiar result

$$i_1(t) = D_1 e^{-\lambda_1 t} + D_2 e^{-\lambda_2 t} \quad (2.54)$$

$$i_2(t) = D_3 (e^{-\lambda_1 t} - e^{-\lambda_2 t}) \quad (2.55)$$

where all three preexponentials,  $D_1$ ,  $D_2$  and  $D_3$  are positive and  $i(t)$  is the rate of emission per initially excited molecule. These equations, 2.54 and 2.55 are of the same form as those encountered for pure monomer decay and pure excimer decay (where the monomer is species 1 and excimer or exciplex is species 2). While it is possible experimentally to obtain essentially pure monomer or exciplex emission separately this is

not generally the case if  $C_1$  and  $C_2$  are conformers of the same chemical species. Since the emission of the conformers is not expected to be spectrally well separated one may observe only the total decay

$$i(t) = i_1(t) + i_2(t) = (D_1 + D_3)e^{-\lambda_1 t} + (D_2 - D_3)e^{-\lambda_2 t}. \quad (2.56)$$

Fischer and coworkers<sup>16</sup> have argued that the positive preexponential factors seen for the fluorescence decay of the trans-1,2-diarylethylene conformers are necessarily indicative of two discrete ground state conformers prior to excitation. Although this will be true if two ground state conformers are initially present<sup>78,79,83</sup> the possibility of a single ground state conformer being responsible for a two component decay with positive preexponentials (via some conversion of  $C_1^*$  to  $C_2^*$  during excited state lifetime) cannot be entirely precluded. If the emission spectra of 1 and 2 overlap strongly the sign of the preexponential factor ( $D_2 - D_3$ ) may not invariably be negative. Where the emission of the derived fluorophore can be spectrally isolated, as in inter- or intramolecular exciplex/excimer formation, the ratio of preexponential factors for this component will, of course, be  $-1 (= D_3/-D_3)$ , as has been verified by experiment.<sup>82,91,92</sup>

A number of other special cases of kinetic Schemes I and II will be recognized;

(i) Fast Interconversion in the Excited State:

This behaviour is observed in inter- or intramolecular photo-physics under conditions of dynamic equilibrium in the excited state, the so-called "high temperature" region.<sup>82,88,92</sup> Under these conditions  $k \gg k_1$  and  $k' \gg k_2$ ; that is, the rates of conversion are faster than



the other deactivation rates of the singlet states  $C_1^*$  and  $C_2^*$ . With  $k \gg k_1$  and  $k' \gg k_2$  the roots,  $\lambda_{1,2}$  reduce to

$$\lambda_1 = (k_1 + k_2)/2 \quad (2.57)$$

$$\lambda_2 = k + k'. \quad (2.58)$$

$\lambda_2$  will be large so the exponential term,  $e^{-\lambda_2 t}$ , will be negligible except at extremely short times.<sup>94</sup> The experimentally measurable lifetime will be

$$\tau = 1/\lambda_1 = 2/(k_1 + k_2) \quad (2.59)$$

and both components will decay with this common lifetime, i.e., the fluorescence decay will be monoexponential.

(ii) No Interconversion in the Excited State:

This implies that  $k$  and  $k' = 0$ , or at least,  $k \ll k_1$  while  $k' \ll k_2$ .

The roots in Equations 2.37 and 2.38 are

$$\lambda_1 = k_1 \text{ and } \lambda_2 = k_2. \quad (2.60)$$

The lifetimes of the two decay components are

$$\tau_1 = (k_{f,1} + k_{nr,1})^{-1} \quad (2.61)$$

$$\tau_2 = (k_{f,2} + k_{nr,2})^{-1}. \quad (2.62)$$

A trivial example of such behaviour is a solution of two chemically distinct fluorescent species, say anthracene and phenanthrene, which cannot interconvert. If the rate of excited state interconversion of conformers of the same chemical species is significantly slower than

the competing radiative and nonradiative return to the respective ground states this behaviour will be approximately realized.

(iii) Uni-directional Conversion in the Excited State:

Two types will be considered:  $C_1^* \rightarrow C_2^*$  but  $C_2^* \nrightarrow C_1^*$  so  $k \neq 0, k' = 0$  and  $C_2^* \rightarrow C_1^*$  but  $C_1^* \nrightarrow C_2^*$  so  $k = 0, k' \neq 0$ . If  $k \neq 0$  while  $k' = 0$  the solutions are

$$\lambda_1 = k_1 + k \quad (2.63)$$

$$\lambda_2 = k_2 \quad (2.64)$$

If  $k$  is comparable to  $k_1, k_2$  then the fluorescence decay following  $\delta$ -pulse excitation will be biexponential whereas if  $k \gg k_1, k_2$  the observed temporal decay will be monoexponential, with

$$\tau = 1/\lambda_2 = 1/k_2 \quad (2.65)$$

For the other case, namely  $k = 0, k' \neq 0$  the roots are

$$\lambda_1 = k_1 \quad (2.66)$$

$$\lambda_2 = k_2 + k' \quad (2.67)$$

Again, depending on the relative magnitudes of  $k'$  and  $k_2$  the observed fluorescence decay may be mono- or biexponential.

All of these kinetic schemes fail to account explicitly for excitation and emission wavelength dependence of the fluorescence decay function. In the most general case the fluorescence intensity should be written as a function of time, the excitation wavelength,  $\lambda_A$ , and the emission or monitoring wavelength,  $\lambda_F$ . Birks and coworkers<sup>11</sup> have

developed this more complete treatment for the limited case where inter-conversion of the emitting species in the excited state is assumed to be noncompetitive with the other deactivation pathways. Their derivation, using Birk's notation, will be reiterated and amplified here.

For a non-interconverting (in  $S_1$ ) system of two fluorescent components the net time-independent, i.e., steady-state, fluorescence spectrum produced by excitation at  $\lambda_A$  will be given by

$$\bar{F}(\lambda_F)[\lambda_A] = f_1[\lambda_A]F_1(\lambda_F) + f_2[\lambda_A]F_2(\lambda_F) \quad (2.68)$$

where square brackets denote fixed parameters while round brackets indicate variable ones.  $F_i(\lambda_F)$  is the time and excitation-independent fluorescence spectrum of the  $i^{\text{th}}$  fluorescent component while  $f_i[\lambda_A]$  is the fraction of excited molecules of species  $i$  excited at wavelength  $\lambda_A$ . This would correspond to  $[C_i^*]/\Sigma[C_i^*]$  at  $\lambda_A$  in the earlier notation. Note also that for two components  $f_1[\lambda_A] + f_2[\lambda_A] = 1$  by definition.

The net absorption spectrum of the mixture of species 1 and 2 will be

$$\bar{\epsilon}(\lambda_A) = \epsilon_1(\lambda_A)C_1/\bar{C} + \epsilon_2(\lambda_A)C_2/\bar{C} \quad (2.69)$$

where the total molar concentration of the two species is

$$\bar{C} = C_1 + C_2. \quad (2.70)$$

One can relate the fractions of excited molecules to these absorption properties by

$$f_1[\lambda_A] = \frac{\epsilon_1[\lambda_A]C_1}{\epsilon[\lambda_A]C} \quad (2.71)$$

and

$$f_2[\lambda_A] = \frac{\epsilon_2[\lambda_A]C_2}{\epsilon[\lambda_A]C} \quad (2.72)$$

With excitation at  $\lambda_A$  the experimental quantum yield of fluorescence will be the weighted average of the true molecular quantum yields of the two species, namely

$$\bar{\phi}_f[\lambda_A] = f_1[\lambda_A]\phi_{f,1} + f_2[\lambda_A]\phi_{f,2} \quad (2.73)$$

The temporal decay of the fluorescence of 1, at fixed excitation wavelength will be

$$I_1(t)[\lambda_A] = f_1[\lambda_A]k_{f,1}e^{-k_1 t} \quad (2.74)$$

with  $k_1 = k_{f,1} + k_{nr,1}$ . Multiplying by  $k_1/k_1$  gives

$$I_1(t)[\lambda_A] = f_1[\lambda_A]\left(\frac{k_{f,1}}{k_1}\right)k_1e^{-k_1 t} = f_1[\lambda_A]\phi_{f,1}k_1e^{-k_1 t} \quad (2.75)$$

By definition

$$\sum_{\lambda_F} F_1(\lambda_F) = \phi_{f,1} \quad (2.76)$$

and

$$\sum_{\lambda_F} I_1(t)[\lambda_A](\lambda_F) = I_1(t)[\lambda_A] \quad (2.77)$$

where the summations (or, more correctly, integrations) are taken over all the emission wavelengths. Taking one  $\lambda_F$  in the above summations one gets

$$I_1(t)[\lambda_A, \lambda_F] = f_1[\lambda_A]F_1[\lambda_F]k_1e^{-k_1 t} \quad (2.78)$$

An analogous expression may be derived for  $I_2(t)[\lambda_A, \lambda_F]$ , and the net fluorescence decay following  $\delta$ -pulse excitation at  $\lambda_A$  with the emission monitored at  $\lambda_F$  will be

$$\begin{aligned} I(t)[\lambda_A, \lambda_F] &= I_1(t)[\lambda_A, \lambda_F] + I_2(t)[\lambda_A, \lambda_F] \\ &= f_1[\lambda_A]F_1[\lambda_F]k_1e^{-k_1t} + f_2[\lambda_A]F_2[\lambda_F]k_2e^{-k_2t} \end{aligned} \quad (2.79)$$

If the deconvoluted experimental data is fit to a biexponential decay law of the form

$$I(t)[\lambda_A, \lambda_F] = \alpha e^{-t/\tau_1} + \beta e^{-t/\tau_2} \quad (2.80)$$

the Equations 2.79 and 2.80 can be equated so

$$\tau_1 = 1/k_1; \tau_2 = 1/k_2 \quad (2.81)$$

and

$$\gamma[\lambda_A, \lambda_F] = (\alpha/\beta)[\lambda_A, \lambda_F] = \frac{f_1[\lambda_A]F_1[\lambda_F]k_1}{f_2[\lambda_A]F_2[\lambda_F]k_2} \quad (2.82)$$

In principle one can then calculate the relative fractions of the two species in the excited state,  $f_1[\lambda_A]/f_2[\lambda_A]$ , if the relative fluorescence intensities,  $F_1[\lambda_F]$  and  $F_2[\lambda_F]$ , can be evaluated at some  $\lambda_F$ .

It will be noted that the ground state equilibrium kinetics do not enter into any of these transient excitation kinetic schemes. Since the electronic changes associated with the absorption process occur very quickly, in about  $\sim 10^{-15}$  s, the initial excited state populations of the two species should reflect the ground state population. For the transient kinetic schemes only those processes subsequent to the  $\delta$ -pulse excitation appear explicitly in the rate equations.

## 2.9 Polycrystalline Matrices and the Shpol'skii Effect

In fluid solution at room temperature the vibrational bands in the fluorescence emission spectrum are found to be very broad, typically several hundred wavenumbers at half-maximum. These broad bands arise from the wealth of specific solute-solvent interactions present in fluid media. However, Shpol'skii<sup>95,96</sup> noted that by judicious choice of solute concentration and n-alkane solvent frozen polycrystalline solutions of aromatic hydrocarbons yield highly resolved absorption and luminescence spectra, with bandwidths less than  $10\text{ cm}^{-1}$  in some cases. It has been found empirically that the sharpest quasilinear spectra are obtained when the molecular dimensions of the solute approximately match those of the solvent, although this "key and-hole rule" has been disputed.<sup>97</sup> For the majority of solute-solvent combinations this size matching criterion does serve as a useful guide and in these circumstances it is believed that a solute molecule occupies a substitutional site in the solvent lattice. These solute molecules may be regarded as isolated and oriented within the crystal lattice and more closely resemble an "oriented" or "cold gas" model than does the corresponding rigid glass solution.

Several different crystalline modifications are possible for many of the matrix-forming solvents, a feature that leads to a multiplet structure in the Shpol'skii emission and absorption spectra. The separation of the multiplet components is usually a few tens of wavenumbers for n-alkane solvents.<sup>98,99</sup>

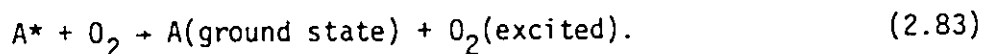
A number of substituted benzenes have demonstrated quasilinear fluorescence and phosphorescence spectra in cyclohexane and methyl-

cyclohexane matrices at low temperature although these solvents are cyclo-, not n-alkanes.<sup>100-104</sup> Cyclohexane is definitely known to have at least two crystal forms, a high temperature cubic form and the low temperature monoclinic form, the proportions varying with the cooling treatment of the sample.<sup>100-105</sup> While heat capacity measurements have indicated only a single modification of methylcyclohexane at 77K<sup>106</sup> recent Raman evidence has been presented that suggests the possibility of two crystalline forms of this solvent at low temperature.<sup>107</sup>

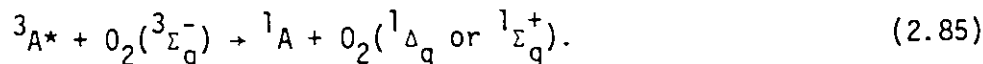
Resolved Shpol'skii spectra in alkane solvents have generally been found only for planar aromatic hydrocarbon solutes, the appearance or non-appearance of quasilines being interpreted as indication of the planarity or nonplanarity of the solute.<sup>29</sup> However, a number of exceptions are known; the slightly nonplanar helicene, 1,2-benzotetraphene does yield a quasilinear fluorescence spectrum although its higher helicene analogs do not.<sup>108</sup> Biphenyl, which is certainly nonplanar in fluid solution<sup>25,109,110</sup> also gives a highly resolved luminescence in alkane matrices.<sup>111</sup> The Shpol'skii effect has recently been employed to distinguish the planar and nonplanar single bond rotational conformers of the trans-1,2-diarylethylenes.<sup>14</sup>

## 2.10 Oxygen Quenching of Fluorescence

In aerated room temperature hydrocarbon solutions molecular oxygen is soluble to the extent of about  $10^{-3}M$ .<sup>112</sup> In addition to the first order deactivation processes for an excited state,  $A^*$ , outlined in Section 2.4, one has the bimolecular quenching step in oxygenated solutions,



For the excited singlet states of aromatic molecules the actual mechanism of oxygen quenching is thought to entail an exchange interaction leading to the aromatic triplet, which is subsequently quenched by a second molecule of oxygen<sup>113,114</sup>



The total rate of depletion of the excited singlet state in the presence of molecular oxygen will then be given by

$$k'_Q = k_f + k_{isc} + k_{ic} + k_Q[O_2] \quad (2.86a)$$

$$= k_f + k_{nr} + k_Q[O_2]. \quad (2.86b)$$

Molecular oxygen is an efficient quencher in fluid solution, the bimolecular quenching rate constant,  $k_Q$ , being approximately the diffusion-controlled rate  $\sim 10^{10} M^{-1} s^{-1}$ .<sup>94,115</sup>

One may write expressions for the fluorescence lifetime and quantum yield in the presence of oxygen by recasting Equation 2.86b



above :

$$\frac{1}{\tau_Q} = \frac{1}{\tau} + k_Q[O_2] \quad (2.87)$$

and

$$\frac{1}{\phi_f} = \frac{1}{\phi_f} + \frac{k_Q}{k_f}[O_2] \quad (2.88)$$

or

$$\frac{\phi_f}{\phi_f} = 1 + k_Q \tau [O_2] \quad (2.89)$$

the last form being the familiar Stern-Volmer equation.

Usually molecular oxygen is rigorously excluded in fluorescence measurements to ensure high signal intensity and to determine the true unimolecular fluorescence lifetime. Deliberate introduction of  $O_2$  can be used to advantage however. If more than one fluorescent species is present the total deactivation rates of the two species in the presence of oxygen will not, in general, be equal, the intrinsically longer lived species being quenched more strongly. Writing individual expressions for the fluorescence lifetime of each species as a function of oxygen concentration one may show that the relative rates of depression of the fluorescence lifetimes with oxygen concentration are given by

$$\frac{d(\frac{\tau_{Q,1}}{\tau_1})}{d[O_2]} = -k_{Q,1}\tau_1(1 + k_{Q,1}\tau_1[O_2])^{-2} \quad (2.90)$$

and

$$\frac{d(\frac{\tau_{Q,2}}{\tau_2})}{d[O_2]} = -k_{Q,2}\tau_2(1 + k_{Q,2}\tau_2[O_2])^{-2} \quad (2.91)$$

where subscripts 1 and 2 refer to the short and long lived species respectively.

If  $k_{Q,1}$  and  $k_{Q,2}$  are taken to be equal ( $=k_Q$ , the diffusion-controlled rate constant) and the quencher concentration is low one has that the differential quenching of the two species will be proportional to the ratio of their unquenched lifetimes. Accordingly a species with a fluorescence lifetime of 100 ns will be quenched 10-fold more strongly than a fluorophore of 10 ns lifetime. Expressions analogous to Equations 2.90 and 2.91 may be derived for the fluorescence quantum yields of the two species.

If only a single fluorescence species is present in fluid solution oxygenation or aeration of the sample should leave the spectral distribution of the steady-state fluorescence emission unaffected but lead to a diminution in total fluorescence intensity. Oxygenation of a solution containing two or more fluorophores of different lifetimes and with non-identical fluorescence emission spectra will lead to selective quenching of the longer-lived components, with concomitant changes in the spectral distribution of the emission. In this manner oxygen quenching experiments serve as a useful diagnostic tool to discern the presence or absence of multiple components in the fluorescence emission in fluid media.<sup>11,16</sup>

## CHAPTER THREE

### EXPERIMENTAL

#### 3.1 Solutes

2,2'-binaphthyl- $\text{h}_{14}$  was obtained from James Hinton Co. (Newport News, Va.) as a zone refined material (purity in excess of 99.5%). As an alternative source 2,2'-binaphthyl was also purchased from K & K Laboratories. 1,1'-binaphthyl- $\text{h}_{14}$  was obtained from James Hinton Co. and K & K while the 1,2'-binaphthyl, of unspecified purity, was purchased from API Reference Materials (Carnegie Mellon University). The 1- and 2- phenylnaphthalenes were obtained from both James Hinton and K & K.

2,2'-binaphthyl- $\text{d}_{14}$  was kindly prepared by Mr. George Timmins and Dr. N.H. Werstiuk by acid catalyzed  $\text{H-D}^{16}$  exchange under the following conditions. 2,2'-binaphthyl (29.5 mg) and 2% w/v  $\text{DCI/D}_2\text{O}$  (5 ml) were placed in a thick-walled glass tube. The solution was degassed by three freeze-pump-thaw cycles and sealed under vacuum. The tube was placed in a steel high pressure bomb (Parr) containing water to equalize the internal tube pressure and the reactor was maintained at  $\sim 280^\circ\text{C}$  for 50 hours. The product was recovered by filtration and washed with water. The yield was 29.1 mg (98.6%). Gas chromatographic product analysis indicated that the starting material had rearranged significantly to the other binaphthyl isomers:<sup>117</sup> 1,1'-binaphthyl - 2.2%; 1,2'-binaphthyl - 19.4%; 2,2'-binaphthyl - 78.4%. The 2,2'-binaphthyl- $\text{d}_{14}$

was separated by reverse phase high pressure liquid chromatography (HPLC) and the extent of deuterium incorporation was estimated by low energy (10 eV) electron impact mass spectrometry to be  $\geq 98\%$ .

2,5-diphenyloxazole (PPO) (Amersham Searle Scintillation Grade) for the relative quantum yield measurements was purified by multiple recrystallizations from 95% ethanol followed by preparative reverse phase HPLC.

The nanosecond lifetime standards anthracene, naphthalene, 1,2-benzanthracene, pyrene and 2,5-diphenyloxazole were derived from commercial materials purified by reverse phase HPLC.

The model compound, 1,2,7,8-dibenzofluorene (13-H-dibenzo[a,i]fluorene) was prepared by dehydration and cyclization of di-(1-naphthyl)carbinol (di-(1-naphthyl)methanol) by the method of Tschitschibabin and Magidson.<sup>118</sup> The di-(1-naphthyl)carbinol was prepared by a Grignard reaction as described by Schmidlin and Massini<sup>119</sup> and outlined below.

50 g (0.24 moles) of 1-bromonaphthalene in ~ 150 ml of dry ether was added dropwise over 1.5 h to 7.5 g (0.31 moles) of Mg turnings in about 50 ml of dry ether. The Mg surface was cleaned and the reaction started by the addition of ~ 0.5 ml of 1,2-dibromoethane. The mixture was refluxed gently with vigorous stirring for 0.5 h after the addition of the 1-bromonaphthalene solution was complete. 7.5 g (0.10 moles) of ethyl formate, fractionally distilled prior to use, was diluted to 50 ml with dry ether and the resulting solution was added dropwise to the Grignard reagent without heating.

After the addition (~ 40 min) the mixture was stirred without heating for a further 0.5 h then the addition complex was decomposed by

the slow addition of ice-cold 5%  $\text{H}_2\text{SO}_4$  solution. The carbinol was extracted with benzene and then recrystallized once from benzene, yielding 19.9 g (.070 moles, 70% yield) of rather crude di-(1-naphthyl) carbinol, m.p. 120-134°C.

A small amount of the carbinol was then treated with twice its mass of anhydrous  $\text{H}_3\text{PO}_4$ <sup>120</sup> in the manner described by Tschitschibabin and Magidson.<sup>118</sup> After extraction of the inorganic salts with boiling  $\text{H}_2\text{O}$  the organic material was extracted with benzene and recrystallized from that solvent. The melting point of the recrystallized material was found to be 234-236°C, uncorrected (literature, 236°C).<sup>119</sup> This recrystallized 1,2,7,8-dibenzofluorene was further purified by preparative reverse phase HPLC and its identity confirmed by several techniques. The UV absorption spectrum was in agreement with that shown by Bergmann et al.<sup>121</sup> Low energy electron impact mass spectrometry and elemental analysis (Guelph Chemical Laboratories; required for  $\text{C}_{21}\text{H}_{14}$  C = 94.70%, H = 5.30%; found C = 94.7 ± .3%, H = 5.6 ± .3%) confirmed this identification.

### 3.2 Solvents

The solvents used were:

- cyclohexane (Caledon Laboratories, ACS Spectrograde) was either used as received or passed through a Woelm alumina column;
- methylcyclohexane (Matheson, Coleman and Bell, Spectro-quality) was used without purification;
- 3-methylpentane (Phillips Pure Grade, 99 mol %), was shaken

four times with BDH 13X molecular sieve then fractionally distilled;

- isopentane (2-methylbutane) was obtained from a number of sources: Phillips Pure Grade and Anachemia Practical Grade were shaken with Linde 10X or BDH 13X molecular sieves then distilled and Matheson, Coleman and Bell (Spectroquality) which was used as received;
- ethanol, absolute (Consolidated Alcohols) was further dried by addition of magnesium and few drops of 1,2-dibromoethane (initiator) to produce the magnesium ethoxide, followed by addition of the bulk of the absolute ethanol, giving a voluminous precipitate of magnesium hydroxide.<sup>122</sup> The dry ethanol (99.95% minimum) was then fractionally distilled out of the reaction flask and stored over Linde 3A molecular sieve;
  - n-pentane, n-hexane, and n-heptane (Matheson, Coleman and Bell, Spectroquality) were used as received;
  - n-octane (Caledon Laboratories, distilled in glass) was used without further purification;
  - 2-methyltetrahydrofuran (Eastman Organic Chemicals) was fractionally distilled immediately prior to use.

All the preceding solvents were checked for spurious emission at 77K and room temperature under the conditions of the emission and decay experiments with no detectable luminescence being observed.

### 3.3 Purification of Solutes

Since fluorescence measurements, both in emission and decay

experiments, were extremely susceptible to the presence of impurities great care was exercised in the purification of the solute species.

Initial attempts were made using fractional vacuum sublimation and zone refining but these proved incapable of producing solutes of assured purity. Zone refining, in principle capable of very good separating, proved totally inadequate for some separation (for example, in removing the phenanthrene impurity in anthracene) in addition to being an extremely time consuming method. Thin layer chromatography (TLC) gave acceptable separation, however, a number of the aromatic hydrocarbons appeared to become sensitized to air oxidation on the silica and alumina TLC plates.

Consequently, high pressure liquid chromatography (HPLC) was employed for most of the analytical and preparative work. The advantages of HPLC were manifold: excellent separation (up to 25,000 plates/m), good scalability from analytical to preparative size, high reproducibility, reasonable speed of separation and the simple, nearly total recovery of the sample. Very small amounts of extremely pure solutes were required so that analytical scale injections ( $\leq 20 \mu\text{l}$ ) were feasible. As an example, to perform an emission or decay experiment required  $\sim 5 \text{ ml}$  of a  $1 \times 10^{-4} \text{ M}$  solution, corresponding to  $130 \mu\text{g}$  of a binaphthyl, an amount easily obtainable from 6-7 analytical injections (at  $1 \text{ mg/ml}$  stock binaphthyl  $\times 20 \mu\text{l}$  injections).

Reverse phase columns were of the C-18 (octadecyl) type, with the Merck Hibar II RP-18 ( $10 \mu$  particle size,  $4.6 \text{ mm} \times 25 \text{ cm}$ ) and Whatman Partisil ODS-2 ( $10 \mu$  particle size,  $4.6 \text{ mm} \times 25 \text{ cm}$ ) used for the analytical and semi-preparative work. The preparative reverse phase

column was a Whatman Magnum-9 ODS-2 (10  $\mu$  particle size, 9 mm x 50 cm). The mobile phases for the reverse phase chromatography were from 0 to 20% V/V water with the balance usually being HPLC grade methanol (Caledon Laboratories). Occasionally acetonitrile was substituted for half of the methanol content, i.e., 45% CH<sub>3</sub>CN; 45% MeOH; 10% H<sub>2</sub>O, with similar results.

Analytical and semi-preparative normal phase separations were performed with an Altex Cyano Ultrasphere Analytical Column (5  $\mu$  particle size, 4.6 mm x 25 cm) using isopropyl alcohol: hexane (1-4% isopropyl alcohol) mobile phases.

Principally two sets of ancillary equipment were used for the HPLC separations. One system consisted of an isocratic solvent pump (Analabs Model B-94), sample injection valve (Valco CFSV-4-HPax) and fixed wavelength (254 nm) absorption detector (Waters Model UV LDC). A Beckman Isocratic Liquid Chromatograph (Model 330) with a Beckman Analytical optical unit and detector (8.0  $\mu$ l flow cell) comprised the second system. The effluent fraction of interest was collected in a round-bottom flask with a standard taper neck, taken to dryness in vacuum and then redissolved in the appropriate solvent. Characterization of the fraction was done by UV absorption spectroscopy and comparison to reference spectra and by electron impact mass spectrometry at low impact energies.

Typically the commercial solutes were dissolved in acetone to ~1 mg/ml, filtered through a Millipore 0.5  $\mu$ m PTFE filter and then injected (10 - 20  $\mu$ l) on a reverse phase analytical column. Mobile phase composition and flow rate were varied to give the best apparent



separation under isocratic conditions. Isocratic, rather than gradient elution was used throughout since the necessary equipment was more readily available and isocratic elution gave acceptable resolution in a reasonable time for the compounds of interest. Once the conditions for separation had been elucidated on the analytical scale it was usually a matter of injecting larger volumes (100-300  $\mu$ l) onto the corresponding preparative column under similar conditions of linear flow rate and solvent composition. All HPLC separations were conducted at ambient temperatures.

To ensure that the collected fraction was indeed a single, pure compound two portions were redissolved, one in acetone, the other in hexane and injected, respectively onto reverse and normal phase analytical HPLC columns. Appearance of a single peak (excluding solvent) on both columns was taken as strong evidence for the presence of only one compound. For further confirmation crucial samples, 2,2'-binaphthyl mostly, were also submitted for capillary gas chromatography. Capillary GC analyses were done on a Varian 3700 instrument using a 20 m Onuska SP2100 (methyl silicone) wall-coated capillary column ( $\sim$  2000 plates/m) with flame ionization detection. Only a single peak was apparent in the traces of the previously purified solutes.

### 3.4 Fluorescence Emission and Fluorescence Excitation Spectra

Figure 3.1 shows the basic apparatus used to obtain the fluorescence emission and excitation spectra. Light from a 450 w Osram xenon lamp, powered by an Oriel Optics Corporation Model C-72-50 DC regulated power supply was focussed onto the entrance slit of a Jarrell-Ash 0.25 m Ebert monochromator fitted with a 2360 grooves/m grating blazed at 300 nm.

- A - LENSES
- B - OPTICAL DEWAR & SAMPLE
- C - PHOTOMULTIPLIER TUBE

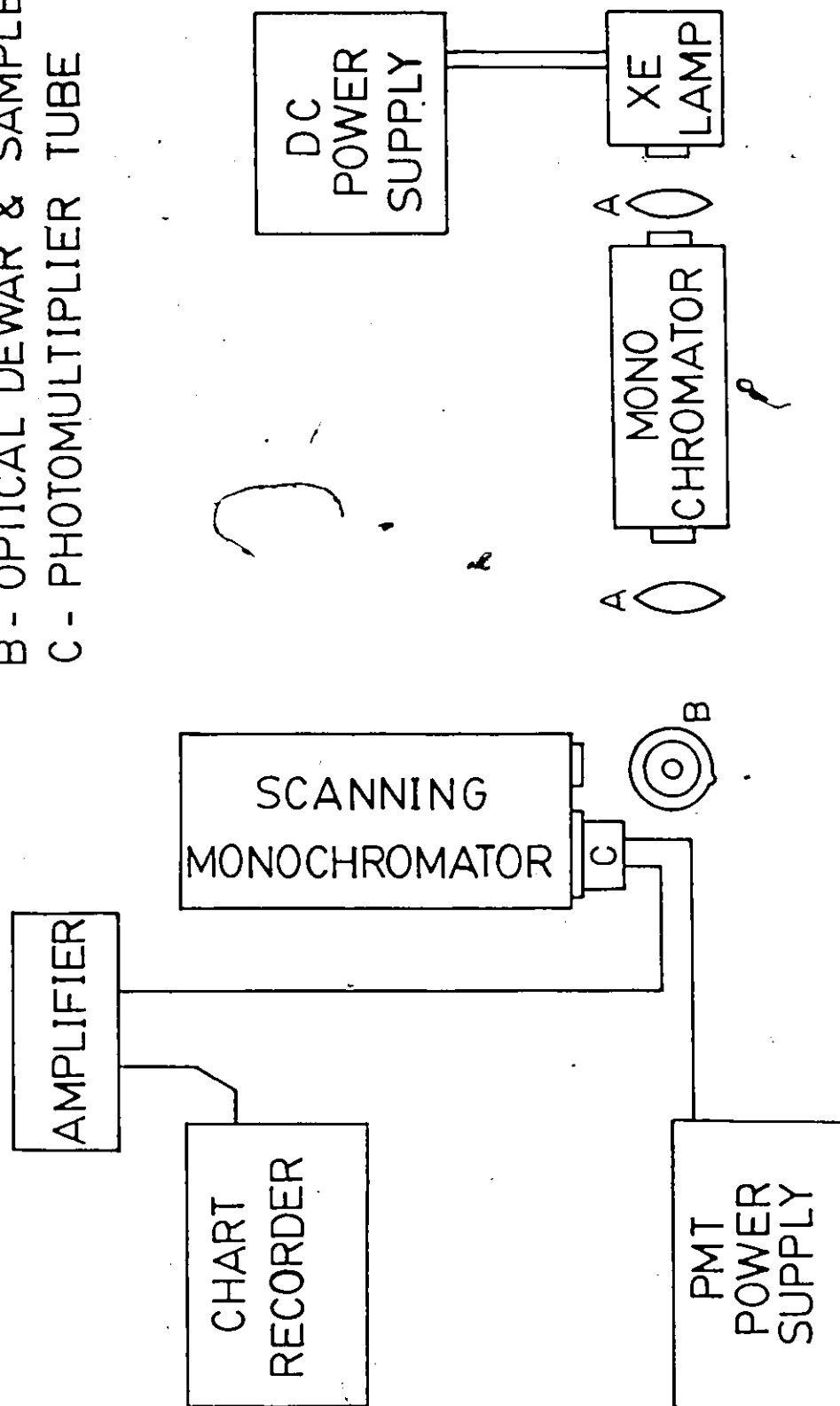


Figure 3.1

# APPARATUS FOR EMISSION EXPERIMENTS BLOCK DIAGRAM

The reciprocal linear dispersion of this grating was 1.65 nm/mm, so that with the three physical slit widths normally employed, 150  $\mu$ m, 650  $\mu$ m and 1000  $\mu$ m the spectral bandpass was, respectively, 0.25 nm, 1.07 nm and 1.65 nm. The radiation leaving this monochromator was focussed by a Spectrosil lens onto the sample and the emission was observed at 90° with respect to the exciting light by a 0.5 m scanning Ebert monochromator (Jarrell-Ash, model 82-000). The dispersive element of this monochromator was a 1180 grooves/mm grating blazed at 400 nm, with a reciprocal linear dispersion of 1.6 nm/mm in the first order. At the monochromator exit slit was mounted an RCA 8575 photomultiplier tube in an Ortec 9201 housing. Amplification was provided by an Ortec single photon counting system operating off of the anode output signal. This amplification system consisted of a Model 454 Timing Filter Amplifier, Model 421 Integral Discriminator and Model 441 Ratemeter. Occasionally, for very weak signals an Ortec Model 9301 Fast Preamplifier with 10X gain was inserted between the anode output and the timing filter amplifier input. The output of the ratemeter was fed to a Varian G-2000 strip chart recorder. Fluorescence emission spectra were usually obtained by exciting in the wavelength region 260 - 335 nm. Except for oxygen quenching studies the samples were thoroughly degassed by at least six freeze-pump-thaw cycles at a pressure of  $\leq 10^{-5}$  torr. Samples were temporarily sealed off under vacuum by means of Rotaflon Teflon stopcocks, which maintained an adequate vacuum for several weeks. For room temperature spectroscopy two sample arrangements were used. A Hellma QS 221 quartz fluorescence cell, 1.000 cm path length with a quartz-glass high vacuum extension was fitted with a pear-shaped side arm ( $\sim 15$  ml volume) and Rotaflon stopcock to permit deoxygenation of the

EVACUABLE FLUORESCENCE CELL

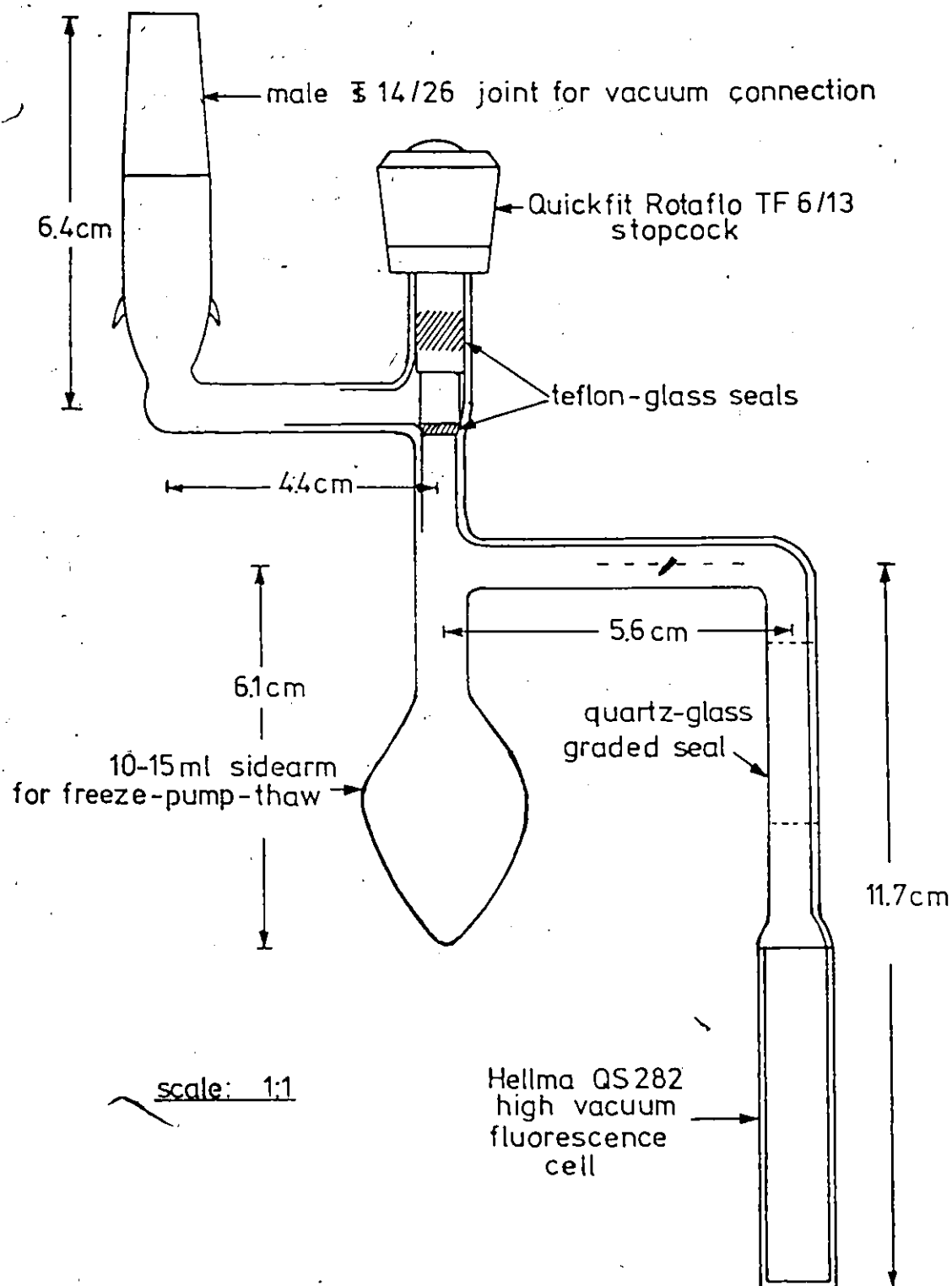


Figure 3.2

solution by multiple freeze-pump-thaw cycles (Figure 3.2). Alternatively, sample solutions were contained in 11 mm o.d. cylindrical tubes of Spectrosil "A" or Suprasil quartz, fitted with Rotaflow stopcocks.

For low temperature emission and excitation spectra the solutions were contained in the aforementioned 11 mm quartz tubes and immersed in a partially silvered Dewar (Spectrosil "A" and commercial grade quartz) containing liquid nitrogen. Low temperature samples were also contained in a cell of ~ 5 ml volume fashioned from a block of OFHC copper 2 cm x 2 cm x 2 cm fitted with three 0.75 inch diameter Si-UV quartz windows (Esco Products, Inc.). This cell was mounted on the tip of a liquid nitrogen insert (Air Products Inc., Model LC-1-110) or on a variable temperature cryogenic liquid transfer refrigerator (Air Products Inc., Model LT-3-110).

Concentrations were generally kept below  $5 \times 10^{-4}$  M to avoid self-quenching and solubility problems. Spectral bandpasses were most frequently 1.07 and 1.65 nm on the excitation side and from .165 to .660 nm (100  $\mu$ m - 400  $\mu$ m) on the emission side. The resultant emission spectra were uncorrected for the wavelength response of the detection system. Accurate calibration of the spectra was achieved by superimposing the resonance lines from a low-pressure 25 w mercury pen lamp directly onto the emission traces. The wavelength accuracy of the bands was estimated to be  $\pm 5 \times 10^{-2}$  nm at best.

Fluorescence excitation spectra were obtained from the same solutions as used for emission measurements. The 0.5 m Jarrell-Ash monochromator was set to the fluorescence emission wavelength of interest and the exciting light was then scanned by means of a

synchronous motor fitted to the 0.25 m Jarrell-Ash monochromator. Excitation scan rates of 5.0, 12.5 or 25.0 nm/minute were available. Typically the emission monochromator was operated at maximum (400  $\mu$ m) slit width whereas the excitation monochromator was fitted with the minimum acceptable slit width (650  $\mu$ m). Wavelength calibration of the excitation spectra was more involved, using back-calibration from the emission monochromator. The 0.5 m Jarrell-Ash monochromator was first calibrated with the Hg pen lamp as mentioned earlier. The 0.25 m monochromator was then set to the most intense peak in the excitation spectrum and the 0.5 m monochromator was scanned through this peak wavelength. The wavelength setting on the 0.5 m emission monochromator at maximum signal was noted and all other bands in the excitation spectra were referred to this wavelength. The cumulative error in the synchronous drives appeared quite small, about 0.1 nm in 100 nm total span.

Polycrystalline matrices of the solutions used in obtaining the fluorescence emission and excitation spectra were produced by placing the tip of the sample tube ~ 2 cm above the liquid level in an unsilvered Dewar containing liquid nitrogen. As the bottom section slowly crystallized the tube was successively lowered until complete crystallization had been effected. The sample was immersed in the liquid nitrogen, then rapidly transferred to the waiting optical Dewar, previously filled with liquid nitrogen. This procedure helped to ensure slow, even crystallization of the solution without the formation of glassy regions.

Organic glasses, both cracked and clear at 77 K, were produced by quickly plunging the quartz tube containing the solution into a Dewar

of liquid nitrogen. After cooling to 77 K the tube was quickly transferred to the quartz optical Dewar.

When the copper block arrangement was employed somewhat poorer control of the cooling rate was obtained. The solutions were first degassed by argon bubbling then transferred to the cell under an argon atmosphere. After cooling the cell and pumping the vacuum shroud the coolant flow was started. Normally the cooling rate was too high for good control of the crystallization process but yielded acceptable glassy solutions.

### 3.5 Absorption Spectra

Most of the absorption spectra were obtained using a Pye Unicam SP8-100 recording UV-visible spectrophotometer with a few also recorded on a Cary Model 14 spectrophotometer.

All the room temperature absorption spectra were obtained using matched 1.000 cm quartz absorption cells with the reference cell containing pure solvent.

Accurate molar absorptivities were calculated from the absorption spectra of standard solutions in cells of known (1.000 cm) path length. The standard solutions were prepared by accurate weighing of the compounds of interest into 10 or 25 ml volumetric flasks followed by dissolution and dilution to the mark with appropriate solvent. If necessary, serial dilutions were performed, using volumetric glassware, until the maximum absorbance was below about 1.5.

### 3.6 Determination of Relative Fluorescence Quantum Yields

The relative fluorescence quantum yields of the phenylanthracenes

and binaphthyls were obtained using an Aminco-Bowman Spectrofluorimeter Model 4-8202. The reciprocal linear dispersion of the excitation and emission grating monochromators was 5.5 nm/mm. PPO (2,5-diphenyl-oxazole) in cyclohexane or 3-methylpentane was chosen as the reference standard since the absorption and emission spectra were quite broad and coincide with the emission spectra of the binaphthyls and phenyl-naphthalenes. PPO was particularly attractive as a reference compound since the quantum yield for fluorescence in cyclohexane has been reported to be near unity, with  $\phi_f = 1.00$  according to Berlman.<sup>34</sup> Recently Abu-Zeid and coworkers<sup>123</sup> have reported  $\phi_f = 0.964$  in cyclohexane at 295 K, although their measured fluorescence lifetime of 2.0 ns is somewhat greater than most other literature values.

In defence of Berlman's value it should be noted that no compound exhibiting a greater quantum yield than that of PPO was encountered in the course of this investigation. Para-quaterphenyl in cyclohexane was explored as an alternative quantum yield standard, however the low solubility of this compound limited its usefulness and made purification difficult. The fluorescence quantum yield of p-quaterphenyl with respect to PPO in cyclohexane was found to be about 0.9, comparing favourable with the  $\phi_f = 0.89$  reported by Berlman<sup>34</sup>; this served as an internal check on the assumption of  $\phi_f(\text{PPO}) = 1.0$  in cyclohexane.

For low temperature quantum yield measurements PPO in 3MP was used as the reference standard. The fluorescence quantum yield of PPO in 3MP was unavailable from literature so the quantum yield of PPO in 3MP at 295 K was measured relative to the same compound in cyclohexane, also at 295 K. Equation 2.22, valid for two solutions of



equal absorbance, excited under identical conditions and observed at normal incidence<sup>51,124</sup> gives

$$\phi_S/\phi_R = \frac{n_S^2 \int F_S(\lambda) d\lambda}{n_R^2 \int F_R(\lambda) d\lambda} \quad (3.1)$$

where  $n$  = refractive index of particular solvent at the emission wavelength and  $S$  and  $R$  represent sample and reference respectively.

For the case at hand it gave

$$\frac{\phi(\text{PPO in 3MP})}{\phi(\text{PPO in cyclohexane})} = \frac{n_{3\text{MP}}^2}{n_{\text{cyclohexane}}^2} \times 1.03$$

where 1.03 was the ratio of areas under the measured fluorescence curves.

Taking  $n_{3\text{MP}}^D = 1.3765$  and  $n_{\text{cyclohexane}}^D = 1.4266$ <sup>125</sup> yields

$$\frac{\phi(\text{PPO in 3MP})}{\phi(\text{PPO in cyclohexane})} = 0.96 \pm 5\% \text{ (3 measurements).}$$

The use of the optical dispersion at the sodium D line, 589.3 nm, was a good approximation since the individual  $n$  values increase only slowly with increasing frequency. At the average emission wavelength for PPO in cyclohexane (370.3 nm<sup>34</sup>) the refractive index of cyclohexane has risen to 1.444<sup>34,126</sup>, an increase of only 1.2%. Dispersion data for 3-methylpentane as a function of wavelength was unavailable, but given that the rate of change of  $n$  with  $\lambda$  is similar for most hydrocarbon solvents studied<sup>126</sup> it is likely that the change in the ratio  $n_{3\text{MP}}^2/n_{\text{cyclohexane}}^2$  was less than 1%.

This value of  $\phi_f = 0.96 \pm 5\%$  at 295 K was also used for the 77 K quantum yield of PPO in 3MP although it may be slightly greater in

reality. Any error in assuming  $\phi_f$  to be 0.96 or 1.00 at 77 K will be much smaller than the inherent experimental error in these low temperature determinations anyway. Sample and reference solutions were accurately matched to an absorbance of approximately 0.5 in 1.000 cm cells at the selected excitation wavelengths. The reference and sample were matched to within 1% or better in all cases. Degassing of the solutions for room temperature measurements was achieved by six cycles of freeze-pump-thaw at  $\leq 10^{-5}$  torr in the pear-shaped side arms of the RotaFlo sealed fluorescence cells described earlier. This method entailed less risk of change in the absorbance of reference and sample than the more commonly used degassing technique of argon bubbling. A check of the absorbance before and after freeze-pump-thaw degassing revealed no significant increase in the absorbance owing to solvent loss during the pump cycles.

Room temperature measurements of  $\phi_f$  were generally conducted in cyclohexane, with a few also measured in 3MP, the solvent employed exclusively for the 77 K quantum yield measurements. The 3-methylpentane solutions were likewise accurately matched at about 0.5 absorbance units in 1.000 cm cells at room temperature. Solutions for low temperature measurements were not degassed prior to use. The usual procedure for relative quantum yield measurements at 77 K was to place the PPO in 3-methylpentane standard in a thin-walled cylindrical quartz tube of  $\sim 6$  mm o.d. on the upper section and  $\sim 1$  mm o.d. on the lower or viewing section. The tube was then plunged into liquid nitrogen contained in one of the partially-silvered quartz optical Dewars provided with the Aminco-Bowman instrument. Following a wait of about one minute for thermal

equilibration the total emission spectrum was rapidly scanned. After discarding the standard solution, acetone washing, and vacuum drying the tube was rinsed 4 - 5 times with the sample solution and returned to the Dewar for recording of the total sample emission. Since the geometry of the sample tube within the Dewar was not precisely reproducible a compromise procedure involved rotation of the sample tube and Dewar until maximum signal amplitude was obtained for both sample and reference. To reduce the fluctuations from this source four separate readings of sample and standard were conducted at each excitation wavelength.

As outlined in the operating manual for the Aminco-Bowman Spectrofluorimeter the emission monochromator was calibrated with a mercury pen lamp, followed by back-calibration of the excitation monochromator. The accuracy of this calibration was no better than the settability of the monochromators,  $\sim 1$  nm. Minimum bandpass, 2.8 nm, was used on the excitation monochromator to reduce the effect of the finite bandwidth of the exciting light on the observed fluorescence quantum yields.<sup>127,a</sup> The fluorescence was observed at right angles with the narrowest practical emission bandpass, usually 2.8 or 5.5 nm. Some comparative experiments were done with the unused cuvette faces masked with matte black paint to reduce internal reflections as recommended by Melhiush.<sup>128</sup> Results of these trials were not significantly different from those obtained with unblackened cuvettes. For

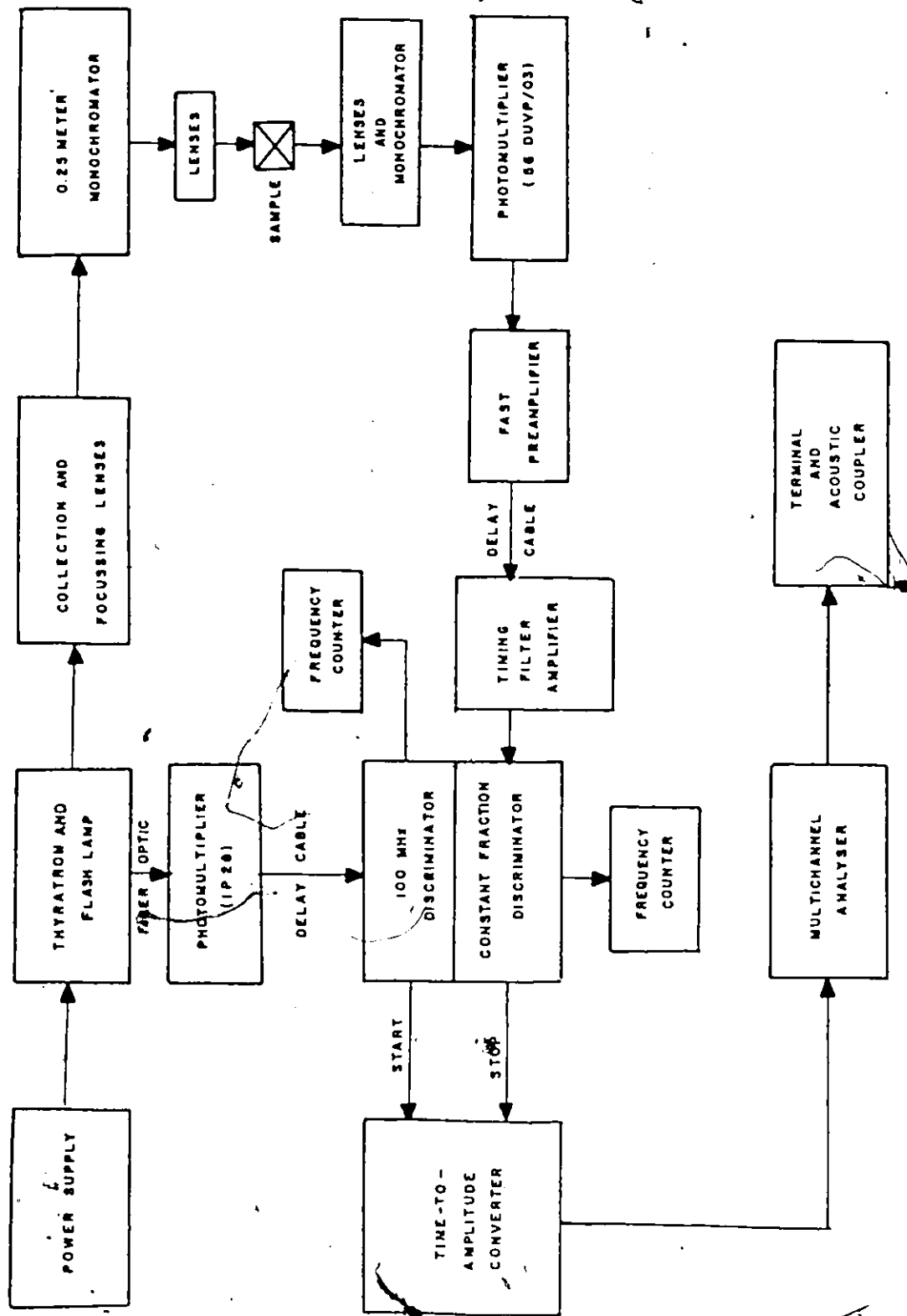
<sup>a</sup> The earlier relationship, Equation 3.1  $(\phi_f)_s = (\phi_f)_r \cdot \frac{F_s}{F_r}$  was derived on the assumption of monochromatic exciting light. For finite bandwidth this is not strictly true but is closely approximated at small bandwidths.

2,2'-binaphthyl excitation wavelengths from 330 - 260 nm at 10 nm increments were used while for the other binaphthyls and the phenyl-naphthalenes two or more excitation wavelengths from 330 - 280 nm were employed.

The photomultiplier signal of the Aminco-Bowman spectrofluorimeter was amplified by the internal electrometer and output as a voltage signal to the y-axis of a Hewlett-Packard 7470A X-Y recorder, while the x-axis input was furnished as a voltage signal from the wavelength drive of the spectrofluorimeter. Each pair of measurements, reference and sample, was repeated three times for the room temperature experiments and four times for those at 77 K. The resulting curves were photoreduced and the relative areas under the emission curves evaluated by the cut-and-weigh technique or by computerized integration of the areas under the curves using an Apple II mini-computer and Apple Graphics Tablet to digitize the spectra. Each area measurement was done in triplicate.

### 3.7 Measurement of Singlet Lifetimes

A more complete description of the principles underlying the time-correlated single photon counting method for the determination of fluorescence lifetimes has been given in Section 2.7. The instrument used in this work, illustrated in block form in Figures 3.3 and 3.4 was designed, built and tested in collaboration with Drs. R.C. Miller, D.A. Condirston and A.J. Yarwood. Some modifications, notably the flashlamp design, emission monochromator and peripheral computing were introduced by the present author. Details of the latest lamp design are shown in Figure 3.5. The electrodes, of  $\frac{1}{8}$ " thoriated tungsten



Block Diagram of Fluorescence Lifetime Apparatus

Figure 3.3

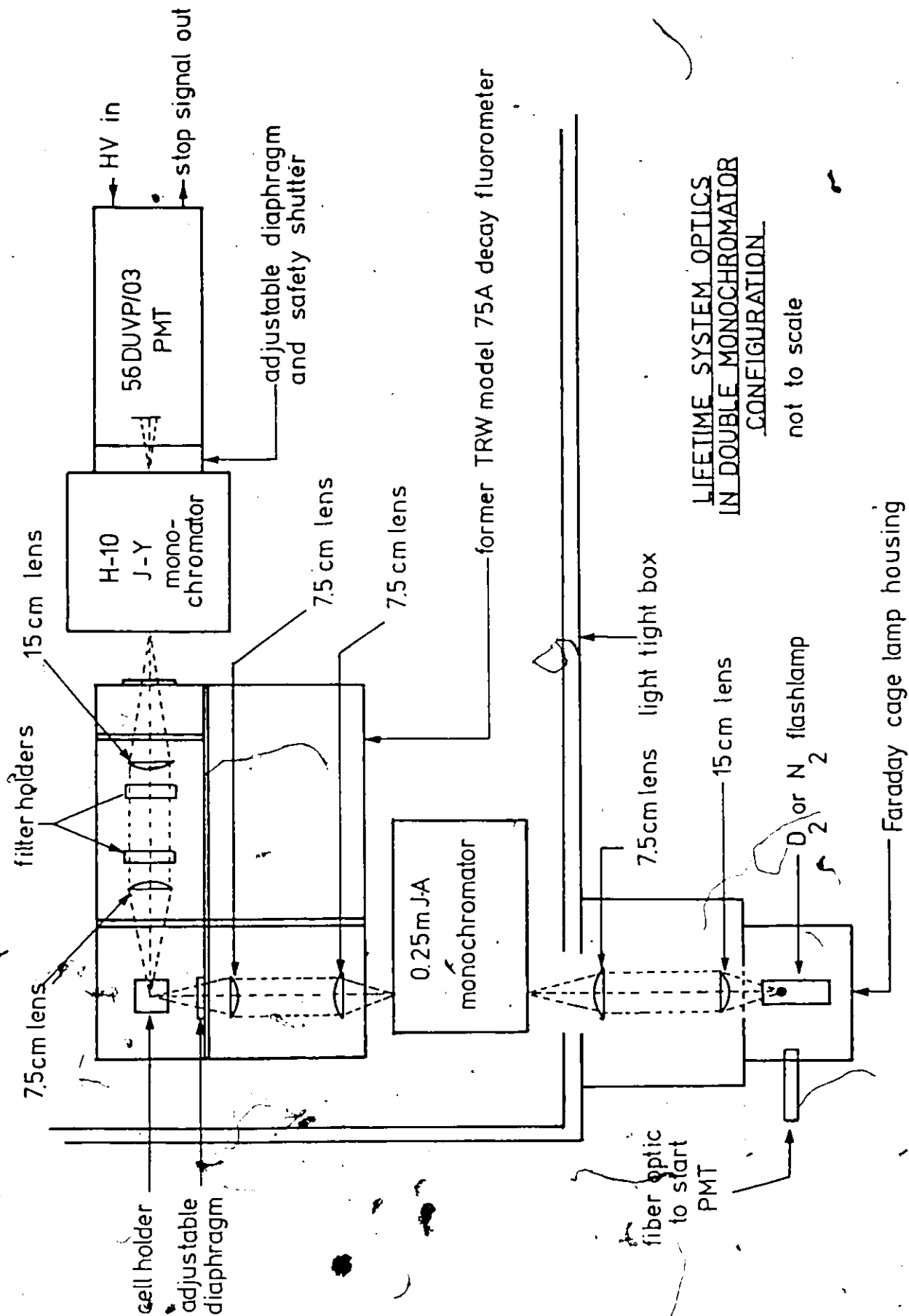


Figure 3.4

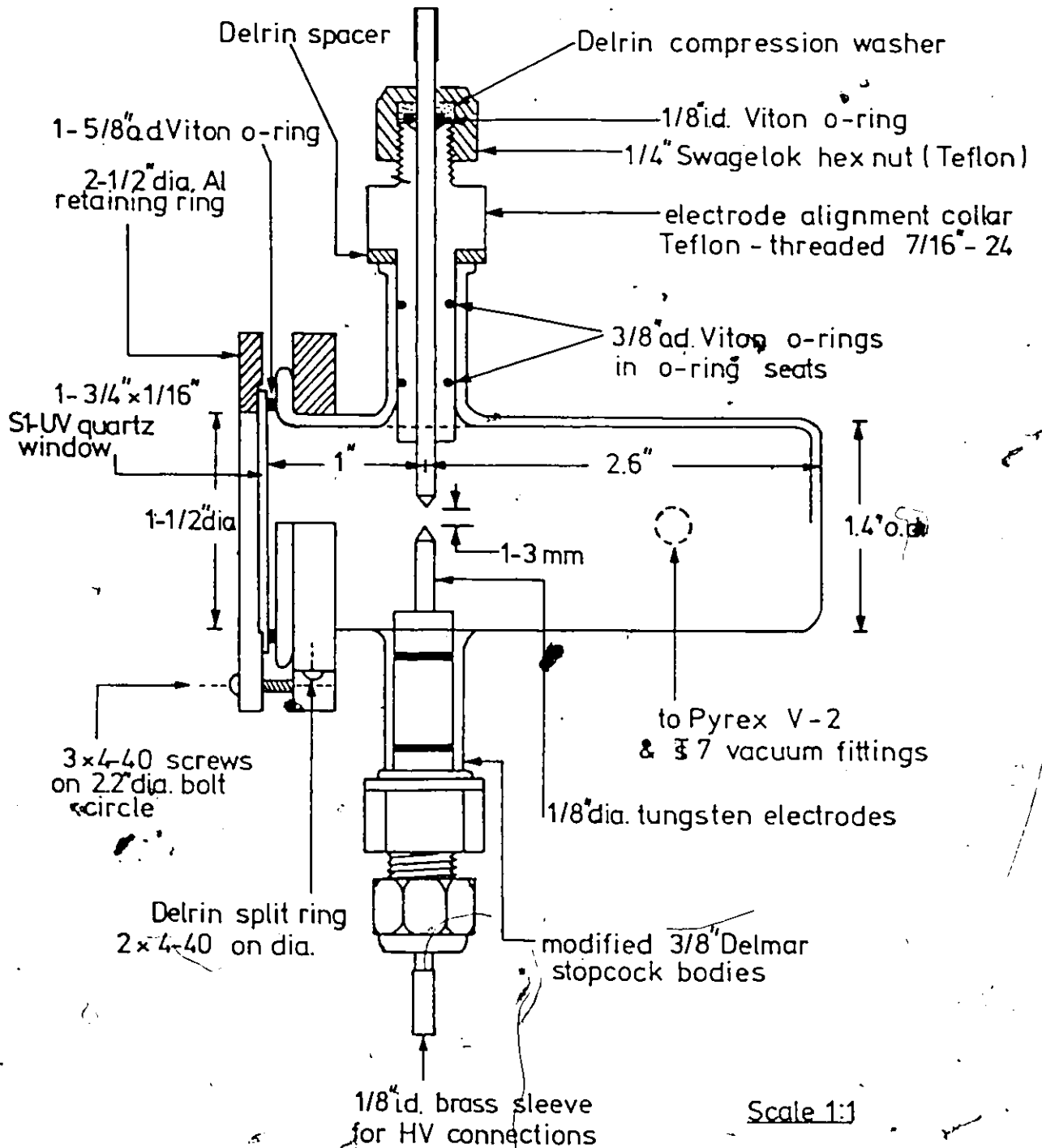


Figure 3.5

Low Pressure Flash Lamp Design

welding rod were accurately ground to conical points of  $40^\circ$  half-angle and the gap between the electrodes adjusted by sliding the electrodes in or out of the o-ring sealed Teflon sleeves. The electrode spacing was varied from 1 - 3 mm with the larger spacing giving rise to greater intensity per flash and greater electrode longevity but at the expense of reduced arc stability, higher applied voltage and greater temporal width of the flashlamp profile. The Teflon sleeves holding the electrodes were, in turn, fitted into the modified glass bodies of Delmar  $\frac{3}{8}$ " o.d. Teflon high vacuum stopcocks. Accurate colinearity of these glass sleeves and hence of the electrodes themselves was ensured at the glassblowing stage by inserting a  $\frac{3}{8}$ " dia. graphite rod through both sleeves while the Pyrex body was still somewhat plastic. The final performance, especially as regards physical stability of the lamp was strongly dependent on the precise alignment of the electrodes. Small adjustments could be made by rotating the electrodes and Teflon holders about their long axes to give the best alignment visually.

The lamp was filled with 200 - 400 torr of  $D_2$  or  $N_2$  gas (prepurified grade, Canadian Liquid Air). Deuterium filling yielded the narrower full-width at half maximum (FWHM), typically 1.0 - 1.5 ns, while with nitrogen the FWHM was  $\sim 4 - 7$  ns. Deuterium emitted a weak continuous spectrum covering the entire UV, corresponding to the transition  $3s^+ \text{ (bound)} \rightarrow 3s^+ \text{ (repulsive)}$ .<sup>129</sup> The  $N_2$  lamp gave a much more intense ( $\sim 100\times$ ) band spectrum characteristic of the  $N_2$  transition  $C^3u \rightarrow B^3g$ .<sup>130</sup> Useful discrete lines were found in the region 280 - 400 nm. Whenever possible  $N_2$  filling was used because of its greater excitation intensity and narrow excitation bands. The lamp was gated with an EG & G HY-2 ceramic-metal hydrogen thyatron. Although



nominally rated to 8 kV hold-off potential the thyratron was occasionally operated without difficulty at 10 kV. The voltage applied to the lamp was in the range 4.5 - 10 kV with the lower values giving improved arc stability with some sacrifice of intensity. The flash repetition rate was the maximum obtainable with the particular home-built trigger generator circuit, 19.5 - 20.0 kHz.

Excitation light from the flash lamp was focussed onto the entrance slit of a Jarrell-Ash 0.25 m Ebert monochromator fitted with 1000  $\mu$ m slits (1.65 nm bandpass). The focussing system for the monochromated exciting light and fluorescence emission and the sample holder and compartment were those from a severely modified TRW Model 31A Decay Time Fluorometer optical system. The optical train, including this modified TRW component is shown in Figure 3.4. The light intensity impinging on the sample could be controlled by an adjustable iris mounted before the sample holder or by the use of neutral density filters (Oriel, quartz substrate filters). Sample emission was monitored at 90° with respect to the exciting light and could be monochromated or discriminated in several manners. In most early experiments Corning glass colour filters, either cut-off or bandpass types, were used. These possessed the advantage of high light throughput but with little selectivity and some problems with filter fluorescence. Colour filters were subsequently replaced by interference filters (Baird-Atomic Inc., 366 nm, 404.7 nm and 410 nm peak wavelengths) giving better scattered light rejection but a poor, fixed range in possible emission wavelengths. Schott KV series cut-off filters proved superior to the corresponding Corning cut-off filters generally. Most exhibited low inherent

fluorescence and an extremely sharp transmission cut-off. The rejection of scattered exciting light was very good but, of course, only the entire emission profile or a large part of it could be selected for observation. To increase the emission wavelength selectivity at the expense of total fluorescence signal a Jobin-Yvon H-10 monochromator was inserted in the emission optical path, after the condensing lenses and immediately before the high gain photomultiplier (Fig. 3.4). The dispersive element was a concave holographic grating with 1200 grooves/mm, blazed at 250 nm and with a reciprocal linear dispersion of 8 nm/mm, giving 4, 8 and 16 nm bandpasses with the supplied 0.5, 1.0 and 2.0 mm slits.

After passage through filter or monochromator the luminescence was detected by an Amperex 56 DUVP/03 high gain single photon counting photomultiplier tube incorporated in a Photochemical Research Associates Inc. Model 520 housing, fitted with a Compur camera shutter and adjustable diaphragm. This safety shutter was controlled by a cable release fitted to the lid of the light-tight box containing the optical components. Opening this lid automatically engaged the safety shutter thereby protecting the highly sensitive photocathode from large ambient light levels. Even with no applied voltage, exposure of the PMT to room lighting resulted in excessive dark counts for ~ 48 h. At the operating voltage of -1990 V this 56 DUVP/03 exhibited 20 - 40 Hz background counts at ambient temperature. The PRA 520 PMT housing was custom tuned for this particular PMT at the factory with some slight adjustments later made to the variable resistors in the inter-dynode and grid-anode chain.

Anode pulses from the photomultiplier passed to an Ortec Model

9301 Fast Preamplifier, giving  $10\times$  gain on the original pulse. This furnished the input signal to an Ortec Model 454 Timing Filter Amplifier. The function of this module was one of further amplification, pulse-shaping and filtering. Gain could be adjusted continuously in the range  $2\times$  to  $200\times$ . Shaping was controlled by independently varying the RC-differentiate time constant at an RC-integrate time constant of less than 2 ns. These settings were determined empirically as those yielding the smoothest, narrowest pulse shape when viewed on a fast oscilloscope. These amplified and shaped timing pulses were fed to an Ortec Model 473 Constant Fraction Discriminator operating in the "constant fraction" mode. Details of the operation of this module may be found in the proprietary literature<sup>131,132</sup> but the salient feature was that all incoming voltage pulses above a selectable threshold value would generate a negative-going logic current pulse which did not vary with input pulse amplitude. These output logic pulses were ideal for timing purposes, being of fixed size and very fast rise time ( $\leq 2.5$  ns) and provided the STOP pulses to the Ortec Model 457 Biased Time-to-Amplitude Converter (TAC). START pulses to the TAC were ultimately derived from an RCA 1P28 photomultiplier tube which viewed the flash lamp via a 3 ft long fiber optic cable. This START photomultiplier was isolated in its own light-tight container and received HV power from the TRW power supply that also supplied the flashlamp high voltage. START pulses from this 1P28 PMT furnished the input to an Ortec Model 436 100 MHz Discriminator. Low level electronic noise was removed by this discriminator, which generated fast (1.4 ns) negative logic pulses suitable for timing applications, in this case as the timing signal to

the START input channel of the TAC. In the majority of experiments so-called delay cables were used on both the START and STOP signal pathways. These delays were usually introduced between the 9301 Preamplifier and 454 Timing Filter Amplifier in the STOP circuit and between the RCA 1P28 output and 436 100 MHz Discriminator on the START side. Physically these delays consisted simply of appropriate lengths of RG58 C/U co-axial cable, for which the velocity of propagation =  $0.659 \times$  velocity of light, corresponding to 5.05 ns/m in this cable. This delay box was kindly constructed by Mr. G.J.G. Hicks of the I.P.A.C.S., McMaster University. Delay of the signals helped to ensure that the detection electronics did not receive spurious noise in the form of radio-frequency radiation from the flashlamp since the START and STOP signal could be delayed until long after a particular lamp pulse and any associated noise had died away and well before the succeeding flash had appeared. In this manner the delay cables appeared to function as high-frequency cut-off filters.<sup>52</sup> Use of variable delays also ensured that the inherent differential delays in the START and STOP circuits could be adjusted such that the START-STOP difference actually fell within the usable voltage domain of the TAC. Experimentally it was found that delays of  $\sim 300$  ns each in both START and STOP circuits gave the best performance. An excellent discussion of the use of delay cables may be found in the review of Knight and Selinger.<sup>53</sup>

The TAC output, a pulse of particular voltage proportional to the START-STOP time difference, was fed to a Nuclear Data Inc. ND 60 Multi-channel Analyzer. This device contained 2048 channels of memory, usually segmented into four groups of 512 channels each. Nominally these

512 channels spanned a voltage range of 0 to +8 V. Incoming pulses from the TAC were then allocated to the corresponding voltage or channel address in the MCA with the many accumulated pulses forming a histogram of pulses versus channel (intensity versus time). Since the TAC time-bases were only very roughly accurate it was necessary to calibrate the TAC and MCA with an Ortec 462 Time Calibrator. The 462 Time Calibrator produced timing signals with a minimum accuracy of  $\pm .01\%$  by means of precision 100 MHz crystal-controlled oscillator.

After acquisition of adequate data, usually  $10^4$  counts at maximum peak height, in the MCA the information was transferred to the main computer system (CDC 6400 and Cyber 170) by telephone line via an ENA Datasystems Inc. Model 112 acoustic coupler and Texas Instrument Silent 743 terminal. In a typical experiment three sets of data were collected: the lamp profile, the observed fluorescence decay and a time calibration run. The molecular decay parameters were obtained by the method of reiterative convolution<sup>57-59,77</sup> to solve the convolution integral (Equation 2.26). The observed data was normally fitted to mono- and biexponential decay laws by the computer programs MRQRDT and TWOEXP respectively, both most generously supplied by Dr. T.L. Nemzek, then at the University of Toronto. These programs were somewhat modified in the course of this work. Observed and fitted decay curves with associated molecular parameters and statistical measures such as  $\chi^2$ , percent differences between observed and fitted curves, and the autocorrelation function<sup>77</sup> of the weighted residuals were plotted by a California Computer Corp. (Calcomp) pen and ink plotter. Performance of the lifetime system was occasionally checked by decay

Table 3.1

Singlet Decay Times of Some Standard Substances

Solute	Measured <sup>a</sup> Lifetime (ns)	Reported <sup>a</sup> Lifetime (ns)	Reference
Pyrene	441.1 $\pm$ 3.4	408 444	133 88
Naphthalene	110.2 $\pm$ 2.2	109 96 120	134 34 135
1,2-Benzanthracene	41.8 $\pm$ 2.2	42 44.1	136 137
Anthracene	4.98 $\pm$ .14	4.9 4.94 5.03	34 138 74
PPO (2,5-diphenyloxazole).	1.50 $\pm$ .13	1.3 1.4 1.6 1.36 1.35	139 34 140 141 142

<sup>a</sup> Solvent used was cyclohexane, degassed and at room temperature.

measurements on dilute solutions of compounds that are generally accepted to exhibit simple, single exponential fluorescence decay kinetics.

Agreement between the lifetimes obtained and those reported in the literature was very good indeed, as seen in Table 3.1. For these standard compounds the fitting of a second exponential component to the decay led to little, if any, improvement in the goodness-of-fit as evaluated by  $\chi^2_v$  and the autocorrelation function of the weighted residuals. By means of illustration an example of an actual decay experiment is given below.

2,2'-Binaphthyl-d<sub>14</sub> Lifetime in Cyclohexane at 295 K

A solution of 2,2'-binaphthyl-d<sub>14</sub> ( $8.6 \times 10^{-5}$  M) in cyclohexane was degassed in a Rotaflo sealed cylindrical Spectrosil "A" tube by six cycles of freeze-pump-thaw at  $\leq 10^{-5}$  torr on a mercury-free vacuum line and then sealed off by means of the Teflon valve. The flashlamp was filled with 350 torr of prepurified N<sub>2</sub> and the 0.25 Jarrell-Ash excitation monochromator was fitted with 1000  $\mu$ m slits and set to the intense nitrogen band at 313.6 nm. A nominal timebase of 400 ns was selected on the TAC, with  $\sim 300$  ns of delay cable inserted in both the START and STOP signal circuits. The lamp was operated at 5 kV and 19.5 kHz while the START and STOP PMTs were operated at -1050 V and -1990 V respectively. The ratio of STOP/START pulses at the appropriate discriminator outputs was adjusted to be  $\leq .05$ . This was crucial to ensure that only single, not multiple photon events were being observed by the STOP PMT and to prevent pulse pile-up in the STOP channel

(Stop PMT, Stop Discriminator, TAC. <sup>54,55,59,138</sup> Collection times at these low STOP/START ratios were not prohibitively long since the quantum yield of the solute was sufficiently high such that the near-maximum detection rate of  $\sim 800$  Hz could be obtained with the H-10 emission monochromator fitted with 1.0 mm slits and set to pass 340.0 nm emission. The STOP/START ratio was controlled by adjustment of the diaphragm in the excitation light path only, since it was known that the instrumental response functions of most photomultipliers, including the 56 DUVF/03 are dependent on the actual portion of photocathode illuminated. <sup>52,138</sup> For this reason the emission optics were set to give full illumination of the photocathode rather than employing a sharply focused image. After collection of  $\sim 10^4$  counts in the peak channel the 2,2'-binaphthyl- $d_{14}$  sample was replaced by a cylindrical tube containing an aqueous suspension of the diffuse, colloidal scatterer Ludox SM (DuPont). The lamp profile was obtained by setting the emission monochromator to the excitation wavelength, 313.6 nm and measuring the Rayleigh scattered light from the Ludox suspension. The apparent optical density of this scatterer was unimportant (if  $< 2.0$ ) since, in contrast to the apparatus of Lewis et al <sup>52</sup>, the use of emission optics assured essentially fixed spatial illumination of the photocathode. Without such optics the capture of a nearly constant solid scattering angle of emission may have proved a significant consideration. In contrast to Eastman's observation, <sup>143</sup> this batch of Ludox was found to be non-fluorescent when excited below 300 nm. Furthermore, substitution of a specular reflector (aluminum foil or front-surface mirror) for the diffuse scatterer yielded identical results on deconvolution of the



observed decay curves. <sup>52,138,144</sup> Following collection of  $10^4$  counts in the peak channel of the lamp profile the nominal 400 nsec timebase was calibrated and the two experimental curves transferred to the computer for reiterative convolution to extract the molecular decay parameters.

Mono exponential fit:  $I(t) = 0.4332 \exp\left(\frac{-t}{33.50}\right)$

$$\chi_v^2 = 36.45$$

Bi exponential fit:  $I(t) = .04789 \exp\left(\frac{-t}{24.39}\right) + .003689 \exp\left(\frac{-t}{99.34}\right)$

$$\chi_v^2 = 1.291$$

The dramatic decrease in  $\chi_v^2$  and the obvious improvement in the randomness of the residuals as evidenced by both the percent deviation plot and the autocorrelation function plot strongly suggested that the decay kinetics more closely resemble those of two excited species, each decaying according to a first order rate law.

## CHAPTER FOUR

### Photophysics of the Phenylanthracenes

#### 4.1 Photophysics of 1-Phenylanthracene

##### 4.1.1 Fluorescence Emission and Excitation Spectroscopy

While the luminescence properties of 1-phenylanthracene in solution have been sporadically examined no comprehensive treatment of temperature and excitation or emission wavelength effects has been previously undertaken. The fluorescence spectrum at room temperature and 77K and the phosphorescence spectrum at the latter temperature have been reported.<sup>34,145</sup> Additionally, quantum yields of fluorescence<sup>34,146</sup> and triplet formation<sup>147</sup> are available at 295K, as is the quantum yield ratio,  $\phi_p/\phi_f$  in low temperature glass.<sup>145</sup> This present study will supplement this existing information to permit calculation of many of the photophysical parameters for the 1-phenylanthracene luminescence in solution. The effect of varied temperature, excitation wavelength and emission wavelength on the steady-state and decay spectroscopy of 1-phenylanthracene has been examined, with a view to confirming the presence or absence of conformeric species and to elucidating approximate torsional geometries of the absorptive and fluorescent states.

The room temperature fluorescence emission and excitation spectra of 1-phenylanthracene in alkane solvents (shown in Figure 4.1) are broad and structureless with maxima at 342.2 nm ( $29\,220\text{ cm}^{-1}$ ) and 295.9 nm ( $33\,800\text{ cm}^{-1}$ ) respectively. At 77K the maximum in the

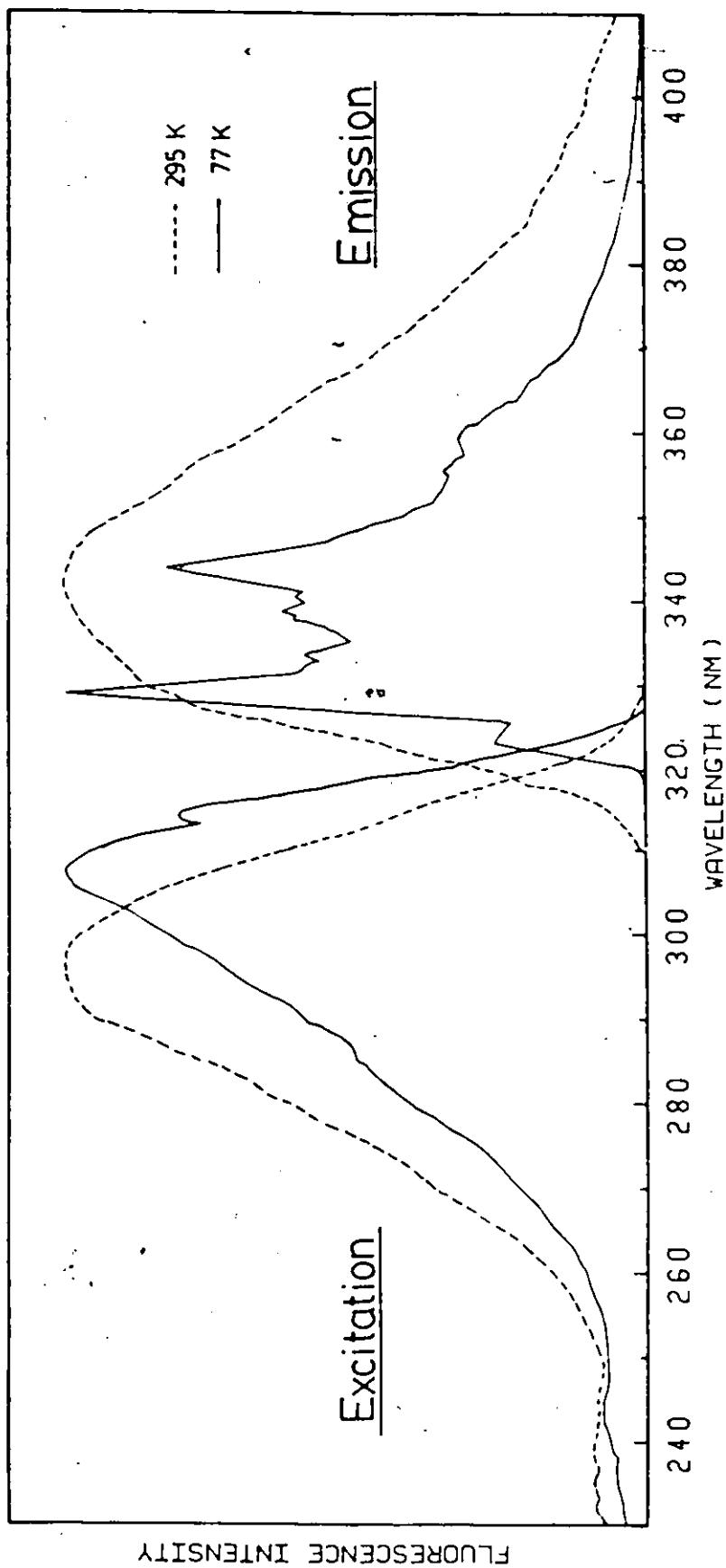


Figure 4.1

Fluorescence Emission and Excitation Spectra of 1-Phenylnaphthalene in Alkane Solvents ( $10^{-4}$  -  $10^{-5}$  M in 3-methylpentane or isopentane) at 295K and 77K

Table 4.1

Fluorescence Emission Bands of  $10^{-4}$  -  $10^{-5}$  M

1-Phenylanthracene in 3MP or Isopentane Glass at 77K

Intensity <sup>a</sup>	$\lambda$ (nm)	$\nu$ ( $\text{cm}^{-1}$ ) $\pm 10 \text{ cm}^{-1}$	$\Delta\nu$ ( $\text{cm}^{-1}$ ) $\pm 20 \text{ cm}^{-1}$	Frequencies ( $\text{cm}^{-1}$ ) and Tentative Assignments in Naphthalene <sup>b</sup>
m	322.7	30 990	0	0; 0-0
vs	327.6	30 530	460	513; $8b_{3g}$ or $9a_g$
w,sh	332.1	30 110	880	937; $7b_{3g}$
m	337.8	29 600	1390	1380; $5a_g$
s	342.6	29 190	1800	1888; 1380 + 513
b,sh	359.2	27 840	3150	3273; 513 + 2 x 1380

<sup>a</sup> s=strong; m=moderate; w=weak; b=broad; v=very; sh=shoulder.

<sup>b</sup> in n-pentane matrix at 77K from refs. 98,99.

excitation spectrum shifts to 307.0 nm ( $32\,570\text{ cm}^{-1}$ ) with a poorly resolved shoulder appearing at 314.9 nm ( $31\,760\text{ cm}^{-1}$ ). The actual onset of absorption as measured from the excitation spectra does not change significantly on going to 77K. The fluorescence emission spectrum on the other hand becomes quite structured at 77K with a small red-shift in the onset of emission (310 nm at 295K, 315 nm at 77K) with an apparent 0-0 band being clearly resolved at 322.7 nm ( $30\,990\text{ cm}^{-1}$ ). The intensity distribution of the fluorescence changes markedly, the maximum blue-shifting  $1310\text{ cm}^{-1}$  to 327.6 nm at 77K.

The emission spectra and lifetimes of 1-phenylnaphthalene were independent of the actual alkane solvent with 3MP and isopentane yielding nearly identical spectra and lifetimes, despite the large viscosity difference at 77K. ( $\eta_{77\text{K}}$  (isopentane)  $\sim 10^6$  poise,  $\eta_{77\text{K}}$  (3MP) =  $2.2 \times 10^{12}$  poise<sup>148,149</sup>).

Positions of the resolved bands in the low temperature fluorescence spectrum are given in Table 4.1. While the bandwidths at half-maximum are large, typically  $350\text{ cm}^{-1}$ , no solvent yielded more structured spectra despite attempts to obtain quasilinear spectra in n-pentane, n-hexane and methylcyclohexane polycrystalline matrices at 77K, with solute concentrations nominally ranging from  $10^{-3}$  to  $10^{-6}\text{M}$ . These polycrystalline matrices in fact gave much broader spectra than those obtained in the clear organic glasses.

These results are similar to those obtained by Hochstrasser for the nonplanar molecule 1,1'-binaphthyl in rigid organic glasses (Section 5.1.1).

The nonplanarity of the electronic ground state for the isolated


1-phenylnaphthalene molecule is amply documented by the available experimental<sup>150,151</sup> and theoretical studies<sup>152-155</sup> which give an interannular angle in the range  $46^{\circ}$  to  $66^{\circ}$ . The large Stokes shift between the fluorescence emission and excitation spectra in the fluid solution at 295K (Figure 4.1) suggests that 1-phenylnaphthalene undergoes a significant geometry change subsequent to excitation in fluid media. Since torsional relaxation about the quasi-single interconnecting bond should be quite facile at 295K it is probable that the emissive state in fluid solution is more planar than the initially formed Franck-Condon excited state (which should have the interplanar angle of the ground state). The calculations of Gustav and coworkers<sup>153</sup> support this contention, with an interannular angle of  $32^{\circ}$  being found for the equilibrium geometry of the first excited singlet state.

At low temperatures or high viscosities this torsional relaxation after excitation will be inhibited, so that the emissive state geometry at 77K will more closely resemble the ground state geometry. Examination of the low temperature spectra confirms this supposition. The large blue-shift of the fluorescence envelope ( $1310\text{ cm}^{-1}$  for the maxima) on going to 77K indicates that the emission does arise from a state of higher energy. Furthermore, the electronic origin of the fluorescence emission of 1-phenylnaphthalene at 77K is at  $30\,990\text{ cm}^{-1}$ , only  $730\text{ cm}^{-1}$  to the red of the naphthalene origin at  $31\,716\text{ cm}^{-1}$ .<sup>98</sup> This points to an excited state in rigid solution with a fairly large interannular angle, i.e., very much like naphthalene.

The slight red-shift in the excitation onset at 77K relative to the room temperature excitation points to the absorptive state at 77K

being, on the average, somewhat more planar than the ground state configuration at room temperature. This is in keeping with a broad and shallow minimum for the ground state potential, whereby various torsional states of  $S_0$  can be moderately populated at room temperature. Such a shallow minimum may, incidentally, account for the wide range of interplanar angles determined experimentally for 1-phenylnaphthalene.

The lack of an excitation or emission wavelength dependence of the fluorescence spectra at 295K and 77K supports the belief that essentially a single conformer or narrow range of conformers are responsible for the fluorescence at these two temperatures. At room temperature, where torsional relaxation in the excited state is expected to be fast the emissive state will likely have the equilibrium excited state geometry, namely  $\theta \sim 32^\circ$ . On cooling to 77K this twisting will be inhibited, so the bulk of the emission will originate from an  $S_1$  state with  $\theta \sim 46-66^\circ$ . This barrier to relaxation in  $S_1$  at 77K may be partially intrinsic (i.e. intramolecular in origin) and partly determined by the viscosity of the solvent. The similar results in isopentane and 3MP at low temperature might be taken to indicate that the contribution of the former is more important; however, the viscosity of even isopentane may already be sufficiently high to impede torsional relaxation. Kordas and El-Bayoumi's study<sup>156</sup> of the intramolecular twisting relaxation in the sterically crowded molecule trans-1,1,4,4-tetraphenyl-2-methylbutadiene indicated that the fluorescence energy depended on the solvent viscosity while the fluorescence quantum yield was a function of both temperature and viscosity. The phenomenology of such solvent matrix effects has been discussed by a number of authors.<sup>157-159</sup>



#### 4.1.2 Fluorescence Quantum Yield Measurements

The fluorescence quantum yields of 1-phenylnaphthalene, measured relative to a PPO reference in cyclohexane at 295K and in 3-methylpentene at 295K and 77K are tabulated below.

Table 4.2

Relative Fluorescence Quantum Yields of 1-Phenylnaphthalene

Solvent	$\phi_f$		$\phi_f$ (literature)
	295K	77K	295K only
cyclohexane	0.36		0.36 <sup>a,146</sup> ; 0.37 <sup>b,34</sup>
3MP	0.42	0.71	

<sup>a</sup> relative to  $\phi_f$  (quinine sulfate) = 0.55 in 1N H<sub>2</sub>SO<sub>4</sub>.

<sup>b</sup> relative to  $\phi_f$  (9,10-diphenylanthracene) = 1.0 in cyclohexane.

These experimental values represent the mean of at least three runs, with an estimated error of about 10% in the room temperature quantum yields, rising to perhaps 20% for the trials at 77K due to the greater difficulty in reproducibly positioning the sample and reference. The  $\phi_f$  of 1-phenylnaphthalene exhibited no dependence on the excitation wavelength at either temperature.

#### 4.1.3 Fluorescence Decay Measurements

The fluorescence decay of 1-phenylnaphthalene in dilute solution could, in all cases, be well described by simple first order kinetics, with the intensity following a decay law of the form

$$I(t) = \alpha \exp(-t/\tau). \quad (4.1)$$



Reduced chi-squared values were generally less than 1.3 and showed no significant improvement if the decay was fitted, instead, to a bi-exponential decay law. Observed fluorescence lifetimes for 1-phenyl-naphthalene in room temperature cyclohexane solution and in 3MP at a number of temperatures are given in the accompanying table.

Table 4.3  
Fluorescence Lifetimes of 1-Phenyl-naphthalene in Dilute Solution  
Fitted to a Monoexponential Decay Law<sup>a</sup>

Solvent	Temperature	$\tau$ (ns)	$\tau$ (literature) (ns)
cyclohexane	295K	12.67 $\pm$ .05	13 <sup>34</sup> ; 9.3 <sup>146</sup>
3MP	295K <sub>b</sub>	14.56 $\pm$ .05	
	195K <sub>b</sub>	16.19 $\pm$ .05	
	77K	24.00 $\pm$ .05	

<sup>a</sup> concentration  $7 \times 10^{-4}$  M:  $\lambda_A = 315.9$  nm,  $\lambda_F = 370.0$  nm.

<sup>b</sup> solid CO<sub>2</sub>/acetone slush, temperature measured with platinum resistance thermometer.

In comparing the measured lifetime in cyclohexane to those in the literature it should be noted that the agreement with Berlman's value of 13 ns<sup>34</sup>, also determined by single photon counting techniques, is excellent whereas the determination of Lentz et al,<sup>146</sup> 9.3 ns, appears to be gravely in error. Their fluorescence lifetimes were calculated by means of a Stern-Volmer scheme of oxygen quenching, viz

$$\tau = \frac{(\phi_f^0/\phi_f) - 1}{k_Q[O_2]} \quad (4.2)$$

where  $\phi_f^0$  and  $\phi_f$  are the quantum yields of fluorescence in the absence and presence of air respectively. This approach is intrinsically less accurate than direct, pulsed methods since the precision and accuracy of the quantum yield measurement for  $\phi_f^0/\phi_f$  is low while constancy of  $k_Q$ , the bimolecular quenching rate constant, for a series of aromatic hydrocarbons is only approximate. The application, by Lentz, of the empirical  $k_Q[O_2]$  term for naphthalene to a series of substituted naphthalenes should be regarded with caution.

#### 4.1.4 Analysis and Discussion of the Photophysics of 1-Phenylnaphthalene

From the experimental values of the observed fluorescence lifetimes and quantum yields the purely radiative lifetime or rate constant may be calculated by the relationship

$$\tau_0 = \tau/\phi_f = 1/k_f. \quad (4.3)$$

Table 4.4

Radiative Lifetimes and Rate Constants for 1-Phenylnaphthalene

Solvent; Temperature	$\tau_0 = \tau/\phi_f$ (ns)	$k_f = 1/\tau_0$ (s <sup>-1</sup> )	$k_f^0 = k_f/n^2, a$ (s <sup>-1</sup> )	n
cyclohexane; 295K	35	$2.8 \times 10^7$	$1.4 \times 10^7$	1.4266
3MP; 295K	35	$2.8 \times 10^7$	$1.5 \times 10^7$	1.3765
3MP; 77K	34	$3.0 \times 10^7$	$1.4 \times 10^7$	1.489

<sup>a</sup> see text.

The second last column in the preceding table shows the radiative rate constant,  $k_f^0$ , after correction for the effect of the

refractive index of the medium using the equation

$$k_f^0 = k_f/n^2. \quad (4.4)$$

This dependence has been predicted theoretically<sup>94,160</sup> and verified for several solutes in both hydrocarbon and ehtanolic solvents over wide temperature regions.<sup>160-163</sup> Olmstead<sup>163</sup> and others<sup>161</sup> have found  $k_f^0$  to vary at least as  $n^{-2}$  and at most as  $n^{-3}$ , their data being consistent with either functional dependence. The refractive index of 3-methylpentane at 77K not being directly available was calculated on the basis of the formula<sup>164-166</sup>

$$\frac{n^2(T) - 1}{\rho(T)\{n(T) + 0.4\}} = b \quad (4.5)$$

where the parameter b can be evaluated from the room temperature refractive index and density  $\rho$  while the density at low temperature is available from contraction data. The values for n and  $\rho$  at ambient temperature are 1.3765 and 0.6643 g/ml respectively.<sup>125</sup> Also,  $V(77K)/V(293K) = 0.7845 \pm 0.0006$  for 3-methylpentane.<sup>167</sup> Using these data,  $n(77K)$  for 3MP = 1.489.

Physically,  $k_f^0$  may be interpreted as the radiative rate constant in a medium of unit refractive index, i.e., gas phase. Table 4.4 indicates that the radiative rate constant is invariant with temperature and solvent after this correction has been applied. This effect has been observed in many other systems.<sup>32,160-163,168-170</sup>

The experimental radiative lifetime of 35 ns is considerably longer than the 5 ns lifetime calculated from the integrated absorption spectrum<sup>34</sup> using the Strickler-Berg<sup>171</sup> relationship

$$k_f = \frac{1}{\tau_0} = 2.88 \times 10^{-9} n^2 \langle \bar{\nu}_f^{-3} \rangle_{AV}^{-1} \int_{\bar{\nu}}^{\bar{\nu}_f} \epsilon d\bar{\nu} \quad (4.6)$$

$$\text{where } \langle \bar{\nu}_f^{-3} \rangle_{AV} = \frac{\int \bar{\nu}^{-3} f(\bar{\nu}) d\bar{\nu}}{\int f(\bar{\nu}) d\bar{\nu}}$$

This discrepancy may arise from the overlap of the  $S_0 \rightarrow S_1$  and  $S_0 \rightarrow S_2$  transitions in absorption, since the integration should be conducted over only that absorption transition ultimately responsible for the fluorescence, i.e., over  $S_0 \rightarrow S_1$  absorption band only. Inclusion of higher transitions leads to erroneously large values for  $\int \epsilon d\bar{\nu}$ , with a commensurate decrease in the apparent  $\tau_0$ . Implicit in the application of the Strickler-Berg relationship is the presumption that the transition moments for fluorescence and absorption are equal. This assumption has merit only if the nuclear configurations of the two relevant states,  $S_0$  and  $S_1$ , are similar. For most systems the effect of large configurational differences between absorptive and emissive states is to make  $\tau_0(\text{experimental}) > \tau_0(\text{calculated})$ .<sup>172</sup> As mentioned in Section 4.1.1 the  $S_0$  geometry of 1-phenylnaphthalene is believed to have a twist angle of  $46 - 66^\circ$  between the aryl rings while the equilibrium  $S_1$  geometry is probably somewhat more planar with  $\theta \sim 32^\circ$ . This geometry change is rather modest, and as indicated by the similar calculated oscillator strengths for absorption and emission transitions in 1-phenylnaphthalene,<sup>153</sup> the transition moments of the participating states are likely not much different. Most of the disparity between observed and calculated  $\tau_0$  values should thus be ascribed to overlap of the two low lying absorption transitions and inclusion of some  $S_0 \rightarrow S_2$  absorption in the Strickler-Berg calculations by Berlman.

In Table 4.3 one may note that the experimental fluorescence lifetime increases with decreasing temperature. From the definitions of the observed singlet lifetime

$$\tau = (k_f + k_{ic} + k_{isc})^{-1} = (k_f' + k_{nr})^{-1} \quad (4.7)$$

and the constancy of  $k_f$  with temperature it is apparent that  $k_{nr}$  ( $= k_{ic} + k_{isc}$ ), the rate constant for nonradiative depletion of the first excited singlet state, decreases with decreasing temperature. Inverting the lifetime expression one may write

$$\tau^{-1} = k(T) = k_f + k_{nr} \quad (4.8)$$

The temperature dependence of the radiationless rate constant is frequently taken to be of the form<sup>94</sup>

$$k_{nr} = k_{nr}^0 + k_{nr}' \exp(-w/kT) \quad (4.9)$$

wherein  $k_{nr}^0$  is temperature independent and the temperature dependent component is comprised of an Arrhenius term with frequency factor  $k_{nr}'$  and activation energy  $w$ . Substitution gives

$$k(T) = k_f + k_{nr}^0 + k_{nr}' \exp(-w/kT) \quad (4.10)$$

Experimental values of  $k(T) = \tau^{-1}$  in 3MP were fitted by nonlinear least squares to a function of the form

$$k(T) = A + B \exp(-C/T) \quad (4.11)$$

with  $A = k_f + k_{nr}^0$ ;  $B = k_{nr}'$ ;  $C = w/k$ . Fitted values of the three parameters were  $A = 2.82 \times 10^7 \text{ s}^{-1}$ ,  $B = 6.09 \times 10^7 \text{ s}^{-1}$  and  $C = 115.7\text{K}$ , so that

$k_f + k_{nr}^0 = 2.82 \times 10^7 \text{ s}^{-1}$ ,  $k'_{nr} = 6.09 \times 10^7 \text{ s}^{-1}$  and  $w = 80.4 \text{ cm}^{-1}$  (0.23 kcal/mole). Since  $k_f = 2.9 \pm .1 \times 10^7 \text{ s}^{-1}$  this implies that  $k_{nr}^0 \sim 0$ .

Furthermore, since the  $S_1 - S_0$  energy gap  $\gg kT$ , the rate of internal conversion  $S_1 \rightarrow S_0$  is usually effectively independent of temperature, so that the temperature-dependent term,  $k'_{nr} \exp(-w/kT)$  refers exclusively to the intersystem crossing  $S_1 \rightarrow T_n$ . Summarizing,  $k_{nr}^0 = k_{isc}^0 + k_{ic} = 0$  and  $k'_{nr} = k'_{isc} = 6.09 \times 10^7 \text{ s}^{-1}$  and  $w_{isc} = 80.4 \text{ cm}^{-1}$ . These values are typical of those found for substituted naphthalenes and anthracenes in dilute solution.<sup>94,173</sup> The activation energy term  $w_{isc}$  may be physically interpreted in the following manner. If  $T_1$  or some higher triplet state  $T_n$  lies significantly below  $S_1$  as in Figure 4.2 then the density of states in  $T_1$  or  $T_n$  at the isoenergetic crossing point will be large and the intersystem crossing process will be effectively independent of temperature (Figure 4.2a). However, if  $T_n$  lies at  $\sim w_{isc}$  above  $S_1$  (Figure 4.2b) then the rate of intersystem crossing  $S_1 \rightarrow T_n$  will be strongly influenced by the thermal population of low-lying vibrational

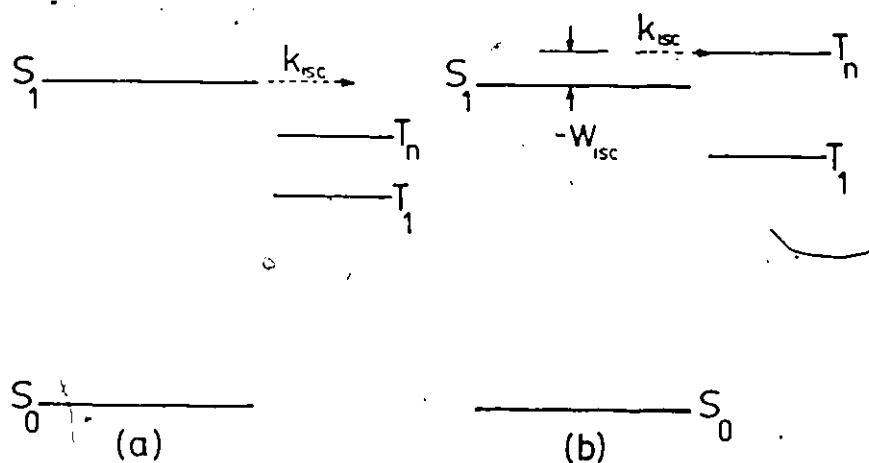


Figure 4.2

- a: Temperature Independent Intersystem Crossing
- b: Thermally Activated Intersystem Crossing

levels in  $S_1$ . Thermal activation or population of these vibrational states  $S_1(v > 0)$  will then lead to crossing to the nearby triplet,  $T_n$ . From the known<sup>145</sup>  $S_0 - S_1$  and  $S_0 - T_1$  energy gaps for 1-phenylnaphthalene in 3MP solution, 31 060  $\text{cm}^{-1}$  (30 990  $\text{cm}^{-1}$  from the 0-0 in fluorescence in this study) and 20 660  $\text{cm}^{-1}$  respectively, the separation  $S_1 - T_1$  may be calculated as 10 400 to 10 330  $\text{cm}^{-1}$ . This large energy difference indicates that  $S_1 \rightarrow T_1$  intersystem crossing should be temperature independent. The state  $T_n$ , if it exists, should lie at about 10 400 + 80 = 10 480  $\text{cm}^{-1}$  above  $T_1$ . Using laser absorption spectroscopy Amand and Bensasson<sup>147</sup> have measured a triplet-triplet absorption at 20 833  $\text{cm}^{-1}$  in a cyclohexane solution of 1-phenylnaphthalene while in 3MP at 77K other workers<sup>174</sup> have found the  $T - T$  absorption of 1-phenylnaphthalene to have a 0-0 at about 20 207  $\text{cm}^{-1}$ , both of which may correspond to the  $T_1 \rightarrow T_8$  absorption in naphthalene and its derivatives.<sup>173</sup> Little is known about the intervening triplet levels in naphthalene derivatives, although  $T_2$  is known to be  $\sim 10\,000\text{ cm}^{-1}$  above  $T_1$  in naphthalene itself. Lending some credence to an assignment of  $T_n$  as  $T_2$  in 1-phenylnaphthalene is the observation that for condensed aromatic hydrocarbons  $k_{isc}^0$  ( $\sim$  zero in this case) is generally small if there are no intervening triplet states between  $S_1$  and  $T_1$ .<sup>173</sup> Failure to observe the triplet level involved in intersystem crossing by  $T_1 \rightarrow T_n$  absorption is not surprising since the pertinent level may be strongly forbidden in radiative combination with  $T_1$ , as indeed is the case for the  $T_1 \rightarrow T_2$  transition in naphthalene and like molecules.

The calculated value,  $k_{nr}^0 = k_{isc}^0 + k_{ic}^0 \sim 0$ , in conjunction with the measured fluorescence quantum yield  $\phi_f = k_f / (k_f + k_{isc} + k_{ic}) = 0.42$  in 3MP at 295K leads to a quantum yield of triplet formation of about 0.58 as calculated from the definition of the quantum yield of triplet formation,

$$\phi_T = \frac{k_{isc}}{k_f + k_{isc} + k_{ic}} \quad (4.12)$$

and the relationship  $\phi_{ic} + \phi_T + \phi_f \equiv 1.0$ .

This figure compares most favourably with the determination (T - T absorption) by Amand and Bensasson who found  $\phi_T = 0.52 \pm 15\%$  for 1-phenylnaphthalene in cyclohexane at ambient temperature.<sup>147</sup>

Using the experimentally determined values for  $k_{ic}$  and  $k_f$  and the temperature dependence of the rate constant for intersystem crossing

$$k_{isc}(T) = 6.09 \times 10^7 \exp(-80.4/kT) \quad (4.13)$$

in conjunction with Gallivan's data<sup>145</sup> for the phosphorescence lifetime,  $\tau_p = 1.2s$  and the quantum yield ratio  $\phi_p/\phi_f = 0.11$  at 77K in 3MP one may solve for many of the photophysical parameters, as shown on the accompanying Jablonski diagram for 1-phenylnaphthalene in 3MP glass.

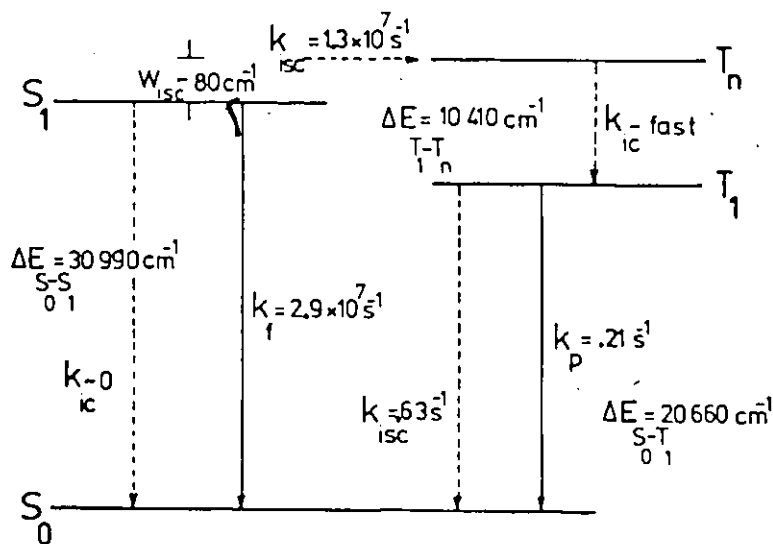


Figure 4.3

Jablonski Diagram for Photophysics of 1-Phenylnaphthalene in 3MP at 77K



The photophysics of 1-phenylnaphthalene is, on the whole, quite straightforward, despite the apparent change in the nature of the emitting state at low temperature. Under all circumstances the fluorescence decay was a simple monoexponential and the radiative lifetime of the unrelaxed, Franck-Condon excited state seen at 77K is essentially identical to that of the equilibrium excited state present in the more fluid media.

#### 4.2 Photophysics of 2-Phenylnaphthalene

##### 4.2.1 Fluorescence Emission and Excitation Spectroscopy

##### 4.2.1a. Fluorescence in Fluid and Glassy Media

The fluorescence emission of 2-phenylnaphthalene in 3MP glass at 77K has been the subject of intensive study by Wharton, Nauman, Hughes and Holloway,<sup>25,26,27</sup> so the results of this present study will be presented in light of their previous work. The aforementioned group concluded that, while the preferred ground state geometry of 2-phenylnaphthalene was twisted with  $\theta \sim 30^\circ$ , there existed, even at 77K, a small but experimentally accessible fraction of molecules having a nearly coplanar,  $\theta \sim 0^\circ$ , geometry. Excitation at the long wavelength edge, ca. 330 nm, was believed to selectively excite primarily these coplanar conformers, leading to a more structured and slightly red-shifted emission than that obtained at  $\lambda_A \leq 320$  nm. This proposed scheme of Wharton et al<sup>25,26,27</sup> may be represented qualitatively in Figure 4.4.

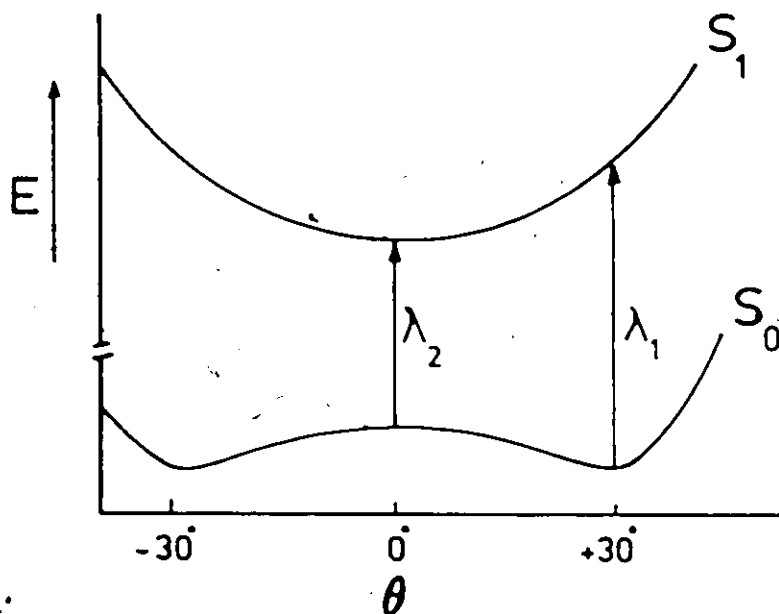


Figure 4.4  
Qualitative Potential Energy Scheme for Two Lowest Singlet States of  
2-Phenylanthracene after Holloway, Nauman, Wharton<sup>26,27</sup>

Energetic excitation at  $\lambda_1$  would produce a wide distribution of conformers with a variety of interannular angles whereas minimum energy excitation at  $\lambda_2$  could excite only that narrow distribution of conformers having geometries near  $\theta = 0^\circ$ . This, they believed would account for their observed red-shifted and structured fluorescence spectrum obtained at  $\lambda_A = 330$  nm. The ground state curve in Figure 4.4 appears to be qualitatively correct in view of the experimental<sup>26,151</sup> and theoretical evidence<sup>152,153,175</sup> pointing to an  $S_0$  geometry of  $\theta = 20 - 34^\circ$ , whereas little is known about the  $S_1$  potential energy curve.

In glasses of 3MP and isopentane Nauman's group found the lowest energy absorption band of 2-phenylanthracene to lie at 322.5 nm ( $31,010 \text{ cm}^{-1}$ ) and the first emission band at 342.0 nm ( $29,240 \text{ cm}^{-1}$ ), a Stokes Shift of about  $1770 \text{ cm}^{-1}$ .

The results of this present study are at variance with those of Wharton with regard to the low temperature emission behaviour.

Figure 4.6 shows the fluorescence spectrum of 2-phenylnaphthalene in 3MP glass at liquid nitrogen temperatures as a function of the excitation wavelength. While the predominant peak at all excitation wavelengths is the 342.5 nm one, as found by Wharton, excitation near the absorption edge with  $\lambda_A = 320$  or 310 nm gives rise to a sharp, moderately strong band at 325.5 nm ( $30\,720\text{ cm}^{-1}$ ) which diminishes in intensity as the excitation becomes progressively more energetic. The fluorescence spectrum of 2-phenylnaphthalene in 3MP at ambient temperatures, shown with the 295K and 77K excitation spectra in Figure 4.5 was found to be independent of the excitation energy while the excitation spectra were invariant with emission wavelength. The 77K and 295K excitation spectra showed a distinct, strong shoulder at 322.7 nm, evidently the 0-0 in absorption as found by Wharton at 322.5 nm. This evidence indicates that Wharton's assignment of the 0-0 in fluorescence to the 342.0 nm band is incorrect, with the band at 325.5 nm being the much more likely candidate. In conjunction with the excitation spectrum at 77K this would mean a Stokes Shift of only  $270\text{ cm}^{-1}$  between the lowest energy absorption band and the highest energy peak in the fluorescence.

Gallivan<sup>145</sup> also reported no fluorescence emission below about 340 nm for  $10^{-3} - 10^{-4}\text{ M}$  solutions of 2-phenylnaphthalene at 77K, although his choice of excitation wavelengths ( $\lambda_A \leq 300\text{ nm}$ ) may have precluded the observation of higher energy fluorescence bands. No concentration effect was found in this present study over the range

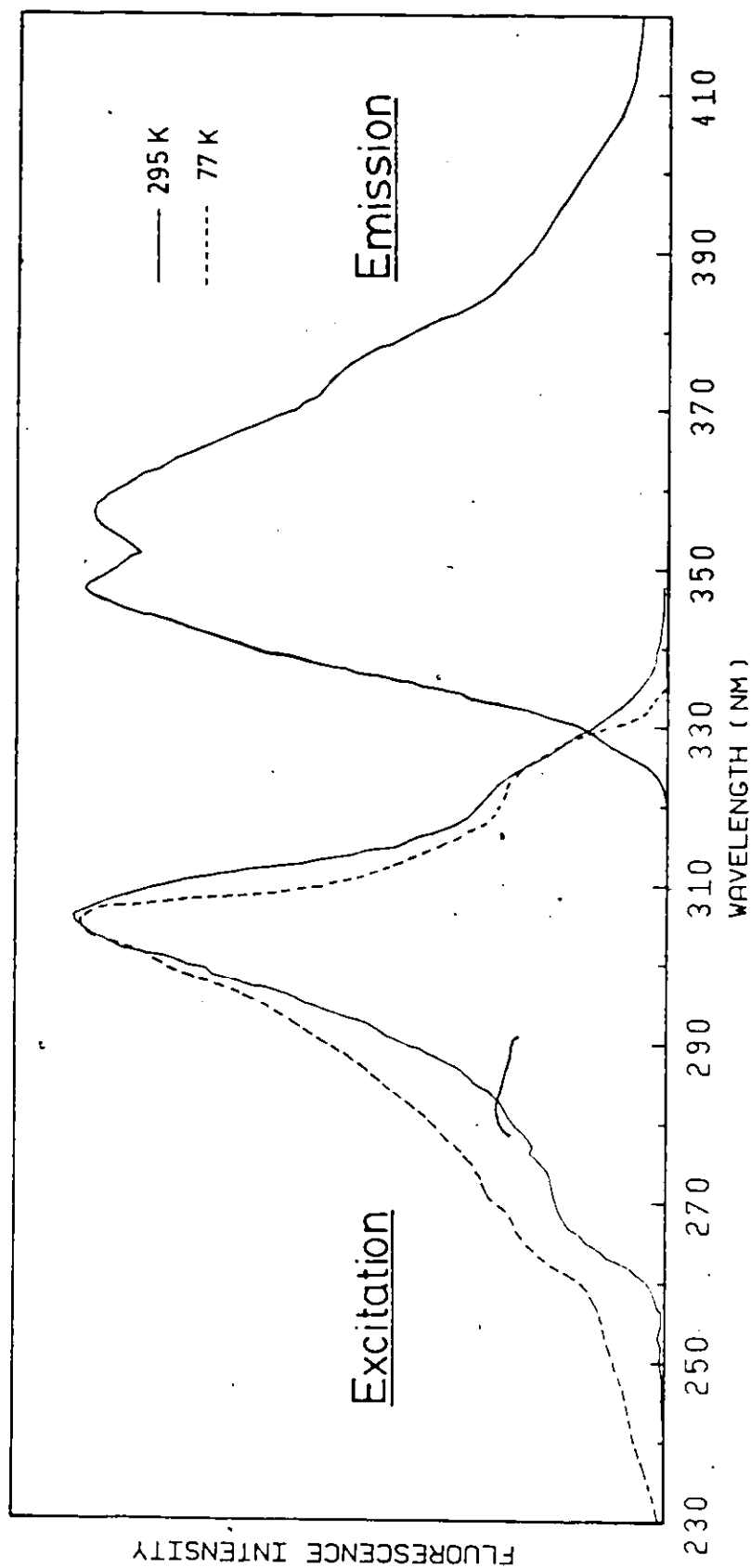


Figure 4.5

Uncorrected Fluorescence Excitation Spectra at 295K and 77K and Uncorrected Fluorescence Emission Spectrum  
at 295K of  $5 \times 10^{-5}$  M 2-Phenylnaphthalene in 3-Methylpentane

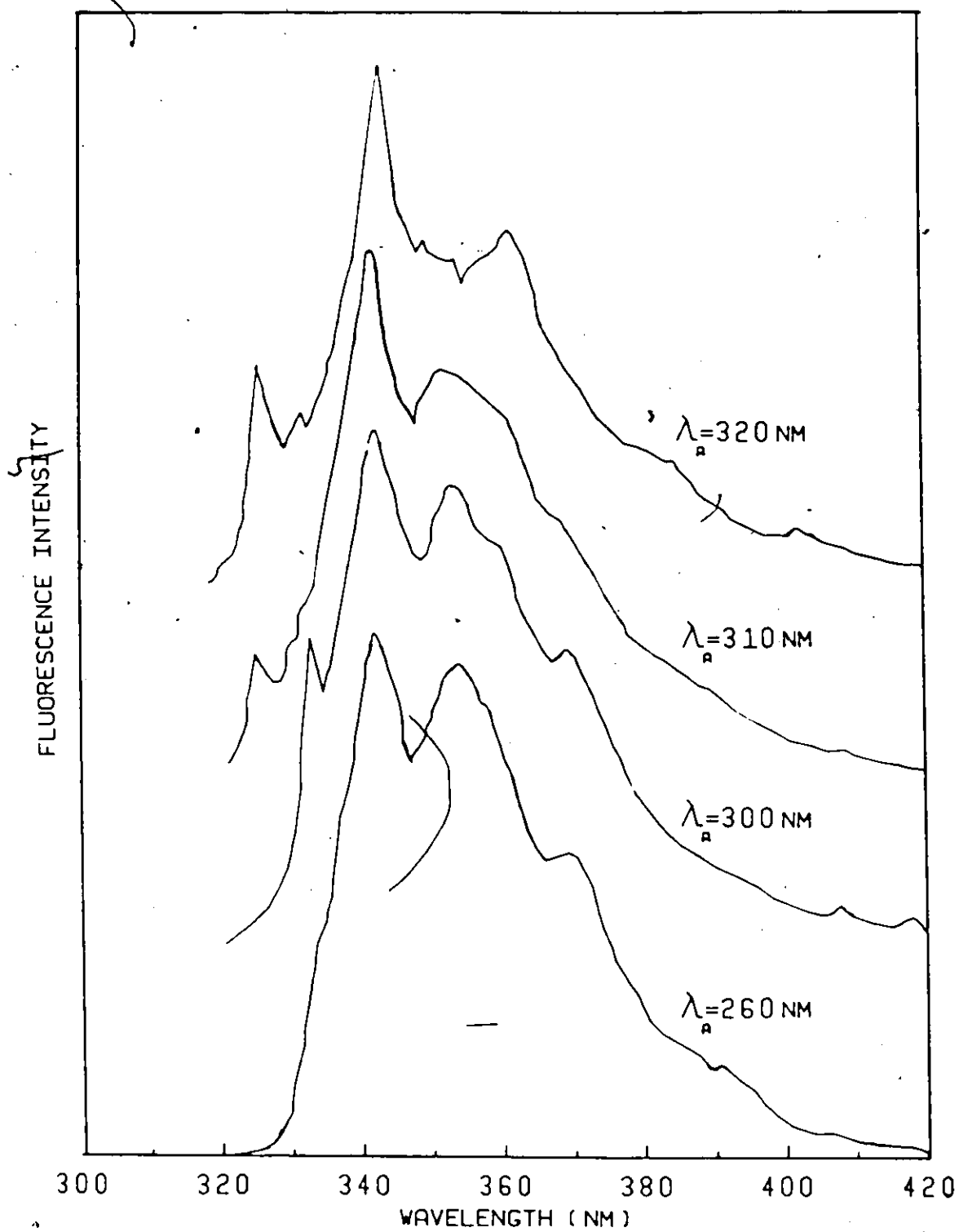


Figure 4.6

Fluorescence Emission Spectrum of  $5 \times 10^{-5} \text{ M}$  2-Phenylnaphthalene in 3-Methylpentane at 77K as a Function of Excitation Wavelength

$10^{-3}$  to  $10^{-5}$  M and any aggregate or crystal fluorescence of 2-phenylnaphthalene would be expected to lie to longer, not shorter wavelengths.

The near-coincidence of the long wavelength shoulder in the excitation spectrum, at 322.7 nm, (also seen by Wharton) and the highest energy fluorescence band at 325.5 nm for 2-phenylnaphthalene in 3MP solution at 77K is strong evidence that this 325.5 nm feature is genuine. Furthermore, the non-appearance of this short wavelength emission band in the quasilinear fluorescence spectrum in methylcyclohexane at liquid nitrogen temperatures (Section 4.2.1b) suggests that this 325.5 nm band is not merely impurity related, the solutes for both sets of experiments having a common origin. It should be remembered that the 2-phenylnaphthalene solute was rigorously purified by HPLC, a technique unavailable at the time of Wharton's and Gallivan's studies.

The highly structured ~~emission~~ reported by Wharton<sup>25</sup> when rigid glassy solutions of 2-phenylnaphthalene were excited at 328.2 nm could not be reproduced in this present work, especially since with  $\lambda_A > 320$  nm the interference of the exciting light precluded useful measurements at the high energy end of the emission envelope.

Wharton and coworkers have argued that at 77K the excitation of nonplanar ground state molecules was followed by torsional relaxation towards a more planar  $S_1$  equilibrium conformation from which emission occurred, hence accounting for the apparently large Stoke's Shift between emission and absorption. This picture cannot be entirely correct, since the appearance of the fluorescence band at 325.5 nm indicates a mirror-image relation to the absorption 0-0 at 322.5 - 322.7 nm. Apparently then, the state prepared by low-energy excitation (as with  $\lambda_F = 320, 310$  nm in

Figure 4.6 ) also emits directly, without significant geometry change, as shown by the small Stokes Shift. This particular feature could be accommodated within Wharton's scheme, as excitation at  $\lambda_2$  in Figure 4.4 i.e., excitation of, and emission from planar or near planar conformers of 2-phenylnaphthalene. That scheme does not however account for the complete excitation wavelength effect.

With excitation at  $\lambda_1$  the fluorescence spectrum should be enhanced in its blue components with respect to the spectra obtained upon very long wavelength excitation, such as at  $\lambda_2$ . If Wharton's scheme is valid then one would expect to see an increase in the higher energy components of the fluorescence as the excitation energy increases. If the excited state initially prepared at excitation wavelength  $\lambda_1$  does relax towards the equilibrium configuration in  $S_1$  the fluorescence should resemble that induced by direct excitation at  $\lambda_2$ . In fact, as seen in Figure 4.6, the high energy excitation enhanced the red, not the blue components, in the fluorescence spectrum at 77K, relative to the weaker bands near 325.5 nm.

Failure to observe a wavelength effect at 295K in the emission and excitation spectra and in the 77K excitation spectrum does not necessarily preclude the presence of ground state conformers of 2-phenylnaphthalene since the spectral broadening at 295K may render it impossible to resolve the expected small variations in spectral distributions of the conformers. The excitation spectra may appear constant for several reasons: the broad excitation bandwidth (1.07 nm) needed for reasonable intensity may have been of insufficient spectral purity to selectively excite the appropriate conformers; the emission

of the conformers may overlap so strongly at  $\lambda_F \geq 340.0$  nm that the net excitation spectra are effectively independent of the particular monitoring wavelength; the emission region of greatest interest,  $320 \text{ nm} \leq \lambda_F \leq 340 \text{ nm}$  could not be examined owing to interference from the exciting light. The other possibility is that the excitation spectra may be truly independent of  $\lambda_F$  if the emitting conformers are produced only after excitation, solely by conversion in the excited state.

Although the emission from degassed room temperature solutions of 2-phenylnaphthalene showed no excitation wavelength effect it was suggested by the fluorescence decay experiments that introduction of a singlet quencher might produce a differential quenching of the steady-state fluorescence if more than one emitting state were present. Anticipating these fluorescence decay measurements, it was found that the room temperature fluorescence decay did indeed indicate two lifetime components, one decaying very rapidly with  $\tau_1 \sim 1$  ns while the other was much longer lived,  $\tau_2$  being approximately 113 - 117 ns. The large difference in fluorescence lifetimes suggested that differential quenching could be of use in elucidating the identity of the components in the steady state fluorescence emission. The effect of a strong singlet quencher like molecular oxygen should be to differentially quench the intensity of the two components in a ratio of about  $\tau_2/\tau_1$ , i.e., the longer-lived emission should be quenched  $\sim 100$ -fold more effectively than the very short component.

The fluorescence of an air-equilibrated solution of  $10^{-4}$  M 2-phenylnaphthalene in 3MP was examined at various excitation wavelengths. Use of 1 atm. of  $O_2$  produced excessive quenching - the sample became non-



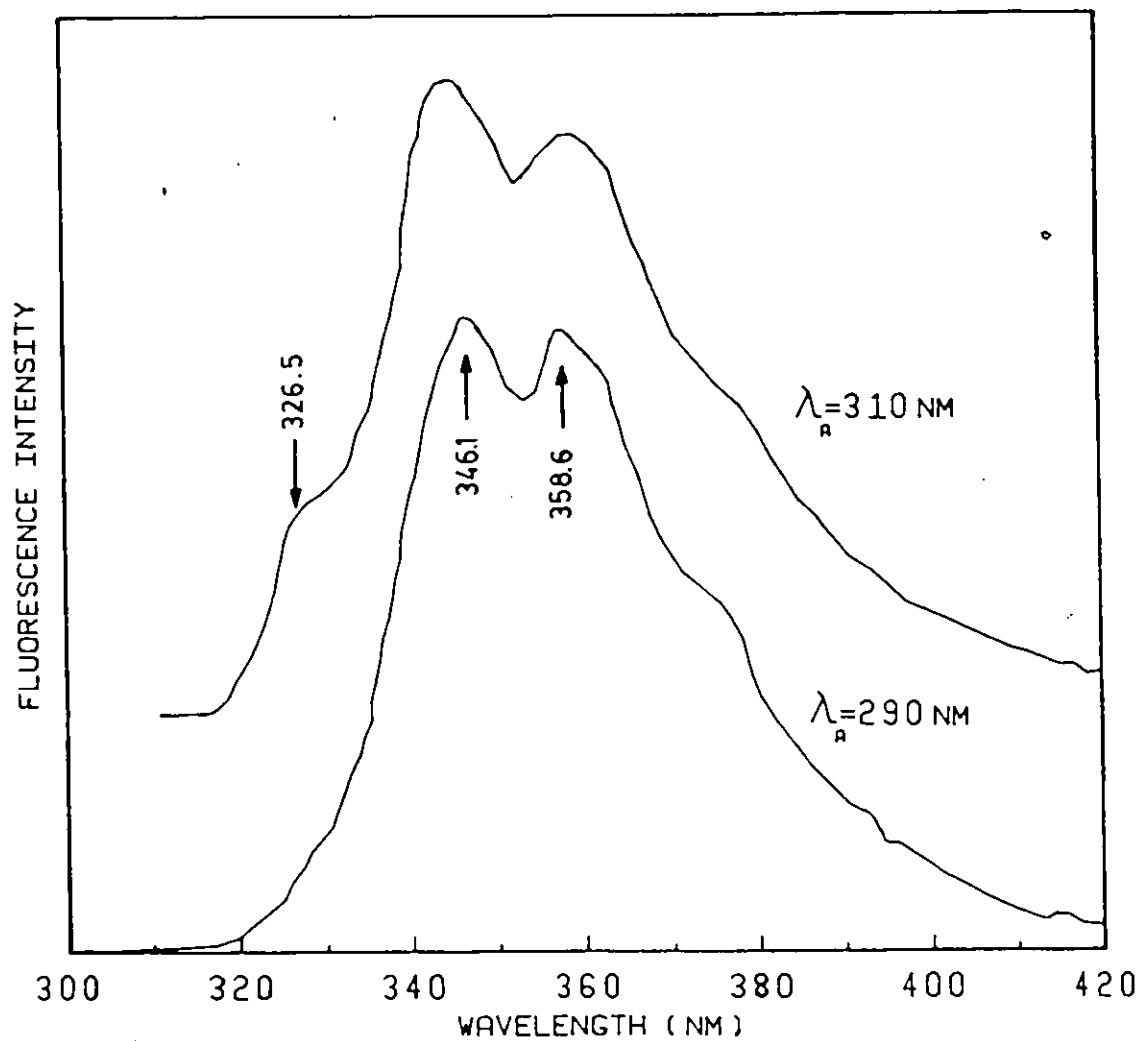


Figure 4.7

Fluorescence Emission Spectrum of  $10^{-4}$  M 2-Phenylnaphthalene  
in Air-Saturated 3-Methylpentane at 295K, as a Function  
of Excitation Wavelength

fluorescent. At wavelengths below 300 nm the air-saturated solutions yielded spectra identical in shape to those obtained from degassed solutions, though much reduced in intensity, while with excitation at 310 nm and 320 nm several differences were noted in the emission of the quenched sample. The relative intensity of the 358.6 nm peak decreased slightly, coupling with the progressive emergence of a shoulder on the blue edge of the fluorescence profile at  $326 \pm 1$  nm. Representative spectra of these oxygen-quenched solutions are shown in Figure 4.7

These spectra show unequivocally that the species responsible for the emission at 325.5 nm at 77K and  $326 \pm 1$  nm at 295K is the short lived ( $\tau_1 \leq 1$  ns) component. This component 1 is likely responsible for the lowest energy absorption at about 322.6 nm in view of the appearance of component 1 most pronouncedly in the steady state spectrum and the decay profile when  $\lambda_A$  is above 300 nm. Species 1 probably contributes to the intensity of the 346.1 nm peak at room temperature judging by its enhancement relative to the 358.6 nm band. As seen from the pulsed and steady state experiments this short-lived component cannot be excited to the exclusion of species 2, the longer-lived and longer wavelength emission component, so the two species or conformers must have very similar absorption energies or be derived from a common intermediate following excitation. Furthermore, component 1 must be a very minor component since even the 100-fold selective quenching of the long lived species was not capable of effecting complete suppression of the species 2 fluorescence.

Introduction of air or oxygen led to no permanent photooxidation products in solution, since the normal, unquenched emission could be easily regenerated by degassing the air or oxygen saturated samples.

No changes in the absorption spectra were noted in the air saturated solutions, indicating no strong tendency of molecular oxygen to form ground state charge transfer complexes with 2-phenylnaphthalene<sup>94</sup>.

#### 4.2.1b. Fluorescence in Polycrystalline (Shpol'skii) Matrices

Unlike the 1-phenyl isomer 2-phenylnaphthalene was found to yield a much sharper quasilinear spectrum (Shpol'skii effect) in polycrystalline matrices of methylcyclohexane or cyclohexane at 77K. The former solvent was preferred, giving slightly better resolution with half-widths of about  $100 \pm 150 \text{ cm}^{-1}$ . This is far from the optimum bandwidths of  $1 - 10 \text{ cm}^{-1}$  obtained for many Shpol'skii matrix-solute combinations and may arise from the imperfect "fit" of the bulky aryl groups into the lattice sites of the methylcyclohexane host. Ethylcyclohexane is an obvious alternative but does not crystallize at low temperatures forming instead a highly viscous glass. Some of the breadth of the spectral lines may arise from low frequency torsional oscillations of the two aryl groups about the interannular bond leading to emission from a moderately broad distribution of torsional conformations of the molecule.

The appearance of a quasilinear fluorescence spectrum for 2-phenylnaphthalene (and 2,2'-binaphthyl) should be contrasted with the observation that 1-phenylnaphthalene, 1,1'- and 1,2'-binaphthyls did not show highly structured emission in any of the n-alkanes or cycloalkanes in the concentration range  $10^{-3} - 10^{-6} \text{ M}$ . This is strong evidence that 2-phenylnaphthalene (and 2,2'-binaphthyl) can assume a planar conformation or conformations in the ground state since the Shpol'skii effect is generally limited to planar aromatic systems.<sup>29</sup>

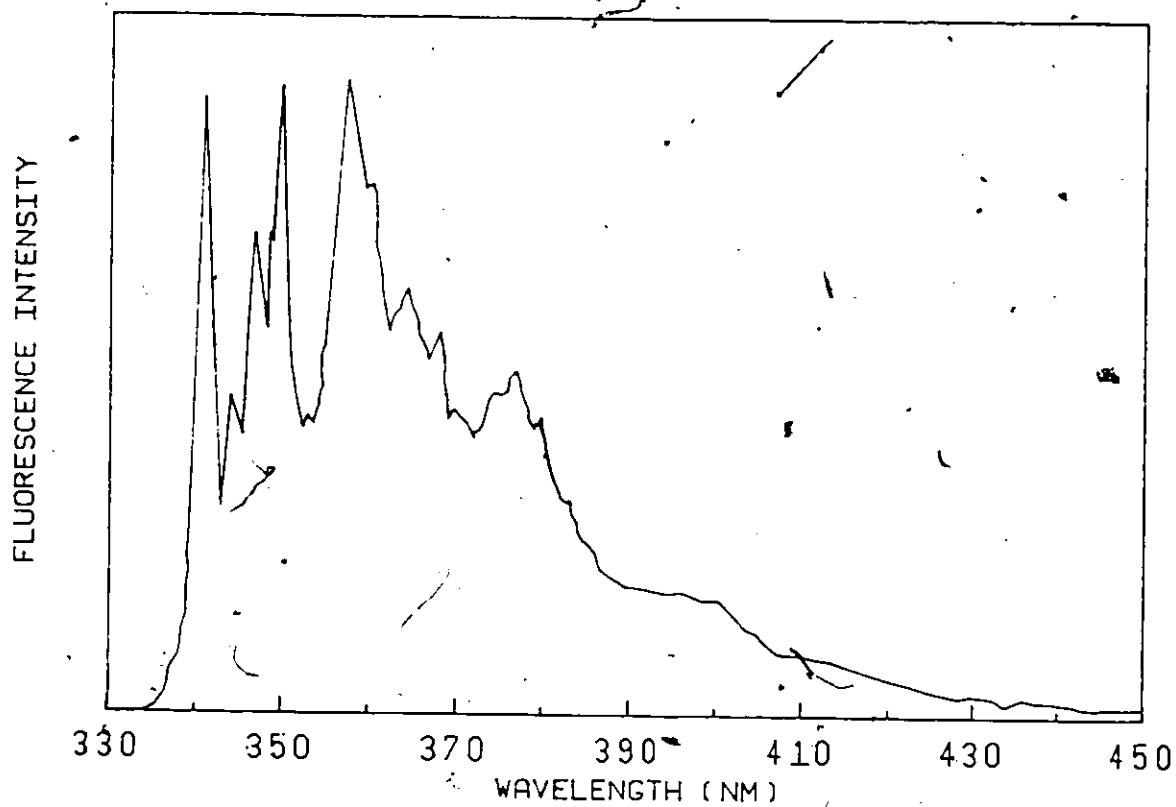


Figure 4.8

Uncorrected Fluorescence Emission Spectrum of  $10^{-4}M$   
2-Phenylnaphthalene in Polycrystalline Methylcyclohexane at 77K

This is not without exception however, since Palewska<sup>108</sup> has shown that the slightly non-planar aromatic hydrocarbon 1,2-benzotetraphene (penta-helicene) does show considerable fine structure superimposed on a diffuse background under Shpol'skii conditions. The more severely nonplanar homologs, hexa- and heptahelicene did not show such structure.

Quasilinear emission spectra have very recently been used to distinguish the planar and nonplanar conformers of the trans-1,2-diarylethylenes<sup>14</sup> with the composite spectrum of the conformers giving sharp quasilines of the planar species superimposed on the broad band spectrum of the non-planar conformers.

Unlike 2,2'-binaphthyl (Section 5.3.1c) the Shpol'skii fluorescence emission of 2-phenylnaphthalene showed no intensity variations of note with changes in the excitation wavelength. This quasilinear fluorescence emission is shown in Figure 4.8, with the emission wavelengths and frequencies tabulated in Table 4.5.

No attempt at a comprehensive assignment or interpretation of these frequencies has been undertaken, however, a few points will be noted.

As expected, the 0-0 in fluorescence for 2-phenylnaphthalene ( $29\,340\text{ cm}^{-1}$ ) is at lower energy than that of naphthalene ( $31\,716\text{ cm}^{-1}$ ).<sup>98,99,176</sup> The first distinct vibronic band is red shifted  $290\text{ cm}^{-1}$  from the origin in 2-phenylnaphthalene with the corresponding frequencies in 2,2'-binaphthyl- $h_{14}$  and  $-d_{14}$  being  $260\text{ cm}^{-1}$  and  $240\text{ cm}^{-1}$ . This is attributable to the vibration described as the aryl-X in-plane bending mode in mono-substituted benzenes<sup>177</sup> and naphthalenes. Since this mode involves a bending of the substituent on the ring it will be sensitive to the force

Table 4.5

Vibrational Frequencies from the Fluorescence Spectrum of  $10^{-4}M$   
2-Phenylnaphthalene in Polycrystalline Methylcyclohexane at 77K

Intensity <sup>a</sup>	$\lambda$ (nm)	$\bar{\nu}$ ( $\text{cm}^{-1}$ ) $\pm 10 \text{ cm}^{-1}$	$\Delta\bar{\nu}$ ( $\text{cm}^{-1}$ ) $\pm 20 \text{ cm}^{-1}$
vs	340.8	29 340	0
m	344.2	29 050	290
s	347.0	28 820	520
vs	350.0	28 570	770
w	353.0	28 330	1010
w,sh	356.2	28 070	1270
vs	357.8	27 950	1390
s,sh	360.0	27 780	1560
w	363.0	27 550	1790
m	364.2	27 450	1890
m	367.8	27 190	2150
m	370.4	27 000	2340
m,b	376.5	26 560	2780
m,b	394.5	25 530	3990

<sup>a</sup> s=strong; m=moderate; w=weak; b=broad; v=very; sh=shoulder.

constant of the atoms involved and the mass of the substituent. This would be in keeping with the progressive shift to higher wavenumber as the substituents become successively lighter from naphthyl- $d_7$  and naphthyl- $h_7$  to phenyl. In the related system of biphenyl and biphenyl- $d_{10}$  Katon and Lippincott<sup>178</sup> have identified the two low frequency modes at  $302\text{ cm}^{-1}$  ( $-d_0$ ) and  $297\text{ cm}^{-1}$  ( $-d_{10}$ ) in the solution phase vibrational spectrum as belonging to this in-plane shear or bend, in agreement with the present designation. Unassigned low frequency vibronic bands were observed in the Shpol'skii fluorescence spectrum of biphenyl- $d_0$  and  $-d_{10}$  and 4,4'-difluorobiphenyl at, respectively, 357, 340 and  $279\text{ cm}^{-1}$  from the electronic origin.<sup>111</sup> In crystalline biphenyl (in which the molecule is planar) the corresponding bending mode appears at  $334\text{ cm}^{-1}$ .<sup>179</sup>

The strong vibronic band at  $\Delta\bar{\nu} = 520\text{ cm}^{-1}$  in 2-phenylnaphthalene can be identified with the moderately strong ones at 540 and  $510\text{ cm}^{-1}$  in the vibronic spectrum of 2,2'-binaphthyl- $h_{14}$  and  $-d_{14}$  and with the very intense band at  $513\text{ cm}^{-1}$  in naphthalene's vibronic spectrum, assigned in the latter case to the  $9a_g$  or  $8b_{3g}$  vibrational modes.<sup>98</sup> Both of these modes may be described as in-plane skeletal distortions of the naphthalene moiety; no clear choice between these two possible assignments may be made on the basis of existing evidence.

The strong band at  $770\text{ cm}^{-1}$  from the electronic origin in 2-phenylnaphthalene appears to be a companion to the bands at 800 and  $750\text{ cm}^{-1}$  in the perprotio- and perdeutero-2,2'-binaphthyls and  $768\text{ cm}^{-1}$  in naphthalene. In general terms this is best envisaged as an in-plane skeletal distortion of the ring systems. In-plane skeletal modes of both the naphthyl and phenyl groups are expected in this frequency

region, with monosubstituted benzene derivatives showing a substituent-sensitive planar deformation in the range  $620 - 830 \text{ cm}^{-1}$ .<sup>177</sup> Physically this mode is rather similar to the  $8a_g$  vibration (in-plane skeletal distortion) at  $768 \text{ cm}^{-1}$  in naphthalene. If a fundamental, the shoulder at  $1270 \text{ cm}^{-1}$  in 2-phenylnaphthalene may be the interannular stretching frequency. The counterparts for this band in the 2,2'-binaphthyls are likely the strong ones seen at  $1190 \text{ cm}^{-1}$  ( $-h_{14}$ ) and  $1150 \text{ cm}^{-1}$  ( $-d_{14}$ ). The frequencies decrease in the expected order for the increasing masses of the substituent ring systems. If 2-phenylnaphthalene is viewed as simply a monosubstituted benzene this  $1270 \text{ cm}^{-1}$  frequency is at the upper end of the usual frequency range of this X-sensitive C-X carbon-carbon stretching frequency,  $1100 - 1280 \text{ cm}^{-1}$ ,<sup>177</sup> and is nearly identical with the frequency assigned to the ring-ring stretch in biphenyl,  $1273 - 1275 \text{ cm}^{-1}$ .<sup>111,178</sup> This apparent lack of mass effect on substitution of a naphthyl group for the phenyl group in biphenyl (i.e., purely in mass terms the ring-ring stretching frequency should be lower in 2-phenylnaphthalene than in biphenyl) may arise from a commensurate increase in the force constant for that stretching mode with introduction of the naphthyl substituent. Indeed, Holloway et al.<sup>27</sup> gives the interannular force constant for 2-phenylnaphthalene as  $6.1 \times 10^5 \text{ dyne.cm}^{-1}$ , 10% greater than Westheimer's value of  $5.5 \times 10^5 \text{ dynes.cm}^{-1}$ <sup>182</sup> for the ring-ring stretch in biphenyl.

The two remaining strong bands in the Shpol'skii spectrum of 2-phenylnaphthalene at  $\bar{\nu} = 1390$  and  $1560 \text{ cm}^{-1}$ , if fundamentals, must be C-C stretching vibrations in the aromatic rings.

One should also attempt to reconcile the behaviour of 2-phenyl-



naphthalene in glassy and polycrystalline solvents at 77K. The apparent electronic origin at  $29\,340\text{ cm}^{-1}$  in the fluorescence in polycrystalline methylcyclohexane at 77K does not correspond to that observed in fluid or rigid glasses. The glassy solutions exhibit the blue component at  $30\,720\text{ cm}^{-1}$  seen on long wavelength excitation and the prominent  $29\,200$  band present at all excitation energies. In room temperature 3MP solution these are red shifted to approximately  $3.06 \times 10^4\text{ cm}^{-1}$  and  $2.89 \times 10^4\text{ cm}^{-1}$  as estimated from the oxygen quenching of the room temperature fluorescence. This non-correspondence of the electronic origins suggests that the geometry in either or both the ground or first excited singlet states is perturbed by the polycrystalline matrix itself. This should be compared with the structurally similar system, biphenyl, wherein the fluorescence origin is practically unshifted on going from polycrystalline n-heptane at 77K (0-0 at  $33\,383\text{ cm}^{-1}$ ) to a rigid 3MP glass (0-0 at  $33\,340\text{ cm}^{-1}$ ).<sup>183</sup> Biphenyl, in the ground electronic state, is known to have a twisted conformation in the vapour and solution with  $\theta = 45 \pm 15^\circ$ <sup>25,109,110</sup> in the former case and about  $20 - 30^\circ$ <sup>25,183</sup> in the latter, while the molecule is planar in the crystal.<sup>184,185</sup>

Theoretical and experimental considerations indicate that the  $S_1$  geometry of biphenyl is planar.<sup>111,155</sup> Although the  $S_0$  geometry of biphenyl is nonplanar in fluid solution this species does yield a quasilinear emission spectrum in n-heptane at 77K. For biphenyl in disordered media (3MP, fluid and glass) the ground and first excited singlet state geometries must be unaffected by temperature since the low temperature (77K) absorption and emission spectra were essentially

identical to their room temperature counterparts.<sup>25,34</sup> This observation, in conjunction with the near coincidence of the fluorescence origin in n-heptane and 3MP, points to a similar, planar geometry for  $S_1$  in the glassy and polycrystalline media. This would also imply that some relaxation from the Franck-Condon excited state geometry, i.e.,  $\theta = 20 - 30^\circ$  toward  $\theta_e = 0^\circ$  is possible within the lifetime of  $S_1$ , even in 3MP at 77K. Whether the ground state geometry of biphenyl in polycrystalline n-heptane is nearer  $\theta = 0^\circ$  or  $\theta = 30^\circ$  is not certain. The barrier for interannular rotation from  $\theta = 30^\circ \rightarrow 0^\circ$  in  $S_0$  is substantial, being estimated at about 2.5 kcal/mole ( $874 \text{ cm}^{-1}$ ) for the isolated biphenyl molecule.<sup>110</sup> The intermolecular packing forces of the lattice may overcome this barrier however, as clearly seen for crystalline biphenyl, wherein the molecular geometry is undeniably planar.<sup>184,185</sup> In the n-heptane matrix then, the biphenyl molecules may have a planar geometry prior to excitation.

The requirement of a net planar ground state geometry sometimes proposed for observation of a Shpol'skii or quasilinear spectrum probably represents only a special case of a more general phenomenon. In principle, one might expect quasilinear spectra from systems in which the solute-matrix combination is capable of restricting the distribution of emitting molecular conformations to a narrow range of twist angles. In the most common cases this arises from intramolecular restriction of the molecular geometry, typified by the inherently rigid planar aromatic hydrocarbons such as fluorene, pyrene, naphthalene, etc. For these systems the emissive state,  $S_1$ , will, of necessity, have a nearly planar geometry since excitation can likely produce only small changes

from the already planar ground state geometry. This accounts for the relatively structured fluorescence of these hydrocarbons even in fluid media. A further narrowing of the conformeric distribution (and spectral bandwidths) is made possible by orientation of the solute molecule within the ordered solvent cage of the polycrystalline environment. The presence of these isolated and oriented solute molecules is the basis of the so-called "cold gas" model for quasilinear spectra.

The  $1380\text{ cm}^{-1}$  shift in the highest energy fluorescence band at 77K from  $30\,720\text{ cm}^{-1}$  in glassy media to  $29\,340\text{ cm}^{-1}$  in the polycrystalline methylcyclohexane for 2-phenylnaphthalene indicates that the polycrystalline matrix is restricting the solute molecules to a more nearly coplanar geometry. The lack of any excitation wavelength dependence of the Shpol'skii fluorescence spectrum of 2-phenylnaphthalene further points to the involvement of a single conformeric species under these conditions. A resulting picture for the fluorescence of 2-phenylnaphthalene in a polycrystalline matrix would then be excitation of the planar ground state conformers, followed by emission from a planar excited state configuration.

#### 4.2.2 Fluorescence Quantum Yield Measurements

The relative fluorescence quantum yields of 2-phenylnaphthalene with respect to PPO are shown for 295K in cyclohexane and 3MP and for 77K in 3MP only. The fluorescence quantum yield showed no dependence on the excitation wavelength used and the values below represent means of the determinations at  $\lambda_A = 320, 300$  and  $280\text{ nm}$ . Estimated errors are similar to those encountered for 1-phenylnaphthalene.

Table 4.6

Relative Fluorescence Quantum Yields of 2-Phenylnaphthalene

Solvent	$\phi_f$		$\phi_f$ (literature)
	295K	77K	295K only
cyclohexane	0.37		0.44 <sup>a,146</sup> ; 0.26 <sup>b,186</sup>
3MP	0.33	0.38	

<sup>a</sup> relative to  $\phi_f$  (quinine sulfate) = 0.55 in 1N H<sub>2</sub>SO<sub>4</sub>.

<sup>b</sup> relative to  $\phi_f$  (9,10-diphenylanthracene) = 1.0 in cyclohexane.

#### 4.2.3 Fluorescence Decay Measurements

In marked contrast to 1-phenylnaphthalene, the fluorescence decay of 2-phenylnaphthalene in fluid or rigid solution could not be adequately described by a monoexponential process. Examination of the observed decay curve and the fitted single exponential model, Figure 4.9 , indicates a serious non-correspondence of the observed and calculated traces, particularly near the maximum in the experimental curve.

At first this "spike" in the decay profile was ascribed to Rayleigh scattered exciting light being detected optically or to spurious radiofrequency noise pick-up by the detection system, since this spike appears in the temporal region expected for these interferences, i.e., at the time of the lamp flash. Usually this spike occurred only 1 channel or 1.3 ns after the known maximum in the temporal profile of the flashlamp. Insertion of additional sharp-cut, broad band, or interference filters or use of an emission monochromator in the fluorescence light path left the relative contribution of this spike to the total decay intensity largely unaltered, as did changes in the excitation

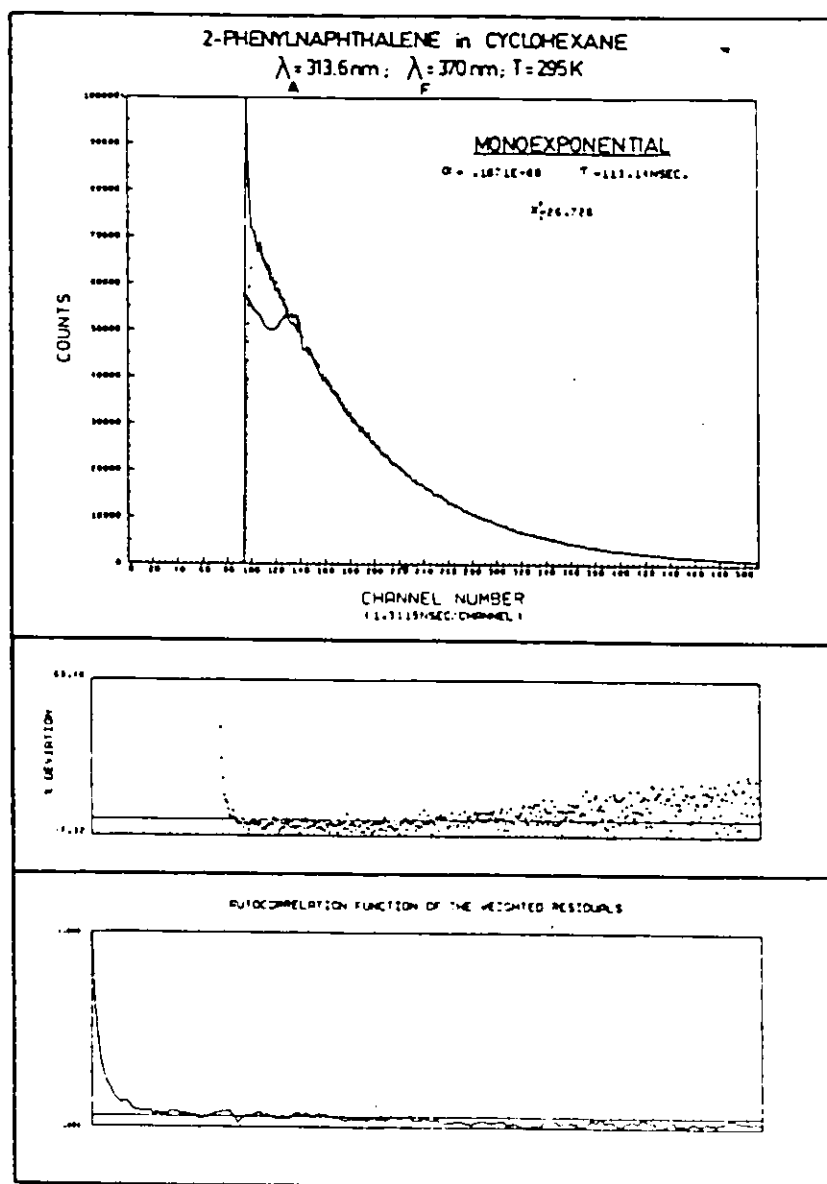


Figure 4.9

Observed and Fitted Monoexponential Fluorescence Decay Curve for  
 $10^{-4}\text{M}$  2-Phenylnaphthalene in Cyclohexane at 295K Showing  
 Presence of Short-lived Component

and emission bandpasses. This short component was unaffected by changes in solvent (methylcyclohexane, cyclohexane, 3MP) and geometry (cylindrical or rectangular fluorescence cells). Significantly, the lifetime standards for this long timebase, pyrene and naphthalene gave normal (i.e., mono-exponential) decay curves under the same conditions. Improved radio-frequency shielding and increased START and STOP discriminator levels in no way diminished this spike in the 2-phenylnaphthalene decay.

In light of these precautions one is forced to conclude that the extremely short component in the 2-phenylnaphthalene decay is genuinely fluorescence occurring in conjunction with an energetically similar but much longer lived major component. Under the conditions of extremely low photon flux used in the lifetime measurements Raman scatter from the solvent is entirely precluded, in addition to being spectrally restricted to frequency differences of about  $3000\text{ cm}^{-1}$  from the exciting light for hydrocarbon solvents. For example, excitation at 315.9 nm could potentially produce a Raman line ca. 347 nm only.

Owing to the enormous difference between the lifetimes of the two contributions,  $\tau_1 \sim 1\text{ ns}$  and  $\tau_2 > 100\text{ ns}$  the observed decay curve resisted most attempts to simultaneously extract both decay parameters by the method of reiterative convolution. Computationally the method usually failed due to excessively large negative arguments ( $\tau_1$  too small) in the exponent term during the search algorithms. Very occasionally a change in the initial guesses for the four parameters  $\alpha$ ,  $\tau_1$ ,  $\beta$  and  $\tau_2$  permitted successful deconvolution to be achieved. This two component decay of 2-phenylnaphthalene points out the inherent limitations of the data reduction method; although this problem is nearly

intractable by reiterative convolution techniques this method is, nonetheless superior to all current alternative approaches such as the method of moments, Laplace or Fourier transforms or modulating functions.<sup>59</sup>

A good estimate of the large component  $\tau_2$  could be obtained by deconvoluting as a monoexponential decay, starting the fitting only a few channels (5 - 10) past the maximum. By this point, 5 - 15 ns after the lamp flash, the intensity of the short component had become negligible and the decay closely resembled that of  $\tau_2$  above. By a judicious choice of experimental conditions it was possible to obtain the long decay component almost exclusively (see Figure 4.9). With excitation below 300 nm the amount of species or component 1 ( $\tau_1 \sim 1$  ns) produced was small, with progressively larger contributions from 1 as  $\lambda_A$  was moved from 300 to 337.1 nm.

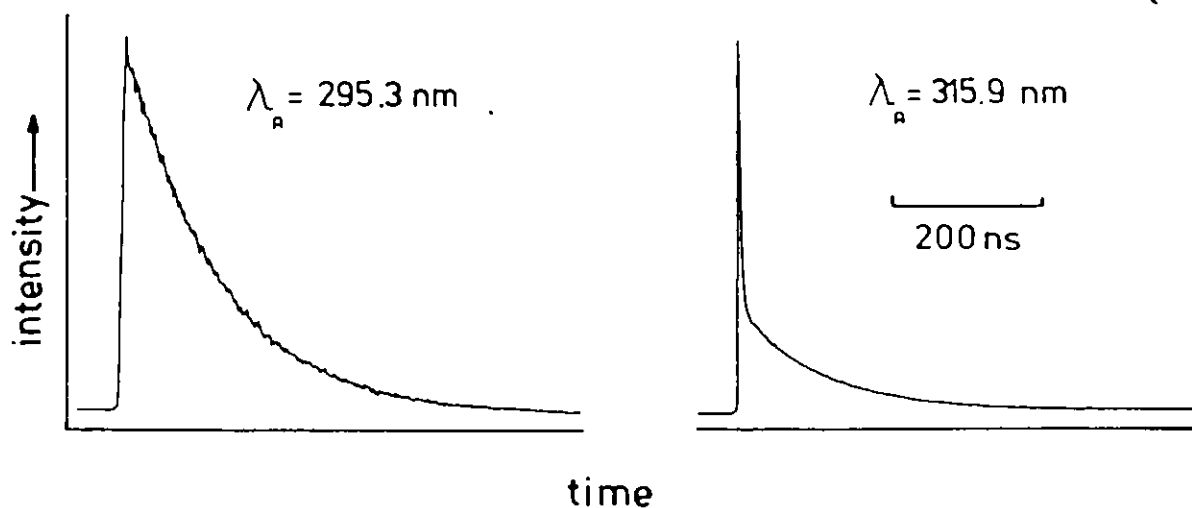


Figure 4.10

Excitation Wavelength Dependence of Observed 2-Phenylanthracene  
Fluorescence Decay in 3MP at 295K;  $\lambda_F = 360.0$  nm in both cases

Excitation at  $\lambda_A < 300$  nm gave decay curves that showed little visible evidence of the early spike seen at 310 nm and above although the presence of a second component was often betrayed by the moderately poor reduced chi squared values obtained, usually  $\chi^2_v = 3 - 6$  if  $\lambda_A$  was 295.3 or 297.7 nm. Attempts to fit those decay curves obtained at  $\lambda_A > 310$  nm to a single exponential function over the entire profile gave  $\chi^2_v$  values of 20 - 200.

The lifetimes extracted for the long component only are indicated in the accompanying table.

Table 4.7  
Fluorescence Lifetimes of the Long Lived Component of  
2-Phenylanthracene in Dilute Solution<sup>a</sup>

Solvent	Temperature	$\tau_2$ (ns)	$\tau$ (literature) (ns)
Cyclohexane	295K	$116.8 \pm 1.0^b$	$114^{34}$ ; $110^{146}$
3MP	295K	$113.8 \pm 1.9^c$	
	77K	$134.7 \pm 1.1^d$	

<sup>a</sup> Concentration  $\sim 10^{-4}$  M.

<sup>c</sup> Mean of 8 trials.

<sup>b</sup> Mean of 5 trials.

<sup>d</sup> Mean of 5 trials.

A crude estimate for the decay time of the short lived component was obtained in several experiments, with values ranging from 0.64 ns to 1.44 ns, with a mean of  $0.9 \pm .4$  ns. Given the large uncertainty it is not known if  $\tau_1$  is solvent or temperature dependent. The relative contributions of the two fluorophores to the fluorescence emission can



be estimated by the quantity  $\alpha\tau_1/\beta\tau_2$  which is found to vary from .008 to .364, depending on the choice of excitation and emission wavelengths. It should be emphasized that these numbers do not indicate directly the ground state fractions of each species as the relative quantum yields and absorbances of the individual species remain unknown.

The oxygen quenching of the steady state fluorescence of 2-phenylnaphthalene (Section 4.2.1a) was incidentally confirmed by fluorescence decay measurements on "old" samples of 2-phenylnaphthalenes. With samples more than several weeks old it was noticed that slow air leakage across the Teflon stopcocks led to a small reduction in  $\tau_2$  to  $\sim 90 - 100$  ns, while the relative contribution of the short component to the total emission intensity increased markedly. This may be ascribed to the preferential quenching of the quantum yields and hence intensities in the ratio of about  $\tau_2/\tau_1$  or  $\sim 100:1$ . The same sample, when freshly degassed and measured under otherwise identical experimental conditions showed a definite decrease in the relative contribution of the short lived species to the observed decay profile.

Quantitative measurements were not possible, owing to the already short lifetime of species 1.

The only other direct measurement of the 2-phenylnaphthalene lifetime was by Berlman,<sup>34</sup> who arrived at a value of 114 ns in cyclohexane, in good agreement with  $\tau_2$ . His failure to detect the short component in the fluorescence decay is not surprising in view of the experimental conditions he employed: excitation at 304 nm, with no monochromation of the fluorescence. Indeed, in the original configuration of his lifetime system, using a D<sub>2</sub> excitation source ( $\lambda_A < 300$  nm) and

colour filtering of the fluorescence this present author also failed to detect the short component.

#### 4.2.4 Analysis and Discussion of the Photophysics of 2-Phenylnaphthalene

A full kinetic treatment of the photophysics such as that given for 1-phenylnaphthalene is not possible for the 2-phenylnaphthalene since individual values of the fluorescence quantum yields for the principal species 1 and 2 are not available. The emission and decay experiments indicate that species 2 predominates, while the observed lack of dependence of  $\phi_f$  on the excitation wavelength for 2-phenylnaphthalene suggests the approximation of the quantum yield for species 2 by the net observed quantum yield. Table 4.8 was calculated on this basis, namely  $\phi_f(2) \sim \phi_f$ .

Table 4.8

Radiative Lifetimes and Radiative and Nonradiative Rate Constants  
for the Long Lived Component in 2-Phenylnaphthalene

Solvent; Temperature	$\tau_0 = \tau/\phi_f$ (ns)	$k_f = 1/\tau_0$ (s <sup>-1</sup> )	$k_f^0 = k_f/n^2$ (s <sup>-1</sup> )	$k_{nr}$ (s <sup>-1</sup> )
Cyclohexane; 295K	316	$3.2 \times 10^6$	$1.6 \times 10^6$	$5.4 \times 10^6$
3MP; 295K	345	$2.9 \times 10^6$	$1.5 \times 10^6$	$5.9 \times 10^6$
3MP; 77K	354	$2.8 \times 10^6$	$1.3 \times 10^6$	$4.6 \times 10^6$

The corrected radiative rate constant,  $k_f^0$  is seen to be approximately independent of temperature and solvent within the limits of uncertainty imposed by the quantum yield measurements.

A value of the total quantum yield of triplet formation at 25°C

in cyclohexane is available from the literature, with  $\phi_T = 0.43 \pm 15\%$ .<sup>147</sup> In conjunction with the net quantum yield of fluorescence, 0.37 under these conditions, one may calculate the total fraction of internal conversion from

$$\phi_{ic} = 1 - \phi_f - \phi_T \quad (4.14)$$

which on substitution gives  $\phi_{ic} = 0.20 \pm 0.12$  or  $k_{ic} = 1.7 \pm 1.0 \times 10^6 \text{ s}^{-1}$ . This is small, but non-zero, perhaps indicative of the competition between radiative and nonradiative processes for the intrinsically long lived component 2 in 2-phenylnaphthalene. Internal conversion in 2-phenylnaphthalene may also have a contribution from interconversion between the excited singlet states identified as 1 and 2.

The accumulated evidence of both the emission and decay experiments strongly supports the contention of Wharton and Hughes et al.<sup>25</sup> that 2-phenylnaphthalene in solution may exist as two or possibly more emissive conformers, which differ principally in their angular rotation about the interannular C-C bond. The finer spectroscopic details of this present work are somewhat at variance with those of the earlier workers however.

Theoretical and experimental evidence points to an equilibrium ground state configuration for 2-phenylnaphthalene wherein the phenyl and naphthyl rings are slightly twisted with respect to one another. Qualitatively it would be expected that this twist angle,  $\theta$ , should be smaller for the 2-phenyl isomer than for 1-phenylnaphthalene, as the nonbonded hydrogen-hydrogen steric repulsions are lower in the former molecule.

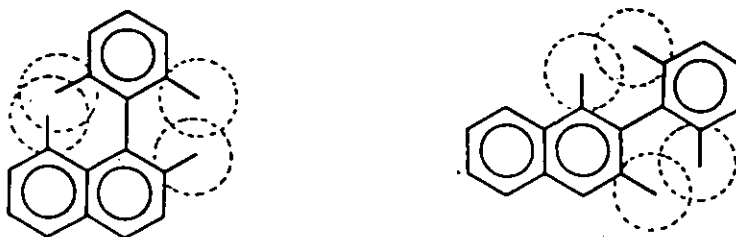


Figure 4.11

Steric Interactions of Nonbonded Hydrogens in 1- and 2-Phenyl-naphthalene; broken circles represent Van der Waals radii for hydrogen

This is borne out by the experimental value,  $20^\circ$ ,<sup>151</sup> and the theoretical ones of  $23^\circ$ ,<sup>153</sup>  $30^\circ$ ,<sup>26,27,175</sup> and  $34^\circ$ .<sup>152</sup> In all cases the uncertainty is large since the minimum is broad and shallow from about  $0^\circ$  to  $40^\circ$ . For 2-phenylnaphthalene the small local maximum at  $\theta = 0^\circ$  is estimated to be no more than 0.7 kcal/mole ( $\sim 230 \text{ cm}^{-1}$ ) above the minimum at  $\sim 30^\circ$ <sup>27</sup> so that at 295K and 77K an appreciable fraction of molecules could have configurations approaching coplanarity.

These calculations by Holloway et al<sup>27</sup> indicate that even at 77K the fraction of  $0^\circ$  conformers should be 1 - 2% of those with the  $30^\circ$  conformation. At angles  $30^\circ \rightarrow 90^\circ$  the ground state potential function rises much more steeply, with the  $\theta = 60^\circ$  conformation lying  $\sim 1600 \text{ cm}^{-1}$  above the  $\theta = 30^\circ$  minimum. Accordingly, the number of conformers in  $S_0$  having  $\theta = 60^\circ$  will be vanishingly small at 77K or at 295K.

The stabilization of 2-phenylnaphthalene in a coplanar configuration by the intermolecular forces in the methylcyclohexane matrix is thus entirely understandable in view of the comparatively

small intramolecular stabilization afforded for the  $\theta = 30^\circ$  ground state conformation.

Like the related biphenyls and polyphenyls<sup>155</sup> 2-phenylnaphthalene is believed to have a minimum near  $\theta = 0 - 1^\circ$  in the first excited singlet state.<sup>153,175</sup>

The predominance of species 2 in the fluorescence emission and the longevity of this species suggests that this must represent an equilibrated, relaxed excited state, i.e., conformer 2 represents an absolute minimum on the excited singlet potential energy surface. Excitation of species 2 occurs with all excitation wavelengths but is favoured relative to species 1 at shorter excitation wavelengths. The emission of this relaxed conformer is found at slightly lower energy than that from the less relaxed, short lived species 1, with the band at 354.6 nm (28 200 cm) in rigid solution and at 358.6 nm (27 890 cm<sup>-1</sup>) in fluid media evincing most clearly the contribution of species 2 emission.

The appearance of a strong species 1 component in the fluorescence emission and decay at wavelengths above 300 nm and the short lifetime of this fluorescence suggests that this component arises from excitation of near-planar ground state conformers, followed by prompt emission from a Franck-Condon (unrelaxed) excited state. This planar or near-planar excited state may not represent the absolute minimum of the upper singlet state surface although a minimum has been calculated near  $0^\circ$ <sup>27,153</sup>; rather this may be a local minimum, with the absolute minimum for  $S_1$  being located at some larger dihedral angle. A semi-qualitative model accounting for the observed emission, excitation

and decay behaviour of 2-phenylnaphthalene in 3MP is pictured below.

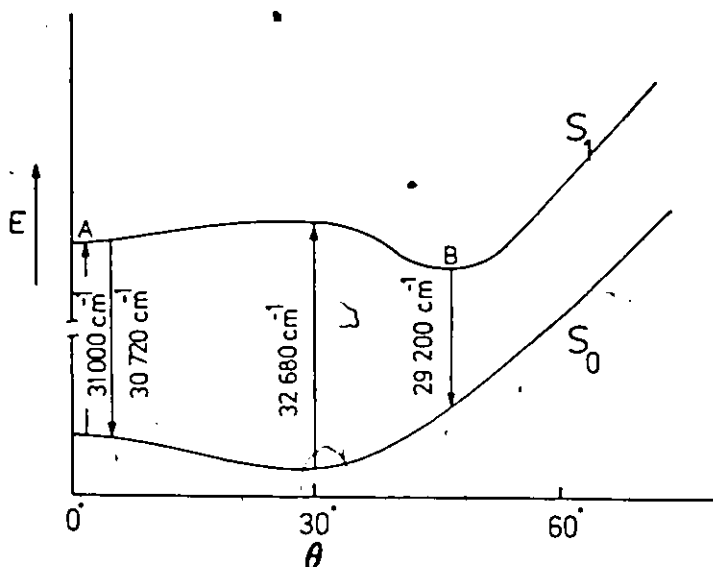


Figure 4.12

Proposed Singlet State Potential Energy Diagram for  
2-Phenylnaphthalene in 3MP at 77K

The bulk of the absorption at  $32\,680\text{ cm}^{-1}$  corresponds to excitation of the  $\theta \sim 30^\circ$  ground state conformers directly to the  $S_1$  surface. The low energy absorption at  $\sim 31\,000\text{ cm}^{-1}$  excites only those conformers having nearly coplanar configurations. No long wavelength absorption by ground state conformers with interannular angles appreciably greater than  $30^\circ$  will be expected because of the insignificant population of such conformers (Figure 4.12 is drawn with the  $S_0$  potential rising steeply for  $\theta > 30^\circ$ ).

Molecules prepared at point A on the upper surface may suffer a number of fates: internal conversion back to  $S_0$ ; intersystem crossing to a triplet state; radiative return to the electronic ground state,

this process perhaps giving rise to the fluorescence originating at 325.5 nm ( $30\,720\text{ cm}^{-1}$ ); torsional relaxation towards the absolute minimum, B, on this potential surface. The extremely short fluorescence lifetime of these molecules points either to very efficient radiative return to  $S_0$  or to very fast nonradiative depletion of this state. The former proposal would require an extremely large oscillator strength for this transition and hence a high quantum yield and intensity.

Since this short lived emission is not dominant this second alternative is to be favoured. For fast conversion  $A \rightarrow B$  the barrier must be quite low. Figure 4.12 envisages this as occurring along a purely torsional coordinate although this need not be strictly accurate. Pure A emission could not be obtained even on low energy excitation, so a very small excess of excitation energy was evidently capable of effecting the conversion from A to B. This conversion implies that rotation of the phenyl substituent about the interannular bond is rapid, even in the moderately viscous 3MP at 77K. The minimum at B must be lower than that at A, with the emission from B to the ground state occurring at slightly longer wavelength than the  $A \rightarrow S_0$  emission. The long lifetime of the molecules at B may be attributable to the higher activation barrier for  $B \rightarrow A$  conversion and to a low transition probability for the  $B \rightarrow S_0$  radiative transition, a possibility suggested by Gustav's study.<sup>153</sup>

While this proposed potential energy scheme may not be the only explanation of the observed emission, excitation (absorption) and decay behaviour it does account for a number of the major features. Any proposal calling for a single minimum for  $S_1$  in the interval  $0 < \theta < 90^\circ$

(2-phenylnaphthalene, like the 1-phenyl isomer will have potential functions symmetric about  $\theta = 90^\circ$ ) must be discounted, since two components are present in fluorescence decay even at room temperature, where torsional relaxation will be fast. A single  $S_1$  minimum would then give emission only from the relaxed, equilibrium configuration and so the fluorescence decay at room temperature would be expected to be monoexponential, not biexponential as seen.

The possibility that the ground state potential has two minima at between 0 and  $90^\circ$  cannot be entirely discounted, though no strong evidence favours this possibility over the single minimum case.

Certainly no fast equilibrium can exist between the excited state conformations even at room temperature, since this would necessitate the emission components decaying with a common lifetime, as seen for the "high temperature" behaviour of excimer or exciplex kinetics.<sup>82,83</sup>

Although the upper state ( $S_1$ ) potential function is described as deriving from a single electronic state with two minima, this surface may also be pictured as arising from the crossing, or rather the avoided crossing of the potential functions of two different and closely lying excited singlet states. Orlandi and Siebrand<sup>187</sup> have set forth such a model for the upper singlet surface of trans-stilbene as a function of the double bond twist angle,  $\omega$ . Their potential energy diagram for trans-stilbene is shown in Figure 4.13, with the avoided crossing of the upper states  $^1A_g$  and  $^1B_u$  leading to a double minimum in the upper singlet surface as a function of twist angle. Gustav's calculations indicate two close lying excited singlet states for 2-phenylnaphthalene too.<sup>153</sup> Recently Riley and coworkers<sup>190</sup> have



described a double minimum of the excited singlet surface of 1,1'-binaphthyl in terms of the avoided crossing of two excited singlet states of different symmetry. These differences in describing the upper surface would appear to be largely a question of semantics or definition.

Photoisomerization studies on trans-stilbene indicate that only  $\sim 1\%$  of the twisted ( $\omega = 90^\circ$ ) form is present in the excited state at 90K.<sup>188</sup> For 2-phenylnaphthalene in solution the torsional barrier will be lower, since rotation about a quasi-single bond, not a double bond is involved. In view of the 1% estimate for  $\omega = 90^\circ$  trans-stilbene, it is not surprising that some significant emission is seen from both the planar and twisted forms of 2-phenylnaphthalene at 77K. Furthermore, as seen in Figure 4.12 or similar schemes, the majority of molecules would require only small angular displacements to reach either minima at A or B following excitation into the initial Franck-Condon excited state at  $\theta \sim 30^\circ$ , in contrast to the  $90^\circ$  rotation required in the trans-stilbene scheme.

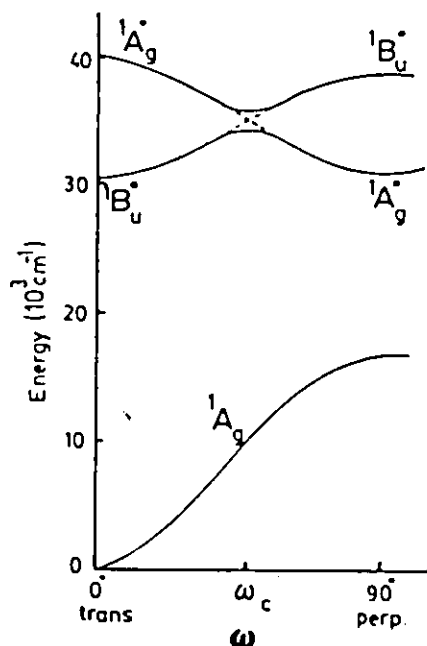


Figure 4.13

Potential Energy Diagram of Ground and Two Lowest Excited Singlet States of Trans-Stilbene as a Function of Rotation Angle,  $\omega$ , about Double Bond<sup>188,189</sup>

CHAPTER FIVE  
PHOTOPHYSICS OF THE BINAPHTHYLS

5.1 Photophysics of 1,1'-Binaphthyl

5.1.1 Fluorescence Emission and Excitation Spectroscopy

The fluorescence emission and excitation spectra of 1,1'-binaphthyl in solution at 77K and 295K are shown in Figure 5.1. Within experimental error these spectra showed no dependence on the excitation or emission wavelengths respectively. Solvent effects were negligible too, with identical spectra being obtained in cyclohexane, 3MP, isopentane or 2-methyltetrahydrofuran (2-MTHF) at 295K and in the last three named solvents at 77K.

In fluid media at 295K the excitation and emission spectra were broad and structureless, with maxima at 302 and 360.5 nm respectively. On cooling to 77K in any of the three glass-forming solvents, 3MP, 2-MTHF or isopentane, the excitation spectrum remained broad and essentially unshifted, with the maximum still at 302 nm ( $33\,110\text{ cm}^{-1}$ ). Some structure did become evident in the low temperature excitation spectrum with distinct peaks being resolved at 312.2 nm ( $32\,030\text{ cm}^{-1}$ ) and 320.9 nm ( $31\,160\text{ cm}^{-1}$ ), the latter peak probably being the 0-0 in absorption.

The change in the fluorescence emission spectrum on cooling was more dramatic, with the maximum shifting fully  $1780\text{ cm}^{-1}$  to higher energy, lying at 338.8 nm ( $29\,520\text{ cm}^{-1}$ ) at 77K. Owing to the breadth of the room temperature emission it was impossible to accurately assess the shift in the 0-0 in fluorescence on cooling to 77K. The emission

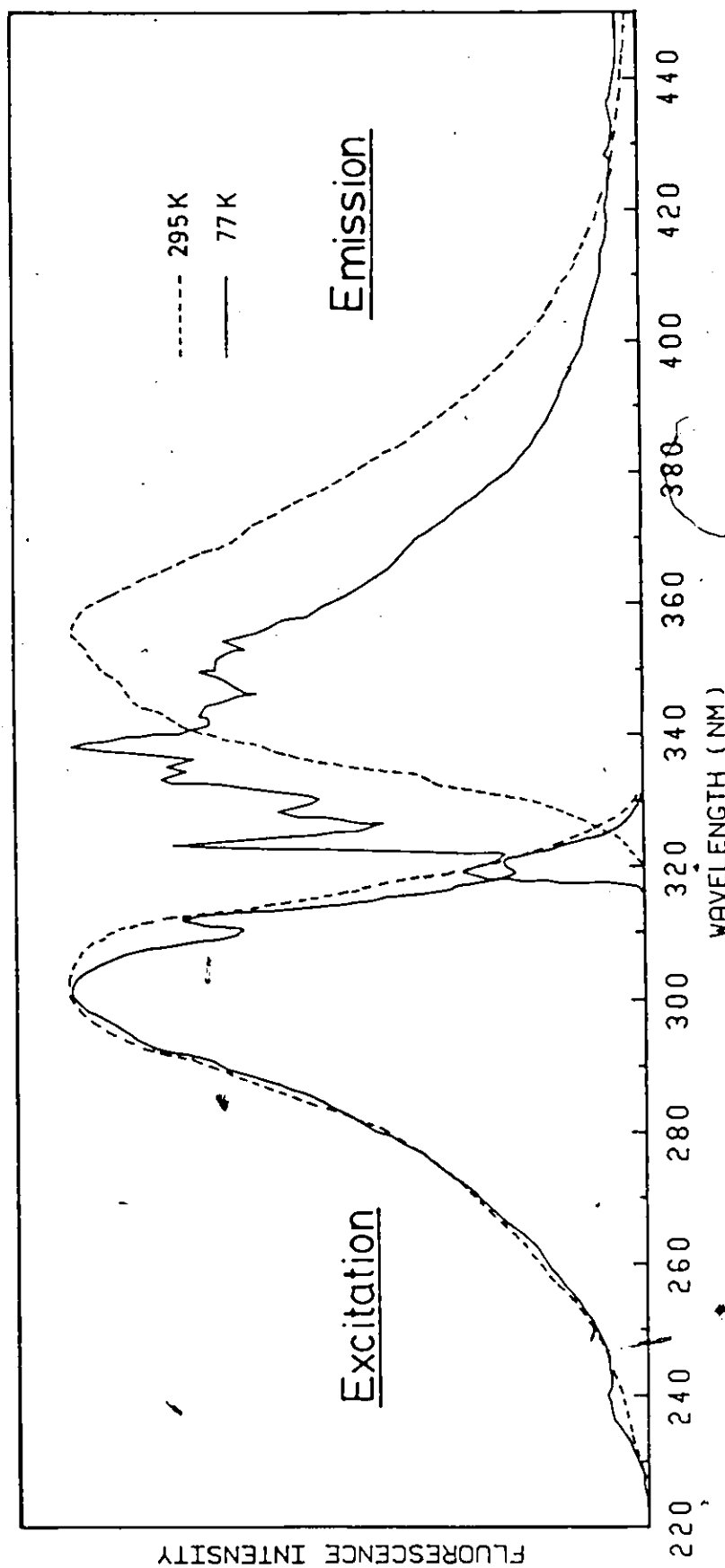


Figure 5.1

Fluorescence Emission and Excitation Spectra of Dilute Solutions of 1,1'-Binaphthyl at 295K and 77K

spectrum of 1,1'-binaphthyl at liquid nitrogen temperatures is also much more structured, with 10 bands plainly discernible, with the breadth of some approaching a mere  $50 \text{ cm}^{-1}$  at half-maximum. This behaviour has been previously noted and studied by several authors.<sup>24,191</sup> Table 5.1 summarizes the vibrational details of the 77K fluorescence spectrum of 1,1'-binaphthyl and additionally shows the striking resemblance to the vibrational structure of the naphthalene quasilinear spectrum, a relationship first pointed out by Hochstrasser.<sup>24</sup> The analysis shown in this table is in general agreement with Hochstrasser's work although the binaphthyl frequencies differ slightly and a more recent and comprehensive survey of the naphthalene vibronic spectrum has been employed for comparison.<sup>98</sup>

The fluorescence origin of 1,1'-binaphthyl at 77K is red-shifted only  $\sim 420 \text{ cm}^{-1}$  from the 0-0 in fluorescence of naphthalene, indicating that the  $\pi$ -electronic interaction between the constituent naphthalene chromophores in 1,1'-binaphthyl must be small; this will be the case if the naphthyl moieties are mutually perpendicular or nearly so.

This new, structured, higher energy emission at 77K cannot be ascribed to precipitation or aggregation of the solute at low temperature since the emission of crystalline 1,1'-binaphthyl is known to be much further to the red, with the maximum at 373 nm.<sup>192,193</sup>

This author found that, like 1-phenylnaphthalene, (and unlike the 2-phenylnaphthalene), 1,1'-binaphthyl did not give a quasilinear spectrum in polycrystalline matrices at 77K. Over the concentration range  $10^{-3}$  -  $10^{-5} \text{ M}$  the emission bands in n-pentane, n-hexane, n-heptane,

Table 5.1

Vibrational Structure in the Fluorescence Spectrum of  
1,1'-Binaphthyl and Naphthalene<sup>a</sup> at 77K

1,1'-Binaphthyl			Naphthalene <sup>a</sup>			Analysis	
Intensity <sup>b</sup>	$\lambda$ (nm)	$\bar{\nu}(\text{cm}^{-1})$ $\pm 10\text{cm}^{-1}$	$\Delta\bar{\nu}(\text{cm}^{-1})$ $\pm 20\text{cm}^{-1}$	Intensity <sup>b</sup>	$\bar{\nu}(\text{cm}^{-1})$ $\pm 10\text{cm}^{-1}$	$\Delta\bar{\nu}(\text{cm}^{-1})$ $\pm 20\text{cm}^{-1}$	Naphthalene ; 1,1'-Binaphthyl
s	319.2	31 330	0	s	31 746	0	0-0 ; 0-0
vvs	323.8	30 880	450	vvs	31 233	513	8b <sub>3g</sub> or 9a <sub>g</sub> ; 450
s	328.5	30 440	890	vs	30 809	937	7b <sub>3g</sub> ; 890
s	333.8	29 960	1370	m	30 366	1380	5a <sub>g</sub> ; 1370
s,sh	335.5	29 810	1520	m	30 121	1625	3b <sub>3g</sub> ; 1520
vs	338.8	29 520	1810	s	29 858	1888	1380+513 ; 1370+450
s	343.8	29 090	2240	ms	29 436	2310	937+1380 ; 890+1370
s,broad	350.5	28 530	2800	ms	28 921	2825	937+1380+513 ; 890+1370+450
	354.5	28 210	3120	s	28 473	3275	513+2x1380 ; 450+2x1370
w,broad	369.0	27 100	4230	ms	27 360	4386	1625+2x1380 ; 1520+2x1370

<sup>a</sup> naphthalene in n-pentane at 77K, ref. 98.

<sup>b</sup> s=strong; m=moderate; w=weak; v=very; sh=shoulder.

n-octane, cyclohexane and methylcyclohexane were, if anything, broader than those obtained in glassy media. Very recently, Riley and co-workers<sup>190</sup> have reported structured vibronic spectra for dilute ( $5 \times 10^{-5} \text{M}$ ) solutions of 1,1'-binaphthyl in polycrystalline n-pentane at 4.2K. The failure to obtain such structured emission in this present work is possibly attributable to the higher temperatures used; at liquid nitrogen temperatures it is possible that low frequency torsional motions of the solute molecule are still sufficiently active to cause broadening of the emission bands and consequent loss of detail.

More importantly, Riley et al report the selective excitation of two vibronic subspectra, each arising from a distinct ground state torsional conformer of 1,1'-binaphthyl in the n-pentane matrix.<sup>190</sup> With high excitation energies ( $\lambda_A = 290 \text{ nm}$ ) the fluorescence of a relatively twisted ground state conformer is excited, with an electronic origin at  $31\,767 \text{ cm}^{-1}$  (314.8 nm) while upon lower energy excitation at 340 nm a fluorescence spectrum with a 0-0 at  $26\,917 \text{ cm}^{-1}$  (371.5 nm) is observed. Riley and coworkers attributed this long wavelength emission to a more nearly planar conformation of the 1,1'-binaphthyl solute.

The high energy (314.8 nm) fluorescence seen by Riley undoubtedly corresponds to the fluorescence from glassy solutions at 77K, where the origin is likely 319.2 nm. No evidence of the much longer wavelength fluorescence was discovered for the glassy solutions however, despite variation of the excitation energy. The energy difference between the origins of these fluorescences,  $4850 \pm 10 \text{ cm}^{-1}$  (13.9 kcal/mole) would then represent the sum of the differences in ground state and excited state minima for the two conformers. This is

much larger than the  $1050\text{ cm}^{-1}$  difference estimated by Hochstrasser. The high energy origin observed by Riley at  $31\,767\text{ cm}^{-1}$  is only  $21\text{ cm}^{-1}$  above that of naphthalene, so these authors attribute that fluorescence to 1,1'-binaphthyl molecules with dihedral angles near  $90^\circ$ , while the red-shifted emission arises from binaphthyl molecules having more nearly coplanar geometries.

The spectroscopic evidence from this present study, down to 77K, points to the possibility of a single ground state conformer for 1,1'-binaphthyl. The wavelength independence of emission and excitation spectra points to the presence of a predominant ground state conformer; from the similarity of the low temperature emission to that of naphthalene it is probable that this conformation is highly twisted. This is in accord with the experimental value in solution  $90^\circ - 110^\circ$  (circular dichroism methods) and the various calculated isolated molecule values:  $61^\circ$ ;  $194, 195^\circ$   $68^\circ$ ,  $105^\circ$ ;  $196^\circ$   $60^\circ, 120^\circ$ ;  $175^\circ$   $89^\circ$ ;  $197^\circ$   $90^\circ$   $191^\circ$ . All these indicate a large interannular angle in the ground state. In crystalline 1,1'-binaphthyl the geometry is largely dictated by the packing forces of the lattice. Recent x-ray crystallographic measurements show the existence of two molecular conformations in the solid, with the pure chiral crystal being composed of molecules with  $\theta = 103.1^\circ$  whereas the molecules in the racemic crystal have dihedral angles of  $68.6^\circ$ .  $198^\circ$  The presence of these two crystalline modifications is reasonable if the ground state potential well for 1,1'-binaphthyl is pictured as quite broad and flat over a range of dihedral angles. Such a model could explain the wide range of values found for the experimental and calculated dihedral angles.

Air and oxygen saturation resulted only in a diminution of the total fluorescence intensity without any accompanying alterations in the shape or distribution of the fluorescence emission. This lends some support to the belief that only a single species is responsible for the emission in fluid solution.

### 5.1.2 Fluorescence Quantum Yield Measurements

The fluorescence quantum yields of 1,1'-binaphthyl with respect to a PPO reference are given below.

Table 5.2  
Relative Fluorescence Quantum Yields of 1,1'-Binaphthyl

Solvent	$\phi_f$		$\phi_f$ (literature)	
	295K	77K	295K	77K
Cyclohexane	$.81 \pm .13$		$.87,^{146}$ $.70,^{123}$ $.77,^{34}$	
3 MP	$.88 \pm .08$	$.51 \pm .06$		$.70^a;^{186}$

<sup>a</sup> in absolute ethanol.

These tabulated values represent the mean of measurements with  $\lambda_A = 320, 300$  and  $280$  nm. No systematic variation with excitation wavelength was seen at 295K but the scatter was quite large for these measurements. At 77K in 3 MP  $\phi_f$  exhibited a slight increase with excitation wavelength, going from 0.46 at 280 nm to 0.49 at 300 nm and 0.58 at 320 nm. There is fair agreement between this present study and the literature at 295K but the quantum yield at 77K in 3 MP, 0.51, appears anomalously low. All other factors being equal the nonradiative



rate constants for depletion of  $S_1$  should decrease with decreasing temperature, leading to a larger, not smaller value of  $\phi_F$ . Some of this anomaly may arise from the large blue shift of the fluorescence on cooling. This would reduce the overlap of the PPO and 1,1'-binaphthyl emission curves and necessitate a different detection-response correction for the two curves, a response correction that has hitherto been considered equal for both sample and reference. The alternative possibility is that the quantum yield is truly smaller at 77K as a result of some change in the photophysics at this temperature.

### 5.1.3 Fluorescence Decay Measurements

The fluorescence decay of 1,1'-binaphthyl in dilute solution in cyclohexane, 3MP, isopentane and 2 MTHF at 295K/could, in all cases, be best described by a single exponential decay law. The reduced chi-squared parameter was generally  $\leq 1.3$  for a monoexponential fit and showed no significant improvement if fit to a biexponential decay instead. The autocorrelation function of the weighed residuals showed the residuals of the monoexponential fit to be random. Occasionally some slight improvement in  $\chi^2_v$  was noted upon biexponential fitting of the room temperature decay data but no consistent second lifetime component could be extracted from the fit to

$$I(t) = a \exp(-t/\tau_1) + b \exp(-t/\tau_2) \quad (5.1)$$

indicating that the slightly poor fit is more likely due to some transient instrumental artifact than to a genuine second fluorescent component. At these short timebases the decay measurements are experimentally more difficult and particular attention must be paid to

scattered light rejection and radiofrequency shielding. Variation of the flashlamp temporal profile can be a problem on this timescale too. The room temperature singlet lifetimes obtained by deconvolution are tabulated for the various solvents in Table 5.3. Within experimental error there is no solvent dependence of the measured fluorescence lifetimes.

Table 5.3

Fluorescence Lifetime of 1,1'-Binaphthyl in Dilute Solution at 295K;  
Fitted to a Monoexponential Decay Law

Solvent (concentration of solute moles/l)	$\tau$ (ns)	$\tau$ (literature) (ns)
Cyclohexane ( $1.6 \times 10^{-5}$ )	$3.20 \pm .18$	$3.0;$ <sup>34</sup> $3.1;$ <sup>123</sup> $2.70$ <sup>199</sup>
3MP ( $1-4 \times 10^{-5}$ )	$3.36 \pm .22$	
isopentane ( $8.5 \times 10^{-5}$ )	$3.38 \pm .21$	
2 MTHF ( $2 \times 10^{-5}$ )	$3.10 \pm .11$	$3.5$ <sup>200</sup>

The tabulated values are the means and standard deviations of from five to ten trials for each solvent, obtained at various combinations of excitation and emission wavelengths. The agreement with the literature values is good.

At 77K the fluorescence decay becomes considerably more complex, although superficial inspection of the monoexponential fit showed the single component lifetime to be nearly unaltered from its room temperature

value. Closer examination showed that, in glasses of 3MP, isopentane or 2 MTHF at 77K, the monoexponential decay model no longer adequately described the fluorescence decay of 1,1'-binaphthyl. Attempts to fit a monoexponential decay to the observed decay curves at low temperature invariably gave values of  $\chi^2_v$  of 6 - 90, with the single component lifetime varying from 3 - 7 ns, depending on the particular excitation and emission wavelengths.

Fitting a biexponential decay law to the observed curves produced a drastic improvement in the goodness-of-fit, while the decay was resolved into a major component with  $\tau_1$  about 2 - 3 ns and with  $\tau_2$  about 11 - 24 ns. These parameters are summarized in Table 5.4. These solutions were necessarily dilute ( $2 \times 10^{-5} M$ ) so the choice of useful emission and excitation wavelengths and slit widths was rather limited, with  $\lambda_A$  chosen as 315.9 nm or 295.3 nm and  $\lambda_F$  from 360 - 370 nm. The short component,  $\tau_1$ , was nearly constant in all solvents with a means of  $2.57 \pm .30$  ns while  $\tau_2$  appeared to fall into two distinct ranges of values. Excitation at 315.9 nm yielded  $\tau_2 = 12.7 \pm 1.5$  ns whereas at higher excitation energy, 295.3 nm,  $\tau_2$  was  $23.9 \pm .5$  ns. This lack of constancy for  $\tau_2$  is probably a result of the very small amount of long lived component excited with 315.9 nm radiation; this is reflected in the ratio of the preexponential factors,  $\alpha/\beta$  being 23 - 45. At these low levels of relative intensity the lifetime of the minor constituent cannot be determined with a high degree of confidence, although the values obtained under a fixed set of conditions will remain approximately constant, i.e., excitation at  $\lambda_A = 315.9$  nm and  $\lambda_F = 360 - 370$  nm will always give,  $\tau_2 \sim 13$  ns. Excitation at 295.3 nm evidently

Table 5.4

Fluorescence Decay Parameters of 1,1'-Binaphthyl in Dilute, Glassy Solution at 77K

Solvent	$\lambda_A^b$ (nm)	$\lambda_F^c$ (nm)	Biexponential Fit		$\alpha/\beta$	$\chi^2_v$	$\tau$ (ns) and $(\chi^2_v)$ for monoexponential fit
			$\tau_1$ (ns)	$\tau_2$ (ns)			
3 MP	315.9	360.0	2.20	11.77	23.5	1.06	3.27 (18.7)
	370.0	370.0	2.40	11.40	23.8	1.04	3.29 (8.2)
			$2.30 \pm .10$	$11.58 \pm .28$	$23.6 \pm .2$		
Isopentane	315.9	360.0	2.40	14.33	39.3	1.28	3.22 (37.6)
	360.0	360.0	2.13	11.61	23.5	1.07	3.17 (15.8)
	360.0	360.0	2.96	15.01	32.9	1.35	3.76 (36.5)
			$2.50 \pm .42$	$13.65 \pm 1.80$	$33.1 \pm 8.5$		
2 MTHF	315.9	360.0	2.63	11.44	36.3	1.19	3.21 (6.2)
	370.0	370.0	2.49	13.34	45.8	0.98	3.06 (11.06)
			$2.56 \pm .07$	$12.39 \pm 0.95$	$41.0 \pm 4.8$		
	295.3	360.0	2.81	24.53	11.6	1.00	6.76 (50.1)
		360.0	3.04	23.72	9.6	1.40	7.10 (88.4)
					$10.6 \pm 1.0$		
.295.3	366 <sup>d</sup>		2.65	23.58	18.6	1.54	4.98 (49.4)
			$2.83 \pm .20$	$23.94 \pm .51$			

mean of  
5 = 2.72  
+ .21 ns

<sup>a</sup> conc.  $\sim 2 \times 10^{-5}$  M.

<sup>b</sup> 0.25 m J-A monochromator, 1.0 mm slits.

<sup>c</sup> H-10 J-Y monochromator, 2.0 mm slits unless otherwise noted.

<sup>d</sup> 366 nm interference filter.

produced relatively more of the minor component,  $\alpha/\beta$  decreasing to about 11. It is expected that the value obtained for  $\tau_2$  at this wavelength is closer to the true figure, that is  $\tau_2$  is probably  $\geq 24$  ns. This problem is quite general; with reiterative deconvolution the presence of a very minor component can still be detected at levels where the actual lifetime of the component cannot be accurately extracted.

With the short lifetimes encountered for 1,1'-binaphthyl temporal instability in the light source during the data acquisition period can also produce larger relative error in the experimental lifetimes.

These low temperature decay parameters are at variance with the results of Post and coworkers.<sup>200</sup> While that group arrived at similar values for the room temperature decay of 1,1'-binaphthyl with 3.5 ns in 2 MTHF and 4.5 ns in EPA (ether/isopentane/ethanol (5:5:2 v/v)) they found the fluorescence lifetime to increase to 48 ns (2 MTHF) and 54 ns (2-methylpentane) at 77K. This present study found no evidence for such a long lived decay from the highly purified solute in any of the glass-forming solvents. While solvent impurities could explain Post's results in 2 MTHF (wherein hydroquinone or butylated hydroxytoluene are used as stabilizers) it fails to explain the result in 2MP unless the 1,1'-binaphthyl solute were itself contaminated. Post et al<sup>200</sup> also worked with solutions of 1,1'-binaphthyl about 10-fold more concentrated ( $2.8 \times 10^{-4}$  M) than this present work ( $2.5 \times 10^{-5}$  M). As this material is only sparingly soluble it is possible that their observed behaviour might be attributable to microcrystallite formation at low temperature. The microcrystallite emission spectrum should

resemble that of the bulk solid, which is known to be broad with a maximum at about 373 nm at low temperature as noted earlier.

The 77K emission spectra in this study and in Post's paper show no evidence of such a species however.

#### 5.1.4 Analysis and Discussion of the Photophysics of 1,1'-Binaphthyl

Of these simple biaryls 1,1'-binaphthyl has undoubtedly been the most extensively studied. Friedel<sup>201</sup> was the first to point out the similarity of the absorption spectrum of 1,1'-binaphthyl in fluid solution to that of naphthalene. He interpreted this resemblance to be indicative of slight interaction between the naphthalene moieties in the ground state of 1,1'-binaphthyl probably owing to a large dihedral angle between the two halves of the double molecule. This molecule has also attracted considerable attention since, by virtue of its restricted internal rotation, it is the simplest unsubstituted biaryl exhibiting optical activity.<sup>202-204</sup> The rate of thermally induced racemization of chiral 1,1'-binaphthyl in solution has been determined by a number of workers in a wide range of solvents<sup>202,205,206</sup> with the average enthalpy of racemization being  $22.0 \pm .5$  kcal/mole ( $7.69 \times 10^3$  cm<sup>-1</sup>). This figure has been nicely confirmed by the theoretical study of the configurational inversion of 1,1'-binaphthyl by Carter and Liljefors<sup>197</sup> who predicted a barrier to inversion on the trans- or anti-side of 20.4 kcal/mole ( $7.12 \times 10^3$  cm). As expected qualitatively (Figure 5.2) passage of the naphthyl rings on the cis-side was found to be energetically much less favourable, with a barrier of at least 34 kcal/mole.

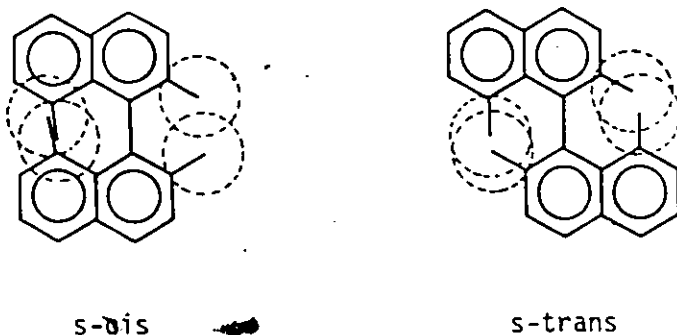


Figure 5.2

Qualitative View of Steric Restrictions for s-cis versus s-trans Racemization in 1,1'-Binaphthyl (broken circles represent Van der Waals radii for hydrogen)

These enthalpies of racemization correspond approximately to the potential energy difference between the equilibrium ground state configuration and the configuration with an interplanar angle of  $180^\circ$  as measured from the s-cis configuration as  $0^\circ$ . Figure 5.3 is drawn with the s-cis barrier of Carter and Liljefors,<sup>197</sup> the experimental racemization enthalpy and an approximate equilibrium ground state configuration,  $68 - 70^\circ$ . The minima in Figure 5.3 are intentionally drawn to be rather flat and broad since the dependence on  $\theta$  is believed rather weak over the range  $\theta = 60 - 120^\circ$ , as discussed in Section 5.1.1.

The very small shift in the fluorescence origin of 1,1'-binaphthyl at 77K from that of naphthalene ( $418 \text{ cm}^{-1}$  or 1.2 kcal) and the appearance of the typical naphthalene-like vibrational modes in the fluorescence emission of 1,1'-binaphthyl support the contention that the molecule is twisted in  $S_0$ . In the rigid glass the excited

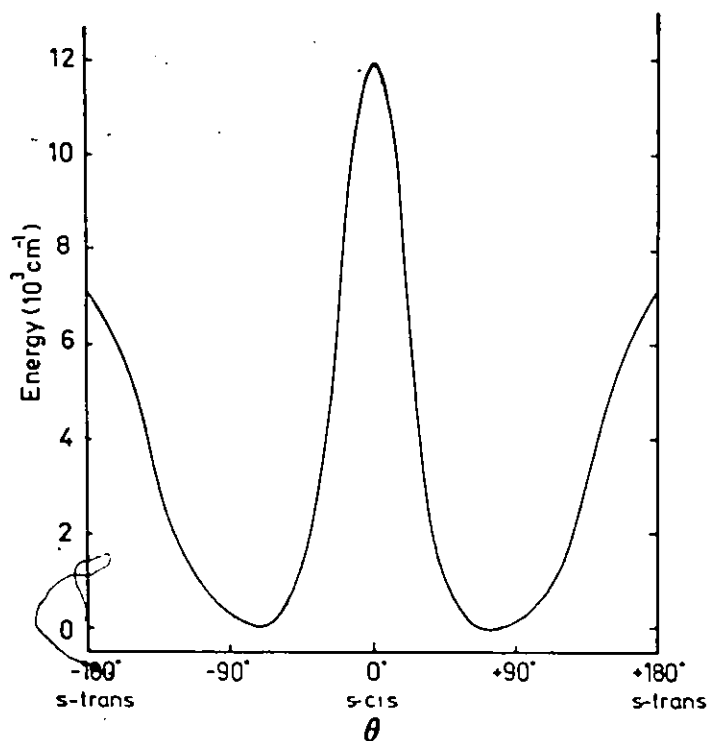


Figure 5.3

Potential Energy as a Function of Dihedral Angle for the  
Electronic Ground State of 1,1'-Binaphthyl

molecule will remain largely unrelaxed by the time emission occurs, so the geometry of the emissive state at 77K should resemble the geometry of the initial, absorptive state,  $S_0$ . In fluid solution this Franck-Condon excited state will rapidly relax towards the  $S_1$  equilibrium configuration. This equilibrium  $S_1$  configuration in fluid solution must be more coplanar than the  $S_0$  geometry, judging from the  $\sim 1800 \text{ cm}^{-1}$  red shift of the fluorescence on passing from rigid to fluid media. The large Stokes Shift,  $3000 \text{ cm}^{-1}$ <sup>34</sup>, between the emission



and absorption spectra at 295K further indicates a substantial geometry change between the emissive and absorptive states in fluid solution.

At intermediate temperatures (142K) Hochstrasser<sup>24</sup> found the fluorescence to show some vibrational details and to be blue-shifted from the room temperature maximum, though not as blue-shifted as the 77K fluorescence.

The intramolecular relaxation times for the torsional relaxation of 1,1'-binaphthyl in  $S_1$  in fluid solution have been measured directly by Shank et al<sup>207</sup> by monitoring the evolution of the  $S_1 \rightarrow S_n$  absorption of the equilibrium excited state configuration. This group found the relaxation times to be 11 - 22 ps at room temperature, with the relaxation times increasing with solvent viscosity. This direct confirmation that  $k_{\text{relax.}} \gg k_f, k_{ic}$  or  $k_{isc}$  under these conditions is proof that the electronically excited molecules will relax totally before any fluorescence emission occurs in fluid solution, thereby accounting for the observation of the purely monoexponential decay of the 1,1'-binaphthyl fluorescence intensity at room temperature.

As Hochstrasser first noted<sup>24</sup> the emission properties of 1,1'-binaphthyl can be accommodated by a model which entails the existence of a double minimum in the upper state potential energy surface. Such a double minimum may explain the appearance of the two types of fluorescence origins seen (relaxed and unrelaxed) and the appearance of a biexponential fluorescence decay at 77K. This double minimum will arise because of the asymmetric nature of the potential energy function in relation to the angle of twist between the two naphthalene rings. This asymmetry will be inherent in molecules of this type, where the s-cis conformation is energetically much less favourable than the

s-trans configuration. The qualitative shape of the  $S_1$  surface has been suggested by earlier spectroscopic work<sup>24,98,191</sup> and has been the subject of some quantitative calculations,<sup>191,194,196</sup> the most comprehensive being the elegant study of McCaskill and Gilbert.<sup>157</sup> Their calculations indicated a local minimum on the  $S_1$  surface at  $\theta = 70^\circ$  (measured with s-cis coplanar as  $0^\circ$ ) and an absolute minimum at  $\theta = 30^\circ$ . They also considered the case of  $\theta = 70^\circ$  (local minimum) and  $\theta = 110^\circ$  (absolute minimum) as possible but the latter case seems less tenable on the grounds that it would necessitate a steeper potential as  $\theta \rightarrow 180^\circ$  than as  $\theta \rightarrow 0^\circ$ , implying the dubious possibility that the s-cis conformation is of lower energy than the s-trans form. The  $S_1$  potential curve calculated by McCaskill and Gilbert is shown below.

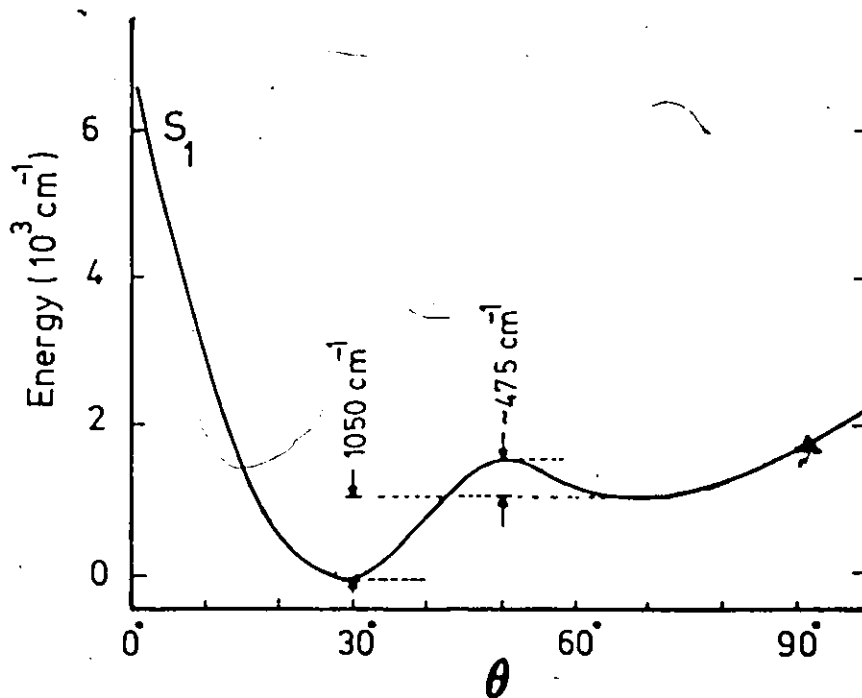


Figure 5.4

Potential Energy of First Excited Singlet State of 1,1'-Binaphthyl as a Function of Dihedral Angle; from McCaskill and Gilbert, ref. 157

The photophysics and spectroscopy of 1,1'-binaphthyl in solution may be explained with the aid of Figure 5.5.

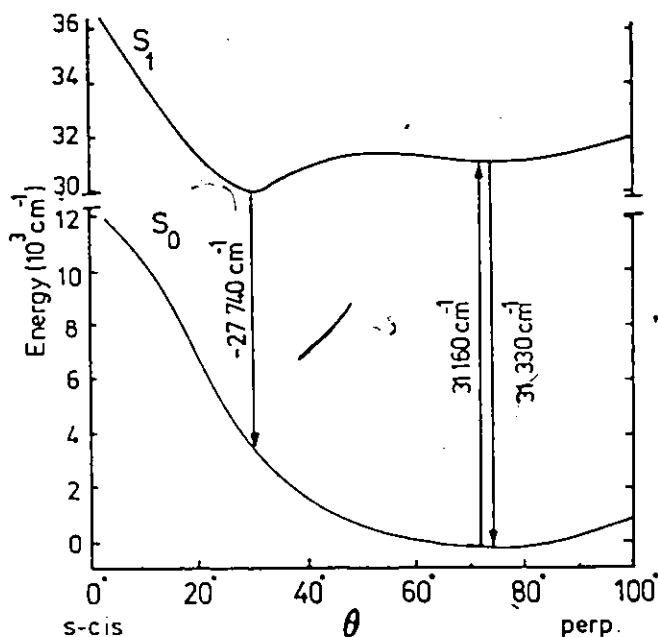


Figure 5.5

Potential Energy of  $S_0$  and  $S_1$  for 1,1'-Binaphthyl as a Function of Dihedral Angle

The geometry of the electronic ground state of 1,1'-binaphthyl at  $\theta \sim 70^\circ$  in fluid or rigid solution will be substantially unchanged immediately following excitation, producing a Franck-Condon excited state at or near  $\theta = 70^\circ$ , the local minimum on the  $S_1$  surface. This local minimum is separated from the absolute minimum by a barrier of about  $400 - 500 \text{ cm}^{-1}$ , a value which may be approximated from the difference between the 0-0 bands in emission for naphthalene and 1,1'-binaphthyl at 77K. This difference represents an upper limit for the

right hand well depth and was found to be  $480\text{ cm}^{-1}$  by Hochstrasser<sup>24</sup> and  $418\text{ cm}^{-1}$  in this study. McCaskill and Gilbert arrived at a very similar figure of  $475\text{ cm}^{-1}$ .

At low solvent viscosity, i.e., 295K, this Franck-Condon excited state will rapidly relax towards the equilibrium excited state conformation with  $\theta \sim 30^\circ$ . At this dihedral angle the  $\pi$ -electron interaction between the constituent naphthalene moieties will increase and the emission shows the expected red shift with respect to the nearly perpendicular naphthalene-like state seen in rigid solution. At high viscosity the emission will originate largely from the unrelaxed local minimum at  $\theta(S_1) \sim 70^\circ$ .

Riley and coworkers<sup>190</sup> very recent observation of an apparently dual emission in the quasilinear vibronic spectrum of 1,1'-binaphthyl in n-pentane Shpol'skii matrices at 4.2K is of considerable importance. Quasilinear spectra could not be obtained by this present author at 77K for this same system at the concentrations used by Riley, despite numerous attempts. One possible explanation is that even at 77K the torsional modes of 1,1'-binaphthyl are still sufficiently active to preclude obtaining very narrow bandwidths. Also, at these temperatures the "fit" of the 1,1'-binaphthyl molecule into the n-pentane lattice may be poor. Selective excitation was found to yield two distinct sub-spectra of 4.2K in Riley's study. At high excitation energies ( $\lambda_A = 290\text{ nm}$ ) a subspectrum with an origin band at  $31\,767\text{ cm}^{-1}$  dominates while at lower excitation energies ( $\lambda_A = 340\text{ nm}$ ) the fluorescence is chiefly from a subspectrum with an apparent 0-0 at  $26\,917\text{ cm}^{-1}$ . No such red-shifted emission was observed by this author in any solvent

at 77K, although the system starting at  $31\,767\text{ cm}^{-1}$  is probably that seen, with poorer resolution, in glassy solution at 77K. Riley ascribes these two subspectra to two conformers of 1,1'-binaphthyl, the red-shifted emission being from the coplanar conformer while the shorter wavelength fluorescence arises from a more twisted conformation of the molecule. Riley also believes both conformers to be present in the ground state, prior to excitation, so the large separation of the two electronic origins in fluorescence,  $4850\text{ cm}^{-1}$  (13.9 kcal/mole) must be the sum of the energy differences between the two conformers in the ground and excited state.

The most important point to note is that the Shpol'skii matrix does not represent a situation of thermodynamic equilibrium. If the difference,  $4850\text{ cm}^{-1}$  was evenly divided between ground and excited state, this would correspond to a ground state energy separation between the two conformers of  $\sim 2425\text{ cm}^{-1}$  or  $\sim 7\text{ kcal/mole}$ . At 4.2K or even room temperature this would dictate a vanishingly small population of the higher energy conformer, if the states were in thermal (Boltzmann) equilibrium. As Riley points out "the ground-state potential of 1,1'-BN in some media may also be a double minimum".<sup>190</sup> This second minimum is solvent induced and is not necessarily present in the purely intramolecular ground state potential function. This is not, as suggested by Riley et al, dependent on solvent polarity, since the nonpolar hydrocarbon glasses behaved identically to the polar glasses, ethanol and 2-MTHF, at 77K.

The likely explanation is that the 1,1'-binaphthyl molecules may occupy, or be forced to occupy the substitutional lattice sites in

n-pentane in two distinct manners. Being a large molecule it seems reasonable that the 1,1'-binaphthyl molecule may span two adjacent substitutional sites in the n-pentane matrix, in one case with the naphthalene moieties being nearly coplanar (the  $26\,917\text{ cm}^{-1}$  emission) while in the other case the two naphthyl groups are mutually perpendicular ( $31\,767\text{ cm}^{-1}$  emission). The low energy fluorescence seen by Riley is surprisingly red-shifted, even for a completely coplanar conformation of the molecule. The rigid planar binaphthyl analog 1,2,7,8-dibenzofluorene has its 0-0 in fluorescence and absorption at  $28\,030\text{ cm}^{-1}$ , fully  $1113\text{ cm}^{-1}$  to the blue of the low energy emission seen by Riley. The absorption spectrum of the planar methylene-bridged 1,1'-binaphthyl analog, 3,4,5,6-dibenzofluorene<sup>121</sup> indicates that the electronic origin of that molecule lies at about  $360.0\text{ nm}$  ( $27\,780\text{ cm}^{-1}$ ), still to the blue of the long wavelength emission in Riley's spectra. This does seem to raise the suspicion that the long wavelength component at  $26\,917\text{ cm}^{-1}$  in the 1,1'-binaphthyl fluorescence might be from a higher condensed hydrocarbon impurity.

The fluorescence lifetime and quantum yield found at ambient temperatures must be those of the equilibrium excited state conformation of 1,1'-binaphthyl. From these data the radiative lifetime and radiative and nonradiative rate constants at 295K may be calculated. At 77K the dominant species, as judged from the relative contributions to the fluorescence decay, would appear to be the species characterized by  $\tau_1 \sim 2.6\text{ ns}$ . Hence the structureless emission seen in the low temperature glasses, originating at  $31\,328\text{ cm}^{-1}$ , must correlate with this same species. The minor, longer lived decay component, in all likelihood, arises via

Table 5.5

Radiative Lifetimes and Radiative and Nonradiative Rate Constants  
for 1,1'-Binaphthyl at 295K

Solvent	$\tau_0 = \tau/\phi_f$ (ns)	$k_f = 1/\tau_0$ (s <sup>-1</sup> )	$k_f^0 = k_f/n^2$ (s <sup>-1</sup> )	$k_{nr}$ (s <sup>-1</sup> )
Cyclohexane	4.0	$2.5 \times 10^8$	$1.2 \times 10^8$	$6.2 \times 10^7$
3 MP	3.8	$2.6 \times 10^8$	$1.4 \times 10^8$	$3.7 \times 10^7$

emission from partially relaxed states. Variation of the excitation energy may, to some small extent, dictate the degree of torsional relaxation possible in the glassy matrix. At higher excitation energies the excess vibrational energy may be sufficient to induce some local heating of the matrix, allowing crossing of the upper state potential barrier. This would be in keeping with the observation that increasing the excitation energy increased the relative amount of lifetime component 2. Such a variation with  $\lambda_A$  may partially explain the variation in the experimental values of  $\tau_2$ , since this observed lifetime would reflect only in an average way the lifetimes of the wealth of contributing states, differing in their degree of torsional relaxation. The second lifetime component,  $\tau_2$ , should not be explicitly identified with the equilibrium conformation of the excited state at  $\theta \sim 30^\circ$  since the purely radiative lifetime of that state should be no longer than about 4 ns, a number derived from the room temperature lifetime and quantum yield.

The net fluorescence quantum yield at 77K must then be a

weighted average of the quantum yields of the emitting species and as such may show some dependence of  $\lambda_A$ . Indeed, the relative fluorescence quantum yield of 1,1'-binaphthyl was found to show a slight systematic increase with increasing excitation wavelength, going from 0.46 at 280 nm, 0.49 at 300 nm to 0.58 at 320 nm. Such a trend seems reasonable qualitatively, as increasing excitation energy would be expected to enhance the nonradiative depletion rate via torsional relaxation.

Since a second component was observable in the fluorescence decay it should also be present in the steady state fluorescence spectrum. No obvious wavelength effect or second component was in fact seen in the fluorescence spectrum. This disparity may be explained by the small absolute amount of second component present. The second component will also have a broad and structureless emission since a large number of emitting species constitute the second emission component. These conformations must not be substantially different from the geometry of the principal Franck-Condon emissive state at  $\theta \sim 70^\circ$  in  $S_1$  as a broad emission feature might be expected to the red of the structured emission at 77K. This structured emission probably hides and overlays the broad background continuum of the second decay component.

As mentioned previously, the low temperature fluorescence lifetime results in this study are very much at odds with the values of 48 ns (2-MTHF) and 54 ns (2-methylpentane) reported by Post and coworkers.<sup>200</sup> These authors noted the similarity of these lifetimes to those of simple alkylated naphthalenes and on this basis and that of the steady state fluorescence proposed that the fluorescence originates from a naphthalene-like state with a dihedral angle approaching  $90^\circ$ .



The theoretical calculations of Gustav, Sühnel and Wild<sup>194</sup> support the hypothesis that, in rigid solution, the emission is principally from a state having  $^1L_b$  character, i.e., with  $\theta(S_1) \sim 70^\circ - 90^\circ$ , a naphthalene-like state; in fluid media they calculate an  $S_1$  geometry more nearly s-cis coplanar with the resulting state being primarily of  $^1L_a$  character more similar to the higher condensed hydrocarbons such as anthracene.

Gustav et al<sup>194</sup> also calculated the oscillator strength of the transition  $S_0(\theta=68^\circ) \rightarrow S_1(\theta=68^\circ)$  to be akin to the  $^1A \rightarrow ^1L_b$  transition of naphthalene, which is approximately zero. The transition is thus forbidden (in the sense of having a small oscillator strength) and the state should be long lived. With a calculated equilibrium geometry of  $41^\circ$  in  $S_1$  Gustav found a large oscillator strength, 0.76, for a fluorescence transition at  $27\,890\text{ cm}^{-1}$  (vs experimental value of  $27\,740\text{ cm}^{-1}$ ), this transition being of  $^1A \rightarrow ^1L_a$  character. The large oscillator strength implies a short lifetime for the upper state, in accord with the observed fluid solution radiative lifetime of 3.8 - 4.0 ns.

While at present no adequate explanation can be offered for the discrepancy between the present lifetime results and those of Post<sup>200</sup> this author is convinced that no long lived decay of the sort reported by Post was present in the fluorescence decay at 77K. Great pains were taken to purify both solute and solvents and no anomalous behaviour was found for these solutions at room temperature, with the experimental fluorescence lifetime being strictly monoexponential and in excellent agreement with the literature values. The solutions were kept dilute to reduce possible precipitation on cooling and the three

solvents, 3MP, isopentane and 2-MTHF yielded very transparent glasses at 77K, free of visible turbidity. Substitution of a pure solvent glass for the sample solution at 77K gave no detectable decay signal in the pulsed lifetime apparatus, further indication that the solvent, sample tube and dewar were free of any spurious fluorescent component.

As a further check on the low temperature performance of the decay fluorometer the lifetimes of several solutes known to have monoexponential decays at 77K were redetermined in conjunction with several of the low temperature 1,1'-binaphthyl runs. Under conditions similar to those used for the 1,1'-binaphthyl both 1-phenylnaphthalene and 1,2,7,8-dibenzofluorene, the rigid methylene-bridged analog of s-cis 2,2'-binaphthyl, were found to exhibit simple monoexponential fluorescence decay. No solubility problems were encountered with the latter solute (nominally  $10^{-5}M$ ), which is expected to have a solubility even lower than that of 1,1'-binaphthyl. These observations reinforce the belief that the biexponential decay seen for 1,1'-binaphthyl at 77K is indeed genuine and not merely an instrumental artifact of the decay fluorometer.

The attempts to correlate the lifetime behaviour with molecular geometry by Gustav<sup>194</sup> and Post<sup>191,200</sup> may be subject to some criticism.

The room temperature absorption spectrum of 1-phenylnaphthalene and 1,1'-binaphthyl show a strong similarity, not surprising in light of their similar ground state geometries, estimated at  $44 - 66^\circ$  dihedral angle for 1-phenylnaphthalene.<sup>150,151</sup> The  $S_1$  equilibrium geometries are also similar with  $\theta \sim 32^\circ$  for 1-phenylnaphthalene.<sup>153</sup> The character of the lowest lying singlet-singlet transition (in fluorescence) is believed to principally of  $^1A + ^1L_a$  character (allowed) for 1-phenyl-

naphthalene<sup>153</sup> yet the radiative lifetime of this molecule is moderately long, 34 - 35 ns at 295K. Furthermore, the radiative lifetime of 1-phenylnaphthalene in rigid solution at 77K is identical to that obtained at room temperature despite some blue shift in the fluorescence and the likelihood that at 77K the transition  $S_0 \rightarrow S_1$  will originate from the more twisted Franck-Condon excited state and would be expected to be of greater  $^1A + ^1L_b$  (forbidden) character.<sup>153</sup> While the correlation between structure and lifetime for the simple alkyl-substituted naphthalenes<sup>34,208</sup> seems reasonably valid similar correlations for aryl-substituted naphthalenes appear less clear-cut.<sup>209-211</sup> For a series of phenyl-substituted naphthalenes given by Berlman<sup>34</sup> the radiative lifetimes are as follows: 1,4-diphenyl, 3.1 ns; 1,5-diphenyl, 3.8 ns; 1,7-diphenyl, 59 ns; 1,4,5,8,-tetraphenyl, 4.6 ns.

## 5.2 Photophysics of 1,2'-Binaphthyl

### 5.2.1 Fluorescence Emission and Excitation Spectroscopy

As opposed to the 1,1'-binaphthyl very little has been reported experimentally about 1,2'-binaphthyl except for the cataloging and brief discussion of its absorption spectrum.<sup>212,213</sup> Indeed of these five simple biaryls 1,2'-binaphthyl is by far the least studied. Superficially the shape of the absorption spectrum resembles that of 1,1'-binaphthyl and 1-phenylnaphthalene both of which are twisted in the ground state.

The fluorescence spectroscopy of 1,2'-binaphthyl is, in many respects, very alike that of 1,1'-binaphthyl. As with the 1,1'-isomer 1,2'-binaphthyl showed fluorescence emission and excitation spectra which were independent of the excitation and emission wavelengths

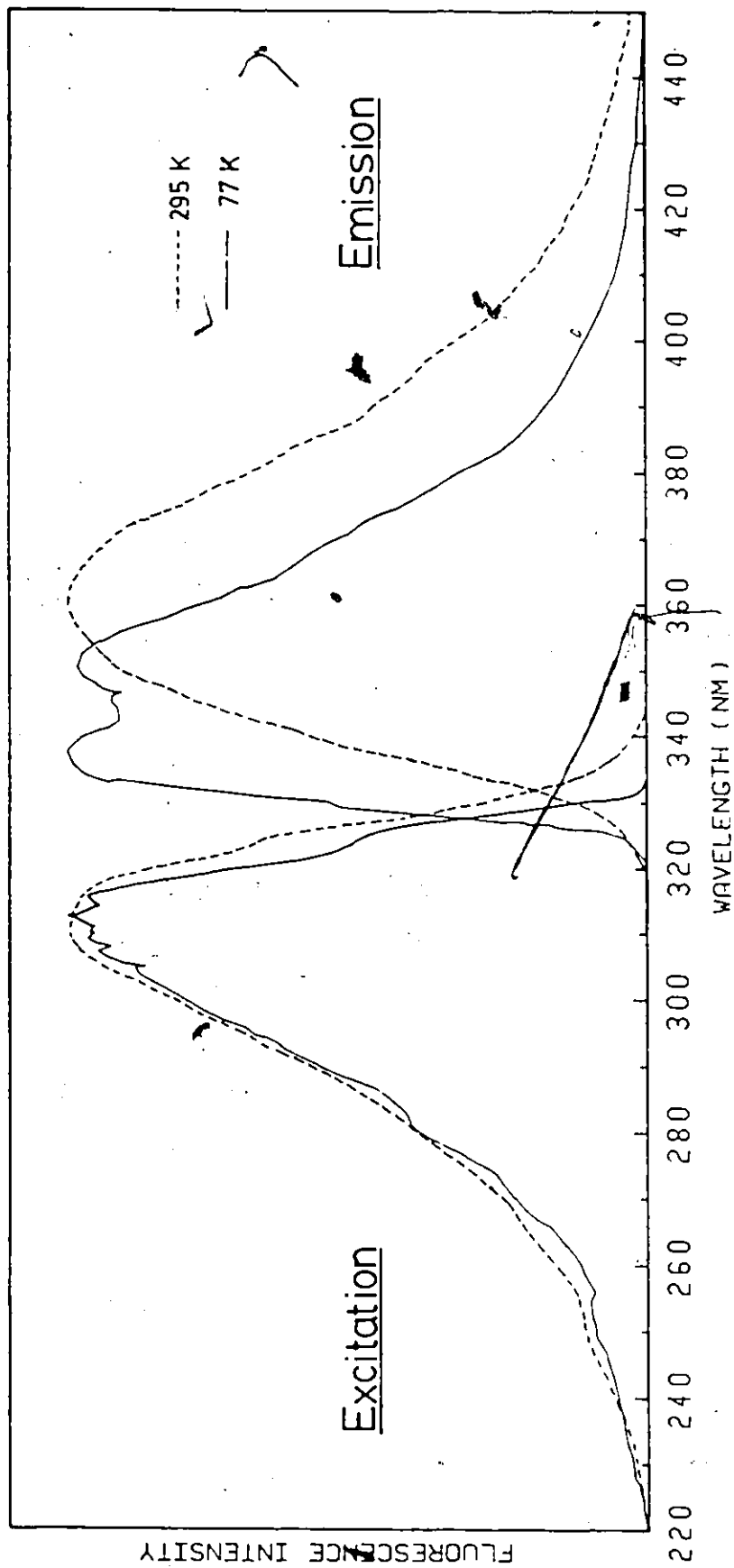


Figure 5.6

Fluorescence Emission and Excitation Spectra of  $10^{-5}M$  1,2'-Binaphthyl in Isopentane at 295K and 77K

respectively and which were, for all purposes, independent of the particular glass-forming solvent. Figure 5.6 shows the emission and excitation spectra of 1,2'-binaphthyl in isopentane at 77K and 295K although this describes the steady state fluorescence in 3MP or cyclohexane (295K only) equally well. 1,2'-binaphthyl gave no highly structured emission at 77K such as seen for 1,1'-binaphthyl in glassy matrices. Attempts to find a solvent yielding a Shpol'skii or quasi-linear spectrum at 77K over the solute concentration range  $10^{-3}$  -  $10^{-5}$ M met with no success. As, with 1,1'-binaphthyl (at 77K) most of the polycrystalline matrices produced even more poorly resolved emission than that obtained from the rigid glasses.

Upon cooling to liquid nitrogen temperatures the fluorescence emission of 1,2'-binaphthyl was found to undergo a substantial blue shift, an effect also observed for 1-phenylnaphthalene and 1,1'-binaphthyl. The emission maximum for solutions of 1,2'-binaphthyl moved fully  $2020\text{ cm}^{-1}$ , from  $27\,680\text{ cm}^{-1}$  at 295K to  $29\,700\text{ cm}^{-1}$  at 77K compared to the  $780\text{ cm}^{-1}$  hypsochromic shift in 1,1'-binaphthyl.

It is apparent that the spectral characteristics of 1,2'-binaphthyl are similar to those of 1,1'-binaphthyl but with both excitation (absorption) and emission shifted to longer wavelength. The exception is the emission maximum at 77K; however both the center of gravity and the highest energy band of the 1,2'-binaphthyl fluorescence lie to the red of the corresponding features in 1,1'-binaphthyl. The highest energy band in the fluorescence of 1,2'-binaphthyl, possibly the 0-0, is  $1410\text{ cm}^{-1}$  from the naphthalene origin and  $990\text{ cm}^{-1}$  from the 1,1'-binaphthyl origin.

This red shift of absorption and emission for the 1,2'-isomer may be produced by several mechanisms. The effects of substitution on the absorption spectra of numerous molecules have been dealt with at length by Jaffe and Orchin,<sup>213</sup> who concluded that extension of a conjugated system in a particular direction by substitution will principally affect those bands whose transition moment or polarization lie in the same direction. Substitution at the 2-position of the naphthalene ring, extending the longitudinal conjugation, should affect most strongly the long-axis polarized  $^1L_b$  band, red shifting it and increasing its intensity in absorption. Because of the strong overlap with the adjacent  $^1L_a$  band in the absorption spectrum of 1,2'-binaphthyl it is difficult to discern such an effect, although the molar absorptivity does seem to show some increase relative to that in the 1,1'-isomer.

The alternative, but related, explanation of the bathochromic shift is to be found in the lower steric repulsion inherent in the 1,2'-structure as compared to the more crowded 1,1'-binaphthyl.

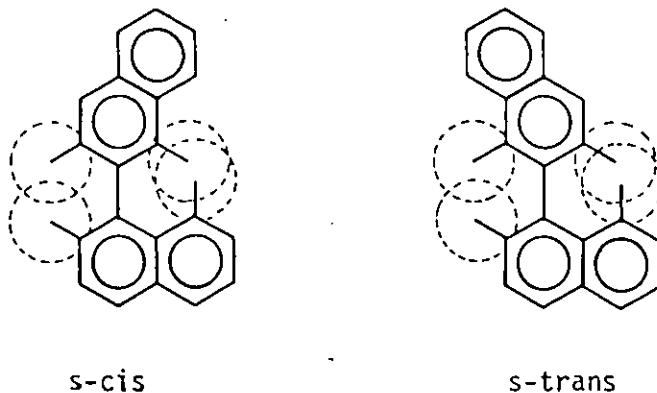


Figure 5.7

Qualitative View of Steric Restrictions for s-cis versus s-trans Conformers of 1,2'-Binaphthyl

For both coplanar forms of 1,2'-binaphthyl the expected non-bonded hydrogen repulsion will be lower than the nonbonded steric repulsion in either s-cis or s-trans coplanar 1,1'-binaphthyl. On this basis alone it is expected that 1,2'-binaphthyl could adopt a more nearly coplanar geometry in the ground or first excited singlet states. It is also obvious that the difference between the s-cis and s-trans coplanar forms in 1,2'-binaphthyl is much smaller than the energy difference expected between the two coplanar 1,1'-binaphthyl conformations. Smaller dihedral angles between the naphthyl moieties would then lead to increased  $\pi$ -electronic interaction between the two aromatic rings and a bathochromic shift in absorption and emission.

Quenching of the steady state fluorescence of 1,2'-binaphthyl at 295K in either air or oxygen saturated (1 atm.) cyclohexane led to a decrease in the total fluorescence intensity but no change in the actual emission profile. This points to the presence of only a single emitting state or species in fluid solution.

#### 5.2.2 Fluorescence Quantum Yield Measurements

Relative fluorescence quantum yields for 1,2'-binaphthyl were determined in the usual manner. No excitation wavelength dependence of the quantum yield was noted over the range from  $\lambda_A = 260$  nm to  $\lambda_A = 320$  nm. Unfortunately no comparative data for this molecule are available in the scientific literature.

The uncertainty in these quantum yields is about 10% at room temperature, increasing to near 15% at 77K.

Table 5.6  
Relative Fluorescence Quantum Yields of 1,2'-Binaphthyl

Solvent	$\phi_f$	
	295K	77K
Cyclohexane	.76	
3 MP	.73	.72

### 5.2.3 Fluorescence Decay Measurements

The singlet decay kinetics of 1,2'-binaphthyl in dilute alkane solution at room temperature follow a monoexponential decay law,  $x_v^2$  being generally  $\leq 1.3$  and the autocorrelation function showing a random distribution of the weighted residuals of the calculated and observed curves. The singlet lifetime of 1,2'-binaphthyl at 295K was, like that of 1,1'-binaphthyl, quite short, 5.2 - 6.6 ns depending on solvent. Lifetimes extracted from a monoexponential fit of the room temperature decay data are given below.

Table 5.7  
Fluorescence Lifetimes of 1,2'-Binaphthyl in Dilute Solution at 295K;  
by Fit to a Monoexponential Decay Law

Solvent (concentration, moles/l)	$\tau$ (ns)
Cyclohexane <sup>a</sup> ( $2.4 \times 10^{-4} M$ )	$5.23 \pm .13$
3 MP <sup>b</sup> ( $3 \times 10^{-4} - 1 \times 10^{-6} M$ )	$6.56 \pm .09$

<sup>a</sup> with both N<sub>2</sub> and D<sub>2</sub> excitation sources; various filter/monochromator combinations.

<sup>b</sup>  $\lambda_A = 313.6 \text{ nm}$  or  $315.9$ ;  $\lambda_F = 370 \text{ nm}$ .



The lifetimes given in Table 5.7 are the means of 8 - 10 measurements each and were highly reproducible from sample to sample and consistent over a long period of time. In 3 MP the lifetime was found to be independent of concentration over more than two orders of magnitude. As with the quantum yield, no literature value of the singlet lifetime was available for comparison.

In rigid 3 MP glass at 77K the kinetics apparently deviate greatly from the simple decay seen at room temperature, as adduced from the deterioration of the monoexponential goodness-of-fit at 77K. A much improved fit was obtained by assuming a biexponential fluorescence decay for 1,2'-binaphthyl at 77K. A comparison of the mono- and biexponential results is given in the accompanying table.

Table 5.8  
Comparison of Mono- and Biexponential Fit of Fluorescence Lifetime Data  
for 1,2'-Binaphthyl in 3 MP at 77K

Solute Concentration (mole/l)	Biexponential Fit				Monoexponential Fit	
	$\tau_1$ (ns)	$\tau_2$ (ns)	$\alpha/\beta$	$\chi^2_\nu$	$\tau$ (ns)	$\chi^2_\nu$
$2.7 \times 10^{-4}$	4.33	15.09	9.31	1.14	6.63	19.26
	4.40	14.29	8.04	1.23	6.80	21.27
$5 \times 10^{-5}$	4.35	14.50	8.25	1.12	6.65	14.84
$1 \times 10^{-6}$	4.30	14.21	7.24	1.26	6.42	5.99

$\lambda_A = 313.6 \text{ nm}$ ;  $\lambda_F = 370 \text{ nm}$

Means:  $\tau_1 = 4.34 \pm .04 \text{ ns}$ ;  $\tau_2 = 14.52 \pm .40 \text{ ns}$ ;  $\alpha/\beta = 8.2 \pm .9$ ;

$\tau = 6.63 \text{ ns}$

The apparent monoexponential decay seen at 77K has a lifetime (6.63 ns) nearly identical to the room temperature value of 6.56 ns. However, the extremely large  $\chi^2_{\nu}$  values (and strong autocorrelation of the residuals, not shown here) suggest that the decay at 77K is not monoexponential. Deconvolution as a sum of exponential terms yielded two constant and characteristic lifetime parameters,  $\tau_1 = 4.34$  ns and  $\tau_2 = 14.5$  ns with the reduced chi-squared values becoming acceptably small. Trials at other excitation and emission wavelengths showed similar lifetime values to those above but with different ratios of the pre-exponential factors,  $\alpha/\beta$ .

Such evidence suggests that, as was the case for 1,1'-binaphthyl, there are at least two distinct fluorophores present in the 1,2'-binaphthyl decay at 77K. Aggregation or microcrystallite formation upon cooling cannot be discounted absolutely but the lack of significant change of the decay parameters on going from  $1 \times 10^{-6}$  to  $2.7 \times 10^{-4}$  M nominal concentration tends to show this not to be the case, unless the solubility limit of 1,2'-binaphthyl is already much below  $10^{-6}$  M at 77K. At these concentrations the 3 MP glass was, to the naked eye, free of turbidity or opalescence.

#### 5.2.4 Analysis and Discussion of the Photophysics of 1,2'-Binaphthyl

From the resemblance of the absorption spectra of 1-phenyl-naphthalene and 1,1'- and 1,2'-binaphthyl one might argue that the ground state of 1,2'-binaphthyl, like those of the other two must be far from coplanar in the absence of strong matrix effects. Direct experimental evidence as to the ground state conformation is lacking but the two published calculations of the  $S_0$  geometry arrived at disparate conclusions.

Gamba et al<sup>175</sup> estimated a dihedral angle of  $60 - 120^\circ$  (the minimum is very shallow) by matching experimental and calculated absorption transition energies and oscillator strengths. Their calculations further indicated that the five biaryls fell into two distinct categories: those with  $S_0$  minima in the region  $60 - 120^\circ$ , encompassing 1,1'-, 1,2'-binaphthyl and 1-phenylnaphthalene and those with a maximum at  $90^\circ$  and minima at  $30^\circ$  and  $150^\circ$ , 2,2'-binaphthyl and 2-phenylnaphthalene being in the latter group. The available experimental evidence supports Gamba's conclusions regarding the angular locations of the minima for 1,1'-, 2,2'-binaphthyl and the phenylnaphthalenes. Gamba also correctly predicts the asymmetry of the 1,1'-binaphthyl ground state potential function.

SCF-CI studies of the steric effects of naphthyl and phenyl substituents by Tinland<sup>152</sup> led that author to conclude that 1,2'- and 2,2'-binaphthyl both have ground state twist angles  $\leq 20^\circ$  (with respect to which initial configuration is not stated), this result being in rough agreement with other published values for the latter molecule whilst the 1,2'-binaphthyl finding is in direct contrast to Gamba's conclusion. Tinland failed to explore angles above  $20^\circ$  however and his fitting criteria, the matching of observed to calculated oscillator strengths and transition energies showed a very weak angular dependence by this method.

On the whole it appears that Gamba's theoretical model for the  $S_0$  potential surface for 1,2'-binaphthyl is in closer accord with the cumulative evidence of this study, and that, while the dihedral angle for 1,2'-binaphthyl is smaller than that for 1,1'-binaphthyl it is not

as small as the  $\theta \leq 20^\circ$  predicted by Tinland. It seems probable that the dihedral angle is nearer that seen for 1-phenylnaphthalene,  $50^\circ$  -  $60^\circ$ . In terms of their nonbonded hydrogen interactions 1-phenylnaphthalene and 1,2'-binaphthyl are quite similar. This ground state minimum is probably very shallow and the potential function will be more symmetric about  $\theta = 90^\circ$  than was the case for 1,1'-binaphthyl since the s-cis and s-trans forms of 1,2'-binaphthyl will be more nearly isoenergetic.

Excitation of 1,2'-binaphthyl in fluid solution will be followed by rapid relaxation towards the equilibrium excited state. From the large Stokes Shift in fluid solution the excited state equilibrium configuration must be at some dihedral angle different from that in the ground state; the  $S_1$  potential surface of 1,2'-binaphthyl is probably similar to that of 1,1'-binaphthyl although not as steep towards  $\theta = 0^\circ$  and  $180^\circ$ . The minimum may be at a lower dihedral angle and shallower. The lack of much vibrational structure in the 1,2'-binaphthyl fluorescence at 77K suggests that the local minimum calculated for the 1,1'-binaphthyl  $S_1$  surface may be much more shallow or entirely absent. A shallow ground and excited state surface would result in a wealth of populated torsional states which could broaden or smear out the vibrational details of the emission. At 77K the fluorescence is shifted to higher energies as the relaxation towards the equilibrium configuration is impeded, with the emission consequently arising from the higher energy Franck-Condon state. These features are summarized in Figure 5.8.

The room temperature lifetime and quantum yield are those of the equilibrium conformation in  $S_1$ . The radiative lifetime and rate constants for that state are given below.

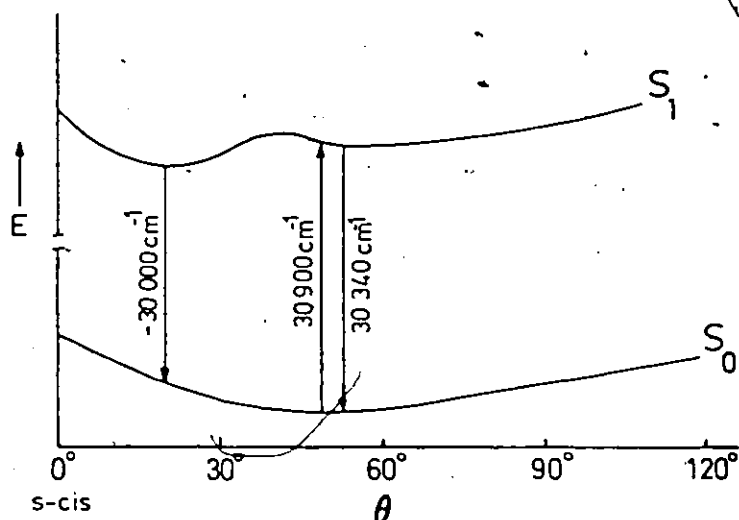


Figure 5.8

Proposed Potential Energy Diagram for Ground and First Excited Singlet States of 1,2'-Binaphthyl

Table 5.9

Radiative Lifetimes and Radiative and Nonradiative Rate Constants for 1,2'-Binaphthyl at 295K

Solvent	$\tau_0 = \tau/\phi_f$ (ns)	$k_f = 1/\tau_0$ (s <sup>-1</sup> )	$k_f^0 = k_f/n^2$ (s <sup>-1</sup> )	$k_{nr}$ (s <sup>-1</sup> )
Cyclohexane	6.9	$1.4 \times 10^8$	$7.1 \times 10^7$	$5.1 \times 10^7$
3 MP	9.0	$1.1 \times 10^8$	$5.9 \times 10^7$	$4.2 \times 10^7$

The 20% difference between  $k_f^0$  in cyclohexane and 3 MP is, in principle, attributable to the error in the quantum yield measurements but the observed fluorescence lifetimes differ by fully 25% too, 5.23 ns in cyclohexane and 6.56 ns in 3 MP. In contrast the greatest difference

for the experimental 1,1'-binaphthyl lifetimes was only 9% for the pair isopentane and 2 MTHF. For all five biaryls the lifetimes measured in, 3 MP were marginally longer than the corresponding values in cyclohexane, so some specific solvent effect may be responsible, over and above the refractive index correction.

In fluid solution the relaxation of 1,2'-binaphthyl should be even more rapid than the already fast equilibration seen for 1,1'-binaphthyl. Under these conditions it is expected that the fluorescence will arise entirely from the equilibrium  $S_1$  conformation, having a small dihedral angle, as depicted in Figure 5.8. This decay has a fluorescence lifetime of 5.23 ns (cyclohexane) to 6.56 ns (3 MP). At 77K this relaxation is inhibited, so much of the emission will now originate from a more highly twisted Franck-Condon type excited state, characterized by a fluorescence lifetime of about 4.33 ns (3 MP) while the longer-lived emission arises from a partially relaxed state or states, with a net fluorescence lifetime of 14.6 ns. The emission from these partially relaxed states should lie to the red end of the fluorescence at 77K. It is not clear whether this long-lived component at 77K actually corresponds to the equilibrium geometry in fluid solution, which decayed with a lifetime of 6.56 ns. The fluorescence lifetime certainly does change in the expected manner, increasing from 6.56 ns to 14.6 ns upon cooling to 77K, if these emissive states are of similar geometry. The seeming invariance of the fluorescence quantum yield with temperature is possibly mostly fortuitous, the projected increase in  $\phi_{f,2}$  being compensated by the decreased amount of the relaxed species 2 at 77K.

### 5.3 Photophysics of 2,2'-Binaphthyl

#### 5.3.1 Fluorescence Emission and Excitation Spectroscopy

##### 5.3.1a Fluorescence Spectroscopy at Room Temperature

Fluorescence emission and excitation spectra of dilute ( $10^{-4}$  -  $10^{-5}$  M) solutions of 2,2'-binaphthyl- $h_{14}$  were obtained in the nonpolar media cyclohexane, methylcyclohexane, 3MP and isopentane and in ethanol at the nominal room temperature, 295K.

The fluorescence excitation spectra in the hydrocarbon solvents at 295K were found to be broad and nearly devoid of structure, with a maximum at 313.8 nm ( $31\,870\text{ cm}^{-1}$ ) and a broad, weak shoulder at 274 nm. These excitation spectra were found to be practically independent of the monitoring wavelength but with the maximum slit width on the emission monochromator, 400  $\mu\text{m}$ , it was necessary to operate the 0.25m excitation monochromator at fairly poor monochromaticity with 1.00 or 0.65 mm slits. Small differences in the relatively structureless excitation spectrum could be lost with such spectrally impure excitation. The apparent red shift of the excitation maximum from the 304 nm absorption peak of the conventional absorption spectrum is likely an artifact of the experiment.

For the nonpolar solvents the emission spectra at 295K were found to be independent of solvent but strongly dependent on the excitation wavelength chosen. The most comprehensive results were obtained in cyclohexane; the fluorescence obtained with excitation wavelengths of 330 nm to 260 nm, at 10 nm intervals is shown in Figure 5.9. The dependence of  $\lambda_A$  was similar for the other hydrocarbons, with some of the wavelength dependent emission also shown for isopentane solution

Figure 5.9

Fluorescence Emission Spectra of  $10^{-4}$  -  $10^{-5}$  M 2,2'-Binaphthyl- $h_{14}$   
in Cyclohexane at 295K as a Function of Excitation Wavelength



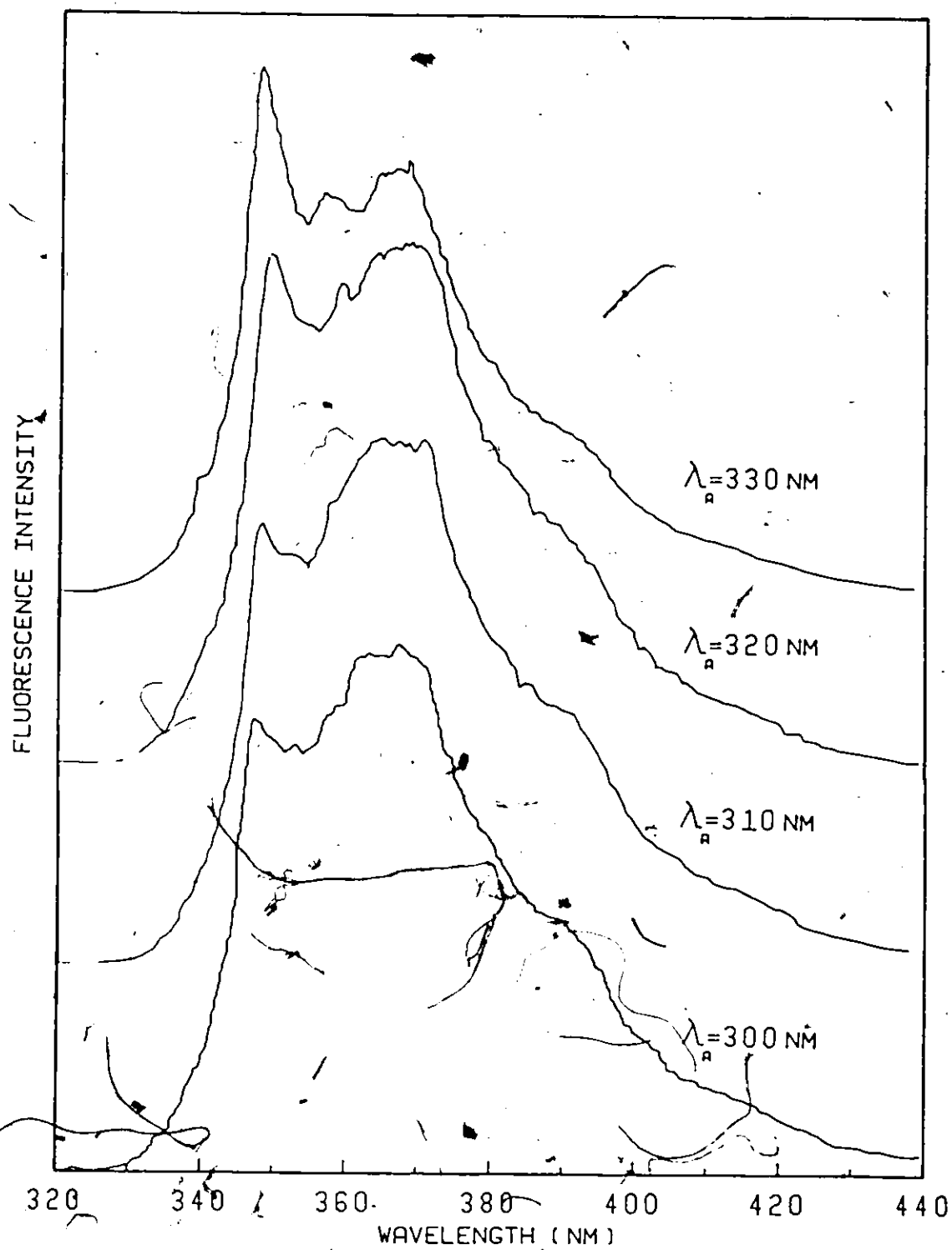


Figure 5.9

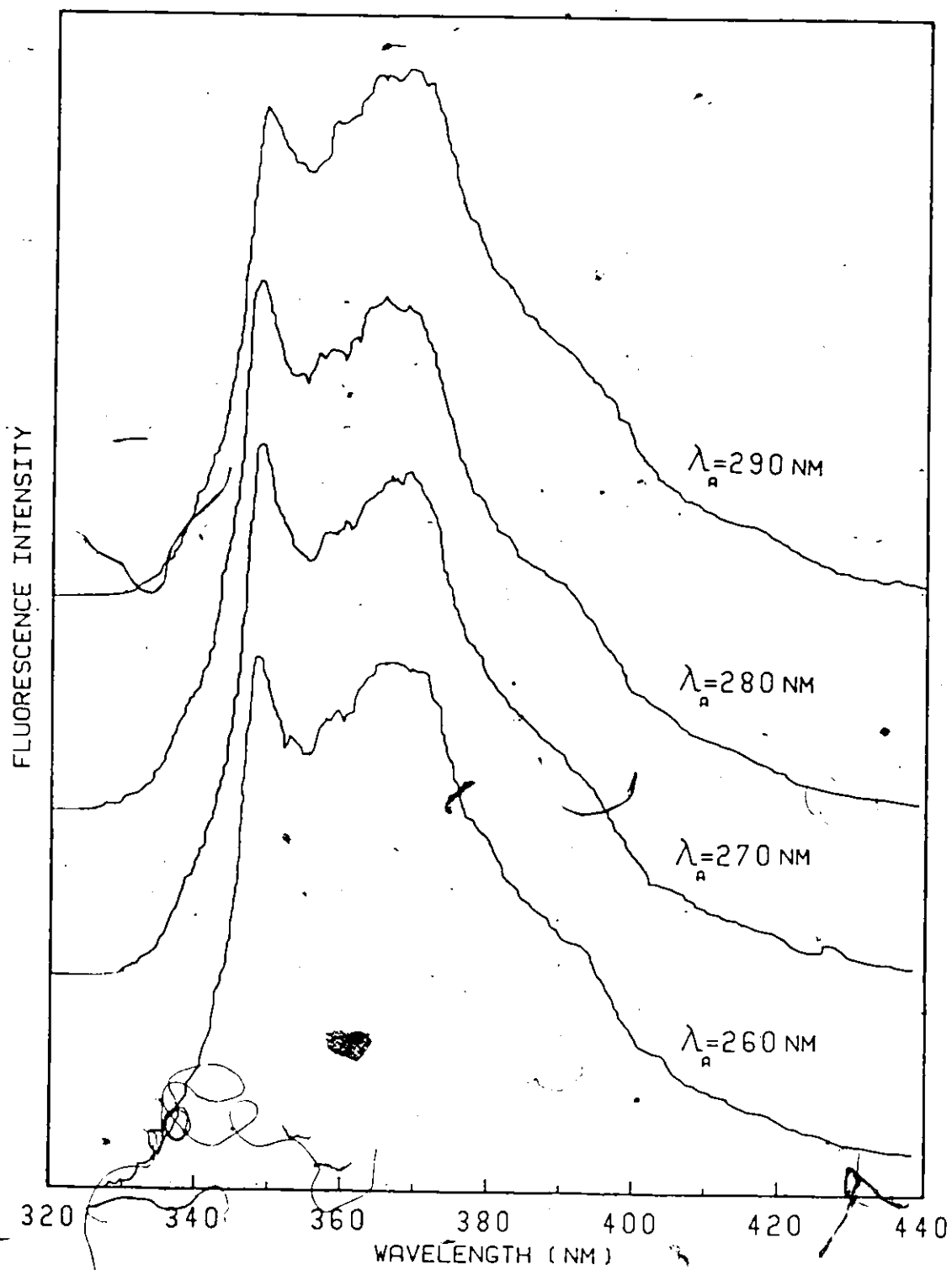


Figure 5.9  
continued

(Figure 5.10).

At all excitation wavelengths three principal bands are seen in the alkane solutions of 2,2'-binaphthyl- $h_{14}$ , at 348.6, 367.6 and 390 nm; the intervals between these bands are  $\sim 1400 - 1500 \text{ cm}^{-1}$ , corresponding to C-C vibrational frequencies. This separation more closely resembles the spacing seen in higher condensed aromatic hydrocarbons than that of benzene, naphthalene and their simple derivatives, usually  $\sim 1000 \text{ cm}^{-1}$ .<sup>94</sup> With both long ( $\lambda_A \geq 330 \text{ nm}$ ) and short ( $\lambda_A \leq 280 \text{ nm}$ ) wavelength excitation the 348.6 nm ( $28\,690 \text{ cm}^{-1}$ ) band dominates the emission while at intermediate excitation energies the peak at 367.6 nm ( $27\,200 \text{ cm}^{-1}$ ) becomes relatively more intense with respect to the 348.6 nm band. This variation suggests the presence of perhaps two or more absorbing species possessing overlapping absorption and emission spectra. Selective excitation at the extreme long wavelength edge of the absorption profile produces a spectrum rich in the 348.6 nm component. With more energetic excitation a second component is significantly excited too, leading to an enhanced emission near 367.6 nm. A further increase in excitation energy, to 280 - 260 nm again reaches a region wherein the absorption of the first component is relatively stronger than that of the second one, again producing an emission similar to that obtained at  $\lambda_A \geq 330 \text{ nm}$ . This behaviour will be treated more fully in conjunction with the detailed fluorescence decay study of 2,2'-binaphthyl and with the discussion of the photo-physics of this system. These results are in qualitative agreement with Horrock's study of the excitation, solvent and temperature dependence of the 2,2'-binaphthyl fluorescence.<sup>28</sup> The spectra shown by

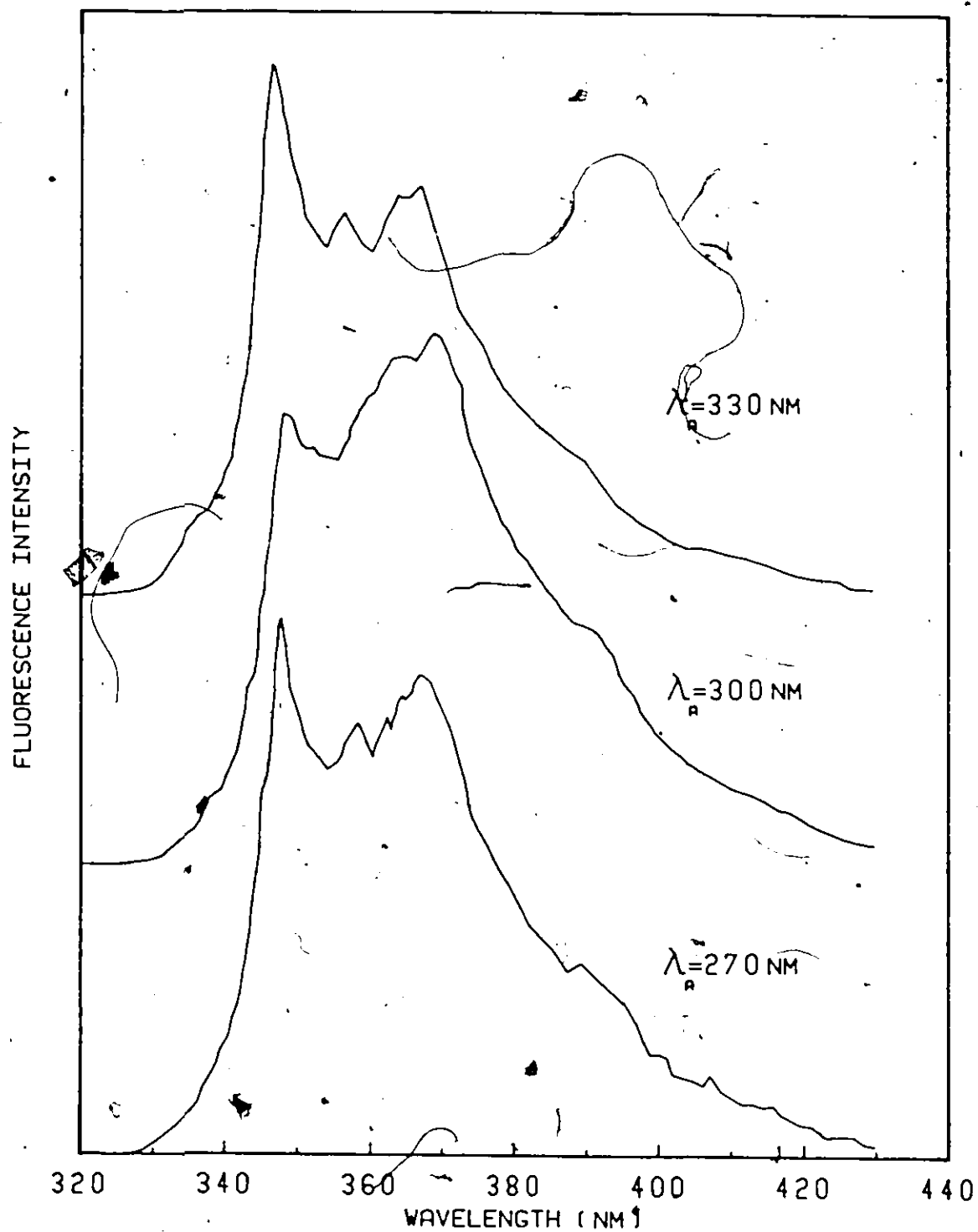


Figure 5.10

Fluorescence Emission Spectra of  $10^{-4}$  -  $10^{-5}$  M 2,2'-Binaphthyl- $h_{14}$  in Isopentane  
at 295K as a Function of Excitation Wavelength

that author are somewhat different in relative intensity, probably as a result of the uncorrected nature of both sets of fluorescence spectra. Additionally, his emission wavelengths are systematically in error, identifying the 348.6, 367.6 and 390 nm peaks as 355, 375 and 395 nm respectively. The spectra obtained at his two excitation wavelengths of 310 and 260 nm show the same qualitative trend as this present work, i.e. the 348.6 nm peak increases with respect to the 367.6 nm peak as the excitation is changed from 300 - 310 nm to shorter wavelengths.

The room temperature fluorescence of 2,2'-binaphthyl in absolute ethanol is somewhat more structured than that in nonpolar solvents, a feature also noted by Horrocks.<sup>28</sup> Although superficially the spectrum in ethanol resembles that found in alkane solutions, under better resolution the broad peaks corresponding to the 348.6 and 367.6 nm peaks in hydrocarbon media were found to be resolved into at least two components each. The fluorescence excitation spectrum of 2,2'-binaphthyl in fluid ethanol solution was as broad and featureless as in alkane solvents but with the maximum slightly to the red of that in the nonpolar solvents (317.7 nm vs 313.8 nm). As in alkane media, the fluorescence excitation at 295K in ethanol was apparently independent of the monitored fluorescence wavelength.

Variation of the excitation energy produced profound changes in the room temperature emission profile in absolute ethanol, as illustrated in Figure 5.11. The variation with  $\lambda_A$  roughly parallels that seen in alkane solvents, with low energy excitation (330 nm) giving rise to a strong high energy component at 348.4 nm. The relative intensity of this band then decreases at  $\lambda_A = 300 - 310$  nm rising again at 280 and

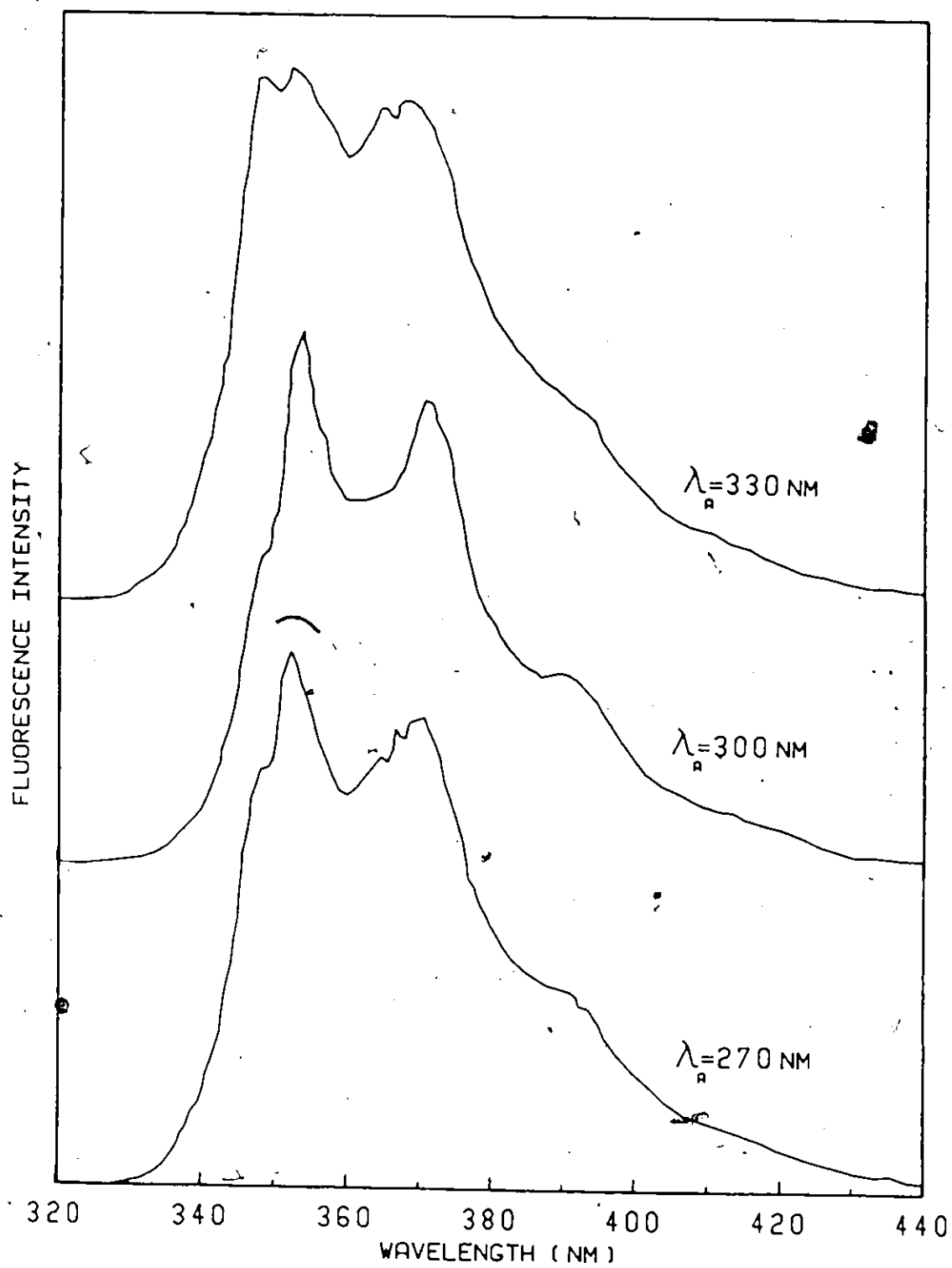


Figure 5.11

Fluorescence Emission Spectra of  $10^{-4}$  M 2,2'-Binaphthyl in Ethanol at 295K  
as a Function of Excitation Wavelength

270 nm excitation. The bands at 353.0 and 370.8 nm appear strongly at all excitation wavelengths.

#### 5.3.1b Fluorescence Spectroscopy in Organic Glasses at 77K

In glasses of 3-methylpentane or isopentane at 77K the fluorescence maximum of 2,2'-binaphthyl is shifted toward longer wavelength, when compared to the 295K results. This is in contrast to the blue shifts observed for 1,1'- and 1,2'-binaphthyl upon cooling. The two principal bands in emission, depending upon the excitation wavelength, are at 367 nm and 387 - 389 nm at 77K. Examples of the low temperature fluorescence excitation and emission spectra for 2,2'-binaphthyl in isopentane and 3 MP are shown in Figures 5.12, 5.13 and 5.14 while some of the salient emission wavelengths are given in Table 5.10.

Relative intensities are not given in the following tables as they were dependent on excitation wavelength. The low temperature spectra in isopentane and 3 MP are quite similar, with a few of the weakest bands in the isopentane solution absent from the 3 MP spectrum. The actual band frequencies found in 3 MP and isopentane are identical within the experimental error and it can be seen that all the bands observed at room temperature are also seen in the 77K spectrum, unshifted in frequency but greatly different in intensity.

The long wavelength region of the low temperature absorption spectrum in 3 MP and isopentane seems somewhat enhanced too; this information is, unfortunately, not directly available from absorption measurements at 77K but may be inferred from the fluorescence excitation spectra and from the fluorescence emission behaviour. The excitation spectra

2  
1

Figure 5.12

Fluorescence Emission Spectra of  $10^{-5}$ M 2,2'-Binaphthyl- $h_{14}$   
in Isopentane at 77K as a Function of Excitation Wavelength



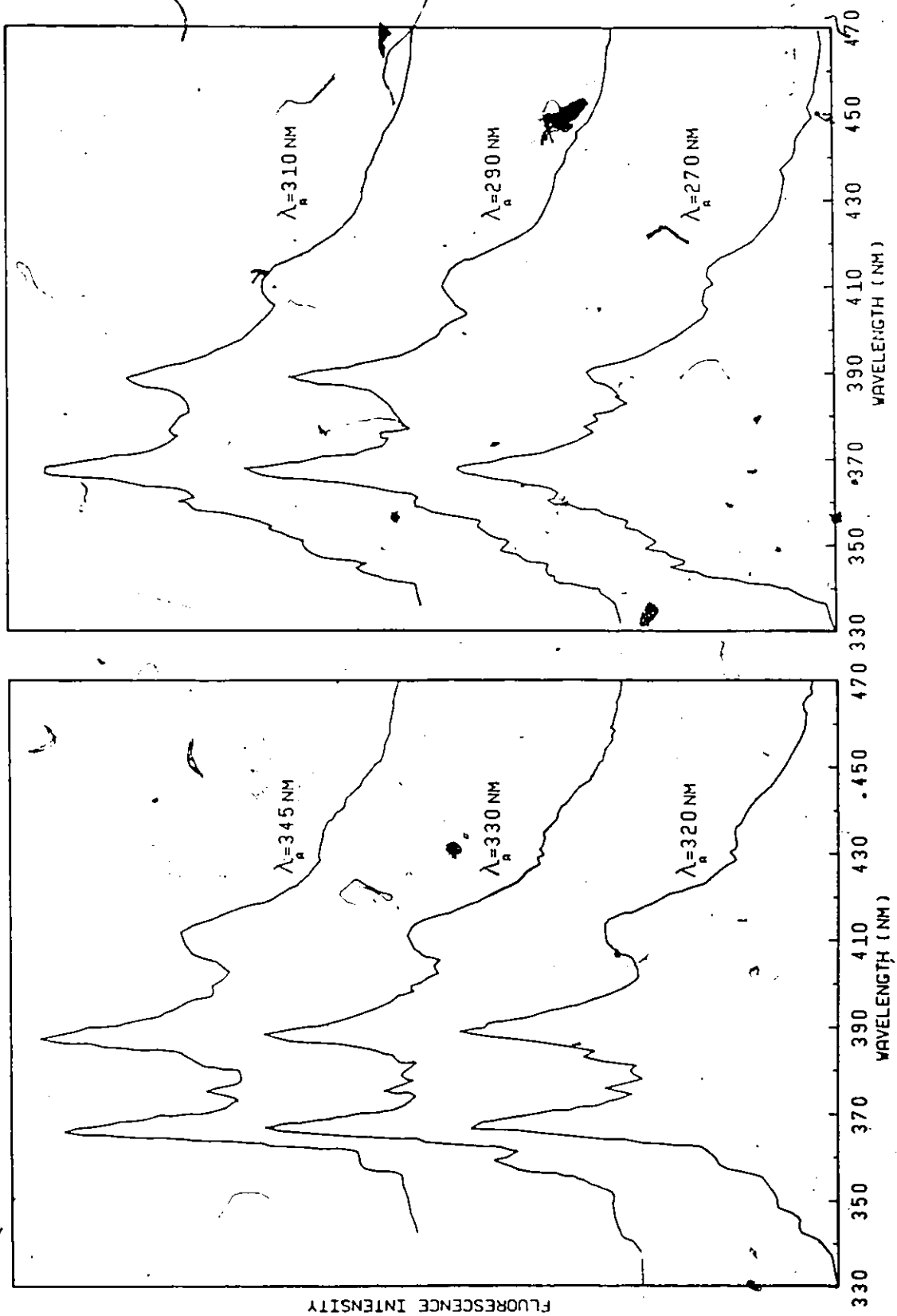


Figure 5.12

Figure 5.13

Fluorescence Excitation Spectra of  $10^{-5}$  M 2,2'-Binaphthyl- $h_{14}$   
in Isopentane at 77K as a Function of Emission Wavelength

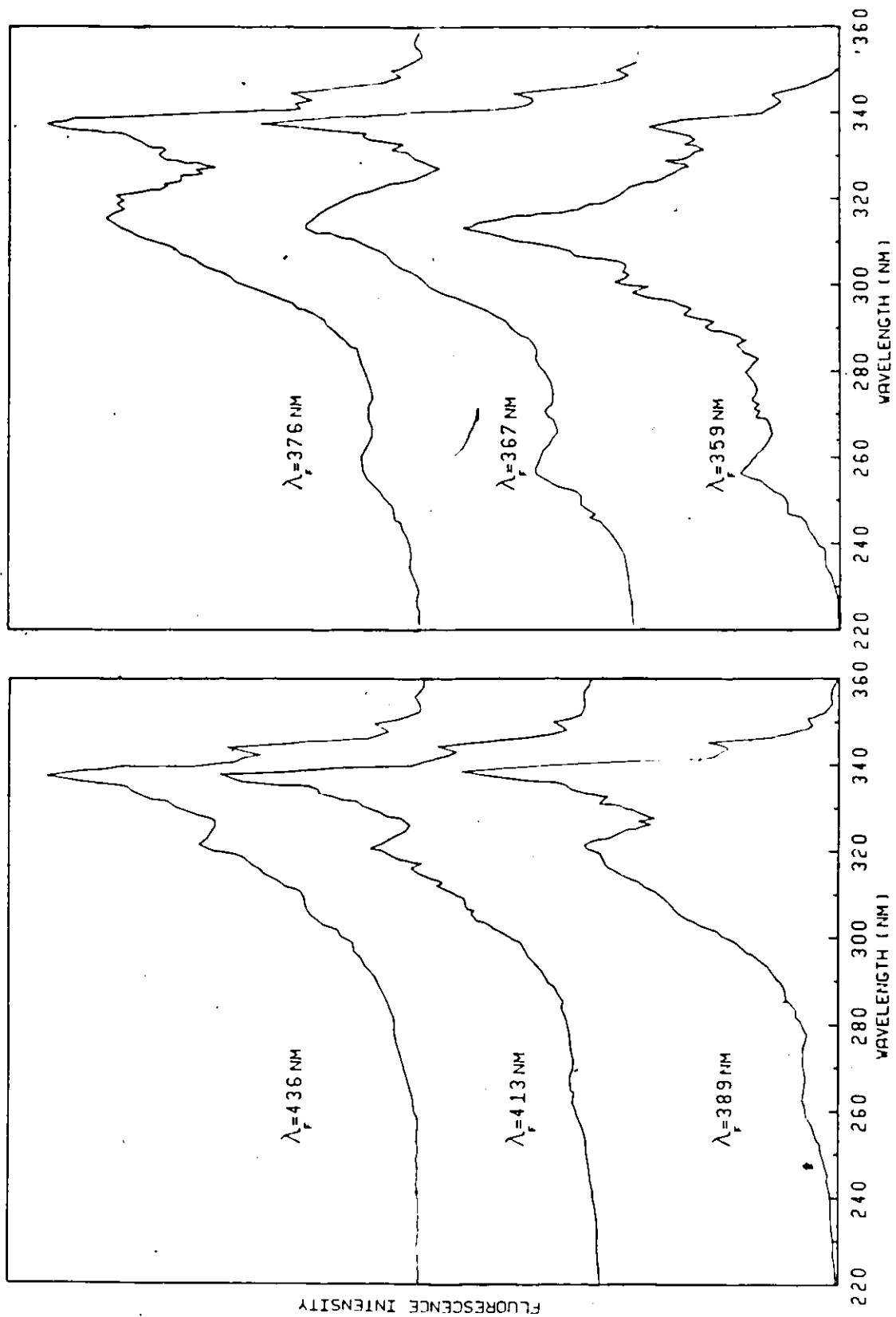


Figure 5.13

Figure 5.14

Fluorescence Emission Spectra of  $10^{-5}$  M 2,2'-Binaphthyl- $h_{14}$   
in 3-Methylpentane at 77K as a Function of Excitation Wavelength

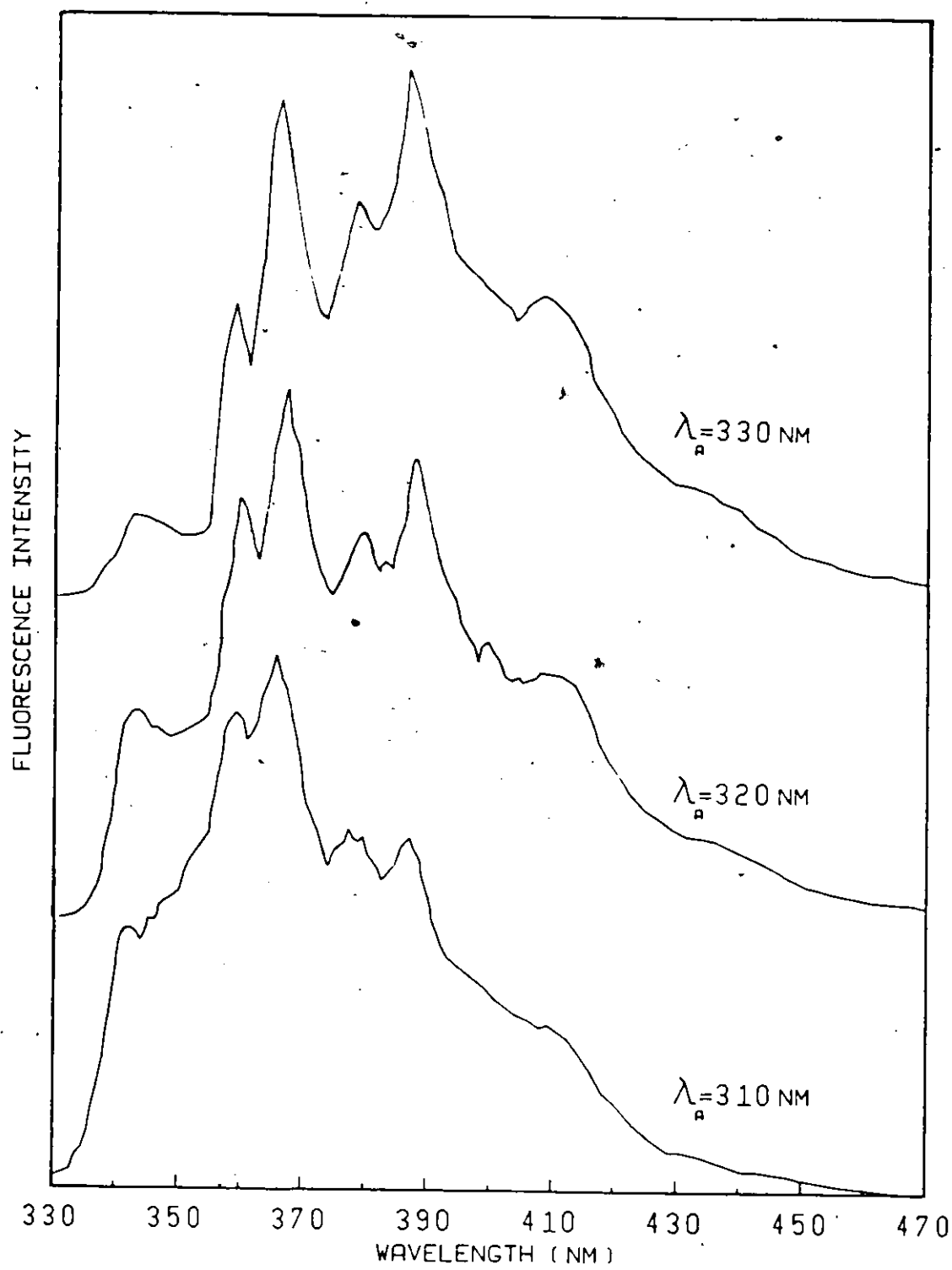


Figure 5.14

Table 5.10  
Emission Wavelengths of  $10^{-4}$  -  $10^{-5}$  M 2,2'-Binaphthyl  
in Alkane Solvents at 295K and 77K

295K		77K			
isopentane, 3-methylpentane cyclohexane or methylcyclohexane		Isopentane		3-Methylpentane	
$\lambda(\text{nm})$	$\bar{\nu}(\text{cm}^{-1})$	$\lambda(\text{nm})$	$\bar{\nu}(\text{cm}^{-1})$	$\lambda(\text{nm})$	$\bar{\nu}(\text{cm}^{-1})$
341.8	29 260	338.6	29 540		
348.6	28 690	343.5	29 110	343.2	29 140
358.8	27 870	348.7	28 680	348.2	28 720
367.6	27 200	352.9	28 330		
390	25 640	359.6	27 810	359.5	27 810
410	24 390	366.8	27 260	366.6	27 280
		376.1	26 590	378.7	26 410
		383.1	26 100		
		388.6	25 730	387.2	25 830
		398.1	25 120		
		412.6	24 240	409.5	24 420
		436.1	22 930	437.6	22 850

show considerable absorption up to  $\sim 350$  nm, while excitation of 2,2'-binaphthyl in isopentane at 77K with  $\lambda_A$  as long as 345 nm was found to yield appreciable fluorescence; in contrast, room temperature solutions of 2,2'-binaphthyl of comparable concentration gave essentially no fluorescence with excitation wavelengths greater than 335 nm.

On cooling to 77K the emission of 2,2'-binaphthyl in rigid ethanol glass is found to remain strongly dependent on excitation wavelength. These variations in relative intensities may arise from the overlap of several individual subspectra constituting the net fluorescence emission spectrum. With excitation at 325 nm the contributions of the subspectra are of similar intensity and the vibronic peaks are more clearly resolved than at either higher or lower excitation energies, with the apparently broad bands at about 350 and 367 nm separating into a number of component peaks, as seen in Figure 5.15 and listed in Table 5.11. The low temperature emission in ethanol is shifted to slightly shorter wavelength relative to the room temperature fluorescence. Using the relative intensities as a guide the shifts appear as follows:  $348.4 \rightarrow 346.1$  nm;  $353.0 \rightarrow 351.5$  nm;  $391.0 \rightarrow 386.4$  nm or about  $150 - 300 \text{ cm}^{-1}$ . The accuracy of this figure is limited by the breadth of the emission lines, particularly at room temperature. Despite this small shift the greatest intensity still lies at the high energy end of the fluorescence at 77K in ethanol. This situation is markedly different from the state of affairs in alkane solvents where the band frequencies were unaltered but where the intensity distribution was enhanced at longer fluorescence wavelengths at liquid nitrogen temperatures.

Fluorescence excitation spectra recorded at 77K in isopentane

Figure 5.15

Fluorescence Emission and Excitation Spectra of  $10^{-4}M$   
2,2'-Binaphthyl- $h_{14}$  in Ethanol at 77K as a Function of  
Excitation and Emission Wavelengths



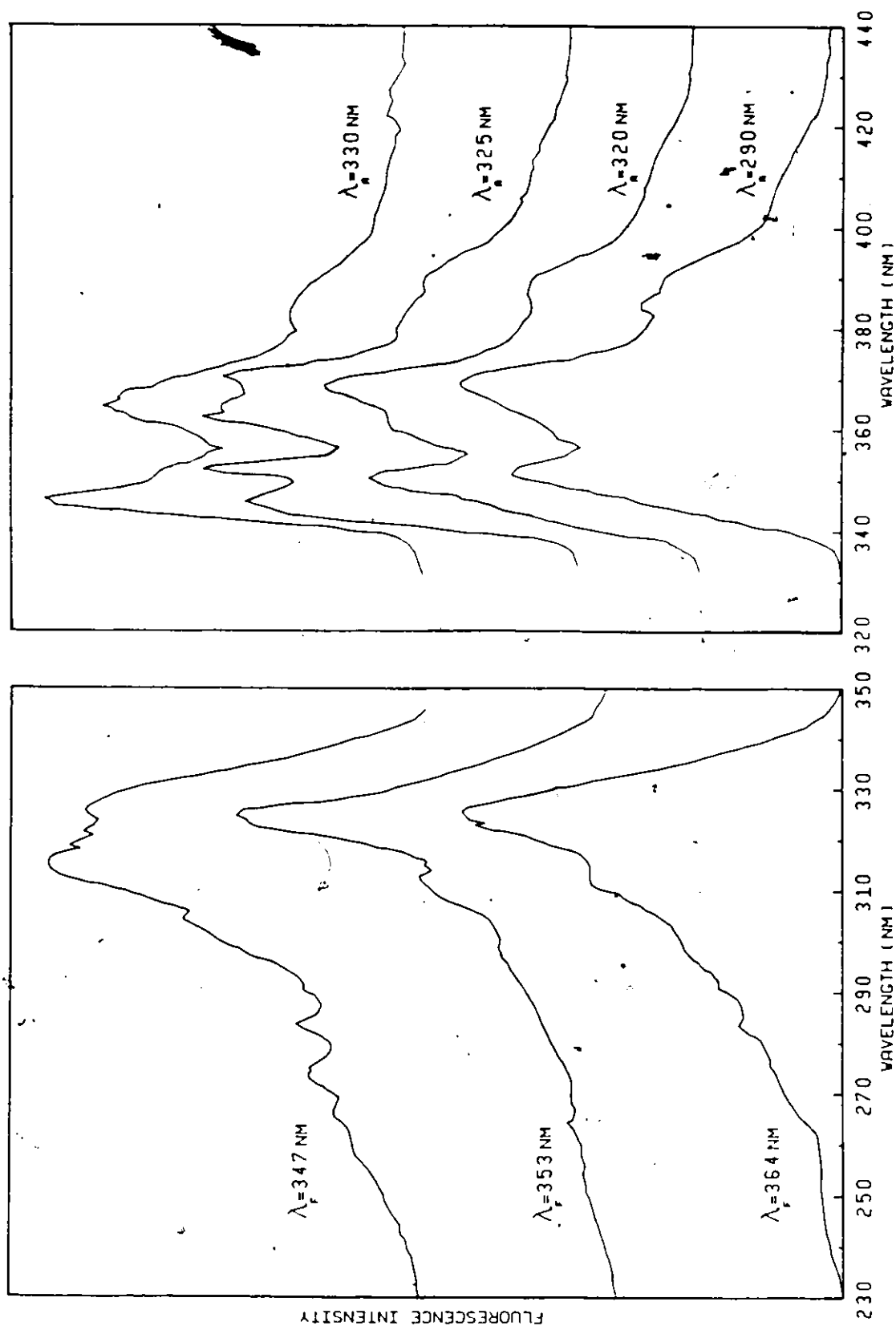


Figure 5.15

Table 5.11  
Emission Wavelengths for  $10^{-5}M$  2,2'-Binaphthyl in  
Absolute Ethanol at 295K and 77K

295K		77K	
$\lambda_F(\text{nm})$	$\bar{\nu}(\text{cm}^{-1})$	$\lambda_F(\text{nm})$	$\bar{\nu}(\text{cm}^{-1})$
344.0 <sup>a</sup>	29 070	350.1 <sup>b</sup> { 348.1 351.5	28 890 28 450
348.4	28 700	366.9 <sup>b</sup> { 362.2 370.2	27 610
353.0	28 330		27 010
370.8	26 970	386.4	25 880
391.0	25 580	410.3	24 370

<sup>a</sup> very weak

<sup>b</sup> with poor resolution

Table 5.12  
Excitation Wavelengths of  $10^{-5}$  M 2,2'-Binaphthyl in  
Absolute Ethanol and Isopentane at 77K

Ethanol		Isopentane			
$\lambda_A^*$ (nm)	$\bar{\nu}$ (cm $^{-1}$ )	$\lambda_A^+$ (nm)	$\bar{\nu}$ (cm $^{-1}$ )	$\lambda_A^+$ (nm)	$\bar{\nu}$ (cm $^{-1}$ )
325.8	30 690	356.8	28 030	307.3	32 540
313.5	31 900	350.9	28 500	300.1 <sup>(a)</sup>	33 320
301.8	33 130	345.4	28 950	294.6 <sup>(a)</sup>	33 940
283.6	35 260	338.6	29 530	292.1 <sup>(a)</sup>	34 240
273.2	36 600	334.6	29 890	286.8	34 870
266.7	37 500	331.4	30 180	283.4 <sup>(a)</sup>	35 290
		322.4	31 010	274.8 <sup>(a)</sup>	36 390
		316.8	31 570		

<sup>a</sup> resolved only in  $\lambda_F = 358.8$  spectrum.


<sup>\*</sup>  $\lambda_F = 363.6, 353.0, 346.7$  nm (see Figure 5.15).

<sup>†</sup>  $\lambda_F = 436.1, 412.6, 388.6, 376.1, 366.8, 358.8$  nm (see Figure 5.13).

and ethanol show a decided wavelength of emission dependence, in addition to becoming somewhat sharper, particularly those in isopentane. The excitation spectrum in isopentane is towards longer wavelength compared with the excitation spectrum in alcohol, in agreement with the observed emission behaviour in these two solvents.

The broad band at 325.8 nm in ethanol glass is believed to have as its counterpart the sharper peak at 338.6 nm in isopentane with the immediately adjacent peaks being unresolved in ethanol; the 0-0 in excitation in ethanol is probably buried under this structureless band centered at 325.8 nm while the longest excitation band in isopentane, although very weak, may be discerned at 356.8 nm. Since the excitation and emission overlap significantly at 77K the apparent difference in the fluorescence excitation spectra monitored at the high energy edge of the emission, both in ethanol and isopentane, may be partially attributable to reabsorption of the fluorescence in this region. Reabsorption may account for the relative weakness of the long wavelength excitation bands for fluorescence monitored at 359 nm in isopentane or 347 nm in ethanol, both in the absorption-emission overlap region. It is unlikely that the entire wavelength effect is due to the distorting effect of possible reabsorption since this would not explain the variation of intensities at 338.6 nm to 322.4 nm in isopentane. This 322.4 nm band in isopentane is believed to be the red shifted counterpart of the peak at  $\sim 313.5$  nm in ethanol.

The differences between the spectra obtained in ethanol as opposed to alkane solvents at 77K could be ascribed to either specific solvent-solute interactions in the polar alcohol solution or to the



high viscosity of the ethanol glasses ( $\eta \sim 2.1 \times 10^{19}$  poise).<sup>214</sup> Trial spectra in highly strained cracked glasses of the hydrocarbon solvent methylcyclohexane ( $\eta \sim 1.2 \times 10^{18}$  poise at 77K)<sup>214</sup> resembled those found in 3 MP at this temperature, suggesting that the spectroscopic differences are primarily the result of some specific solvent-solute interaction in the ethanol solution, a rather surprising result in view of the low polarity of the 2,2'-binaphthyl solute. The difference in the room temperature emission in alkanes and ethanol, wherein the viscosities are comparably low, also supports this contention. The absorption spectrum of 2,2'-binaphthyl at 295K was apparently unaffected by solvent, with the same spectrum being obtained in ethanol and the hydrocarbon solvents.

#### 5.3.1c Fluorescence in Polycrystalline (Shpol'skii) Matrices

In contrast to the broad emission bands obtained in low temperature glassy media the fluorescence emission of 2,2'-binaphthyl- $h_{14}$  and - $d_{14}$  in polycrystalline matrices of methylcyclohexane at 77K yielded a wealth of vibrational structure. In this solvent the half-widths were typically  $100 - 150 \text{ cm}^{-1}$ , still far from the  $1 - 10 \text{ cm}^{-1}$  bandwidths observed in other Shpol'skii guest-host combinations. This is similar to the case of 2-phenylnaphthalene in methylcyclohexane matrices, as discussed in Section 4.2.1b.

Nominal solute concentrations were kept to a maximum of  $10^{-5} \text{ M}$  to avoid possible aggregation or precipitation at the lower temperature. A number of other matrix forming alkane solvents were tried with cyclohexane and n-pentane producing spectra of marginally inferior resolution to those in methylcyclohexane. The normal alkanes, hexane, heptane and octane gave very poorly resolved emission.

Both the  $-h_{14}$  and  $-d_{14}$  fluorescences show a large variation in relative intensities of the quasilines as a function of the excitation wavelength, as shown in the accompanying spectral traces, Figures 5.16 through 5.17. The wavenumbers of the 25 resolved vibronic bands for the  $-h_{14}$  species and 27 vibronic bands for the  $-d_{14}$  species are listed in Table 5.13, with the rough relative intensities with 300 nm excitation being noted.

Isotopic substitution of deuterium for hydrogen produced a small hypsochromic shift of the highest wavenumber band in the  $-h_{14}$  ( $28\,700\text{ cm}^{-1}$ ) and  $-d_{14}$  ( $28\,790\text{ cm}^{-1}$ ) spectra. Blue shifts of this magnitude are frequently seen on perdeuteration and are believed to arise from the decrease in zero-point energies of both ground and excited states upon deuteration, with the decrease being greater in the ground state.<sup>34</sup> A blue shift of comparable size was observed in the room temperature absorption spectrum of the isotopic 2,2'-binaphthyls. Although the  $S_0 \rightarrow S_1$  absorption is largely buried under the adjacent  $S_0 \rightarrow S_2$  band, for the higher energy absorption transitions at 212 and 254 nm the blue shift is  $\sim 80\text{ cm}^{-1}$  on perdeuteration while the molar absorptivities were unaffected.

Fluorescence excitation spectra, Figure 5.18, were obtained for four principal bands in the  $-h_{14}$  emission spectrum at 358.4, 363.6, 368.8 and 373.1 nm. The band of greatest interest, the highest energy band at 348.5 nm could not be monitored directly because of interference with scattered exciting light. It should be noted that the resolution of the fluorescence excitation was rather poor owing to the necessarily large excitation bandwidth. Even considering the large bandwidth it appears that the excitation spectrum is intrinsically broader than the

Figure 5.16

Uncorrected Fluorescence Emission Spectra of  $10^{-5}M$   
2,2'-Binaphthyl- $h_{14}$  in Polycrystalline Methylcyclohexane  
at 77K as a Function of Excitation Wavelength

indicated peaks correspond to monitoring wavelengths for excitation  
spectra, Figure 5.18; a = 358 nm; b = 364 nm; c = 369 nm; d = 373 nm.

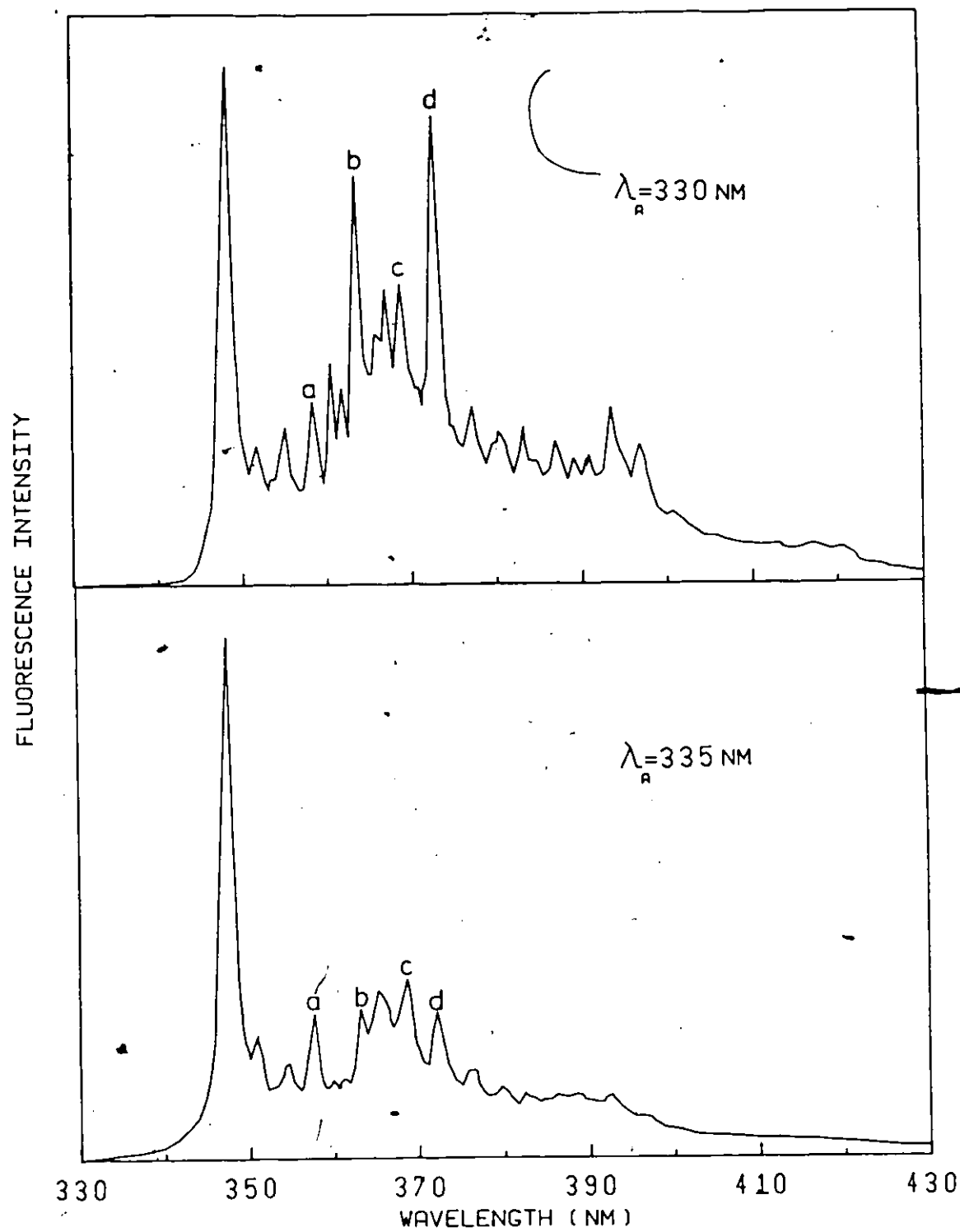


Figure-5.16



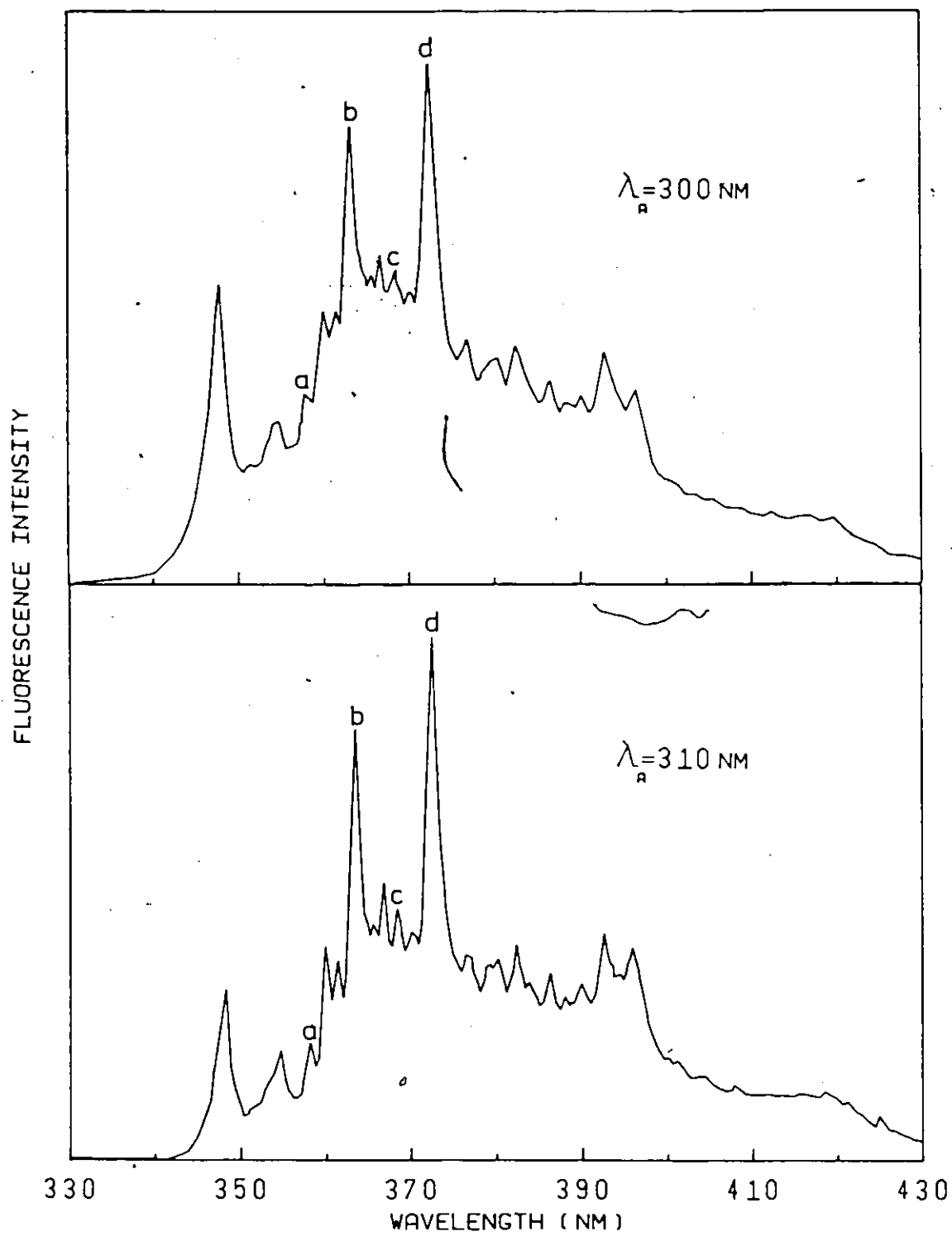


Figure 5.16  
continued

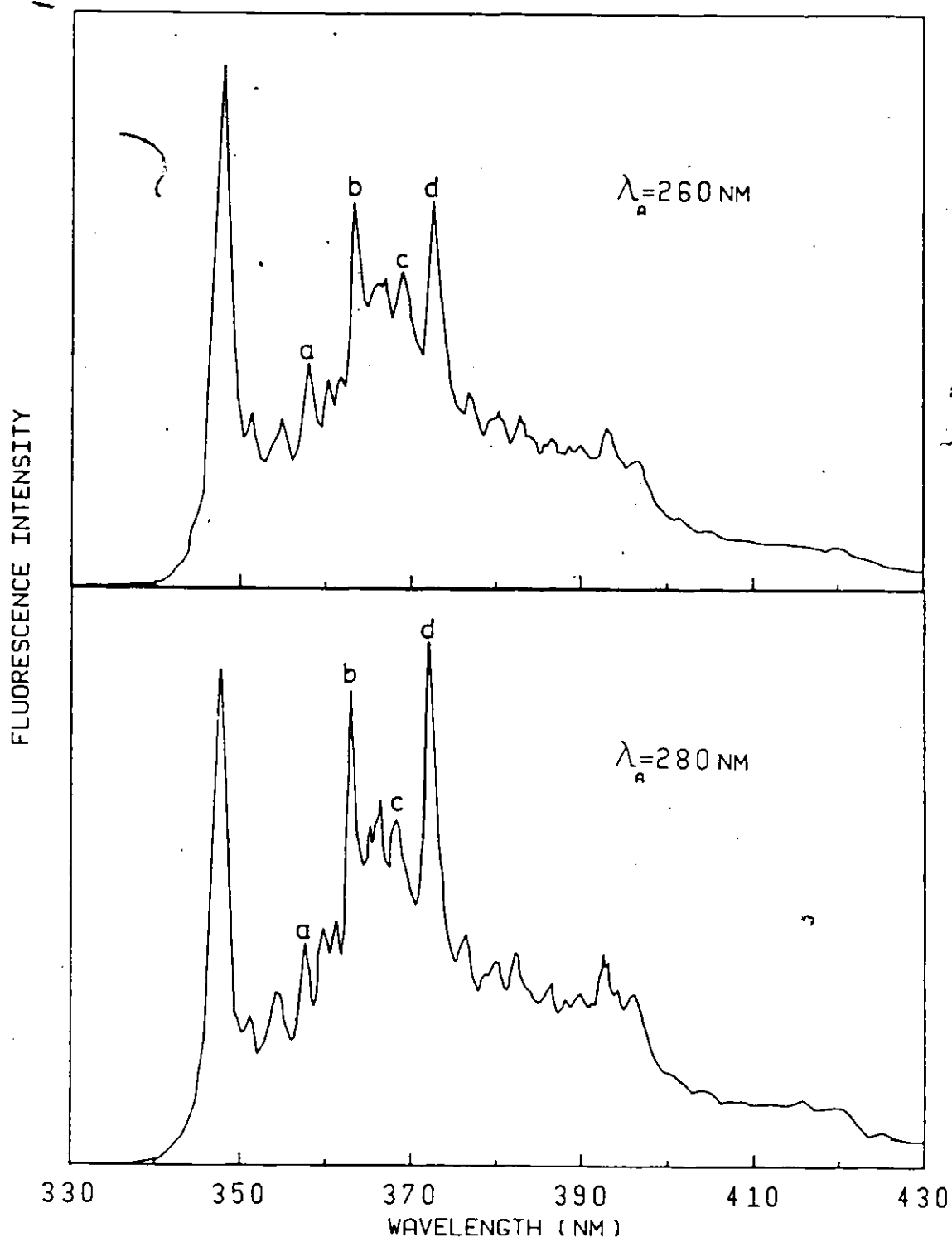


Figure 5.16  
continued

Figure 5.17

Uncorrected Fluorescence Emission Spectra of  $10^{-5}M$   
2,2'-Binaphthyl- $d_{14}$  in Polycrystalline Methylcyclohexane at 77K as a  
Function of Excitation Wavelength

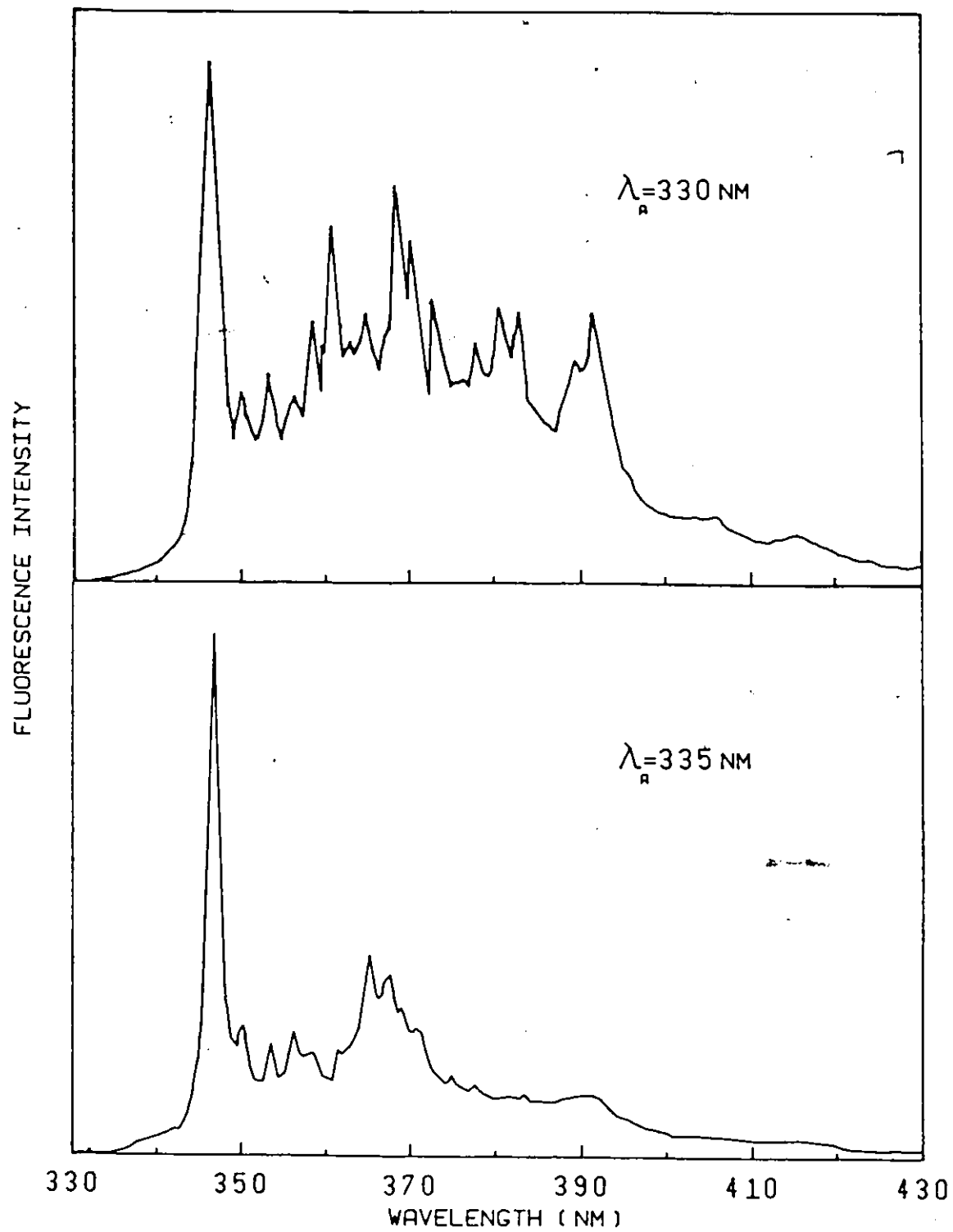


Figure 5.17

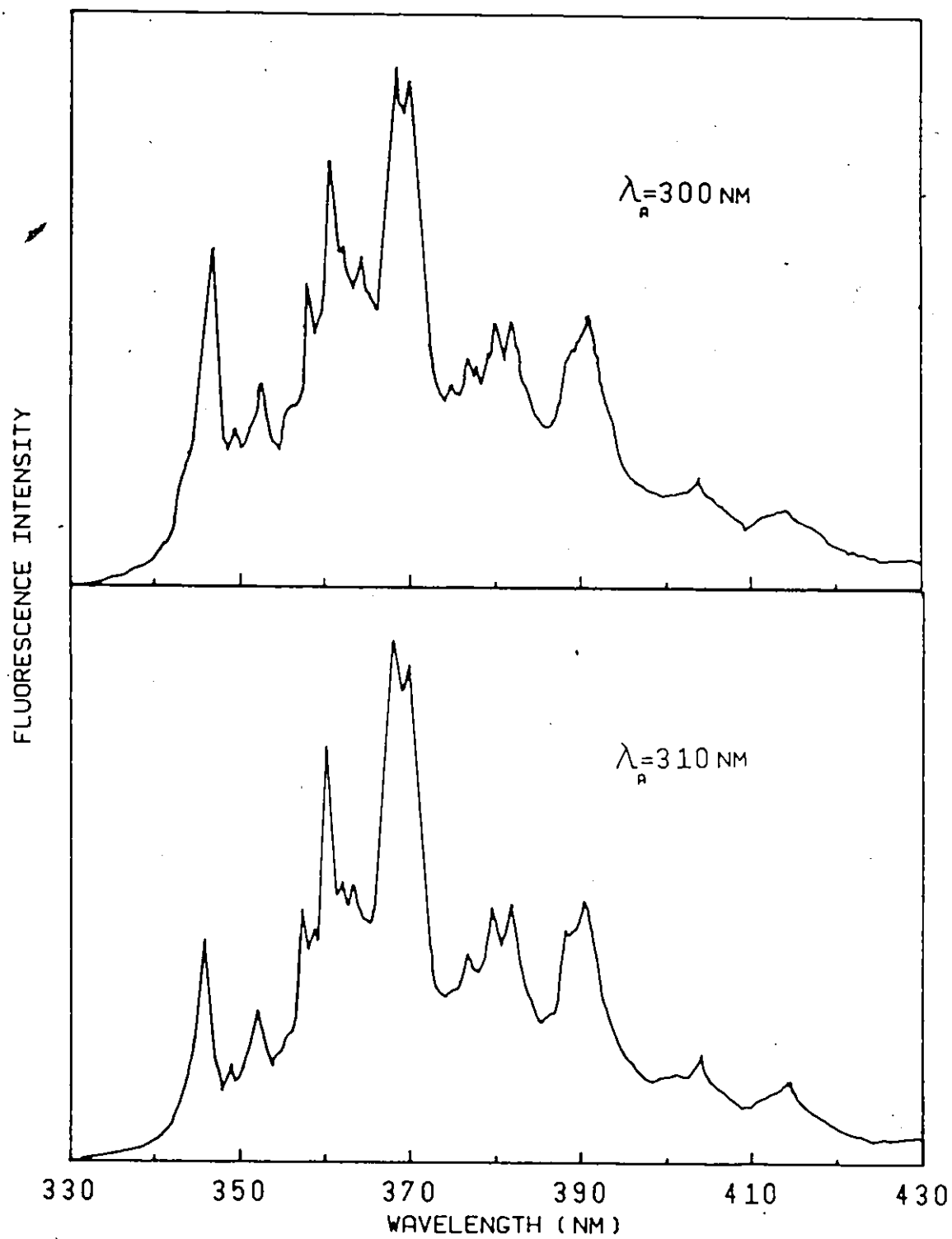


Figure 5.17  
continued

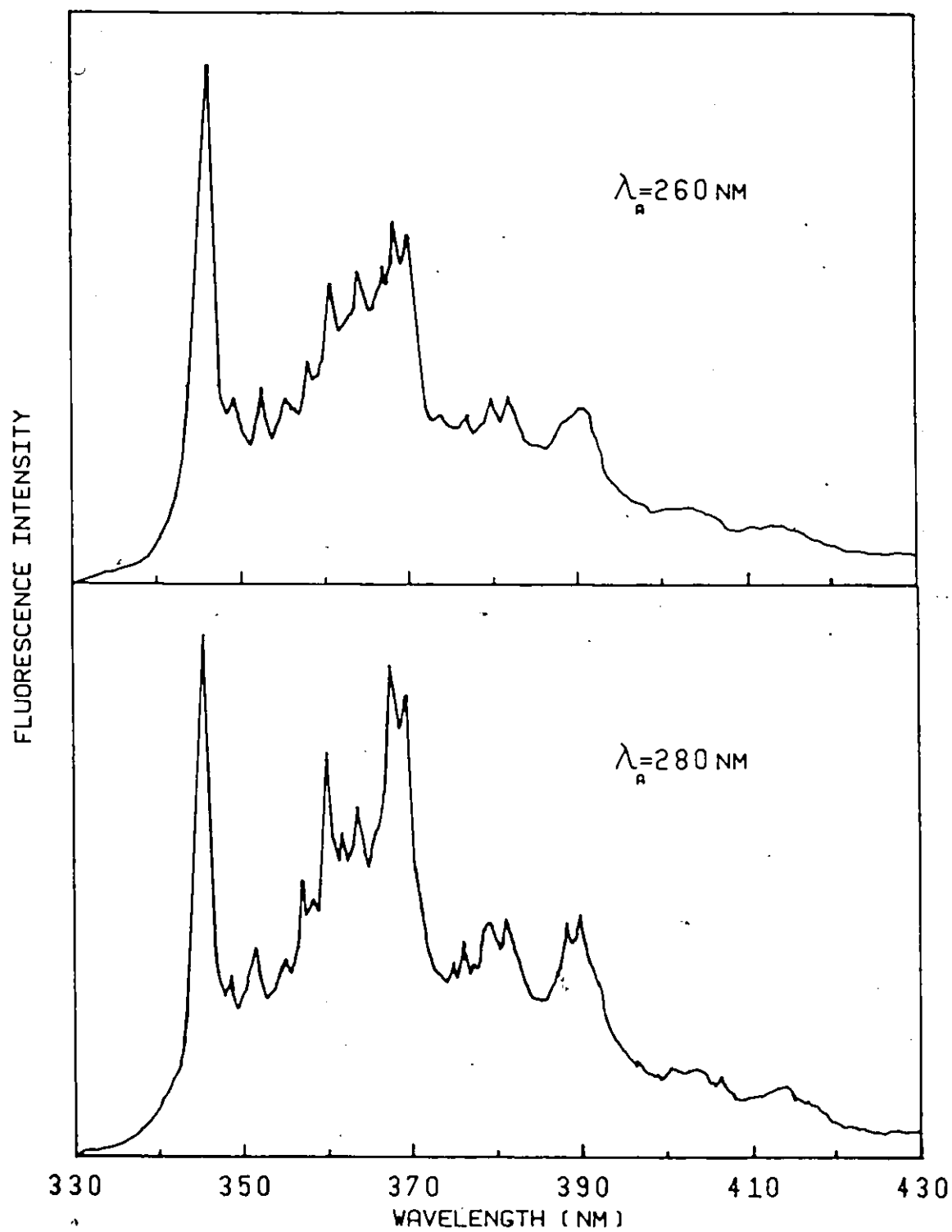


Figure 5.17  
continued

2

Table 5.13

Frequencies from the Fluorescence Spectra of  $10^{-5}M$   
2,2'-Binaphthyl- $h_{14}$  and  $-d_{14}$  in Polycrystalline Methylcyclohexane at 77K

$-h_{14}$		$-d_{14}$	
Relative Intensity <sup>a</sup> at $\lambda_A = 300$ nm	$\nu(\text{cm}^{-1})_{\pm 10 \text{ cm}^{-1}}$	Relative Intensity <sup>a</sup> at $\lambda_A = 300$ nm	$\nu(\text{cm}^{-1})_{\pm 10 \text{ cm}^{-1}}$
s	28 700	s	28 790
m	28 430	w	28 550
m	28 160	m	28 280
m	27 900	w	28 040
m	27 740	m	27 990
m	27 640	s	27 850
vs	27 510	w	27 750
s	27 220	vs	27 640
s	27 110	w	27 480
s	26 970	ms	27 360
vs	26 800	m,sh	27 160
m	26 490	vs	27 070
m	26 280	vs	26 940
m	26 100	s,sh	26 900
m	25 850	vw	26 640
m	25 710	vw	26 560
m	25 610	w	26 430
ms	25 420	vw	26 310
ms	25 200	m	26 230
w	24 940	m	26 080
w	24 720	m	25 630
w	24 650	m	25 500
w	24 520	vw	25 020
w	24 320	vw	24 808
w	23 820	w	24 660
		vw,sh	24 500
		w,broad	24 070

<sup>a</sup> s=strong; m=moderate; w=weak; v=very; sh=shoulder

Figure 5.18

Fluorescence Excitation Spectra of 2,2'-Binaphthyl- $h_{14}$  in  
Polycrystalline Methylcyclohexane at 77K as a Function  
of Emission Wavelength.

Curves are individually height normalized.





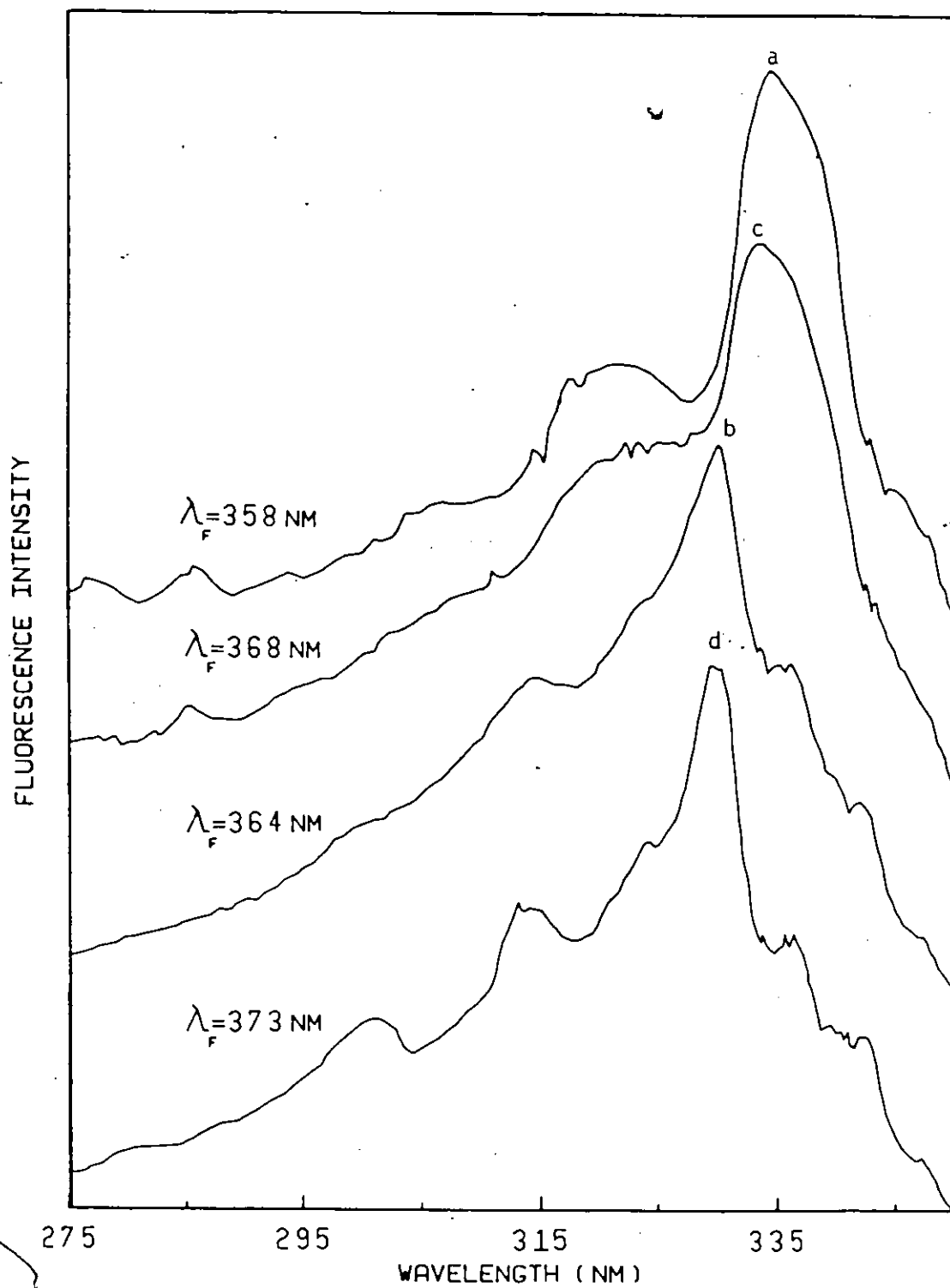


Figure 5.18

emission spectrum.

The excitation spectra indicate the presence of at least two absorbing species in the polycrystalline matrix, with the excitation spectra at 358.4 and 368.8 nm belonging principally to one species and the 363.6 and 373.1 nm spectra arising mostly from the other component. The monitored bands are indicated on the quasilinear emission spectrum for 2,2'-binaphthyl- $h_{14}$ . The excitation curves are individually height normalized so that quantitative comparison of the relative absorbances of the two species at a particular wavelength is difficult.

Examination of the wavelength dependent emission and excitation spectra clearly indicates that at least two fluorescent species are present in the methylcyclohexane matrix at 77K. For both  $-h_{14}$  and  $-d_{14}$  molecules the shortest wavelength band in emission dominates at excitation wavelengths of 335, 330 and 260 nm, while this band is comparatively weak if excitation is at 310 or 300 nm. At  $\lambda_A = 280$  nm the intensity of the  $28\,700\text{ cm}^{-1}$  band ( $-h_{14}$ ) and  $28\,790\text{ cm}^{-1}$  band ( $-d_{14}$ ) is roughly that of the other strong emission bands. With excitation at the extreme absorption edge, at  $\lambda_A = 335$  nm, the emission so obtained should correspond to that of the nearly pure red-absorbing component. On increasing the excitation energy to 300 and 310 nm the intensity of the more red-shifted emission component appears to pass through a maximum, decreasing again at shorter excitation wavelengths. The fluorescence emission of 2,2'-binaphthyl- $h_{14}$  and  $-d_{14}$  has been dissected into subspectra on the basis of the excitation wavelength effect. The apparent electronic origins of these two emissions lie about  $540 - 510\text{ cm}^{-1}$  apart. The assignment of various vibronic bands to one or another subspectrum is made on the basis of the variation of

relative intensities with excitation wavelength, particularly with  $\lambda_A = 335$  nm and 310 nm. These assignments are shown in Tables 5.14 and 5.15

The qualitative behaviour of both isotopic molecules is similar. Surprisingly the  $-d_{14}$  species shows no consistent lowering of the frequencies relative to the  $-h_{14}$  results, as would be expected if the vibrational modes involved much C-H or C-D character. This may simply reflect the low precision in the measurement of the vibrational spacings at these rather wide bandwidths. The separation between the origins of the two subspectra is  $540\text{ cm}^{-1}$  for the  $-h_{14}$  molecule and  $510\text{ cm}^{-1}$  in the  $-d_{14}$  case; these values are identical within the experimental error. The mean figure of  $525\text{ cm}^{-1}$  would then represent the total energy difference,  $\Delta S_0 + \Delta S_1$ , for the two fluorescent components in the emission of 2,2'-binaphthyl in polycrystalline methylcyclohexane at 77K. These observations are much in keeping with the recent results of Riley and co-workers<sup>190</sup> for 1,1'-binaphthyl in Shpol'skii matrices at 4.2K, as discussed in Section 5.1.4. For the 2,2'-binaphthyl the sum of the energy differences between the two proposed conformers in the ground and excited states is the much smaller  $525\text{ cm}^{-1}$ , in contrast to the large difference of  $4850\text{ cm}^{-1}$  proposed for the 1,1'-binaphthyl conformers.<sup>190</sup> Unlike 1,1'-binaphthyl, for 2,2'-binaphthyl the higher excitation energies led to the longer wavelength subspectrum. This would indicate that the 2,2'-binaphthyl conformer strongly excited at 310 and 300 nm must undergo some geometry change or relaxation subsequent to excitation, even at 77K.

The spectral behaviour of 2,2'-binaphthyl in polycrystalline methylcyclohexane at 77K is considerably different from that observed for fluid or glassy solutions of that molecule. This tends to indicate

Table 5.14

Vibrational Subsystems in the Fluorescence Emission Spectrum of  
2,2'-Binaphthyl-h<sub>14</sub> in Polycrystalline Methylcyclohexane at 77K

$\lambda_A = 335 \text{ nm}$			$\lambda_A = 310 \text{ nm}$		
$\bar{\nu} (\text{cm}^{-1})^{\dagger}$ $\pm 10 \text{ cm}^{-1}$	$\Delta \bar{\nu} (\text{cm}^{-1})$ $\pm 20 \text{ cm}^{-1}$	Relative* Intensity	$\bar{\nu} (\text{cm}^{-1})^{\dagger}$ $\pm 10 \text{ cm}^{-1}$	$\Delta \bar{\nu} (\text{cm}^{-1})$ $\pm 20 \text{ cm}^{-1}$	Relative* Intensity
28 700	0,0	vs	28 160	0,0	w
28 430	0,270	m	27 740	0,420	m
27 900(a)	0,800	m	27 640	0,520	m
27 220	0,1480	m	27 510(b)	0,650	vs
27 110(c)	0,1590	vs	26 970	0,1190	w
			26 800(d)	0,1360	vs
			26 400	0,1670	m
			26 280	0,1880	m
			26 100	0,2060	m
			25 850	0,2310	m
			25 710	0,2450	m
			25 610	0,2550	m
			25 420	0,2740	s
			25 200	0,2960	s

<sup>†</sup> bracketted letters refer to bands monitored in excitation spectra and indicated on fluorescence emission spectra, Fig. 5.16

\* v=very; w=weak; m=moderate; s=strong.

Table 5.15

Vibrational Subsystems in the Fluorescence Emission Spectrum of  
2,2'-Binaphthyl-d<sub>14</sub> in Polycrystalline Methylcyclohexane at 77K

$\lambda_A = 335 \text{ nm}$			$\lambda_A = 310 \text{ nm}$		
$\bar{\nu} (\text{cm}^{-1})$ $\pm 10 \text{ cm}^{-1}$	$\Delta \nu (\text{cm}^{-1})$ $\pm 20 \text{ cm}^{-1}$	Relative* Intensity	$\bar{\nu} (\text{cm}^{-1})$ $\pm 10 \text{ cm}^{-1}$	$\Delta \nu (\text{cm}^{-1})$ $\pm 20 \text{ cm}^{-1}$	Relative* Intensity
28 790	0,0	vs	28 280	0,0	m
28 550	0,240	m	27 850	0,430	s
28 040	0,750	m	27 750	0,530	s,sh
27 990	0,800 <sup>†</sup>	m	27 640	0,640	vs
27 360	0,1430	s	27 480	0,800	m
27 160	0,1630	s	27 070	0,1210	m
			26 940	0,1340	vs
			26 900	0,1380	s,sh
			26 640	0,1640	w
			26 560	0,1720	m
			26 430	0,1850	m,sh
			26 310	0,1970	m,sh
			26 230	0,2050	s
			26 080	0,2200	s
			25 630	0,2650	s
			25 500	0,2780	s

<sup>†</sup> poorly resolved.

\* v=very; w=weak; m=moderate; s=strong; sh=shoulder.

that the geometries of the conformers in the methylcyclohexane matrix are largely dictated by the crystalline environment, that is, the potential in polycrystalline methylcyclohexane is partially, if not chiefly intermolecular in origin. In fluid solution it is believed that the potential functions of the participating singlet states of 2,2'-binaphthyl will be more nearly intramolecular in nature. Similar conclusions may be drawn for the 1,1'-binaphthyl work of Riley (Section 5.1.4).

The actual geometries of the two 2,2'-binaphthyl conformers in the polycrystalline matrix are not known but the two subspectra clearly do not show similar progressions, merely displaced with respect to one another. This observation, in conjunction with the  $525\text{ cm}^{-1}$  shift, suggests that the dual emission is not a trivial consequence of the possible presence of two crystalline modifications of methylcyclohexane at 77K. The dissimilar vibrational progressions for the two conformers points to two fluorescent species with different geometries. It is unlikely that both conformers could be planar, as the planar s-cis and s-trans forms of 2,2'-binaphthyl might be expected to exhibit nearly identical vibrational details in their fluorescence emission spectra. The fluorescence origins of the 2,2'-binaphthyl emission in the polycrystalline matrix may be compared with the emission origins of the model compounds naphthalene and 1,2,7,8-dibenzofluorene (1,2,7,8-DBF). This latter compound was synthesized as a model for the coplanar s-cis conformation of 2,2'-binaphthyl wherein rotation about the C-2-C-2' bond is eliminated by the restraining methylene bridge.

Given the rigidity of the molecular skeleton 1,2,7,8-DBF is probably planar in both its ground and first excited singlet states.

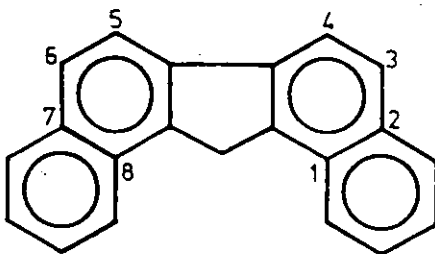


Figure 5.19

Structural Formula and Numbering for 1,2,7,8-Dibenzofluorene

Room temperature and low temperature excitation and emission spectra, Figures IV.1 and IV.2, in Appendix IV, show considerable vibrational structure typical of rigid aromatic systems, in addition to a coincidence of the origins in absorption (excitation) and emission at  $28\,030\text{ cm}^{-1}$  (356.8 nm). This latter feature in addition to the substantial mirror-image symmetry about the 0-0 indicates that this model compound is planar in both  $S_0$  and  $S_1$ .

The fluorescence origin for naphthalene in a low temperature Shpol'skii matrix lies at  $31\,746\text{ cm}^{-1}$ .<sup>98</sup> On the basis of these two model geometries it may be conjectured that the fluorescent conformers of 2,2'-binaphthyl in the polycrystalline matrix, with probably origins of  $28\,700\text{ cm}^{-1}$  and  $28\,160\text{ cm}^{-1}$ , have considerable  $\pi$ -electronic interaction between the constituent aromatic rings and are both closer to planar species than to perpendicular ones. Neither species show distinct naphthalene-like vibronic progressions.

The excitation spectra of the polycrystalline solutions of 2,2'-binaphthyl obtained at various emission wavelengths nicely complement the emission results. As mentioned earlier the presence of at least two,

emitting species is revealed in these curves. The conclusion that the emission bands labelled "a" (358.4 nm,  $27\,900\text{ cm}^{-1}$ ) and "c" (368.8 nm,  $27\,110\text{ cm}^{-1}$ ) belong chiefly to the species absorbing at longer wavelength is directly borne out in Figure 5.18. This figure also confirms that the bands "b" (363.6 nm,  $27\,510\text{ cm}^{-1}$ ) and "d" (373.1 nm,  $26\,800\text{ cm}^{-1}$ ), strong in the  $\lambda_A = 310, 300\text{ nm}$  emission spectra, are more strongly excited at shorter wavelength.

The cumulative evidence would point to at least two fluorescent conformers for 2,2'-binaphthyl in the polycrystalline matrix, the geometries of which are more nearly planar than perpendicular. These geometries are most likely imposed on the molecule by the lattice restraints, rather than arising from a purely intramolecular potential. Furthermore these conformers are spectroscopically distinguishable in the steady-state emission and excitation spectra, the sum of the differences in the ground and excited state minima amounting to about  $525\text{ cm}^{-1}$ .

#### 5.3.1d Oxygen Quenching of the Steady-State Fluorescence of 2,2'-Binaphthyl at Room Temperature

To further explore the question of possible conformers of 2,2'-binaphthyl in fluid solution and in anticipation of the fluorescence lifetime studies singlet quenching experiments using molecular oxygen were conducted on cyclohexane solutions of 2,2'-binaphthyl nominally at 295K. This technique has been applied successfully by several authors to study the differential quenching of the emission spectra of the conformers of 1,2'-diarylethylenes.<sup>11,16</sup>

The fluorescence emission spectra of a dilute ( $1.2 \times 10^{-4}\text{ M}$ ) solution of 2,2'-binaphthyl- $\text{h}_{14}$  in cyclohexane, equilibrated under 1



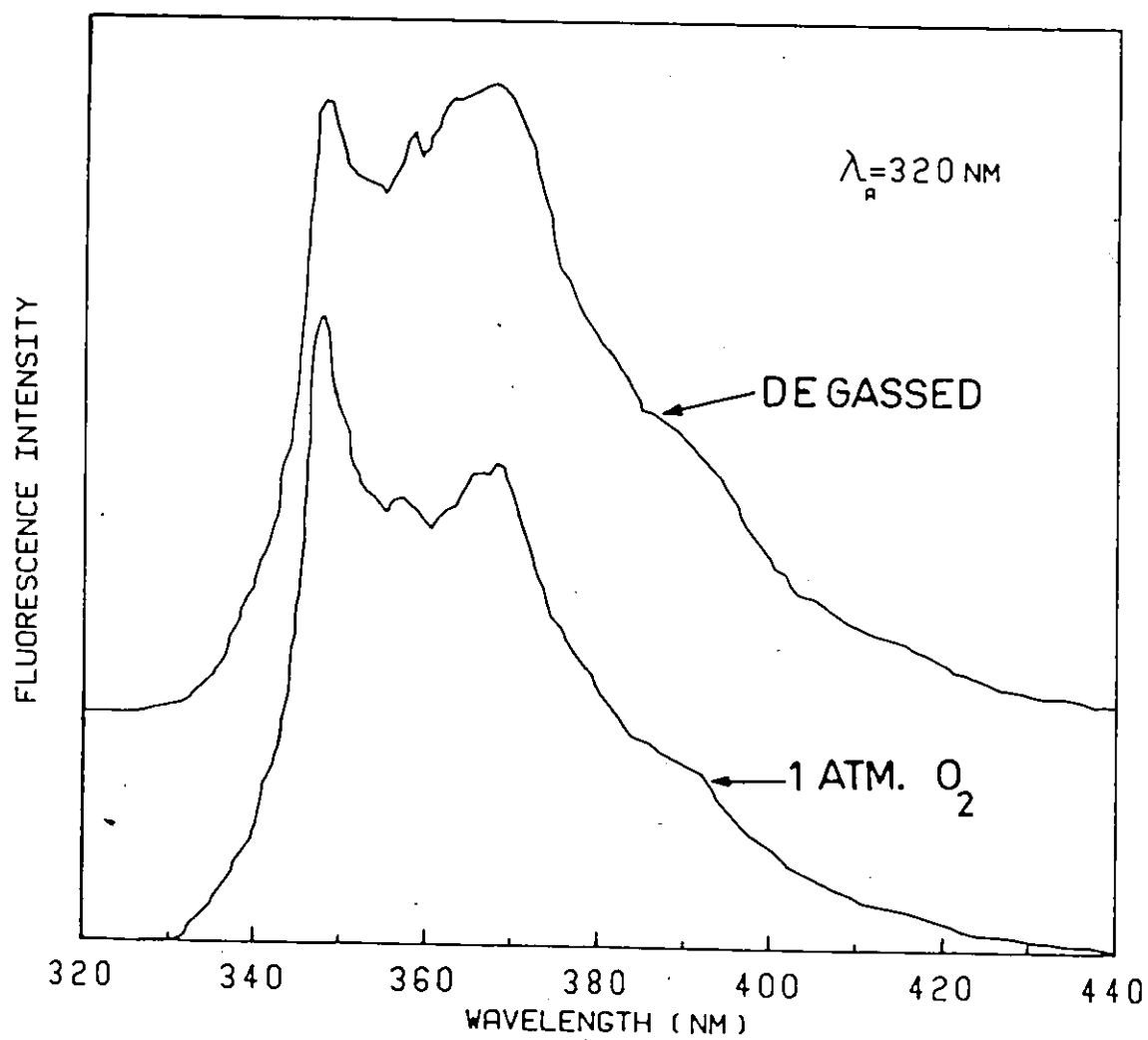


Figure 5.20  
Fluorescence Emission of  $1.2 \times 10^{-4} \text{ M}$  2,2'-Binaphthyl in  
Cyclohexane at 295K with  $\lambda_A = 320 \text{ nm}$   
upper curve: degassed by 6 cycles of freeze-pump-thaw  
lower curve: under 1 atmosphere of oxygen

atmosphere of  $O_2$ , were recorded as a function of the excitation wavelength. In contrast to the degassed solutions these oxygenated solutions showed practically no excitation wavelength dependence. In all quenched solutions the 348.6 nm band dominates the fluorescence spectrum. Figure 5.20 clearly illustrates the selective quenching of the red shifted, and presumably longer-lived component upon the addition of the singlet quencher. Both solutions in Figure 5.20 were excited at the common wavelength, 320 nm, but in the degassed solution the emission maximizes in the region 365 - 375 nm. Introduction of oxygen apparently quenches the species emitting in this region rather more strongly than the shorter wavelength component, leaving the 348.6 nm band as the most intense feature of the oxygen saturated solution. Excitation of the oxygenated solutions anywhere in the range 335-260 nm produced spectra practically identical to those shown for  $\lambda_A = 320$  nm in Figure 5.20. These alterations in spectral properties are not the result of irreversible photochemical reaction of  $O_2$  with the 2,2'-binaphthyl solute, as any single sample could be repeatedly cycled from a degassed to oxygenated condition with no accompanying irreversible changes in the emission characteristics, including fluorescence lifetime. Moreover, no contact charge-transfer absorption was evident in the oxygenated solutions above 260 nm.<sup>94</sup>

This steady-state quenching evidence suggests that at least two fluorescent species, characterized by different fluorescence lifetimes and emission spectra are present in the room temperature cyclohexane solution of 2,2'-binaphthyl. That the longer-lived species, which fluoresces somewhat to the red of the shorter-lived component, is nearly totally quenched at one atmosphere of oxygen quencher is apparent from

the lack of excitation wavelength effect on the fluorescence emission of the oxygenated solutions. It is expected that the lower curve (oxygenated solution) in Figure 5.20 will reflect the fluorescence emission of the nearly purely short-lived component. This spectrum is similar to those obtained in degassed solutions upon excitation at either wavelength extreme at 330 nm or 270 and 260 nm. At intermediate excitation energies in degassed solution the longer-lived component contributes substantially to the total intensity, leading to an emission maximum at 368 nm, rather than the 349 nm maximum seen at  $\lambda_A = 330$  nm or in oxygenated solutions.

### 5.3.2 Fluorescence Quantum Yield Measurements

The relative fluorescence quantum yields of 2,2'-binaphthyl were determined at 295K in cyclohexane and at 295K and 77K in 3 MP in the usual manner. Both ambient and low temperature fluorescence quantum yields showed a distinct variation with excitation wavelength, contrary to expectation if Vavilov's law is obeyed for this system. In the range  $\lambda_A = 320 - 270$  nm the room temperature quantum yield in cyclohexane was practically constant (at  $\phi_f \sim 0.61 \pm .02$ ) but it declined sharply outside this range of excitation energies to 0.39 at  $\lambda_A = 330$  nm and 0.46 at  $\lambda_A = 260$  nm. The results for the  $-h_{14}$  isotopic molecule are tabulated in the two succeeding tables.

The quantum yield of the  $-d_{14}$  isotope was determined by measurement relative to the perprotio-species. Absorbances of the two solutions in cyclohexane were  $\sim 0.5$  (in 1 cm cells) and matched to within 1% at the three excitation wavelengths, 320, 300 and 280 nm. In all cases the areas under the fluorescence emission curves for both species were identical to within 3%, indicating that the fluorescence quantum yield

Table 5.16  
Relative Fluorescence Quantum Yields of  
2,2'-Binaphthyl in Cyclohexane as a Function  
of Excitation Wavelength at 295K<sup>a</sup>

$\lambda_A$ (nm)	$\phi_f$	$\lambda_A$ (nm)	$\phi_f$
330	0.39	290	0.60
320	0.64	280	0.59
310	0.58	270	0.60
300	0.63	260	0.46

<sup>a</sup> measured in triplicate at each  $\lambda_A$ .

Table 5.17  
Relative Fluorescence Quantum Yields of  
2,2'-Binaphthyl in 3-Methylpentane at 295K and 77K  
as a Function of Excitation Wavelength<sup>a</sup>

$\lambda_A$ (nm)	$\phi_f$ (295K)	$\phi_f$ (77K)
320	0.58	0.64
300	0.57	0.34
280	0.66	0.85

<sup>a</sup> measured in triplicate at each  $\lambda_A$  and temperature.

of 2,2'-binaphthyl-d<sub>14</sub> was in no way different from the quantum yield of the -h<sub>14</sub> species. A number of other authors have also found  $\phi_f$  to be invariant upon deuteration for a large selection of aromatic hydrocarbons.<sup>33,34</sup>

Berlman<sup>34</sup> gives  $\phi_f$  of 2,2'-binaphthyl in cyclohexane at room temperature as 0.41 with 265.0 nm excitation in fair agreement with the present measurement. Lentz and coworkers<sup>146</sup> arrived at a somewhat higher figure, 0.55, in cyclohexane at 25°C, ( $\lambda_A = 254$  nm), measured relative to quinine sulfate solution. On the whole the quantum yields determined by this latter group appear to be systematically slightly larger than those measured by other workers for a variety of other naphthalene derivatives so this discrepancy in actual values of  $\phi_f$  is not viewed as serious.

### 5.3.3 Fluorescence Decay Measurements

The most striking feature of all the fluorescence decay measurements on 2,2'-binaphthyl-h<sub>14</sub> and -d<sub>14</sub> was that under no conditions could the intensity versus time data be adequately described by a monoexponential decay law of the form

$$I(t) = \alpha \exp(-t/\tau). \quad (5.2)$$

The fluorescence decay of the 2,2'-binaphthyls at 77K or 295K in the various solvents could, in all cases, be well fitted to a biexponential decay function

$$I(t) = \alpha \exp(-t/\tau_1) + \beta \exp(-t/\tau_2) \quad (5.3)$$

where the lifetimes  $\tau_1$  and  $\tau_2$  remained invariant for a given solvent,

Table 5.18

Fluorescence Decay of  $10^{-4}$  M 2,2'-Binaphthyl in Cyclohexane at 295K

Fit to Biexponential Decay Model: Comparison of Nitrogen and  
Deuterium Filled Excitation Sources.<sup>a</sup>

Excitation Source	$\tau_1$ (ns)	$\tau_2$ (ns)	$\alpha/\beta$	$\chi^2_\nu$
D <sub>2</sub>	21.06	103.8	1.32	1.61
( $\lambda_A = 300$ nm)	20.06	102.6	1.37	1.25
	21.34	105.6	1.37	1.52
N <sub>2</sub>	21.84	103.0	1.37	1.36
( $\lambda_A = 297.7$ nm)	<u>22.94</u>	<u>107.1</u>	<u>1.41</u>	1.29
means	21.45 $\pm$ 1.06	104.4 $\pm$ 1.9	1.37 $\pm$ .03	

<sup>a</sup>  $\lambda_F =$  KV399, KV408 filters in series.

temperature and solute concentration whereas the preexponential factors (or better, their ratio  $\alpha/\beta$ ) varied with both  $\lambda_A$  and  $\lambda_F$ .

The fluorescence decay was examined in greatest detail in cyclohexane at 295K but experiments were also conducted in 3 MP, isopentane and ethanol at 295K and 77K. In all cases the excitation wavelength was selected by means of a monochromator whereas the emission wavelengths were selected variously by colour filters, sharp-cut filters, interference filters or by a second monochromator. Both  $D_2$  and  $N_2$  excitation sources were used except where the use of the second monochromator mitigated against the use of the 100-fold weaker deuterium source. Essentially identical results were obtained using either excitation source, as shown by Table 5.18.

The preceding table shows the close agreement obtained with either gas filling. The reduced chi-squared parameter for the biexponential fit was somewhat larger than desirable but typical of those obtained using the Schott KV Series sharp-cut filters. This is probably the result of some very long lived residual emission of the filters themselves, albeit at a rather low level. This problem has been reported for these particular filters by other workers in the field;<sup>215</sup> this effect persists in the results given in Table 5.18 too, giving rather large values of  $\chi^2_\nu$  even for the biexponential fit. Incomplete blocking of the scattered exciting light by the Schott filters is considered the less likely culprit since the published transmission curves indicate a very efficient scattered light rejection (transmission down to  $\sim 10^{-5}$  by 20 nm below cut wavelength) for these filters. Inclusion of a scattered light component would also tend to systematically shorten both characteristic lifetimes

with a lesser effect on the reduced chi-squared value.

Table 5.19 shows the results of deconvoluting some of the room temperature 2,2'-binaphthyl decay data both as a mono- and a biexponential decay, with the reduced chi-squared being applied as the criterion for the goodness-of-fit.<sup>53</sup> It is apparent that the fluorescence decay of 2,2'-binaphthyl-h<sub>14</sub> is not well described by a single exponentially decaying fluorescent component, with the reduced chi-squared routinely exceeding 50. Furthermore the lifetime deduced from the monoexponential fit varies greatly with the choice of excitation wavelength, contrary to expectation for a single emitting state or species. This variation of  $\tau$  (mono) as a function of  $\lambda_A$  (at fixed emission conditions) is smooth but not monotonic, passing through a maximum at 300 - 310 nm excitation.

A dramatic improvement in the goodness-of-fit was obtained upon fitting a biexponential model to the experimental decay data,  $\chi^2_v$  dropping to about  $\leq 2$  in all cases.  $\chi^2_v$  values significantly above 1 for the biexponential fit likely result from those sources discussed earlier. Most importantly, the decay at all excitation wavelengths can be characterized by two invariant lifetime arguments,  $\tau_1 = 22.09 \pm 1.07$  ns and  $\tau_2 = 103.6 \pm 1.7$  ns, whose relative contributions, as measured by the ratio of pre-exponential factors,  $\alpha/\beta$ , are the only variables.

The high degree of reproducibility of  $\tau_1$ ,  $\tau_2$  and  $\alpha/\beta$  at a particular  $\lambda_A$  strongly suggests that the appearance of a second component in the fluorescence decay is not merely the result of some transient instrumental artifact such as radiofrequency noise or sample contamination since the replicate experiments were performed on different samples at widely separated times.



Table 5.19

Comparison of Mono- and Biexponential Fitting of Decay Data<sup>a</sup> for  
10<sup>-4</sup>M 2,2'-Binaphthyl in Cyclohexane at 295K

$\lambda_A^b$ (nm)	Biexponential Fit				Monoexponential Fit	
	$\tau_1$ (ns)	$\tau_2$ (ns)	$\alpha/\beta$	$\chi^2_v$	$\tau$ (ns)	$\chi^2_v$
335.0	24.02	106.2	7.94	1.48	41.93	74.62
332.5	23.97	105.9	7.00	1.57	42.80	75.46
330.0	23.12	101.2	5.84	1.58	44.60	113.3
	23.66	103.8	6.03	1.53	44.41	77.64
327.5	23.81	104.7	4.62	1.22	51.78	77.65
325.0	23.05	105.9	3.11	1.35	61.71	80.79
	22.32	101.0	3.00	1.36	59.83	75.71
320.0	22.55	103.3	2.00	1.17	70.58	63.92
	22.29	105.2	1.98	1.26	72.36	65.91
310.0	22.01	105.4	1.30	1.37	81.12	69.96
	20.81	101.8	1.27	1.39	79.21	69.84
300.0	21.06	103.8	1.32	1.61	80.31	69.10
	20.06	102.6	1.37	1.25	78.70	49.30
	21.34	105.6	1.37	1.52	80.56	74.72
290.0	21.72	104.9	1.60	1.29	76.90	57.47
280.0	21.27	101.6	2.48	2.16	65.07	113.3
	21.72	103.7	2.58	1.78	65.61	117.2
270.0	21.65	101.0	2.68	1.48	63.12	78.69
	21.49	102.9	2.72	1.85	63.56	81.73
260.0	21.62	101.6	2.08	1.57	69.23	67.21
	21.36	102.9	2.10	1.68	69.77	102.5
250.0	21.65	103.4	1.85	1.76	72.83	93.74
	21.57	103.9	1.96	1.76	72.31	64.75
means	22.09±1.07	103.6±1.7			65.68±12.76	

<sup>a</sup>  $\lambda_F$  = Schott KV399, KV408 filters in series.

<sup>b</sup> D<sub>2</sub> filled lamp.

These results then imply the presence of at least two emitting states or species in the 2,2'-binaphthyl solution, each characterized by its own singlet lifetime and having overlapping fluorescence spectra. The ratio  $\alpha/\beta$  gives a rough estimate of the contribution of each to the intensity as a function of time after excitation.<sup>16</sup> A better estimate may be obtained by integration of Equation 5.3 over time

$$\int_{t_0}^{\infty} I(t) dt = \int_{t_0}^{\infty} \{ \alpha \exp(-t/\tau_1) + \beta \exp(-t/\tau_2) \} dt \quad (5.4)$$

$$= \alpha \tau_1 + \beta \tau_2$$

so that  $\alpha \tau_1$  and  $\beta \tau_2$  are, respectively, the contributions of the short-lived (1) and long-lived (2) species to the total fluorescence intensity. Figure 5.21 is derived from the data of Table 5.19, using the mean lifetimes of  $\tau_1 = 22.09$  ns and  $\tau_2 = 103.6$  ns, and shows the smooth variation of  $\alpha \tau_1 / \beta \tau_2$  with excitation wavelength at the fixed emission conditions. This figure indicates that the long lived species 2 dominates the emission at excitation wavelengths below 330 nm while above 330 nm the contribution of species 1 increases rapidly, implying that while the absorption spectra of 1 and 2 overlap strongly they are not entirely coincident with species 1 absorbing somewhat more strongly at the red end than species 2. Excitation at the long wavelength edge of the electronic absorption band of 2,2'-binaphthyl may then be expected to selectively excite the shorter lived species 1, while excitation in the region 300 - 310 nm, where  $\alpha \tau_1 / \alpha \tau_2$  is a minimum may be expected to favour the longer lived species 2. These observations are in agreement with the corresponding steady-state room temperature emission properties of 2,2'-binaphthyl, in particular

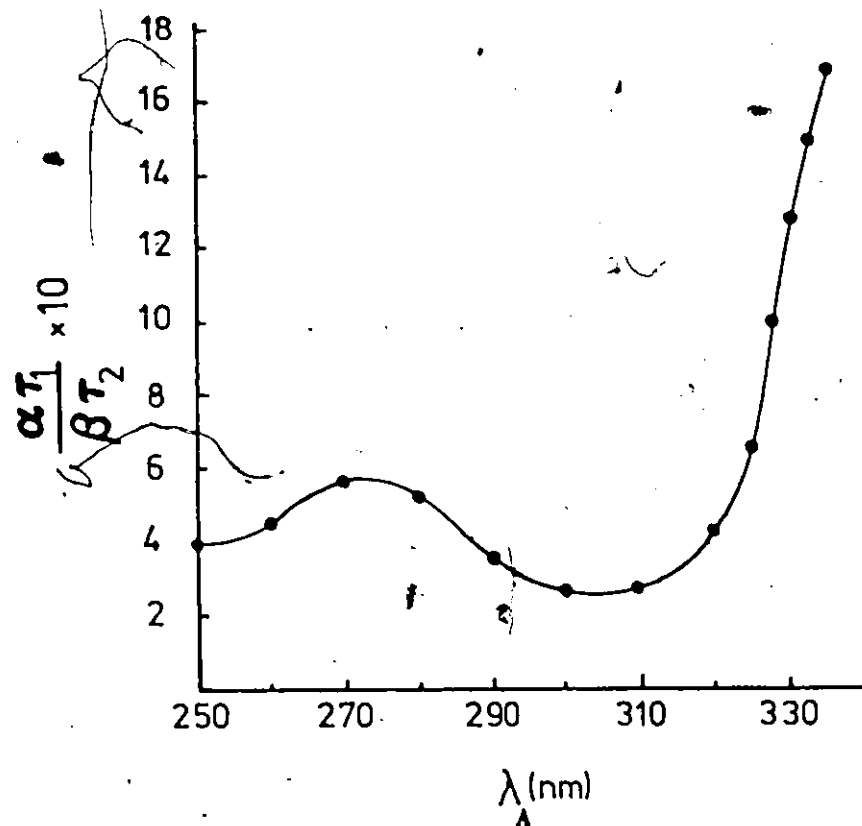


Figure 5.21

Relative Contribution of Species 1 and Species 2  
to Total Decay Intensity as a Function of  
Excitation Wavelength; derived from Table 5.19

the wavelength dependence of the emission and the identification, by oxygen quenching, of the short lived component as that one primarily excited at  $\lambda_A = 330$  nm and at  $\lambda_A = 260 - 270$  nm.

It should be emphasized that Figure 5.21 gives only the relative contributions of the two lifetime components; this would represent the ratio of absolute contributions to the total decay intensity only if the steady-state fluorescence intensities of the two species were identical at the wavelength or wavelengths (for filtered emission) of emission. In general there is no reason to suppose that the intensity of the two emissions will be equal at each and every emission wavelength since the emission spectra of species 1 and 2 will not necessarily be coincident nor will the two species have the same fluorescence quantum yields.

From the wavelength dependence of the emission spectra and the observation of two lifetime components in the fluorescence decay of 2,2'-binaphthyl even in fluid solution at room temperature it appears probable that 2,2'-binaphthyl may exist as discrete conformers in the electronic ground state at 295K. Since the absorption process is much faster ( $\sim 10^{-15}$  s) than any possible interconversion in the ground state these conformers, two or possibly more, will be prepared in their distinct Franck-Condon states immediately after excitation. Unlike, for example, the case of 1,1'-binaphthyl in fluid solution, it appears that conversion or interconversion of the excited conformers cannot be occurring much faster than the other photophysical processes, especially radiative return to the ground states, since the decay is characterized by two lifetimes even in fluid solution. Under conditions of rapid interconversion in the excited state the two species would decay with a common lifetime given by

Equation 2.59

$$\tau = 2/(k_1 + k_2).$$

The kinetic schemes have been more fully outlined in Section 2.8.

Failure to obtain a monoexponential decay for 2,2'-binaphthyl at room temperature is strong evidence that the rate of interconversion or conversion of the excited conformers is comparable to, or slower than the radiative depletion of the excited states.

Birks and coworkers<sup>11</sup> have given a full kinetic analysis of the fluorescence of such systems, applied specifically to the conformeric emission in solutions of trans-2-styrylnaphthalene (1-phenyl-2-naphthylethylene). The fluorescence decay as a function of time at fixed excitation and emission wavelengths was given by Equation 2.79

$$I(t)[\lambda_F, \lambda_A] = f_1[\lambda_A]F_1[\lambda_F]k_1e^{-k_1t} + f_2[\lambda_A]F_2[\lambda_F]k_2e^{-k_2t}$$

and the fractions of the two conformers in the excited state were given by Equations 2.71 and 2.72.

$$f_1[\lambda_A] = \frac{\epsilon_1[\lambda_A]C_1}{\epsilon[\lambda_A]C}$$

$$f_2[\lambda_A] = \frac{\epsilon_2[\lambda_A]C_2}{\epsilon[\lambda_A]C}$$

Equation 2.82, which gave a relationship between the experimental quantity,  $(\alpha/\beta)[\lambda_A, \lambda_F]$ , the ratio of pre-exponential factors, and the molecular parameters  $f_i[\lambda_A]$ ,  $F_i[\lambda_F]$  and  $k_i$  can be rearranged to give

$$\alpha\tau_1/\beta\tau_2 = \frac{f_1[\lambda_A]F_1[\lambda_F]}{f_2[\lambda_A]F_2[\lambda_F]} = \frac{\epsilon_1[\lambda_A]C_1}{\epsilon_2[\lambda_A]C_2} \times \frac{F_1[\lambda_F]}{F_2[\lambda_F]} \quad (5.5)$$

Hence the ratio  $\alpha\tau_1/\beta\tau_2$  may be physically interpreted as the relative absorbances of the two species at wavelength  $\lambda_A$  modified by their fluorescence emission,  $F_i$ , at wavelength  $\lambda_F$ . While the individual values of  $\epsilon_i$ ,  $C_i$  and  $F_i$  are obviously desirable, they may not be elucidated from the information of Table 5.19 since the fluorescence emission is not strictly monochromatic, but is merely filtered, so that the fluorescence decay was monitored simultaneously at all wavelengths above the filter cut-off, approximately 400 nm (KV 408 filter). Under these conditions neither  $F_i[\lambda_F]$  nor  $f_i[\lambda_A]$  can be easily characterized.

Consequently, it was seen that the only definitive decay experiment would be one wherein both excitation and emission could be fairly strictly monochromated. Introduction of the second (emission) monochromator dictated the use, perforce, of the nitrogen excitation source, with a concomitant reduction in the available excitation wavelengths. Nonetheless the fluorescence decay experiments are not, in themselves, sufficient to solve for the individual parameters of the proposed species 1 and 2 since both the relative absorbances of the two species  $\epsilon_1[\lambda_A]C_1/\epsilon_2[\lambda_A]C_2$  and the relative fluorescence intensities,  $F_1[\lambda_F]/F_2[\lambda_F]$  remain unknown. The net emission properties of the mixture will be determined by the contributions of the individual components via the fractions  $f_1[\lambda_A]$  and  $f_2[\lambda_A]$ .

The net or experimentally observable fluorescence quantum yield was given by Equation 2.73, namely

$$\bar{\phi}_f[\lambda_A] = f_1[\lambda_A]\phi_{f,1} + f_2[\lambda_A]\phi_{f,2}$$

where the individual quantum yields  $\phi_{f,1}$  and  $\phi_{f,2}$  are defined in the usual manner.

$$\phi_{f,1} = \frac{k_{f,1}}{k_{f,1} + k_{ics,1} + k_{ic,1}} \quad (5.6)$$

$$\phi_{f,2} = \frac{k_{f,2}}{k_{f,2} + k_{isc,2} + k_{ic,2}} \quad (5.7)$$

Similarly the usual steady-state fluorescence spectrum produced by continuous excitation at  $\lambda_A$  was shown as Equation 2.68, namely

$$F(\lambda_F)[\lambda_A] = f_1[\lambda_A]F_1(\lambda_F) + f_2[\lambda_A]F_2(\lambda_F)$$

where  $F_1(\lambda_F)$  and  $F_2(\lambda_F)$  are the fluorescence spectra of species 1 and 2 respectively. The individual fluorescence spectra are written as independent of excitation wavelength, in accord with Vavilov's law.

Since species 1 and 2 have overlapping absorption and emission spectra it is likely that there exists at least one or more isoemissive wavelengths,  $\lambda_F'$ , at which the intensities of species 1 and 2 are equal, i.e.,  $F_1[\lambda_F'] = F_2[\lambda_F']$ . Experimentally the isoemissive wavelengths of the 2,2'-binaphthyl emission in cyclohexane can be determined by examination of the normalized fluorescence spectra obtained at different excitation wavelengths. The need for normalization stems from the wavelength dependence of  $\phi_f(\lambda_A)$  and hence the need to express all the fluorescence spectra in terms of a common relative fluorescence quantum intensity. In practice this is accomplished by setting the ratio of the integrated fluorescence spectral area to the fluorescence quantum yield, both obtained at a common excitation wavelength, equal to a constant. Figure 5.22 shows the results of normalizing the fluorescence emission for solutions of 2,2'-binaphthyl- $h_{14}$  in cyclohexane (295K) for  $\lambda_A = 330$  to 310, at 10 nm intervals, to the expression

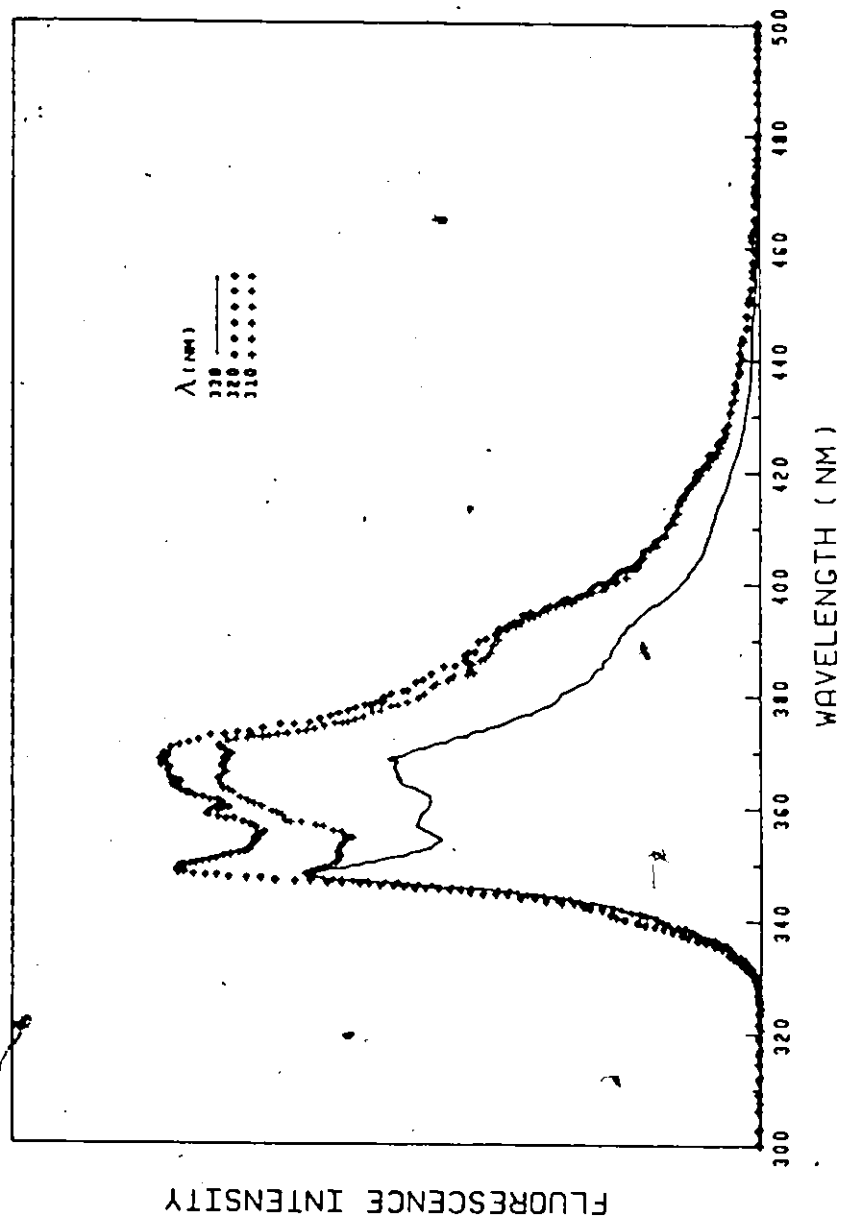


Figure 5.22  
Fluorescence Emission of 2,2'-Binaphthyl- $h_{14}$  in Cyclohexane at 295K  
Normalized Such That Area Under Emission Curve Divided by  $\bar{\phi}_f[\lambda_A] \approx 1.0$



$$\int_{\lambda_F} \bar{F}[\lambda_A] d\lambda_F / \bar{\phi}_f[\lambda_A] = 1.00 \quad (5.8)$$

over all

i.e., the area under the curve divided by the quantum yield at the same  $\lambda_A$  is set equal to unity. This normalization procedure indicates that the entire short wavelength edge of the fluorescence emission is an isoemissive region, within the rather large experimental uncertainty imposed by the quantum yield measurements. Similar normalizations over the other excitation wavelengths 300 - 260 nm lead to the same conclusion but have been omitted from Figure 5.22 for clarity. In this region, 330 - 350 nm, the normalization is actually fairly insensitive to changes in  $\bar{\phi}_f[\lambda_A]$ ; even assuming  $\bar{\phi}_f$  to be constant for all excitation wavelengths lead to the same conclusion regarding the isoemissive wavelengths. For trans-2-styrylnaphthalene in n-hexane (295K) Birks<sup>11</sup> found a number of isoemissive wavelengths both on the edges of vibronic emission bands, where  $dF/d\lambda_F$  is large, and in the flatter regions of the fluorescence spectrum, where  $dF/d\lambda_F$  is small. Isoemissive wavelengths of the latter sort are preferable since the decay experiments would then be relatively insensitive to small errors in  $\lambda_F$  or bandwidth effects but, unfortunately, the only isoemissive region for 2,2'-binaphthyl was found to be on the edge of the emission band where  $dF/d\lambda_F$  was large.

Choosing the isoemissive wavelengths as  $\lambda_F' = 340$  nm one has that  $F_1[\lambda_F'] = F_2[\lambda_F']$  reducing Equation 5.5 to

$$a\tau_1/b\tau_2 = \frac{f_1[\lambda_A]}{f_2[\lambda_A]} = \gamma[\lambda_A] \quad (5.9)$$

Remembering the relation

$$f_1[\lambda_A] + f_2[\lambda_A] = 1$$

at each  $\lambda_A$  one may rearrange to get expressions for the fractions of excited conformers at each choice of  $\lambda_A$ , namely

$$f_1(\lambda_A) = \frac{\gamma(\lambda_A)}{1 + \gamma(\lambda_A)} \quad (5.10)$$

and 
$$f_2(\lambda_A) = \frac{1}{1 + \gamma(\lambda_A)} = 1 - f_1(\lambda_A). \quad (5.11)$$

Hence, determination of the ratio  $\alpha\tau_1/\beta\tau_2 = \gamma(\lambda_A)$  with  $\lambda_F' = 340$  nm permits evaluation of the fractions of the two species present in the excited state as a function of the excitation wavelength.

Table 5.20 presents the decay parameters obtained for  $10^{-3} - 10^{-4}M$  solutions of 2,2'-binaphthyl- $h_{14}$  in cyclohexane nominally at 295K, monitoring the fluorescence at 340 nm and varying the excitation wavelength. The need to employ the more intense nitrogen excitation source restricted the usable excitation wavelengths to the region 281 - 337 nm. As noted previously the decay data could best be described by a biexponential model with constant lifetime parameters and variable pre-exponential factors. The fit to the biexponential model was better for the monochromated emission of Table 5.20 than for the filtered emission experiments of Table 5.19, as shown by all the  $\chi^2_v \leq 1.15$ . This is most likely the result of the better stray light rejection of the monochromator and the elimination of potential low-level filter fluorescence from the Schott KV series cut-off filters.

Some values obtained at  $10^{-3}M$  solute concentration are included for completeness, although the lifetimes clearly indicate some concentration quenching of the fluorescence at these levels, the short component

Table 5.20

Fluorescence Decay Parameters for 2,2'-Binaphthyl- $h_{14}$  in  
Cyclohexane at 295K;  $\lambda_F = 340 \text{ nm}^{a,b}$

$\lambda_A^d$ (nm)	Biexponential Fit				Monoexponential Fit	
	$\tau_1$ (ns)	$\tau_2$ (ns)	$\alpha/\beta$	$\chi^2_v$	$\tau$ (ns)	$\chi^2_v$
337.1	24.99 25.10	133.8 127.9	72.48 77.50	1.02 1.05	27.29	9.14
333.9	24.69	104.8	42.25	1.05		
330.9	24.84 21.19	97.08 98.60	48.72 30.60	1.12 1.15	24.98	19.29 <sup>c</sup>
328.5	25.22 25.14 21.04 21.09	106.4 110.6 96.68 92.23	42.55 47.63 23.90 23.30	0.94 1.03 1.06 1.07	28.18 25.95 26.22	11.19 27.38 <sup>c</sup> 24.18 <sup>c</sup>
326.8	24.98 25.08	107.0 110.7	29.89 38.24	0.96 1.08		
315.9	24.76	103.6	13.77	0.96		
313.6	24.95 25.34	103.9 111.8	11.94 14.41	1.02 0.96	35.54	43.83
311.7	24.39	99.11	10.44	1.00		
297.7	24.94 25.01	104.7 104.6	12.01 12.63	1.03 1.05	35.53	47.51
296.2	24.81	103.9	12.90	1.07		
295.3	24.81	103.6	12.64	1.06		
281.9	24.39	99.40	17.92	1.08		
281.4	24.13 24.27	105.9 104.3	16.36 14.71	1.15 1.05		

Means	$10^{-4}M$	$10^{-3}M$
$\tau_1$	$24.83 \pm .33 \text{ ns}$	$21.11 \pm .08 \text{ ns}$
$\tau_2$	$104.8 \pm 4.0 \text{ ns}^e$	$95.84 \pm 3.27 \text{ ns}$

<sup>a</sup> emission bandpass = 8 nm

<sup>b</sup> concentration  $10^{-4}M$  except where noted

<sup>c</sup> concentration  $10^{-3}M$

<sup>d</sup>  $N_2$  filled source

<sup>e</sup> excluding values at  $\lambda_A = 337.1 \text{ nm}$

decreasing 15% and the long one about 8.5%. This concentration quenching must be ascribed to a self-quenching mechanism whereby the excited singlets are quenched by ground state solute molecules since the alternative mechanism, concentration quenching by self-absorption (followed by subsequent re-emission) must produce longer, not shorter, lifetimes.<sup>94,216</sup>

On the basis of self-quenching alone it might be expected that the longer component,  $\tau_2$ , should be quenched more strongly than the shorter lived one,  $\tau_1$ , if one assumes that the rate constants for self-quenching of the two species or conformers are equal.

These rate constants are frequently taken to be simply the purely diffusional rate constants and hence equal<sup>11,217</sup> although it is known that the self-quenching rate constants typically vary over a greater range than the corresponding rate constants for oxygen quenching, some differing by a factor of three in hydrocarbon solvents.<sup>218</sup> This difference in self-quenching rates may also be related to the geometry of the species involved, it generally being argued that chromophores capable of assuming a planar configuration are more susceptible to self-quenching, while nonplanar solutes are practically immune to this effect.<sup>28,219,220</sup> Horrocks has shown the twisted 1,1'-binaphthyl to be immune to concentration quenching over the range of about  $2 \times 10^{-3}$  M to .4M in various solvents, while solutions of 2,2'-binaphthyl showed a sharply diminished fluorescence intensity with increased concentration.<sup>28</sup> It is not surprising then that different conformers of 2,2'-binaphthyl would exhibit somewhat different rate constants for self-quenching.

At concentrations  $\leq 10^{-4}$  M at room temperature 2,2'-binaphthyl solutions showed no further increase in the fluorescence lifetimes. To

avoid the complication of concentration quenching further discussion and calculation will be based only on those decay parameters obtained at concentrations of  $\leq 10^{-4}M$ , so that the mean values of  $\bar{\tau}_1 = 24.83$  ns and  $\bar{\tau}_2 = 104.8$  ns in Table 5.20 will be accepted as the true molecular lifetime parameters.

Typical fluorescence decay curves are shown in Figures 5.23a and 5.23b, in conjunction with plots of the percent residuals and autocorrelation functions of the weighted residuals, illustrating the improved fit of the biexponential model to the observed decay curves. Additional plots of the results used to obtain Table 5.20 are catalogued in, Appendix III. As  $\lambda_A$  is moved progressively toward the long wavelength absorption edge the observed decay comes to resemble more closely that of component 1 alone, as evidenced by the increased ratio  $\alpha/\beta$ , the approach of  $\tau$  (monoexponential) to  $\tau_1$  and the improvement in the reduced chi-squared measure of the monoexponential fit. With excitation at the extreme absorption edge at 337.1 nm the longer lived component is present to such a minor extent that its lifetime can no longer be accurately extracted from the experimental data, the values of  $\tau_2$  of 133.8 and 127.9 ns being much too long. Some of these difficulties and limitations of data reduction and detection levels are discussed at greater length in Appendix II.

From the data furnished in Table 5.20 one may then calculate  $\gamma[\lambda_A]$  ( $= (\alpha/\beta)[\lambda_A] \times (\tau_1/\tau_2)$ ),  $f_1[\lambda_A]$ ,  $f_2[\lambda_A]$  and the relative absorptivities of the two species,  $\epsilon_1[\lambda_A]C_1/\bar{C}$  and  $\epsilon_2[\lambda_A]C_2/\bar{C}$ , tabulated below.

$\bar{\epsilon}(\lambda_A)$  is simply the conventional absorption spectrum of both species, at known total concentration. The calculated relative molar

Figures 5.23 a and b

Mono- and Biexponential Fitting of the  
Fluorescence Decay Curve for  $10^{-4}$  M 2,2'-Binaphthyl  
in Cyclohexane at 295K

$\lambda_A = 297.7$  nm;  $\lambda_F = 340$  nm

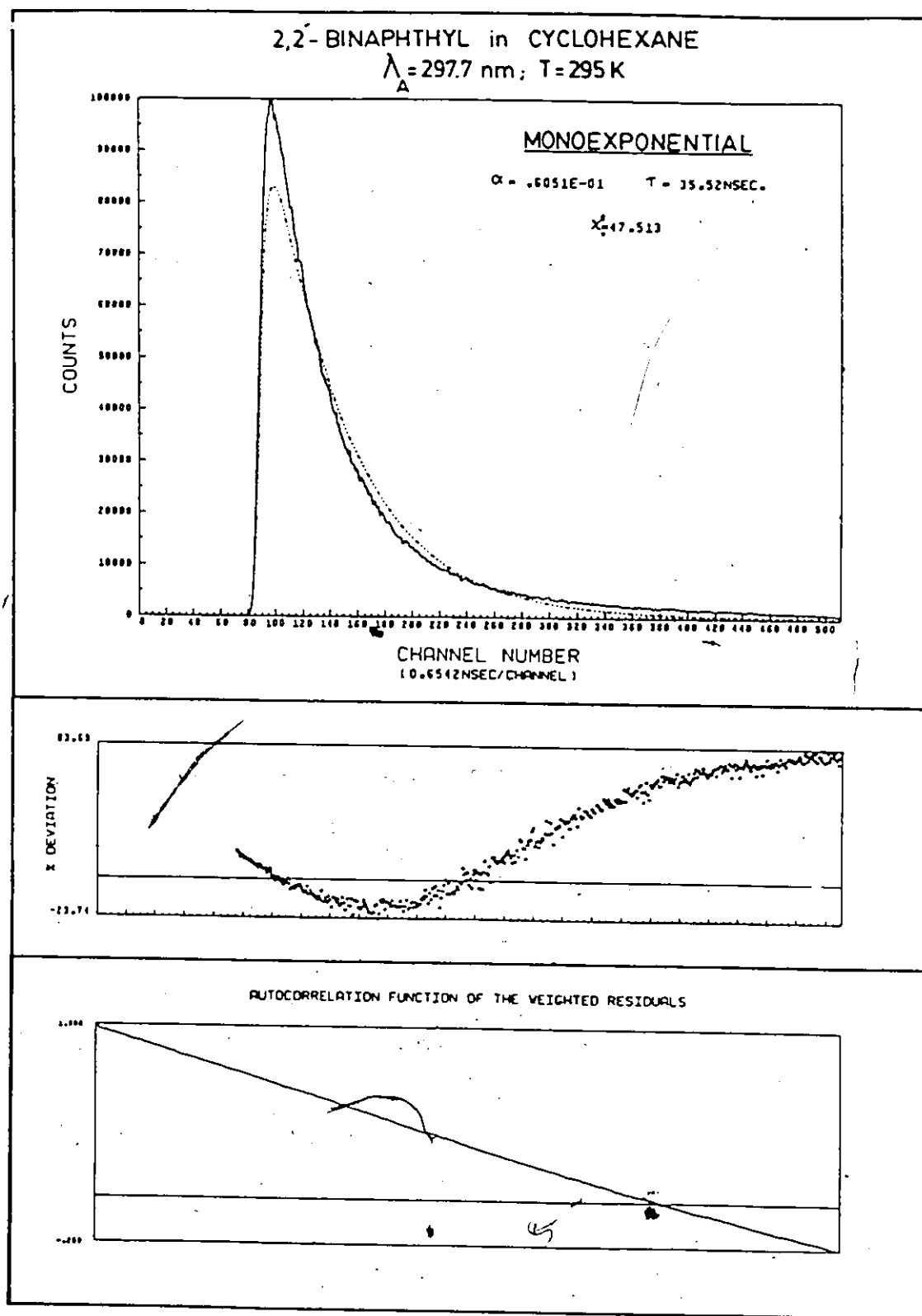


Figure 5.23a

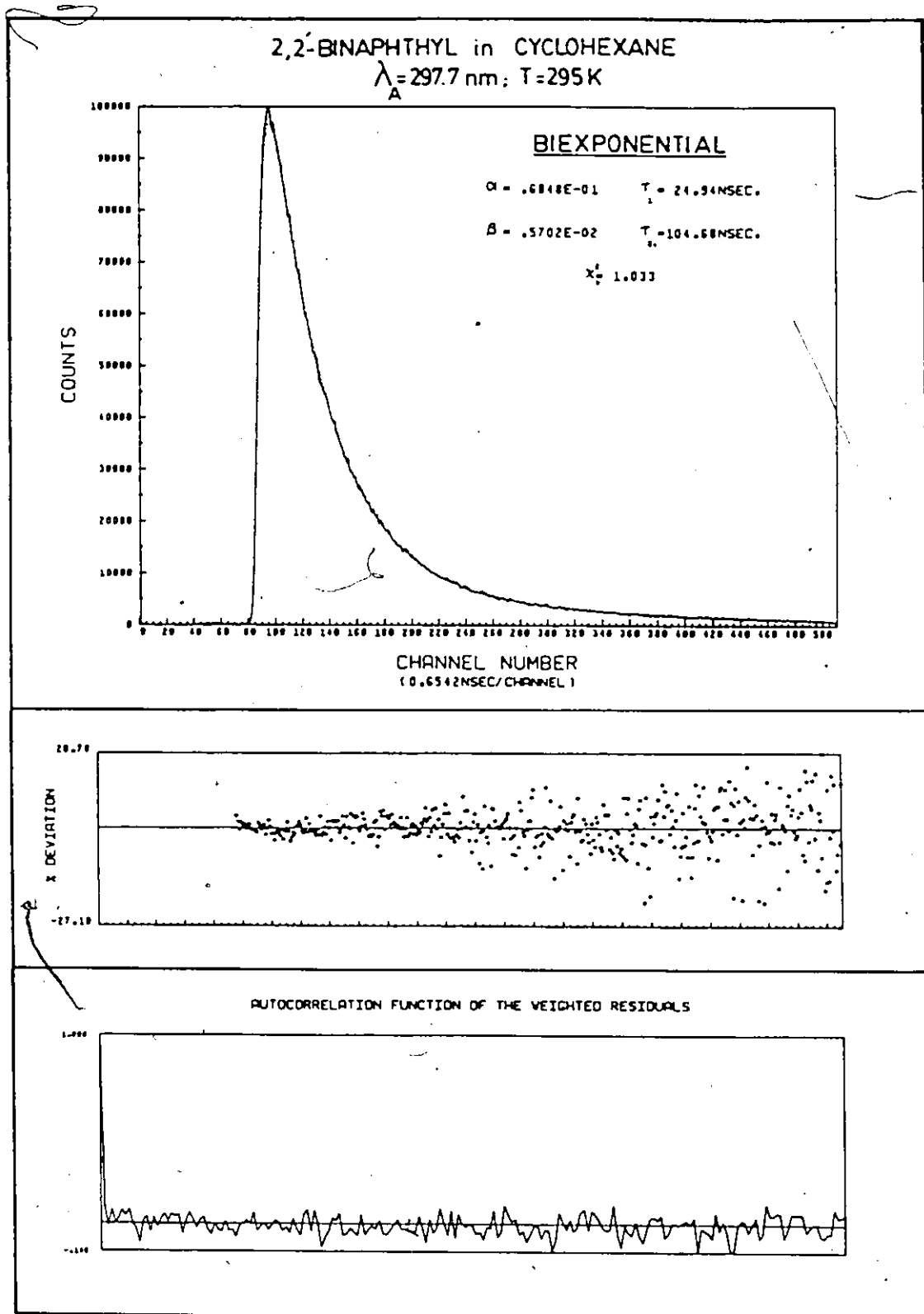


Figure 5.23b



Table 5.21

Fractional Excited State Populations and Absorbances for  
Conformers of 2,2'-Binaphthyl in Cyclohexane at 295K

$\lambda_A$ (nm)	$\gamma[\lambda_A]^a$	$f_1[\lambda_A]$	$f_2[\lambda_A]$	$\epsilon[\lambda_A]$ ( $\ell \cdot \text{mole}^{-1} \cdot \text{cm}^{-1}$ ) $\times 10^{-3}$	$\epsilon_1[\lambda_A]C_1/\bar{C}$ ( $\ell \cdot \text{mole}^{-1} \cdot \text{cm}^{-1}$ ) $\times 10^{-3}$	$\epsilon_2[\lambda_A]C_2/\bar{C}$ ( $\ell \cdot \text{mole}^{-1} \cdot \text{cm}^{-1}$ ) $\times 10^{-3}$
337.1	17.8	.947	.053	.745	.706	.039
333.9	10.0	.909	.091	1.22	1.11	.11
330.9	11.5	.920	.080	1.84	1.70	.14
328.5	10.7	.914	.086	2.70	2.47	.23
326.8	8.10	.890	.110	3.57	3.18	.39
315.9	3.26	.765	.235	13.8	10.6	3.2
313.6	3.12	.757	.243	16.0	12.1	3.9
311.7	2.47	.712	.288	17.5	12.5	5.0
297.7	2.92	.745	.255	19.6	14.6	5.0
296.2	3.06	.754	.246	19.2	14.5	4.7
295.3	3.00	.750	.250	19.0	14.3	4.8
281.9	4.25	.809	.190	18.6	15.0	3.6
281.4	3.68	.786	.214	18.8	14.8	4.0

<sup>a</sup> using  $\tau_1 = 24.83$  ns and  $\tau_2 = 104.8$  ns

Figure 5.24

Calculated Relative Molar Absorptivities  
of Two Proposed Conformers of 2,2'-Binaphthyl  
in Cyclohexane at 295K

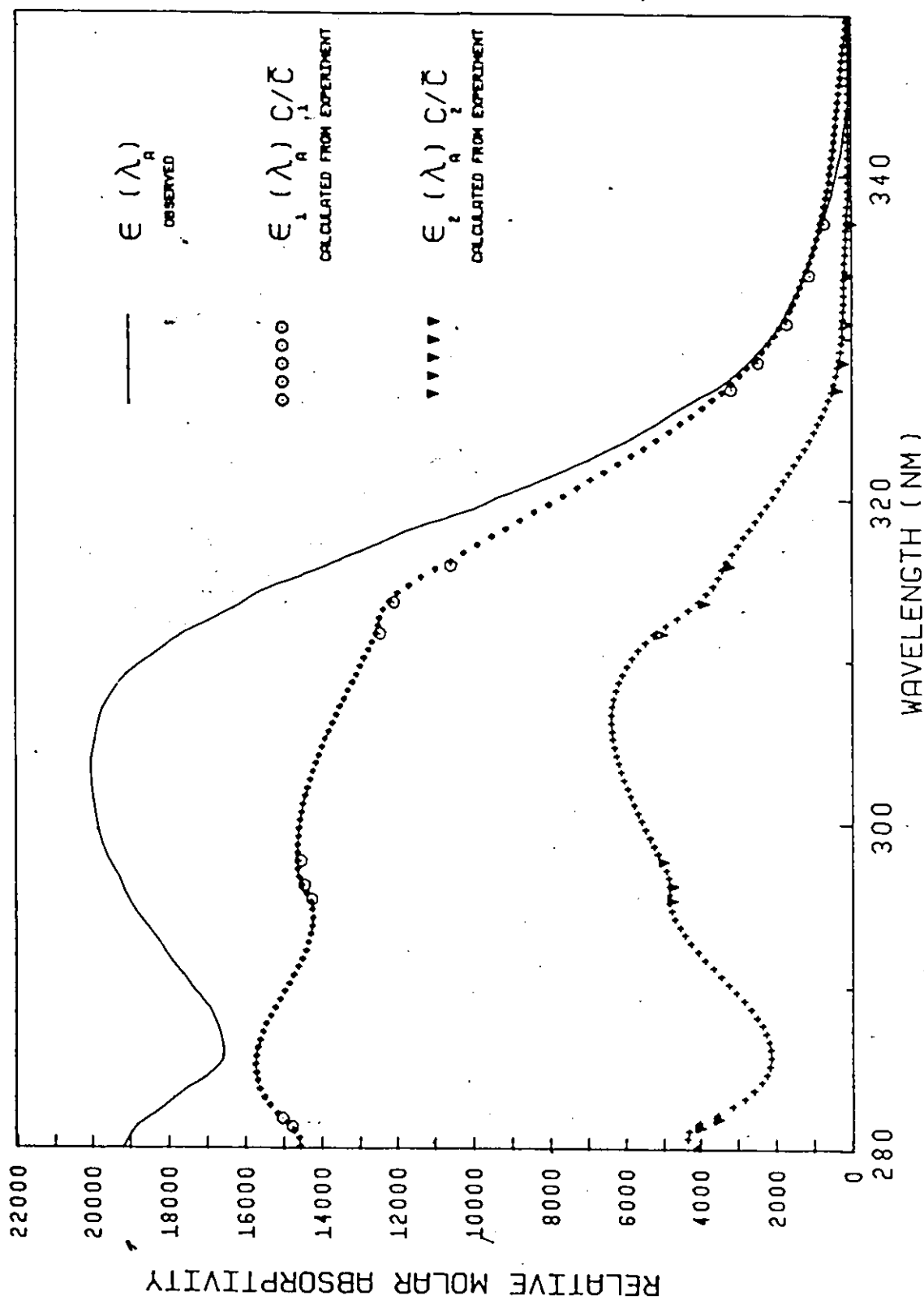


Figure 5.24

absorptivities of species 1 and 2 are plotted in Figure 5.24 where the smooth curves drawn through the two calculated data sets were determined by quartic interpolation between pairs of experimental points. The limitations of the band spectrum of the nitrogen source causes the paucity of experimental data in the three regions 326.8 - 315.9 nm, 311.7 - 297.7 nm and 295.3 - 281.9 nm so the curves drawn for these interpolations must be regarded as highly speculative.

The results obtained in the double monochromator experiments are in good agreement with those of the filtered emission experiments as indicated by a comparison of the normalized  $\alpha\tau_1/\beta\tau_2$  values for each. Figure 5.25 shows the values of  $\gamma[\lambda_A]$  from Table 5.21 renormalized to coincide with the curve from Figure 5.21 at the minimum at  $\lambda_A = 311.7$  nm. After normalization it is apparent that the values of  $\alpha\tau_1/\beta\tau_2$  deduced from the two types of experiment are in good agreement. This normalization factor should correspond to

$$\begin{aligned} \frac{(\alpha\tau_1/\beta\tau_2)_{\text{Table 5.19}}}{(\alpha\tau_1/\beta\tau_2)_{\text{Table 5.21}}} &= \frac{\frac{\epsilon_1[\lambda_A]C_1}{\epsilon_2[\lambda_A]C_2} \times \frac{F_1[\lambda_F \geq 400 \text{ nm}]}{F_2[\lambda_F \geq 400 \text{ nm}]}}{\frac{\epsilon_1[\lambda_A]C_1}{\epsilon_2[\lambda_A]C_2} \times \frac{F_1[\lambda_{F'}]}{F_2[\lambda_{F'}]}} \\ &= \frac{F_1[\lambda_F \geq 400 \text{ nm}]}{F_2[\lambda_F \geq 400 \text{ nm}]} = 0.12 \end{aligned} \quad (5.12)$$

The magnitude of this factor would suggest that the bulk of the emission of species 2 lies to the red of the emission from species 1. In principle it should be possible to calculate the individual fluorescence spectra of the two species,  $F_1(\lambda_F)$  and  $F_2(\lambda_F)$  from the

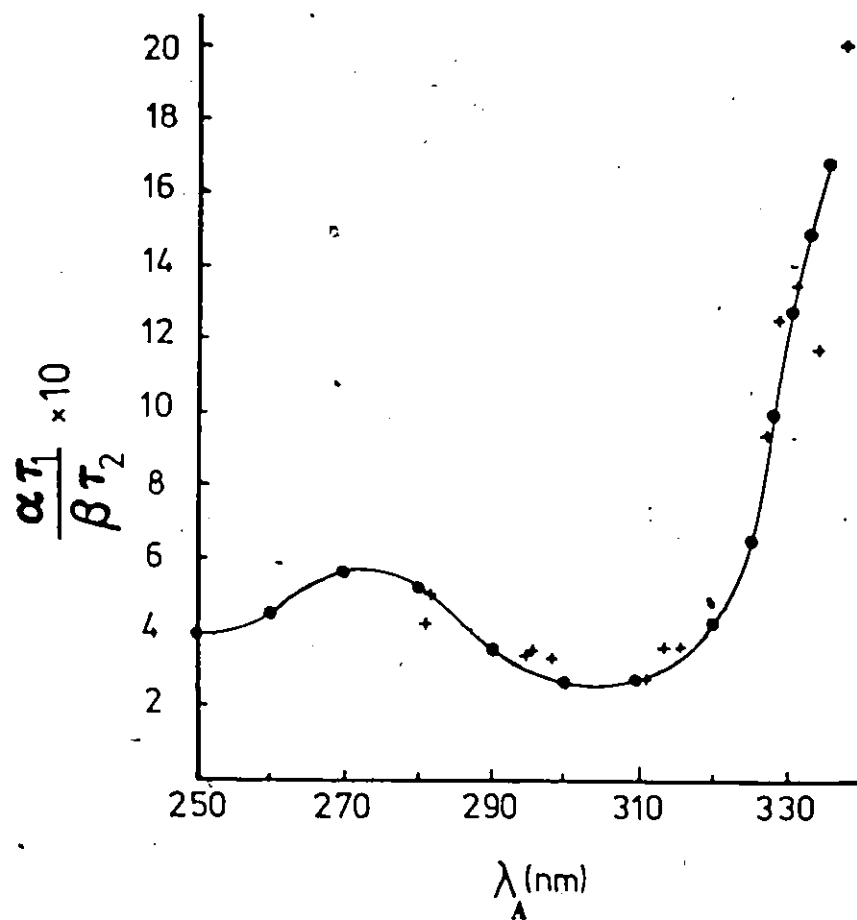


Figure 5.25

Comparison of Ratios  $\alpha\tau_1/\beta\tau_2$  for Filtered and Monochromated Emission Decay of 2,2'-Binaphthyl Fluorescence:

• - filtered; + - monochromated;

monochromated values normalized to scale of Figure 5.21.

relations

$$F_1(\lambda_F) = \frac{\bar{F}(\lambda_F)[\lambda_x]f_2[\lambda_y] - \bar{F}(\lambda_F)[\lambda_y]f_2[\lambda_x]}{f_2[\lambda_y] - f_2[\lambda_x]} \quad (5.13)$$

and

$$F_2(\lambda_F) = \frac{\bar{F}(\lambda_F)[\lambda_y]f_1[\lambda_x] - \bar{F}(\lambda_F)[\lambda_x]f_1[\lambda_y]}{f_1[\lambda_x] - f_1[\lambda_y]} \quad (5.14)$$

where  $\lambda_x$  is some value of excitation wavelength where contribution of species 1 is large,  $\lambda_y$  is some value of excitation wavelength where contribution of species 2 is large, and  $\bar{F}(\lambda_F)[\lambda_x \text{ or } \lambda_y]$  represents the fluorescence spectrum excited at  $\lambda_x$  or  $\lambda_y$  and normalized to unit relative quantum intensities in each case.

The excitation wavelengths of choice were  $\lambda_x = 330 \text{ nm}$  and  $\lambda_y = 310 \text{ nm}$  since the fluorescence quantum yields and fluorescence spectra are known at these wavelengths while the fractions  $f_1$  and  $f_2$  are known at the nearby wavelengths 330.9 nm and 311.7 nm. These computed fluorescence spectra of species 1 and 2 are illustrated in Figure 5.26 with the ratio of relative intensities being about 1:3 as noted. The spectra seem to confirm the earlier speculation that the long lived component 2 has its maximum to the red of the species 1 maximum, at 371.5 nm ( $26\,918 \text{ cm}^{-1}$ ) versus 347.5 nm ( $28\,777 \text{ cm}^{-1}$ ).

That species 1 is indeed the short lived component is nicely confirmed by examination of Figure 5.27 which shows the correlation between the fluorescence spectrum,  $F_1(\lambda_F)$ , of species 1 as calculated from Equation 5.13 and the total fluorescence spectrum of 2,2'-binaphthyl in room temperature cyclohexane solution, oxygen saturated at one atmosphere of oxygen pressure. That species 2 is not completely quenched may be evinced by the intensity of the  $\sim 370 \text{ nm}$  peak and the

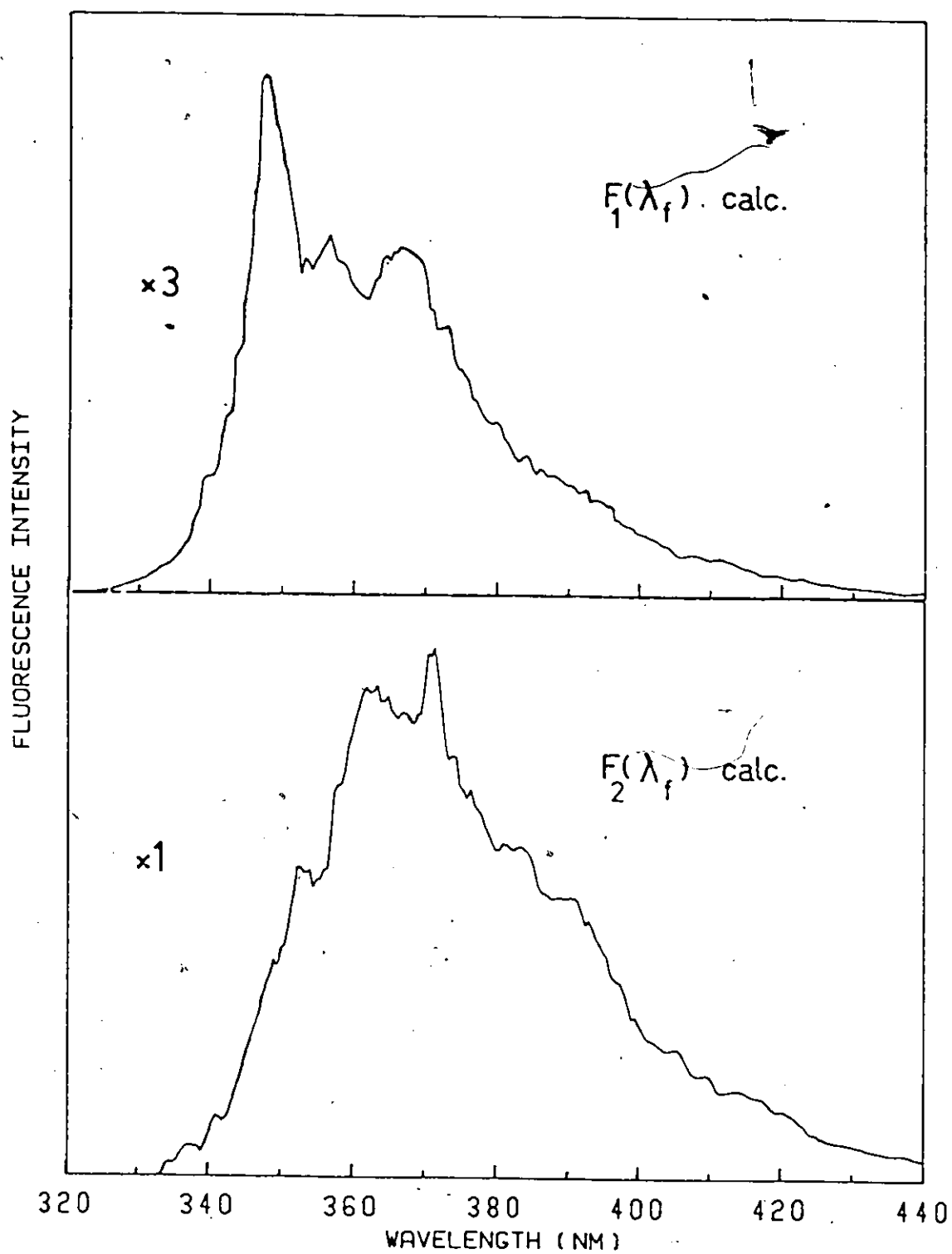


Figure 5.26

2,2'-binaphthyl in cyclohexane, 295K

Upper:  $F_1(\lambda_f)$  as calculated from equation 5.13

Lower:  $F_2(\lambda_f)$  as calculated from equation 5.14

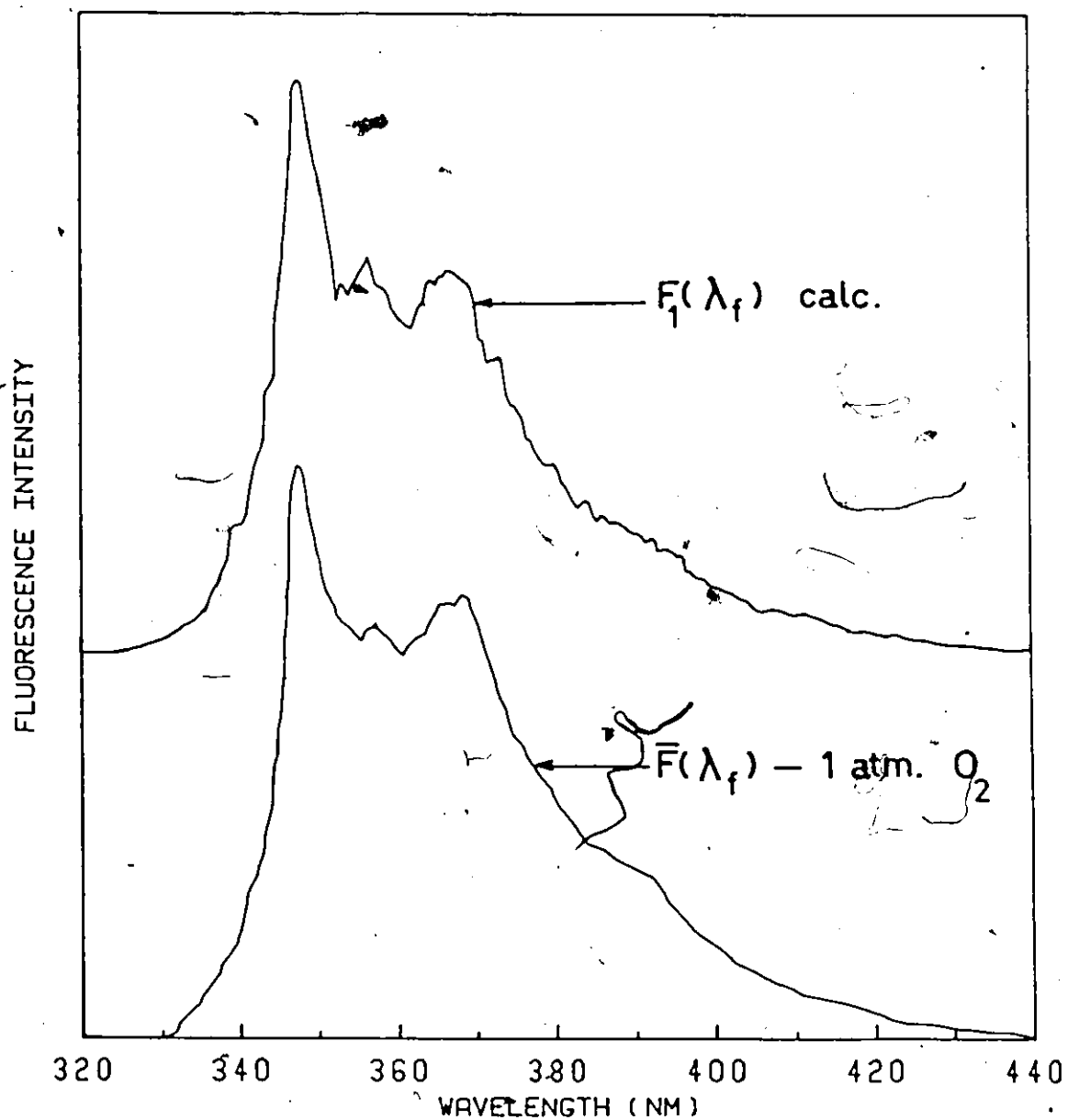


Figure 5.27

Fluorescence of 2,2'-binaphthyl in cyclohexane, 295K:

Species 1 fluorescence by calculation and quenching

Upper curve: fluorescence spectrum of species 1 derived from Equation 5.13

Lower curve: fluorescence in presence of 1 atm.  $O_2$  from Figure 5.20



shoulder at about 390 nm in the quenched emission as compared to the calculated  $F_1(\lambda_F)$ .

The individual fluorescence quantum yields for the two species can be calculated from equations analogous to those used to calculate the fluorescence spectra, namely

$$\phi_{f,1} = \frac{\bar{\phi}_f[\lambda_x]f_2[\lambda_y] - \bar{\phi}_f[\lambda_x]f_2[\lambda_x]}{f_2[\lambda_y] - f_2[\lambda_x]} \quad (5.15)$$

$$\phi_{f,2} = \frac{\bar{\phi}_f[\lambda_y]f_1[\lambda_x] - \bar{\phi}_f[\lambda_x]f_1[\lambda_y]}{f_1[\lambda_x] - f_1[\lambda_y]} \quad (5.16)$$

where  $\lambda_x$  and  $\lambda_y$  were chosen as before.

Substitution of the appropriate values gives  $\phi_{f,1} = 0.31$  and  $\phi_{f,2} = 1.25$ . Since  $\phi_f$  obviously cannot exceed unity this quantum yield for species 2 is in error by at least 25%. This is not unexpected since the terms  $\bar{\phi}_f[\lambda_x]$  and  $\bar{\phi}_f[\lambda_y]$  are each subject to 10 - 15% experimental error even without considering the additional uncertainty introduced in  $f_1$  and  $f_2$ . If  $\phi_{f,2}$  is tentatively assumed to be near unity ( $\pm 25\%$ ) then  $\phi_{f,1}$  can be calculated in an average sense rather than from Equation 5.15. The areas under the calculated curves  $F_1(\lambda_F)$  and  $F_2(\lambda_F)$  will give the ratio of  $\phi_{f,1}/\phi_{f,2}$  and hence  $\phi_{f,1}$  if  $\phi_{f,2}$  is taken as unity. After correcting for the intensity difference in Figure 5.26  $\phi_{f,1}$  is found to be  $\sim 0.25$ . If  $\phi_{f,1}$  is calculated from Equation 2.73

$$\bar{\phi}_f[\lambda_A] = \phi_{f,1}f_1[\lambda_A] + \phi_{f,2}f_2[\lambda_A]$$

with  $\phi_{f,2} = 1.0$  then larger values of  $\phi_{f,1}$ , in the range .4 - .5, are obtained. The cumulative experimental error is obviously a serious obstacle to accurately assessing the individual quantum yields for the

two components and at best one could only state that  $\phi_{f,2} \sim 1 \pm .25$  while  $\phi_{f,1} \sim .25 - .50$ .

One may incidentally obtain a very rough confirmation of the normalization constant of Equation 5.12, with  $F_1[\lambda_F \geq 400 \text{ nm}]/F_2[\lambda_F \geq 400 \text{ nm}] = 0.12$  by taking the areas under the calculated fluorescence curves  $F_1(\lambda_F)$  and  $F_2(\lambda_F)$  above 400 nm. This ratio proved to be  $(1 \times 194)/(3 \times 531) = 0.12$ . The high degree of agreement is, no doubt, somewhat fortuitous since the choice of exactly 400 nm is somewhat arbitrarily taken as the step-function cut-off of the KV408 filter. Also, the accuracy of  $F_1(\lambda_F)$  and  $F_2(\lambda_F)$  is ultimately determined by the accuracy of the quantum yields  $\bar{\phi}_f[\lambda_A]$ . Nonetheless, the agreement between the two values does to some measure bolster one's confidence in the information derived from the lifetime experiments and serves as a rough check on the self-consistency of the analysis.

The fluorescence decay of the perdeuterated 2,2'-binaphthyl proved nearly identical to that of the  $-h_{14}$  isotopic species, as seen from Tables 5.22 and 5.20.  $\tau_1$  for the  $-d_{14}$  and  $-h_{14}$  molecules is identical while the longer component seems genuinely shorter for the perdeutero-compound, albeit by only 6%. Both the ratios  $\alpha/\beta$  and  $\alpha\tau_1/\beta\tau_2$  are unchanged by deuteration too, a not unreasonable outcome, since this latter ratio in particular should reflect the relative populations of the two conformers, a feature that should be essentially invariant with the isotope. As previously noted the fluorescence quantum yields were unaltered on going from the  $-h_{14}$  to  $-d_{14}$  species; since the purely radiative lifetime of the singlet state is usually taken to be independent of isotope effect<sup>32</sup> the experimental fluorescence lifetimes should also

Table 5.22  
Fluorescence Decay Parameters for  $10^{-4}$  M 2,2'-Binaphthyl- $d_{14}$   
in Cyclohexane at 295K.  $\lambda_F = 340$  nm<sup>a</sup>

$\lambda_A^b$ (nm)	Biexponential Fit				Monoexponential Fit	
	$\tau_1$	$\tau_2$	$\alpha/\beta$ $(\alpha/\beta - h_{14})^c$	$\chi^2_v$	$\tau$	$\chi^2_v$
337.1	25.32	143.7	79.64 (74.99)	1.24	27.70	13.87
328.5	24.87	99.85	44.22 (45.09)	1.21	27.61	8.66
315.9	23.41 24.35 <sup>d</sup>	97.02 99.01	13.28 12.77 (13.77)	1.43 1.21	32.24 33.67	42.91 43.03
313.6	24.39	99.34	12.98 (13.18)	1.29	33.50	36.45
297.7	24.12	96.41	11.05 (12.32)	1.21	34.78	41.79
295.3	24.07	96.00	11.22 (12.64)	1.24	33.85	40.32
$\bar{\tau}_1 = 24.36 \pm .61$ ns $\bar{\tau}_2 = 97.94 \pm 1.66$ ns <sup>e</sup>						

<sup>a</sup> emission band pass = 8 nm

<sup>b</sup> N<sub>2</sub> filled source

<sup>c</sup> mean  $\alpha/\beta$  for  $-h_{14}$  isotope under these conditions

<sup>d</sup> emission selected by Schoeffel QPM-30 monochromator

<sup>e</sup> excluding  $\lambda_A = 337.1$  nm trial

be unaffected by deuteration, as is approximately the case.

The decay parameters of a more dilute solution in cyclohexane ( $1 \times 10^{-5} \text{ M}$ ) are very similar to those determined at  $10^{-4} \text{ M}$  concentration of the 2,2'-binaphthyl- $\text{d}_{14}$ . These are shown in Table 5.23, as a function of the emission wavelength, with the excitation wavelength fixed at 315.9 nm. The emission was selected by means of a quartz prism monochromator (Schoeffel QPM-30) or interference filters, with excellent agreement between the two methods. With constant excitation energy it will be noted that the contribution of the second emission component,  $\tau_2$ , increases with increasing emission wavelength as evidenced by the decrease in the ratio of preexponential factors  $\alpha/\beta$ .

To ensure that no significant D-H exchange had occurred with time in the dilute hydrocarbon solutions a bulk solution of the 2,2'-binaphthyl- $\text{d}_{14}$  was taken to dryness in vacuum and submitted to mass spectral analysis. From this analysis it was apparent that no amount of incorporated deuterium had been exchanged with the solvent.

The fluorescence decay spectroscopy of 2,2'-binaphthyl- $\text{h}_{14}$  was also studied in the three glass-forming solvents, 3MP, isopentane and absolute ethanol at room temperature and at 77K. As in cyclohexane, 2,2'-binaphthyl in these three solvents exhibited a biexponential fluorescence decay under all conditions. The statistics for the goodness-of-fit, though not explicitly shown in the accompanying tables, were entirely analogous to those found for the cyclohexane solutions. When fitting to a single exponential component was attempted, the calculated lifetime varied widely while the reduced chi-squared measure was above 10 in all cases. Both  $\tau$  and  $\chi^2_{\nu}$  diminished as the excitation wavelength

Table 5.23

Lifetimes and Ratios of Preexponential Factors for Fluorescence Decay  
of  $10^{-5}$  M 2,2'-Binaphthyl- $d_{14}$  in Cyclohexane at 295K as a  
Function of Emission Wavelength:  $\lambda_A = 315.9$  nm

$\lambda_F^a$ (nm)	$\tau_1$ (ns)	$\tau_2$ (ns)	$\alpha/\beta$	$\lambda_F$ (nm)	$\tau_1$ (ns)	$\tau_2$ (ns)	$\alpha/\beta$
430	20.91	99.16	1.75	370	23.68	102.8	3.54
420	21.40	99.56	1.85	365	23.19	99.55	3.74
410	22.40	101.2	1.91	360	23.55	99.17	4.66
410 <sup>b</sup>	21.95	101.8	1.93	355	23.72	99.31	6.55
404.7 <sup>b</sup>	22.26	100.9	2.15	350	23.84	98.93	8.31
400	21.62	100.0	2.08	345	23.81	96.29	10.8
390	22.84	100.9	2.27	340	23.35	99.01	12.8
380	22.97	100.5	2.73	335	24.13	103.1	11.4

Means  $\bar{\tau}_1 = 22.85 \pm .99$  ns

$\bar{\tau}_2 = 100.1 \pm 1.7$  ns

<sup>a</sup> Schoeffel QPM-30 monochromator, except where noted.

<sup>b</sup> Baird Atomic interference filters.

Table 5.24

Fluorescence Decay Parameters for 2,2'-Binaphthyl-h<sub>14</sub>  
in 3-Methylpentane at 295K and 77K<sup>a</sup>

$\lambda_A^b$ (nm)	$\lambda_F^c$ (nm)	T = 295K				T = 77K			
		$\tau_1$ (ns)	$\tau_2$ (ns)	$\alpha/\beta$		$\tau_1$ (ns)	$\tau_2$ (ns)	$\alpha/\beta$	
315.9	370.0	29.21	103.6	2.91	2.95 $\pm$ .08	22.59	104.8	1.65	1.88 $\pm$ .17
		28.52	105.6	2.90		22.73	104.7	1.85	
		29.32	107.8	3.04		23.04	105.8	2.05	
						22.84	106.1	1.96	
315.9	340.0	29.57	107.8	12.18	11.98 $\pm$ .29	23.10	104.0	11.19	
		29.83	102.7	11.77					
Mean Lifetimes		295K				77K			
		$\bar{\tau}_1 = 29.29 \pm .49$ ns;				$\bar{\tau}_1 = 22.86 \pm .21$ ns;			
		$\bar{\tau}_2 = 105.5 \pm 2.31$ ns				$\bar{\tau}_2 = 105.1 \pm .87$ ns			

<sup>a</sup> concentration  $\leq 10^{-5}$  M.

<sup>b</sup> N<sub>2</sub> filled source.

<sup>c</sup> Jobin-Yvon H-10 monochromator.

Table 5.25  
Fluorescence Decay Parameters for 2,2'-Binaphthyl- $h_{14}$   
in Ethanol at 295K and 77K<sup>a</sup>

$\lambda_A^b$ (nm)	$\lambda_F^c$ (nm)	T = 295K				T = 77K		
		$\tau_1$ (ns)	$\tau_2$ (ns)	$\alpha/\beta$		$\tau_1$ (ns)	$\tau_2$ (ns)	$\alpha/\beta$
337.1	340.0	22.97	91.80	50.46				
315.9	340.0	22.34 23.41	64.54 69.56	8.00 6.44	7.22 $\pm$ 1.10	22.36	85.50	4.39
313.6	340.0	23.14	69.08	5.52		22.42	82.06	4.88
311.7	340.0	22.49	65.96	4.18		22.28	80.86	5.13
297.7	340.0	22.90	67.06	4.50		22.98	84.97	4.26
296.2	340.0	23.10	67.50	5.15		22.34	81.71	4.87
Mean Lifetimes		295K <sup>d</sup>				77K		
		$\bar{\tau}_1 = 22.65 \pm 0.59$ ns;				$\bar{\tau}_1 = 22.48 \pm 0.29$ ns;		
		$\bar{\tau}_2 = 65.95 \pm 2.29$ ns <sup>e</sup>				$\bar{\tau}_2 = 83.02 \pm 2.08$ ns		

<sup>a</sup> concentration =  $1 \times 10^{-4} M$

<sup>b</sup> N<sub>2</sub> filled source

<sup>c</sup> J-Y H-10 monochromator

<sup>d</sup> includes 9 other trials not shown

<sup>e</sup> excluding  $\lambda_A = 337.1$  nm trial

Table 5.26

Fluorescence Decay Parameters for 2,2'-Binaphthyl-h<sub>14</sub>  
in Isopentane at 295K and 77K

$\lambda_A^b$ (nm)	$\lambda_F^c$ (nm)	T = 295K			$\alpha/\beta$	T = 77K			$\alpha/\beta$
		$\tau_1$ (ns)	$\tau_2$ (ns)			$\tau_1$ (ns)	$\tau_2$ (ns)		
337.1	410	32.98	101.8	12.68		36.97	106.4	28.51	
315.9	410					33.86	110.3	6.89	
313.6	410	28.47	104.9	1.14	1.24 $\pm$ 1.10	34.90	108.7	11.45	10.58 $\pm$ 1.24
		29.59	108.5	1.34		32.16	102.8	9.70	
Mean Lifetimes		295K <sup>d</sup>				77K			
		$\tau_1 = 29.19\pm.9$ ns;				$\tau_1 = 34.47\pm2.01$ ns;			
		$\tau_2 = 106.0\pm4.0$ ns				$\tau_2 = 107.0\pm3.3$ ns			

<sup>a</sup> concentration  $\leq 10^{-5}$  M

<sup>b</sup> N<sub>2</sub> filled source

<sup>c</sup> interference filter

<sup>d</sup> includes 4 other trials not shown



progressed toward the red end of the absorption envelope. Employing a biexponential decay model greatly improved the agreement between the observed and calculated curves with all  $\chi^2_{\nu}$  parameters dropping below 1.2 and the autocorrelation functions exhibiting a random distribution of the residuals. As with the cyclohexane result, the observed fluorescence decay could be decomposed into two exponentially decaying components of invariant lifetime but differing in their relative contributions to the total decay, as seen by the variable  $\alpha/\beta$  values.

From these tables and the earlier results in cyclohexane solution it is apparent that both  $\tau_1$  and  $\tau_2$  are fairly constant in all the hydrocarbon solvents at room temperature but that  $\tau_2$  is definitely shorter in ethanol. While the correction of the radiative lifetimes for the refractive index of the medium

$$k_f^o = k_f/n^2 = \frac{\phi}{\tau n^2} \quad (5.17)$$

cannot strictly be applied in the absence of quantum yield data for the two species in all solvents one may make an approximate correction for the index effect at room temperature if  $\phi_1$  and  $\phi_2$  are assumed to be independent of solvent. This is probably a reasonable supposition for the three hydrocarbon solvents, but may be far from true for the polar alcoholic solvent. Nonetheless if  $\phi_1$  is taken as constant then the product  $\tau n^2$  should be constant ( $= \phi/k_f^o$ ) if  $k_f^o$  is independent of solvent.<sup>94,163</sup> That this is not so for ethanol solutions is evident in Table 5.27.

The absorption spectrum of 2,2'-binaphthyl at room temperature was unaffected by solvent while the steady-state fluorescence and fluorescence decay at this temperature were seen to be considerably

Table 5.27

Refractive Index Correction Applied to Observed Lifetimes  
for 2,2'-Binaphthyl at 295K

Solvent	$n_{20}^{D 125}$	$\tau_1 n^2$ (ns)	$\tau_2 n^2$ (ns)
Cyclohexane	1.4266	50.53	213
3 MP	1.3765	55.50	200
Isopentane	1.3537	53.50	194
Ethanol	1.3611	41.96	122

different in alcoholic and hydrocarbon solvents. This difference between absorption and emission spectra may be rationalized as follows: the absorption spectra will not reveal relaxation or specific solvation processes occurring subsequent to absorption, since it only probes the unrelaxed Franck-Condon upper state; similarly, fluorescence will not reveal details of the solvent relaxation or interactions after de-excitation into the Franck-Condon ground state. If the polarity of the excited electronic state is greater than that of the ground state then solvent polarity will be expected to have a greater influence on the fluorescence than the absorption properties. The converse will be true if the ground state is more polar than the first excited singlet electronic state. The small red shift in the room temperature fluorescence in ethanol,  $\sim 190 \text{ cm}^{-1}$  agrees with this picture, the energy of the solvent equilibrated excited states being lower in the polar solvent.

Several trials with perdeuterated solute ( $5 \times 10^{-5} \text{ M}$ ) in ethanol at room temperature yielded results similar to those for the  $-h_{14}$  isotope in that solvent, so the effect of deuteration was not pursued further.

The quenching effect of molecular oxygen on the decay kinetics of 2,2'-binaphthyl in solution was examined, in addition to the steady-state effects mentioned earlier. Fluorescence lifetime measurements on a solution quenched with 1 atmosphere of oxygen indicated a nearly mono-exponential decay of the fluorescence, with a lifetime of  $\sim 2.1 \text{ ns}$ . Very slight improvement of the fit was obtained on fitting a biexponential model to the data with  $\tau_1 = 2.0 \text{ ns}$  and  $\tau_2 = 2.2 \text{ ns}$ ; this probably represents nearly the limit of the capabilities of the reiterative convolution method to distinguish two short lifetimes so nearly identical.

Separate expressions of the form of Equation 2.86b may be written for the rates of depletion of the fluorescent states of species 1 and 2 in the presence of oxygen quencher

$$k'_{Q,1} = k_{f,1} + k_{nr,1} + k_{Q,1}[O_2] \quad (5.18)$$

and

$$k'_{Q,2} = k_{f,2} + k_{nr,2} + k_{Q,2}[O_2] \quad (5.19)$$

where  $k_{nr,i} = k_{isc,i} + k_{ic,i}$ . Recasting in terms of the experimental fluorescence lifetimes

$$\frac{1}{\tau_{Q,1}} = \frac{1}{\tau_1} + k_{Q,1}[O_2] \quad (5.20)$$

and

$$\frac{1}{\tau_{Q,2}} = \frac{1}{\tau_2} + k_{Q,2}[O_2] \quad (5.21)$$

where the  $\tau_{Q,i}$  are the lifetimes observed in the presence of oxygen.

To obtain values for  $k_{Q,i}[O_2]$  the singlet lifetimes of air saturated solutions of 2,2'-binaphthyl in cyclohexane ( $10^{-4}M$ ) were measured. Use of air in lieu of pure oxygen reduced the quenching rate to levels where the lifetime components were more readily separable. The mean values of  $\tau_{Q,1}$  and  $\tau_{Q,2}$ , found with six measurements at various combinations of  $\lambda_A$  and  $\lambda_F$ , were  $\tau_{Q,1} = 10.02 \pm .50$  ns and  $\tau_{Q,2} = 16.91 \pm .46$  ns, with  $\chi^2_v \leq 1.2$  for all trials. Taking the unquenched lifetimes  $\tau_1 = 24.83$  ns and  $\tau_2 = 104.8$  ns and substituting into Equations 5.20 and 5.21 gives

$$k_{Q,1}[O_2] = (5.95 \pm .55) \times 10^7 \text{ s}^{-1}$$

and

$$k_{Q,2}[O_2] = (4.96 \pm .20) \times 10^7 \text{ s}^{-1}$$

where the error limits correspond to the standard deviations of the experiment lifetimes.

As noted in many studies<sup>114,115,221</sup> the value of  $k_Q$  is only approximately constant for different aromatic solutes in a common solvent so a slight difference between the two quenching rates is not surprising. With the concentration of oxygen in an equilibrated cyclohexane at 25°C as  $2.1 \times 10^{-3} \text{ M}$ <sup>112</sup> one gets the bimolecular quenching constants for the two species

$$k_{Q,1} = 2.8 \times 10^{10} \text{ l} \cdot \text{mole}^{-1} \cdot \text{s}^{-1}$$

$$k_{Q,2} = 2.4 \times 10^{10} \text{ l} \cdot \text{mole}^{-1} \cdot \text{s}^{-1}$$

These figures are within a factor of three of those predicted by simple diffusion-controlled quenching obeying the Stokes-Einstein relation<sup>94</sup>, which gives

$$k_{\text{diff}} = k_Q = \frac{8RT}{2000 \eta} = 9.6 \times 10^9 \text{ l} \cdot \text{mole}^{-1} \cdot \text{s}^{-1} \quad (5.22)$$

at  $T = 298 \text{ K}$  and  $\eta(\text{cyclohexane}) = 1.02 \text{ centipoise}$ .<sup>125</sup> Ware has shown<sup>115</sup> that the 2-4 times faster true quenching rates likely arise from an underestimation of the diffusion coefficient for the small oxygen molecule in the Stokes-Einstein equation from which the relation above is derived.

As an extra check on the consistency of this analysis the lifetimes expected at 1 atmosphere of oxygen pressure may be calculated as  $\tau_{Q,1} = 2.3 \text{ ns}$  and  $\tau_{Q,2} = 2.5 \text{ ns}$ , with  $[O_2] \sim 1.5 \times 10^{-2} \text{ M}$  at 1 atmosphere oxygen pressure, in reasonable agreement with experimental values of 2.0 and 2.2 ns respectively. In fact these calculated values may be somewhat high since  $k_Q$  is known to increase slightly with increased

quencher concentration.<sup>94</sup> Of course, at sufficiently high oxygen concentrations the quenching terms  $k_{Q,i}[O_2]$  will dominate the rate expressions and the observed lifetimes  $\tau_{Q,1}$  and  $\tau_{Q,2}$  will become coincident and experimentally indistinguishable, a situation very nearly reached at 1 atmosphere of applied oxygen pressure.

Overall the oxygen quenching of the fluorescence decay reinforces the belief that the appearance of a biexponential decay for the 2,2'-binaphthyl emission in fluid solution is not the result of any instrumental or experimental artifact external to the sample itself, since such artifacts would be unaffected by oxygenation of the sample. The high purity of the solvent and the solute (by HPLC) indicate that the two emission components can, most reasonably, be attributed to conformers of 2,2'-binaphthyl, derived by rotation about the interannular bond.

#### 5.3.4 Analysis and Discussion of the Photophysics of 2,2'-Binaphthyl

With estimates of the fluorescence lifetimes and quantum yields for the two species or conformers in room temperature cyclohexane solution now available one may calculate the radiative and nonradiative rate constants for the depletion of the singlet states involved. Using the very approximate values of 0.35 for  $\phi_{f,1}$  and 1.0 for  $\phi_{f,2}$  gives  $k_{f,1} = 1.4 \times 10^7 \text{ s}^{-1}$ ,  $k_{nr,1} = k_{ic,1} + k_{isc,1} = 2.6 \times 10^7 \text{ s}^{-1}$ ;  $k_{f,2} = 9.5 \times 10^6 \text{ s}^{-1}$  and  $k_{nr,2} = k_{ic,2} + k_{isc,2} \sim 0$ . The purely radiative lifetime or rate constant is usually considered to be independent of isotopic substitution,<sup>32</sup> as is the rate constant for intersystem crossing from  $S_1$  to  $T_n$ .<sup>32,222,223</sup> In contrast, the rate constant for internal conversion is expected to show a significant dependence on isotope. As Robinson and Frosch<sup>33,34</sup> pointed out the radiationless transition probabilities are governed by

the Franck-Condon overlap factor between the vibrational wavefunction of the upper state and the isoenergetic vibrational wavefunction of the lower state. If the electronic energy gap between the states is large the energetic C-H (ca.  $3000\text{ cm}^{-1}$ ) and C-D (ca.  $2250\text{ cm}^{-1}$ ) stretching modes principally determine the magnitude of this Franck-Condon factor.<sup>41,42</sup> The  $S_1 - S_0$  gap of  $\sim 29\,400\text{ cm}^{-1}$  for 2,2'-binaphthyl would correspond to about ten quanta of a C-H stretching vibration but about thirteen quanta of C-D vibration. Since the Franck-Condon factor decreases rapidly with increasing vibrational quantum number<sup>42</sup> this factor will be much smaller for the deuterated molecule, with the radiationless transition probability being correspondingly reduced.

Since both the fluorescence lifetimes and quantum yields of 2,2'-binaphthyl were found to be unaffected by isotopic substitution the rate constants for internal conversion,  $S_0 + S_1$ , of the two conformers must both be nearly zero already, that is  $k_{ic} \ll (k_f + k_{isc})$  for the two species of 2,2'-binaphthyl in room temperature solution. This observation is in keeping with the situation prevailing for many aromatic hydrocarbons, namely  $k_{ic} \sim 0$ .<sup>94</sup> This was also found to be the case for 1-phenyl-naphthalene, whereas the rate of internal conversion in the related biaryl, 2-phenylnaphthalene, was found to be small but non-zero with  $k_{ic} \sim (1.7 \pm 1.0) \times 10^6\text{ s}^{-1}$ . For this latter molecule  $k_f$  for the dominant conformer or species was found to be intrinsically small ( $3 \times 10^6\text{ s}^{-1}$ ) so the normally slow internal conversion can then become competitive with radiative depletion of  $S_1$ .

Incidentally, deuteration was found to profoundly affect the rate of intersystem crossing from the triplet state in 2,2'-binaphthyl

evidenced by the increase in the phosphorescence lifetime from  $2.7 \pm .1s$  to  $9.2 \pm 1.1s$  upon deuteration, as measured by flash methods in alkane glasses at 77K. The low temperature phosphorescence of 2,2'-binaphthyl appears at about 487 nm (possible 0-0) with the maximum at 496 nm, indicative of a  $T_1 - S_0$  gap of  $\sim 2.05 \times 10^4 \text{ cm}^{-1}$ . This observed increase in the phosphorescence lifetime can be ascribed to the reduced rate of  $S_0 + T_1$  radiationless processes for the  $-d_{14}$  species, similar to that outlined for the radiationless  $S_0 + S_1$  process. The radiative rate constant  $k_p$  has usually been assumed to be free of isotope effect,<sup>224</sup> although recent evidence has been found for a small radiative deuterium effect upon the triplet states of aromatic molecules.<sup>33,225</sup>

The fluorescence properties of 2,2'-binaphthyl in fluid, glassy and polycrystalline media clearly point to the presence of at least two emitting conformers or species. As discussed at greater length in Section 5.3.1c the geometries of the emissive states in the polycrystalline matrices are more likely those imposed by solvent matrix constraints rather than geometries solely determined by any intrinsic intramolecular potential. By comparison with the observed fluorescence origins in the model compounds naphthalene and 1,2,7,8-dibenzofluorene it appears that both fluorescent species seen in the Shpol'skii emission spectra of 2,2'-binaphthyl are probably more nearly coplanar in their excited state. At the very least the emissive species are probably not very twisted about the interannular bond. Given the  $\sim 525 \text{ cm}^{-1}$  separation in probable fluorescence origins for the two subspectra in the quasilinear spectrum of 2,2'-binaphthyl in polycrystalline methylcyclohexane and the very different fluorescence (and, apparently, absorption) envelopes of the



two subspectra it is clear that the geometries of the two conformers are sufficiently different to permit their spectroscopic differentiation.

The situation in fluid solution at room temperature may be examined in light of the kinetic schemes discussed in Section 2.8. If one considers there to be two ground state conformers for 2,2'-binaphthyl (Scheme I of Section 2.8) then it follows that interconversion of the two conformers in the excited state cannot be extremely rapid, since rapid interconversion would result in a monoexponential fluorescence decay and no excitation wavelength dependence of the emission spectrum. The kinetic scheme proposed by Birks<sup>11</sup> to describe the photophysics of the s-cis and s-trans conformers of trans-2-styrylnaphthalene in fluid solution envisaged no interconversion of these conformers in their excited states. An alternative approach was adopted by Donzel and co-workers<sup>83</sup> in their study of the conformeric equilibria of several tryptophanyl diketopiperazines. These workers considered that rates of interconversion in the excited state to be a significant perturbation of the ground state equilibrium in fluid solution. Donzel assumed that the molar absorptivities of the two species (folded and open conformations of the tryptophanyl residue) were identical. From the Strickler-Berg relationship<sup>171</sup> these authors then equated the radiative rate constants of the two conformers, namely if  $\epsilon_1 = \epsilon_2$  then  $k_{f,1} = k_{f,2}$ . While this may be a reasonable approximation for the weakly interacting chromophores of the tryptophanyl diketopiperazines it is not likely to be valid for the biaryls wherein the  $\pi$ -electronic interaction of the aryl constituents will be large and will vary quite markedly with conformation. The probable lack of a Strickler-Berg relationship for the specific case of

2,2'-binaphthyl will be dealt with at greater length shortly.

In view of the known fast torsional relaxation of 1,1'-binaphthyl in room temperature fluid solution it is very probable that Birks's supposition that excited state interconversion of conformers is negligible is not strictly true for the conformers of 2,2'-binaphthyl. The true state of affairs for 2,2'-binaphthyl likely lies between the two extremes of no interconversion in the excited state or extremely rapid interconversion in the excited state, i.e., some geometry changes of the 2,2'-binaphthyl conformers must be possible subsequent to excitation.

Although the method of Birks et al.<sup>11</sup> has been used to calculate the relative molar absorptivities of the two conformers of 2,2'-binaphthyl in cyclohexane solution as a function of the excitation wavelength (Table 5.21) as

$$\epsilon_1[\lambda_A]C_1/\epsilon_2[\lambda_A]C_2 \quad (5.23)$$

the separate value of the relative concentrations of the two components cannot be extracted without further information about  $\epsilon_1[\lambda_A]/\epsilon_2[\lambda_A]$ . Birks dealt with the problem of evaluating  $\epsilon_1[\lambda_A]/\epsilon_2[\lambda_A]$  by assuming that a Strickler-Berg type relationship could be used, relating the molar absorptivity of the transition giving rise to the emission and the radiative rate constant for emission.<sup>171,172</sup> If the geometry change upon excitation is not large then  $\epsilon_{0-0}(S_0 \rightarrow S_1)$  is proportional to  $k_f$ . From this Birks evaluated relative absorptivities of the origin band of each conformer as

$$\epsilon_1(0-0)/\epsilon_2(0-0) \sim k_{f,1}/k_{f,2} \quad (5.24)$$

Such an approach fails in the case of the 2,2'-binaphthyl conformers since the origins of emission and absorption of the two conformers do not occur at a common wavelength, the absorption origin of species 1 lying to the red of the origin in absorption of species 2. The Strickler-Berg relationship is also predicted on the assumption that no large geometry change occurs upon excitation. This is not the case for at least one of the conformers of 2,2'-binaphthyl. In a room temperature solution in cyclohexane species 1, with  $\tau_1 = 24.83$  ns, absorbs more strongly at longer wavelength than does species 2; this is apparent from a number of observations, including the wavelength dependence of the steady state emission and the pre-exponential factors in the fluorescence decay experiments. This conformer 1 appears to suffer little geometry change on excitation as its emission lies immediately to the red of its absorption. The emission of 1 has a maximum at about 348.6 nm ( $28\,690\text{ cm}^{-1}$ ) and is probably that obtained with  $\lambda_A = 330$  nm in the degassed samples (Figure 5.9), upon oxygen quenching of the fluorescence (Figure 5.20), or calculated as  $F_1(\lambda_F)$  in Figure 5.26.

Species or conformer 2, with  $\tau_2 = 104.8$  ns, appears to have its relative absorption maximum near 300 - 310 nm. This may be deduced from the steady state fluorescence emission. From Figure 5.18 it is seen that the height of the 367.6 nm band reaches a maximum at  $\lambda_A = 300$  and 310 nm. Confirmation is obtained from the ratio of fluorescence intensities,  $\alpha_1/\beta\tau_2$ , obtained by the fluorescence decay experiments, with this ratio passing through a minimum (hence maximum contribution from 2) at  $\lambda_A = 300 - 310$  nm as evinced in Figures 5.21 and 5.25. Analysis of these values led to the calculated relative molar absorptivities, Figure 5.24,

which clearly shows the maximum is species 2 absorption near 300 - 310 nm.

The emission of 2 appears to be red-shifted with respect to both species 1 emission and the species 2 absorption. As noted in the steady state emission spectrum the intensity at  $\sim 368$  nm is chiefly attributable to the conformer 2 absorption at about 300 to 310 nm, while the fluorescence intensity of this peak was selectively quenched by the introduction of oxygen, clearly apparent in Figure 5.20. Decay experiments performed at a fixed excitation wavelength but variable emission wavelengths for room temperature solutions show the relative contribution of species 2 to increase at longer emission wavelengths, as gauged by the decrease in the ratio of pre-exponentials to longer wavelength.

Tinland has suggested an  $S_0$  minimum for 2,2'-binaphthyl in fluid solution at an interplanar angle of  $10^\circ$  or less although he has not examined torsional angles above  $20^\circ$ .<sup>152</sup> Gamba and coworkers<sup>175</sup> have proposed a model  $S_0$  potential for 2,2'-binaphthyl that is symmetric about  $\theta = 90^\circ$  with minima at  $35^\circ$  and  $145^\circ$  and barrier heights of  $\sim 770$   $\text{cm}^{-1}$  at  $90^\circ$  and  $\sim 1600$   $\text{cm}^{-1}$  at  $0^\circ$  and  $180^\circ$ . Unlike the potential surfaces for 1- and 2-phenylnaphthalene the potential for 2,2'-binaphthyl will not, in principle, be truly symmetric about the perpendicular configuration,  $\theta = 90^\circ$ , although one may qualitatively expect the potential functions for  $S_0$  and  $S_1$  to be less asymmetric than those of the 1,1'- and 1,2'-binaphthyls.

Figure 5.28 is proposed as qualitatively accounting for a number of the observed features of the steady state and decay spectroscopy of 2,2'-binaphthyl in nonpolar solvents at 295K and 77K. A double minimum is depicted in both the ground and first excited singlet states at

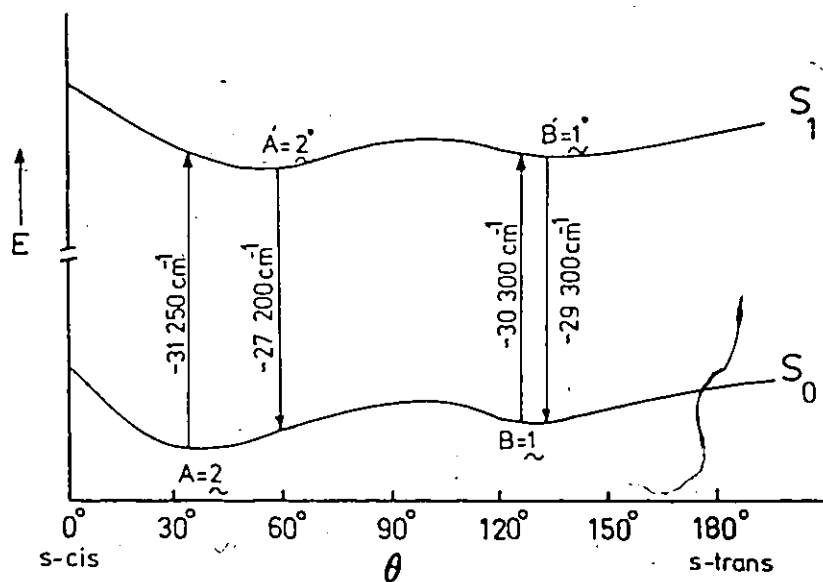


Figure 5.28

Proposed Potential Energy Diagram for the  
Ground and First Excited Singlet States of  
the 2,2'-Binaphthyl Conformers.

points A, B, A' and B'. The actual angular location of these points is open to question but on the basis of Gamba's calculations<sup>175</sup> and by analogy with the other biaryls it is likely that conformer or species 2 has a broad minimum at point A with a dihedral angle of about 30°. Conformer 1 has a more twisted geometry, possibly within 30° of the perpendicular conformation. For purposes of illustration this has been set to ~ 120°, the minimum of point B on Figure 5.28. This local minimum B is believed to be at somewhat higher energy than that of species 2 at A. At first glance this appears contrary to the result calculated from the room temperature decay experiments, namely that  $\epsilon_1[\lambda_A]C_1/\epsilon_2[\lambda_A]C_2$  is greater than unity. If the molar absorptivities of species 1 and 2 were equal at all values of  $\lambda_A$  then the ground state population of conformer 1 must be larger than the ground state population of 2, that is  $C_1 > C_2$ . However, the low temperature emission spectra in alkane glasses seem to belie this possibility, as these spectra show a definite increase in the intensity of the red component of the emission and enhanced structure in that region. This implies that the relative population of the more coplanar species 2 increases upon reducing the temperature and that this conformer is the thermodynamically more stable form. One may reconcile this observation with  $\epsilon_1[\lambda_A]C_1/\epsilon_2[\lambda_A]C_2 > 1$  if the actual absorptivity or molar extinction coefficient of conformer 1 is greater than that of conformer 2. This is not an unreasonable supposition since one might expect a higher absorptivity to be associated with the shorter lived species.<sup>94</sup>

When cooled to 77K in the relatively fluid isopentane glass a small fraction of 2,2'-binaphthyl molecules appear to have nearly

coplanar configurations as evinced by the appearance of a weak band at 356.8 nm in the excitation spectrum (Figure 5.13 and Table 5.12). This is precisely the position of the 0-0 in fluorescence and absorption of 1,2,7,8-DBF. It was also noticed that the fluorescence of 77K solutions of 2,2'-binaphthyl in isopentane could be excited at much longer excitation wavelengths, up to 345 nm, than could the same solutions at room temperature.

The barrier height between conformers 1 and 2 in the ground state must be small, so that a significant proportion of the 2,2'-binaphthyl molecules will have rather twisted geometries at 295K. Relatively low energy excitation of molecules at point B in Figure 5.28 will lead to fluorescence from a conformation such as B'. As the excitation energy is increased direct excitation from A becomes possible, leading to the long lived and red shifted emission from A'. This may account for the unusual wavelength dependence seen for 2,2'-binaphthyl in fluid solution, with the peak at 349 nm dominating the emission upon excitation at  $\lambda_A \geq 330$  nm, while the emission component at 368 nm becomes more pronounced at  $\lambda_A \sim 300 - 310$  nm.

Upon cooling to 77K the preferred or average conformation will be the more coplanar one, although some fraction of twisted conformers is probably still present, since the ground state torsional barrier is unlikely to be very high. The increased solvent viscosity at 77K will modify the true torsional barriers, while Figure 5.28 only attempts to depict the intramolecular potential in a qualitative manner. At higher excitation energies the blue lying emission component ( $\sim 343$  nm) arising from species 1 increases in relative intensity in the emission

spectra in isopentane and 3MP at 77K, indicating the presence of production of a twisted configuration even at liquid nitrogen temperatures.

While the lifetime  $\tau_2$  was relatively unaffected by temperature,  $\tau_1$  seemed to vary with temperature or viscosity. The observation that  $\tau_2$  is practically invariant with temperature incidentally confirms that the value of  $\phi_{f,2}$  could be near unity. If  $\phi_{f,2}$  was, as calculated, near unity then one would expect a decrease in the observed  $\tau_2$  of  $\sim 15\%$  on going from 3MP solution at ambient temperatures to 77K in that same solvent, that decrease being determined by the increased refractive index, all other factors being equal. The observed  $\tau_2$  does not decline by this amount but remains essentially constant, indicating that the fluorescence quantum yield for species 2 is slightly less than unity. In light of the very similar lifetimes of species 2 at 77K and 295K it is likely that the excited state geometries are not greatly different at these temperatures.

The shorter decay component was identical in isopentane and 3-methylpentane at room temperature, with  $\tau_1 = 29.19$  ns in the former and  $\tau_1 = 29.29$  ns in the latter solvent. This pair of solvents have similar refractive indices at this temperature while in the more dispersive solvent, cyclohexane,  $\tau_1$  was found to be somewhat shorter (24.83 ns), as expected. The low temperature behaviour of  $\tau_1$  was found to be different in isopentane and 3-methylpentane;  $\tau_1$  decreased to 22.86 ns in the more-rigid ( $\eta = 2.2 \times 10^{12}$  poise) 3MP glass while increasing to 34.47 ns in the relatively fluid ( $\eta \sim 10^6$  poise) isopentane glass at 77K. This longer fluorescence lifetime of species 1 upon cooling in isopentane points to a decrease in the radiationless rate constants at 77K; the



lack of a deuterium effect on the experimental values of  $\tau_1$  or  $\tau_2$  in isopentane (or other solvent, for that matter) indicates that intersystem crossing is the principal mechanism for nonradiative depletion of the excited singlet states. The increase in  $\tau_1$  in isopentane on cooling must stem from the decrease in  $k_{isc}$ . The fluorescent states for species 1 in isopentane at 295K and 77K are likely very similar, the low viscosity permitting considerable torsional relaxation at either temperature.

The decrease in  $\tau_1$  observed in 3MP is larger than expected on the basis of the refractive index effect alone. If the emissive states at 295K and 77K in 3MP were the same the largest decrease in  $\tau_1$  expected on the basis of an  $n^{-2}$  refractive index correction alone would be about 10%, going to about 25 ns instead of the 22.86 ns observed. It is probable then that the geometry of the shorter lived emissive state in the rigid 3MP is somewhat different from that giving rise to the 34.47 ns component in isopentane at 77K. In the more viscous solvent this excited state conformation would resemble more closely that of the initial ground state configuration whereas the equilibrium excited state geometry of species 1 lies at some interplanar angle different from that of the ground state of conformer 1. For this reason point B' is not drawn vertically above the point B on the lower potential energy curve.

It cannot be determined with certainty whether the absolute minimum of  $S_0$  (i.e., species 2) lies to the s-cis or s-trans side. The curves in Figure 5.28 may, in fact, be reflected about the  $\theta = 90^\circ$  line approximately. The particular configuration of  $\sim 30^\circ$  from the coplanar s-cis configuration was chosen on the basis of the trend established for

1,1'-binaphthyl, where the ground and excited state absolute minima were found to both lie on the cis side. The torsional barrier  $A' \rightleftharpoons B'$  in the excited state is drawn to be lower than the corresponding torsional barrier  $A \rightleftharpoons B$  in the ground state. The bond order of the nominally single interannular bond is normally considered to increase upon excitation, with a commensurate shortening of this connecting carbon-carbon bond.<sup>24,27,194</sup> Mulliken<sup>226</sup> first predicted this increased bond order for the  $C_2-C_3$  quasi-single bond upon excitation of 1,3-butadiene, while a similar effect has been predicted for the more pertinent systems, 1-phenylnaphthalene,<sup>153</sup> 2-phenylnaphthalene<sup>27,153</sup> and 1,1'-binaphthyl.<sup>24,194</sup> Despite this shortening of the interannular bond upon excitation the non-bonded steric repulsions in both 2-phenylnaphthalene and 1,1'-binaphthyl were not believed to be much different in the ground and first excited singlet states since the adjacent C-C ring bonds were found to lengthen upon excitation.<sup>153,194</sup> The net effect is to increase the  $\pi$ -conjugation energy in  $S_1$ , with no increase in the nonbonded H-H steric repulsion. This results in a lesser dependence of the total energy upon the twist angle and a reduced torsional barrier in the excited state as compared to the ground state.<sup>24</sup>

The fluorescence lifetime alone does not seem to be an adequate basis for assigning a structure to the two conformers of 2,2'-binaphthyl. The rigid *cis* binaphthyl-analog 1,2,7,8-DBF has a fluorescence lifetime (25.09 ns in 3MP at 295K) more closely resembling that of the more twisted conformer 1 ( $\tau_1 = 29.29$  ns) than the more nearly planar conformer 2 ( $\tau_2 = 105.5$  ns) under the same solvent and temperature conditions.

## CHAPTER SIX

### SUMMARY

The fluorescence spectroscopy and photophysics of the phenyl-naphthalenes and binaphthyls have been examined for evidence of excited conformeric states of these molecules in solution.

The fluorescence properties of 1-phenylnaphthalene proved quite unexceptional and indicated the presence of a single predominant conformation of this molecule with a relatively large dihedral angle between the aromatic rings. This large interannular angle has been inferred from the small shift ( $730\text{ cm}^{-1}$ ) of the electronic origin of the 1-phenylnaphthalene fluorescence from that of naphthalene, and from the naphthalene-like vibrational modes seen in the low temperature emission. This correlation does not extend to the fluorescence lifetimes with  $\tau_f = 12.7\text{ ns}$  for 1-phenylnaphthalene and  $\tau_f = 110\text{ ns}$  for naphthalene.

Wharton, Nauman, Hughes and Holloway's<sup>25,26,27</sup> earlier work on the steady-state spectroscopy of 2-phenylnaphthalene had pointed to the existence of single bond rotational conformers for that molecule. This has been confirmed by the fluorescence decay measurements on dilute fluid and glassy solutions and by the excitation wavelength dependence of the fluorescence from oxygenated fluid solutions of 2-phenylnaphthalene, whereas the corresponding degassed solutions showed

no such effect. Both at 295K and 77K the fluorescence of 2-phenyl-naphthalene could be analyzed in terms of a very minor short-lived ( $\sim 1$  ns) blue-emitting component and a longer-lived (114 - 135 ns) lower energy component, apparently representing different molecular configurations.

A moderately detailed fluorescence spectrum was obtained from 2-phenylnaphthalene in a polycrystalline methylcyclohexane matrix at 77K. Under these conditions no excitation wavelength effect was noted while the emission showed a distinct red-shift compared to that found in glassy media at 77K, the highest energy band lying at  $29\,340\text{ cm}^{-1}$  in the former and  $30\,720\text{ cm}^{-1}$  in the latter medium. This is likely the result of the intermolecular restraint of the polycrystalline matrix on the conformation of the 2-phenylnaphthalene guest molecule, leading to a single and generally more coplanar configuration.

At room temperature the photophysics and fluorescence spectroscopy of the 1,1'-binaphthyl were found to agree with the results of previous studies.<sup>24,191,200,207</sup> The lack of any excitation wavelength dependence, the monoexponential singlet decay and the large Stokes shift between fluorescence and absorption of 1,1'-binaphthyl in fluid solution points to emission from the equilibrium conformation of the  $S_1$  surface only. On cooling to 77K the principal fluorescent state changed, becoming more naphthalene-like and blue shifting considerably. Under these circumstances it is probable that this  $S_1$  conformation more closely resembles the  $S_0$  equilibrium geometry and has a dihedral angle approaching  $90^\circ$ . Results of the singlet decay measurement of 1,1'-binaphthyl in rigid media were at variance with those found by Post et al.,<sup>200</sup> a bi-

exponential fluorescence decay being observed at 77K with no long-lived emission akin to that reported by Post. The source of this discrepancy is not clear but the materials used in this present work were rigorously purified and apparently free of any spurious fluorescence. A model involving local and absolute minima in the first excited singlet state is proposed to account for this biexponential decay behaviour.

While this author found no quasilinear emission from 1,1'-binaphthyl in polycrystalline solvents at 77K, Riley very recently reported quasilinear fluorescence from 1,1'-binaphthyl in an n-pentane matrix at 4.2K. Since similar concentrations and solvents were previously examined by this author it is possible that the heat treatment or cooling rate of the solution may be particularly critical for this solute-solvent pair or that some torsional modes are sufficiently active at 77K (versus 4.2K) to cause a loss of vibrational detail in the fluorescence spectrum. In addition Riley found this to be a dual quasilinear fluorescence, with two electronic origins separated by fully  $4850\text{ cm}^{-1}$ ; he attributes this dual emission to two different molecular conformations of 1,1'-binaphthyl in the polycrystalline matrix.

The spectroscopy of the 1,2'-isomer is very similar to that of 1,1'-binaphthyl but with both absorption and fluorescence shifted to longer wavelength, suggesting a more coplanar arrangement of the naphthalene rings.

This would be in keeping with the expected smaller steric repulsion between the two groups in the 1,2'-compound than in the 1,1'-binaphthyl. A single fluorescent state is present in fluid solution but the fluorescence decay becomes distinctly biexponential at 77K, like that of 1,1'-binaphthyl. Again, this is most readily accommodated by a scheme

entailing a double minimum on the  $S_1$  potential energy surface. The fluorescence lifetime and quantum yield have been measured for the first time and the corresponding radiative and nonradiative rate constants calculated.

The fluorescence of 2,2'-binaphthyl is further red shifted from that of 1,1'- and 1,2'-binaphthyl indicating on average a more coplanar conformation of that molecule, as expected qualitatively on the basis of the reduced steric interactions. At least two fluorescent conformers of 2,2'-binaphthyl coexist in fluid solution, as evinced by the pronounced excitation wavelength dependence of the fluorescence emission spectrum and quantum yield and by the biexponential fluorescence decay, with characteristic lifetimes of about 25 and 105 ns in cyclohexane. The singlet lifetime measurements proved a very powerful method for discriminating temporally between two species with very similar and overlapping spectral distributions. Both the fluorescence lifetime measurements and differential oxygen quenching of the steady-state emission show the longer-lived component to be somewhat red shifted with respect to the shorter-lived conformer. While the absorption spectra of these two conformers overlap strongly the shorter-lived species may be selectively excited at the extreme absorption edge. The spectrum so obtained agrees well with that seen in oxygenated samples at all wavelengths, although the shorter-lived species has the higher molar concentration in fluid solution. Indeed, the low temperature experiments would suggest that the red-lying, long-lived species 2 is the predominant, equilibrium conformation of the molecule. Both conformations are likely

rather coplanar, possibly with one being cis-inclined and the other trans-inclined with respect to the configuration with both aryl rings mutually perpendicular.

2,2'-binaphthyl did give quasilinear spectra in polycrystalline methylcyclohexane, although the bandwidths were relatively broad. These too were found to be strongly dependent on the excitation wavelength employed. From the variations in relative intensities of the quasilines and from the fluorescence excitation spectra these Shpol'skii spectra could be analyzed as two fluorescence subspectra, with electronic origins separated by  $\sim 525 \text{ cm}^{-1}$ . When compared with the model planar compound 1,2,7,8-dibenzofluorene it is apparent that the two fluorescent conformers in the polycrystalline matrix are close to, but not completely coplanar. These two conformers are probably different from those seen in fluid or glassy media, being largely determined by the intermolecular or random solvent effects.

Behaviour of the perdeuterated 2,2'-binaphthyl parallels that of the  $-h_{14}$  molecule. Both rate constants  $k_{nr}$  and  $k_f$  proved independent of deuterium substitution. The deuterated species did show a somewhat different relative intensity distribution in the quasilinear spectrum.

This work suggests that the occurrence of relatively stable, spectroscopically distinguishable molecular conformers differing in their orientation with respect to a single bond may be a more widespread phenomenon than is commonly recognized. This should be particularly true where that bond is of somewhat increased bond order, as with those conjugated between nominally double bonds. While the steady-state

fluorescence can provide much useful information, the measurement and

analysis of the fluorescence decay spectrum provides a powerful method of probing systems with strongly overlapping absorption and emission spectra. Use of the selective oxygen quenching of the longer-lived component proved a useful method of enhancing otherwise subtle spectroscopic differences.



## APPENDIX I

### Room Temperature Absorption Spectra of 1- and 2- Phenyl naphthalene; 1,1'-, 1,2'- and 2,2'-Binaphthyl and 1,2,7,8-Dibenzofluorene

These spectra, Figures I.1 through I.6, were measured at room temperature in cyclohexane solution with pure cyclohexane as the reference. Molar absorptivities were determined by accurate weighing of the solute followed by dissolution and appropriate dilutions. The units of molar absorptivity are  $\text{litre} \cdot \text{mole}^{-1} \cdot \text{cm}^{-1}$ . The long wavelength region of each spectrum is shown in greater detail in the upper right quadrant of each spectral trace. The assignment of transitions is generally taken from Jaffe and Orchin<sup>213</sup> but that of 2,2'-binaphthyl is re-interpreted in light of the 1,2,7,8-dibenzofluorene absorption spectrum. To coincide with Jaffe and Orchin's discussion the Platt classification<sup>227</sup> of electronic states of aromatic hydrocarbons is used. The ground states  $S_0$  are denoted  $^1A$  in all cases so the transitions are frequently designated by the upper state label alone.

#### 1-Phenyl naphthalene:

1-phenyl substitution red shifts and slightly enhances the transversely polarized  $^1L_a$  band with respect to the parent molecule naphthalene (at 286 nm in naphthalene). The weak, long-axis polarized transition  $^1L_b$  is at roughly 310 nm but is practically buried under the adjacent, stronger  $^1L_a$  band ( $\log \epsilon = 3.95$ ) centered at 288 nm. The strong band ( $\log \epsilon \sim 4.8$ ) at 227 nm probably corresponds to the longitudinally polarized  $^1B_b$  band which occurs at 221 nm in naphthalene.

Figure I.1 - I.6

- 1: 1-Phenylnaphthalene
- 2: 2-Phenylnaphthalene
- 3: 1,1'-Binaphthyl
- 4: 1,2'-Binaphthyl
- 5: 2,2'-Binaphthyl
- 6: 1,2,7,8-Dibenzofluorene

Absorption Spectra in Cyclohexane Solution at Room Temperature

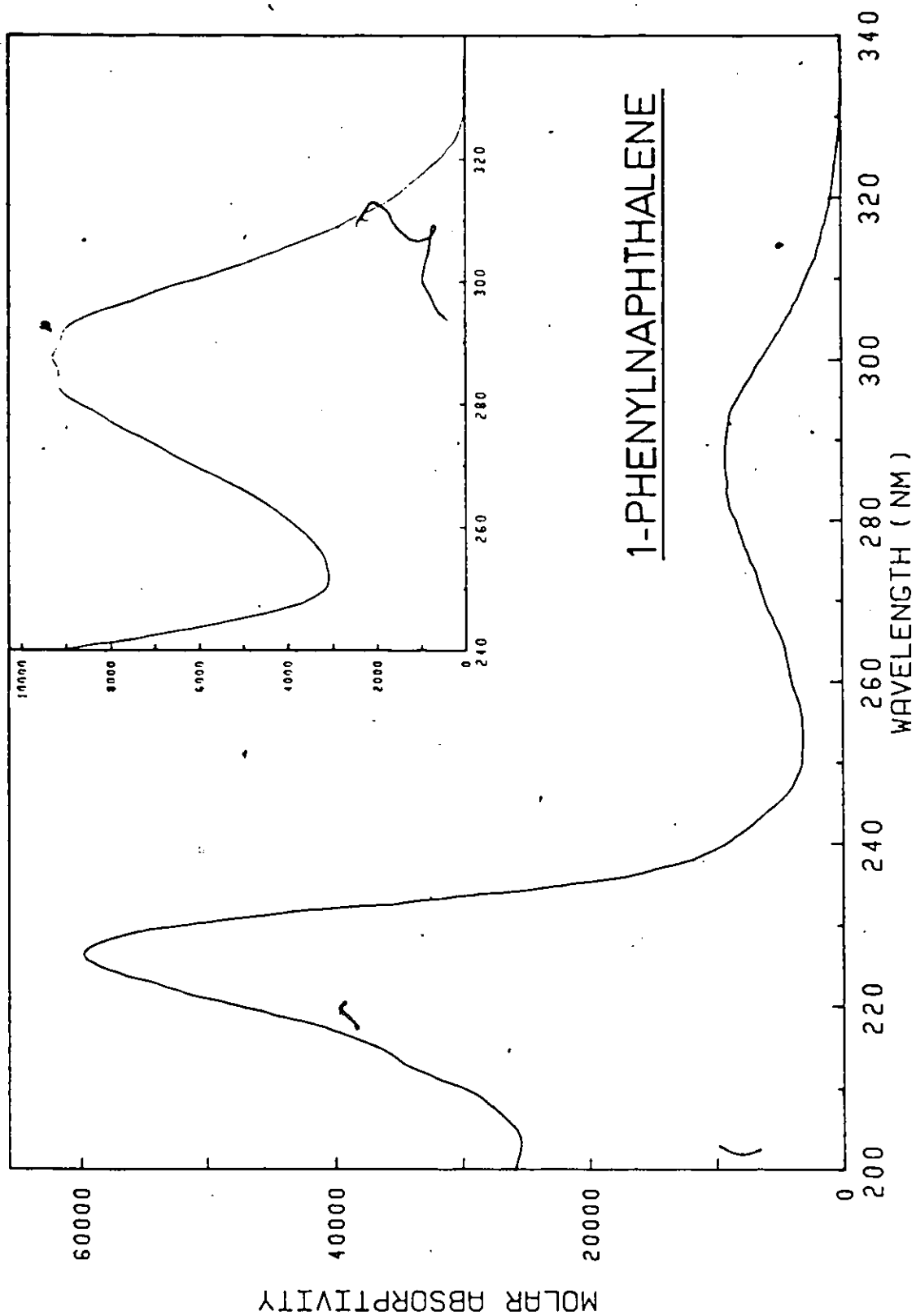


Figure I.1

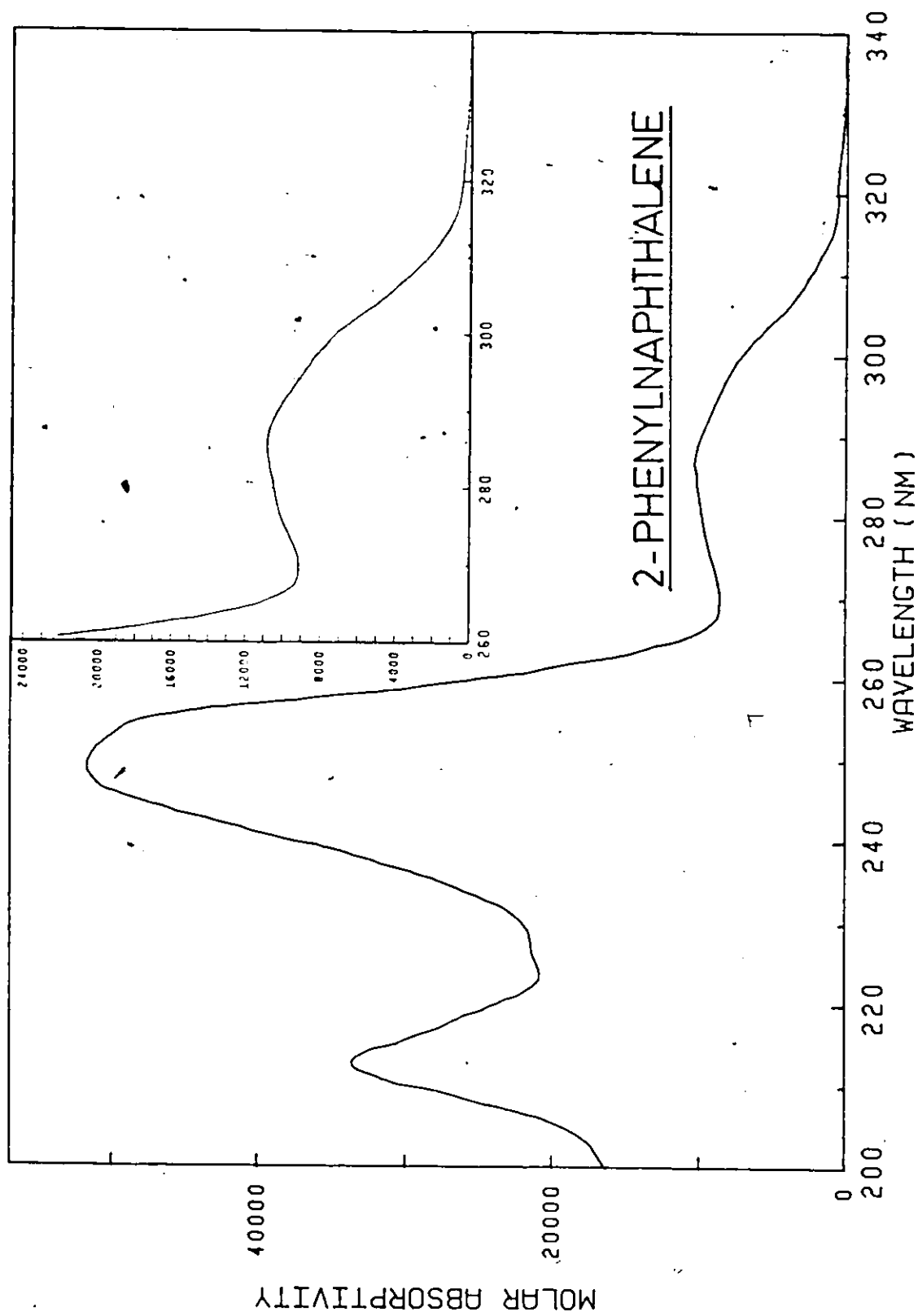


Figure 1.2

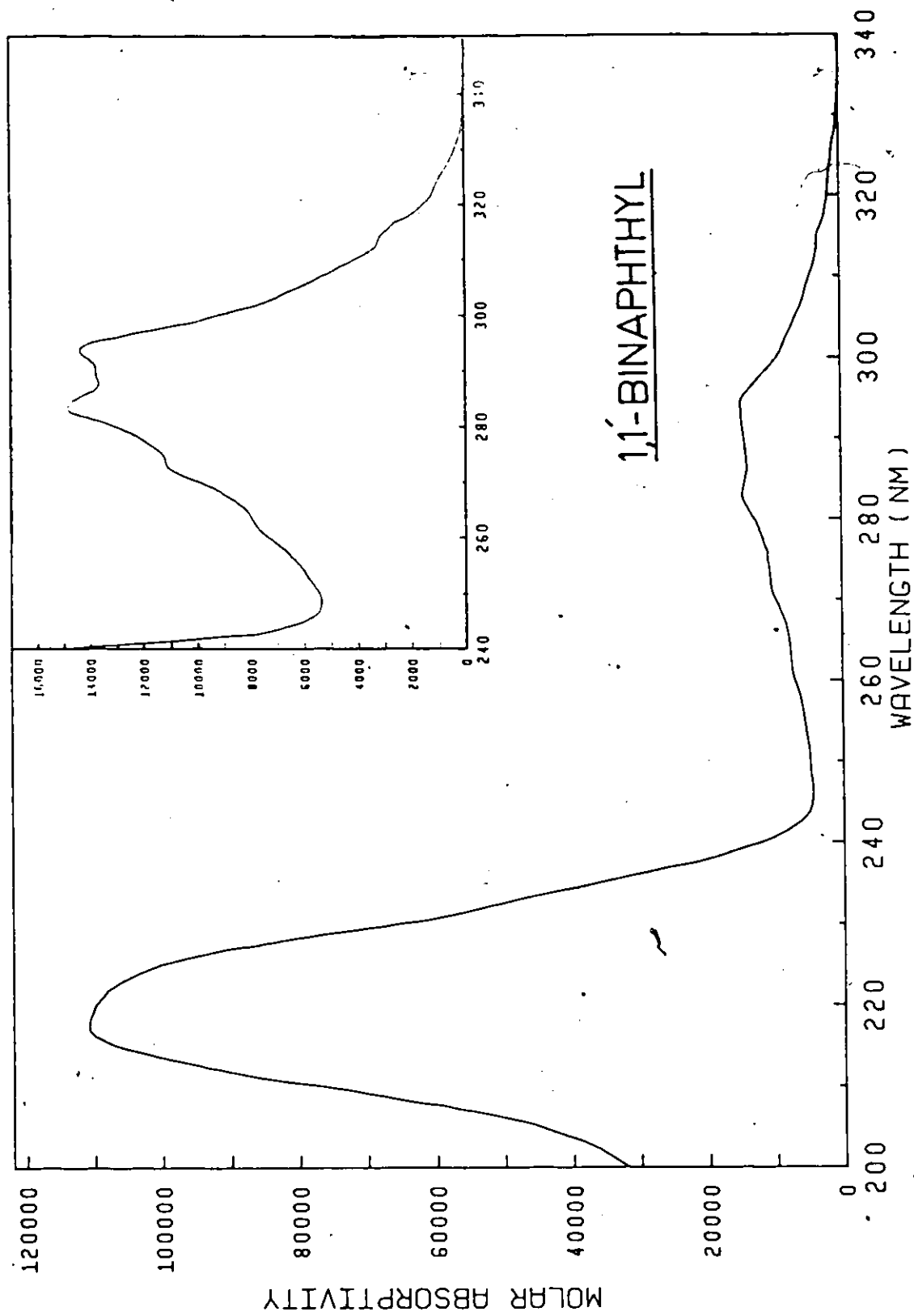


Figure I.3

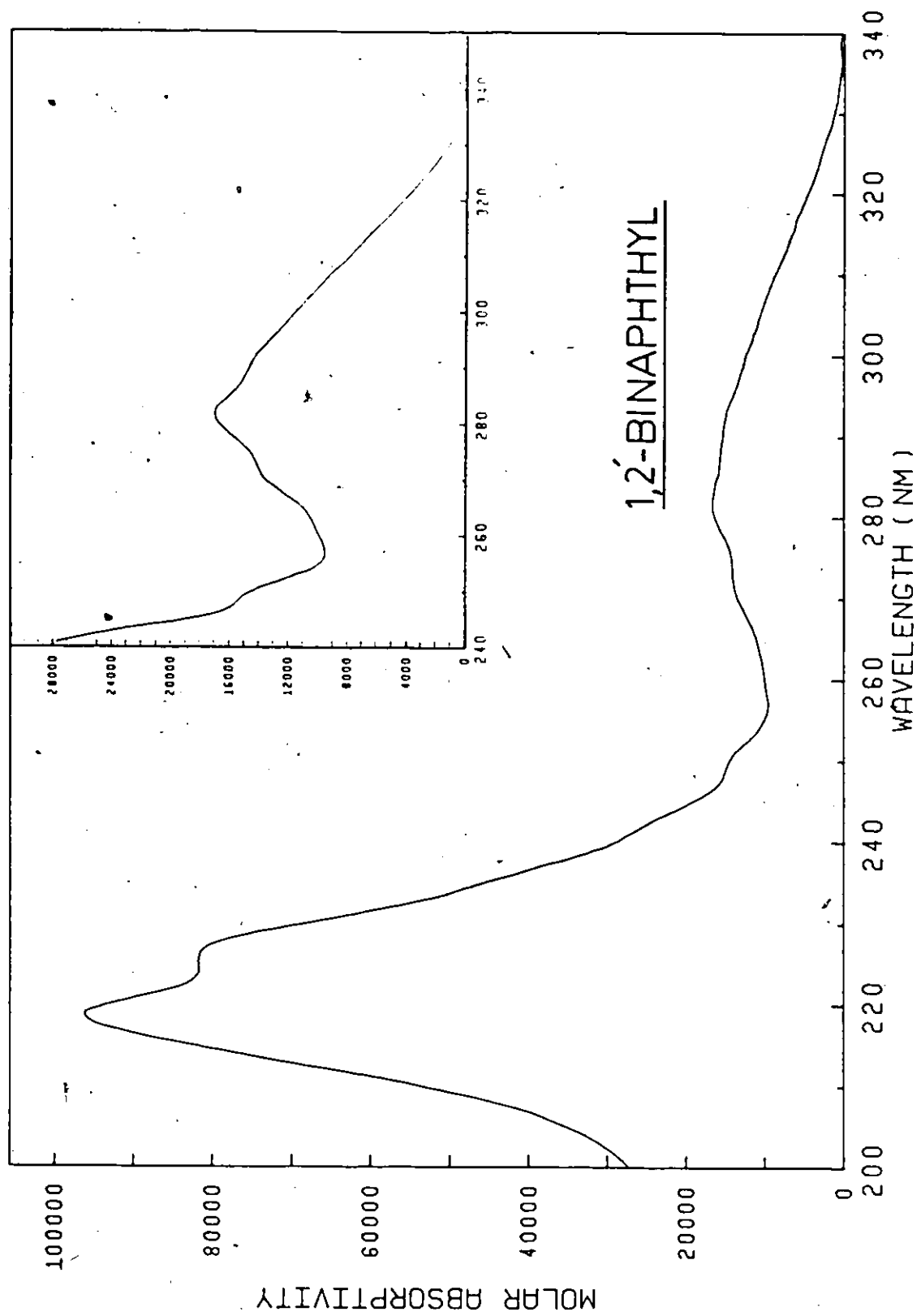


Figure I.4

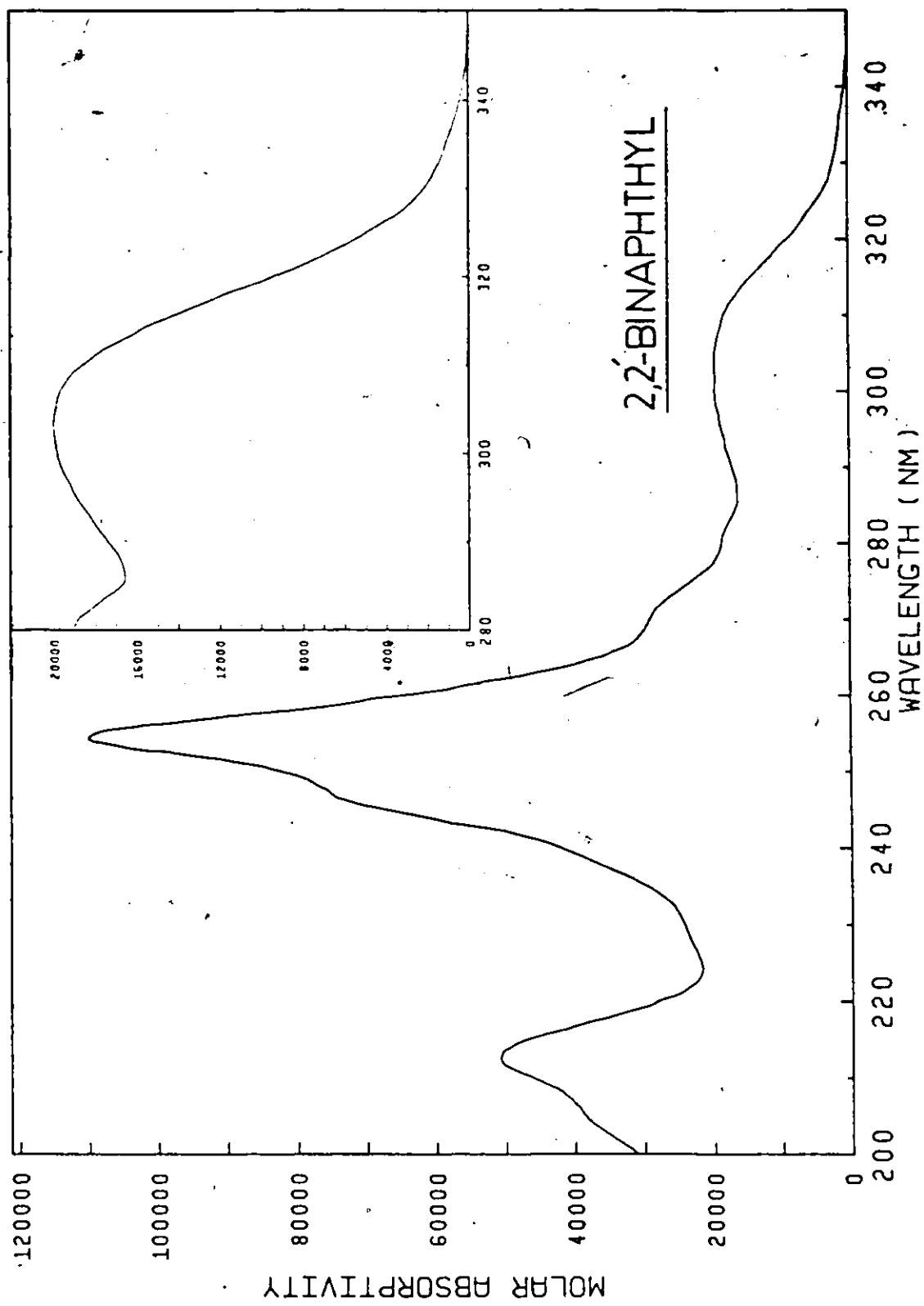


Figure 1.5

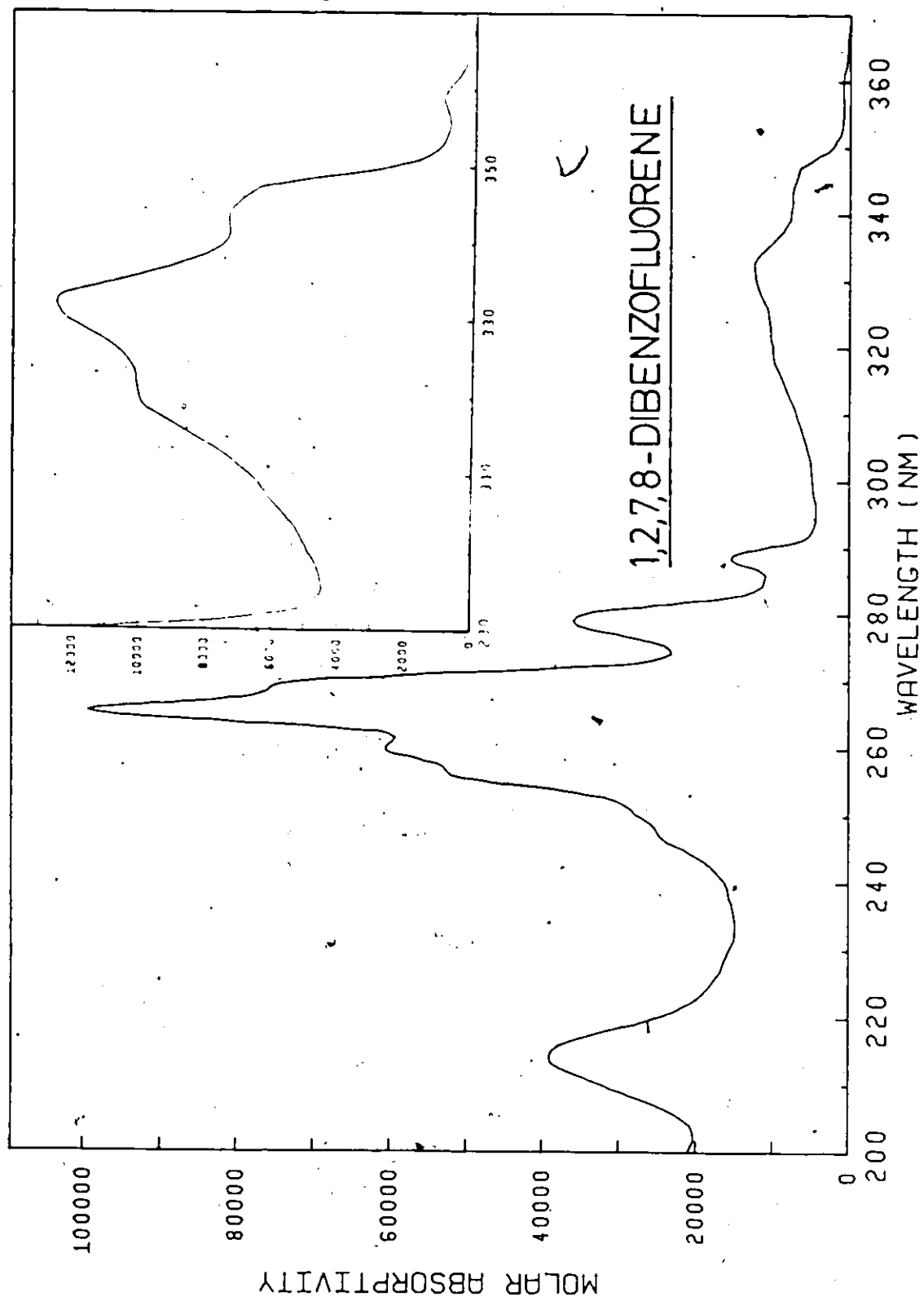


Figure I.6



### 2-Phenylnaphthalene:

Substitution in the 2-position is expected to intensify and red-shift the long-axis polarized  $^1L_b$  band relative to naphthalene, although this is difficult to assess, owing to the poor resolution of this region. The  $^1L_a$  transition at 286 nm is unaffected by introduction of the phenyl substituent in the 2-position on the naphthalene nucleus. That conjugation in the longitudinal direction will affect transitions polarized in that direction is apparent from the behaviour of the  $^1B_b$  transition which undergoes a large bathochromic shift from 221 nm in naphthalene to 250 nm in 2-phenylnaphthalene. The band at 212 nm in the 2-phenylnaphthalene absorption spectrum is most likely the  $^1C_b + ^1A$  transition which is formally forbidden in the centrosymmetric naphthalene but allowed in derivatives of reduced symmetry.

### 1,1'-Binaphthyl:

The absorption spectrum of this compound bears more than a passing similarity to that of 1-phenylnaphthalene. Both long wavelength bands, the  $^1L_b$  at 318 nm and the  $^1L_a$  at 297 nm have undergone some red-shift relative to the corresponding bands in naphthalene, the shift being larger for the transversely polarized  $^1L_a$  transition, as anticipated for 1-substitution. The other longitudinally polarized transition, the  $^1B_b$  at 222 nm is practically unaffected (221 nm in naphthalene). These observations indicate that the  $\pi$ -electron interaction between the rings in 1,1'-binaphthyl is very small and that the coupling is chiefly through the interannular bond, affecting the short-axis polarized transitions only.

### 1,2'-Binaphthyl:

The absorption spectrum of this compound shows characteristics of both a 1- and 2- substituted naphthalene. The gross features show a closer resemblance to those of 1-phenylnaphthalene and 1,1'-binaphthyl, the  $^1L_b$  and  $^1L_a$  bands being nearly coalesced while the  $^1B_b$  transition appears distinctly at 218 nm. The  $^1L_b$  is submerged by the stronger adjacent  $^1L_a$  band but this absorption seems somewhat red-shifted with respect to naphthalene.

### 2,2'-Binaphthyl:

This spectrum is similar to that of 2-phenylnaphthalene, but with the extended conjugation red-shifting the long axis polarized  $^1L_b$  and  $^1B_b$  transitions somewhat. Jaffe and Orchin believed the  $^1L_b$  and  $^1L_a$  bands to be at 335 and 305 nm respectively,<sup>213</sup> indicating a large effect on transitions of both polarizations. However, in view of the greatly enhanced resolution obtained in the absorption spectrum of the rigid 2,2'-binaphthyl analog 1,2,7,8-dibenzofluorene (infra vide) their assignments of the  $^1L_a$  transition's origin should be revised. The weak shoulder 335 nm is likely the electronic origin of the low lying  $^1L_b$  transition, the peak at  $\sim 305$  nm being a vibrational band of this same electronic transition. The poorly resolved band at 282 nm in 2,2'-binaphthyl is the more probable candidate for the electronic origin of the  $^1L_a$  transition, with an adjacent ill-resolved vibrational band at 272 nm,  $\sim 1300\text{ cm}^{-1}$  away. This indicates that the transversely polarized  $^1L_a$  transition is practically unaffected by the extended longitudinal conjugation.

Further strong bands appear in the 2,2'-binaphthyl absorption at

255 nm ( $^1B_b$ ) and 212 nm ( $^1C_b$ ); these are similar to those bands seen for 2-phenylnaphthalene but quite red-shifted from those of naphthalene.

1,2,7,8-Dibenzofluorene:

The absorption spectrum of this rigid analog of 2,2'-binaphthyl bears a striking similarity to that of the unrestrained 2,2'-binaphthyl. The increase extent of the  $\pi$ -electron system in this planar compound red-shifts the  $^1L_b$  absorption considerably, to 358 nm. More vibrational structure is evident in this rigid 2,2'-binaphthyl than in its flexible parent, a behaviour noted by Jaffe and Orchin<sup>213</sup> in comparing the absorption spectra of the phenylnaphthalenes and their rigid analogs, the benzofluorenes. This vibrational detail in the 1,2,7,8-dibenzofluorene absorption spectrum seems to indicate that the previously mentioned re-interpretation of the 2,2'-binaphthyl absorption spectrum is in order. The four bands of 1,2,7,8-DBF in the region 300 - 360 nm appear to be vibrational bands of the single electronic transition  $^1L_b + ^1A$ . The sharp band at 288 nm is then the origin of the  $^1L_a$  transition (282 nm in 2,2'-binaphthyl, 286 nm in naphthalene and 2-phenylnaphthalene) with vibrational spacings between successive bands of about 1100 - 1300  $\text{cm}^{-1}$ . The peaks at 279, 269, 260 and 251 nm are the vibrational components of this  $^1L_a + ^1A$  transition whose electronic origin is at 288 nm. The very intense absorption at 265 nm is probably the  $^1B_b$  origin (255 nm in 2,2'-binaphthyl, 250 nm in 2-phenylnaphthalene and 221 nm in naphthalene) with weaker vibrational components at 256 and 246 nm, again a spacing of  $\sim 1200 \text{ cm}^{-1}$ . The high energy absorption at 214 nm is assigned to the transition  $^1C_b + ^1A$  (212 nm in 2,2'-binaphthyl and 2-phenylnaphthalene).

#### Summary of the Absorption Properties:

The absorption spectra clearly fall into two categories, those resembling naphthalene fairly strongly and those showing substantial deviation from the naphthalene absorption. The first group contains 1-phenylnaphthalene, 1,1'-binaphthyl, and 1,2'-binaphthyl. For these molecules the  $\pi$ -interaction between the aryl moiety is small, with transitions of both polarizations being little affected. No  $^1C_b + ^1A$  transition is apparent in their absorption spectra, indicating that the perturbing influence of the aryl substituent is insufficient to relax the electronic selection rules of the centrosymmetric naphthalene substantially.<sup>227</sup>

The second group is comprised of those molecules exhibiting a large  $\pi$ -electronic interaction of the aryl moieties, namely 2-phenylnaphthalene, 2,2'-binaphthyl and 1,2,7,8-dibenzofluorene. Being less sterically hindered, the ground states of these molecules are more nearly planar with a concomitant increase in the  $\pi$ -electronic delocalization over both ring systems. The long-axis polarized transitions generally show large bathochromic shifts and with the reduction of molecular symmetry the transition  $^1C_b + ^1A$  becomes allowed and so appears with moderate intensity in the absorption spectra of all three compounds.

## APPENDIX II

### Testing of the Deconvolution Procedures

The deconvolution routines MRQRDT and TWOEXP were tested on simulated and real data sets to assess the ability of these programs and the experimental method in determining or retrieving the fluorescence decay parameters. Of particular interest were trials designed to find the levels at which a true second component in the fluorescence decay could be detected and quantified. At sufficiently low levels it is expected that the genuine biexponential decay would no longer be distinguishable from the monoexponential decay of the major component.

### Deconvolution of Synthetic Data Sets

The efficacy of data handling method for the time-correlated single photon counting technique of fluorescence lifetime determination has been evaluated by a number of authors using various simulations of the convoluted decay data.<sup>58,59,69,72,77,84,228</sup>

Since the fluorescence decay of 2,2'-binaphthyl in fluid solution appears to be biexponential it was decided to model the fluorescence decay of this particular system. The temporal dependence of the model excitation (lamp) function is chosen to be of the form

$$E(t) = At^2 e^{-0.5t} \quad (II.1)$$

where  $t$  is the time in channel numbers; for the typical time base of the real 2,2'-binaphthyl decay experiments, 0.6550 ns, which approximates that of the  $N_2$ -filled flashlamp. The normalization factor  $A$  is chosen to give  $10^4$  counts at the maximum of the lamp function. This smooth,

analytic lamp function is then convoluted with an impulse fluorescence decay function of the form

$$I(t) = \alpha e^{-t/\tau_1} + \beta e^{-t/\tau_2} \quad (II.2)$$

To simulate the 2,2'-binaphthyl decay  $\tau_1$  and  $\tau_2$  are chosen to be 25.0 and 100.0 ns respectively while  $\alpha$  and  $\beta$  can be varied to give the different relative contributions of the two decay components to the total decay intensity. The convolution integral

$$G(t) = \int_0^t E(t') I(t-t') dt' \quad (II.3)$$

is integrated numerically using the trapezoidal rule. The resulting curve is smooth, since no noise has been added and the expressions for  $E(t)$  and  $I(t)$  are exact. This smooth, convolved curve is normalized to  $10^4$  counts at the maximum again. This maximum number of counts is chosen since it represents a value normally realizable at reasonable collection times for the real decay experiments. This maximum is sometimes used to specify the signal-to-noise ratio in photon counting experiments.<sup>58,77</sup> For  $y_i$  counts in channel  $i$  the S/N ratio will be  $y_i/\sqrt{y_i}$  hence, for  $10^4$  counts maximum the S/N will be 100; 100-fold longer collection times ( $10^6$  counts maximum) result in only a 10-fold improvement in S/N. Such long collection times pose many experimental difficulties.

The statistical counting noise for the single photon counting method will be Poisson distributed about a mean of  $y_i$  in channel  $i$ . For  $y_i$  reasonably large (even  $y_i = 10$  is adequate) this Poisson distribution is closely approximated by the Gaussian distribution. To the smooth

convoluted curve is then added Gaussian distributed random noise.

This Gaussian noise is generated by means of the IMSL subroutine GGNML by the call statement "Call GGNML(DSEED,NR,R)" where NR = the number of channels (512), R is a vector of dimension NR and DSEED is a double precision number (integral) selected by the user. The vector R contains output random deviates of the normal distribution having a mean of zero and variance of one. Hence for channel i having  $y_i$  counts in the noiseless function G(t), the generated noisy value will be

$$y_i(\text{noisy}) = y_i(\text{smooth}) + [y_i(\text{smooth})]^{1/2} \times r_i \quad (II.4)$$

where  $r_i$  is the  $i^{\text{th}}$  random deviate generated by GGNML and contained in the vector R. The value of DSEED is changed on every run since a given DSEED will generate the same vector of random deviates each time.

Starting with  $\tau_1 \equiv 25.0$  ns and  $\tau_2 \equiv 100.0$  ns synthetic decay curves were generated with the ratio of preexponentials,  $\alpha/\beta$ , ranging from 100:1 to 1:100. Some of the results of deconvolution of these data sets are shown in Table II.1:

A more meaningful measure of the relative contributions of the short and long-lived components than  $\alpha/\beta$  itself is the quantity  $(\alpha\tau_1)/(\beta\tau_2)$ , which represents the relative contributions of the two to the total decay, since

$$\int_{t=0}^{t=\infty} I(t)dt = \int_{t=0}^{t=\infty} \{\alpha e^{-t/\tau_1} + \beta e^{-t/\tau_2}\}dt = \alpha\tau_1 + \beta\tau_2 \quad (II.5)$$

Thus  $\alpha/\beta$  of 100:1 actually corresponds to relative intensities of 25:1 for short:long components. From Table II.1 it is seen that the presence of the long-lived component can be clearly detected even at an intensity

Table II.1

Deconvolution of Noisy Synthetic Data for Biexponential Decay Law

$$I(t) = \alpha e^{-t/25.0} + \beta e^{-t/100.0}$$

$\alpha/\beta$ given	$\alpha/\beta$ found	$\Delta(\alpha/\beta)$ %	$\tau_1$ (ns) found	$\Delta\tau_1$ %	$\tau_2$ (ns) found	$\Delta\tau_2$ %	$\chi^2$	Residuals Correlated
100	54.1	-45.9%	24.73	-1.08%	72.26	-27.7%	1.07	no
	-	-	26.40	+5.60%	-	-	4.47	strongly
20	19.7	-1.36%	24.97	-1.12%	97.27	-2.73%	0.98	no
	-	-	31.25	+25.0%	-	-	28.23	strongly
10	9.64	-3.54%	24.81	-0.76%	96.89	-3.11%	1.02	no
	-	-	37.31	+49.2%	-	-	50.63	very strongly
1	0.985	-1.53%	25.08	+0.32%	99.62	-0.38%	1.01	no
	-	-	-	-	81.28	-18.7%	26.21	strongly
0.10	0.0954	-4.57%	23.94	-4.24%	99.67	-0.33%	1.01	no
	-	-	-	no convergence with monoexponential fit				
0.05	0.0457	-8.59%	20.09	-19.64%	99.37	-0.63%	1.02	no
	-	-	-	-	98.47	-1.53%	1.16	slightly
0.01	0.0190	+90.0%	11.58	-53.68%	99.74	-0.26%	1.05	no
	-	-	-	-	97.55	-2.45%	1.72	strongly
	-	-	-	-	99.49	-0.51%	0.95	no



of only 4% that of the major, short-lived, component, as witnessed by the sharp decrease in  $\chi^2_v$  and improved randomness of the residuals on going from a monoexponential to a biexponential fit. The actual value extracted for  $\tau_2$  is highly inaccurate however, being fully 28% low. At the other extreme, very low intensity of the short-lived component, the behaviour is similar, with the presence of the minor constituent reliably detectable down to  $\alpha/\beta = 0.05$  (1:80 relative intensities). The minor component is, again, underestimated. The trial with  $\alpha/\beta = 0.05$  is of particular interest since  $\chi^2_v$  only is insufficient basis for deciding between the mono- and biexponential fit with  $\chi^2_v$ , being 1.02 and 1.16 respectively, both being statistically acceptable. However, the autocorrelation function of the weighted residuals for the monoexponential fit clearly indicates some non-randomness the differences at short times and betrays the existence of the additional short component. At very low amounts of the short-lived fluorophore,  $\alpha/\beta = 0.01$  or relative intensities of 1:400, this second component can not be reliably detected. Sample deconvolutions of this "true" biexponential decay as a monoexponential produce roughly equal numbers of good and bad fits. Two examples are given in Table II.1 one trial yielding  $\chi^2_v = 1.72$  with very non-random residuals while a second, independent trial gave  $\chi^2_v = 0.95$  with no autocorrelation of the residuals, i.e., the second decay component would pass undetected. From these observations it would appear that if the decay components have lifetimes of 25 and 100 ns the minor decay component can be detected at levels of roughly 2% of the total intensity. On this time-base the lifetime of the long-lived component can be accurately determined

(< 5% error) only if it contributed about 15% or more to the total intensity whereas the short lifetime can be calculated to better than 5% accuracy if this fluorophore contributed more than ~ 3% of the total intensity. This greater sensitivity toward the shorter component is probably the result of the particular time-base chosen, 0.655 ns/channel. A formula relating the fluorescence lifetime to the optimal channel width has been given recently by Hall and Selinger<sup>87</sup>

$$T_o = \tau x_o(m) \quad (II.6)$$

where  $T_o$  is the optimal channel width (ns/channel),  $\tau$  is the fluorescence lifetime and  $x_o(m)$  is a minimizing parameter and is a function of the number of channels used. With  $x_o(512) = 0.0331$ <sup>87</sup>  $T_o$  for a 100 ns fluorescence lifetime will be 3.31 ns/channel while for a 25 ns fluorescence lifetime the optimal channel width is 0.828 ns/channel, closer to the 0.655 ns/channel width used for these simulations. No single timebase will be ideal for both components of a biexponential decay.

The reiterative deconvolution of these decay curves by the routines MRQRDT and TWOEXP is most satisfactory, with reliable detection and recovery of the decay parameters down to very low intensities of the minor component. The expected values of the parameters  $\tau_1$ ,  $\tau_2$  and  $\alpha/\beta$  were recovered with reasonable accuracy and the reduced chi-squared statistic for the biexponential fit was near unity in all cases, as demanded for Poisson distributed counting noise. It should be noted in passing that  $\chi^2_v$  may occasionally be slightly less than one for the noisy curves. Trials in which smooth synthetic decay curves were generated by convolution (i.e., no Gaussian noise added) gave reduced

chi-squared values near zero ( $\chi^2_{\nu} < 10^{-3}$ ) upon deconvolution. This result could be anticipated, since the sum of squares of the residuals for such initial and fitted curves should be zero, within the rounding errors of the calculations. Thus  $\chi^2_{\nu}$  will be  $\sim 0$  for such fitted curves.

A cursory examination of the effect of scattered light on the results of the deconvolution was undertaken. Smooth synthetic decay curves were normalized to  $10^4$  counts at the maximum and to which were added varying amounts of the lamp excitation function with the normalization factor in Equation II.1 being adjusted to give the appropriate fraction of scattered light. Scattered light amounting to 5% (500 counts at maximum) or 15% (1500 counts at maximum) was added to the smooth synthetic curve, which was then re-normalized to  $10^4$  counts at the peak. Gaussian distributed random noise was then added. Even 15% scattered light was found to have virtually no effect on the 100 ns component. On a time-base of 0.6550 ns/channel and with no short component ( $\alpha/\beta = 0$ ) the recovered lifetime was 99.85 ns with  $\chi^2_{\nu} = 1.03$  and random residuals, despite the inclusion of 15% scattered light. For a 25 ns component on the same time scale the effect of scattered light was more pronounced. With  $\beta/\alpha = 0$  (no long component) the extracted lifetime with 5% scattered light was only slightly low, 24.81 ns, and the reduced chi-squared of 1.26 was quite good but the autocorrelation function of the weighted residuals clearly showed the presence of a non-random variation at short times. At equal pre-exponential factors ( $\alpha/\beta = 1$ ) the scattered light at a 5% level will pass virtually undetected. The extracted parameters,  $\alpha/\beta$  (final) =

0.99,  $\tau_1 = 25.06$  ns and  $\tau_2 = 99.31$  ns are very accurate, while the goodness-of-fit criteria,  $\chi^2_v (= 1.02)$  and the autocorrelation function, give no hint of the presence of the 5% scattered light. Evidently scattered excitation light is only detectable and only a problem where short fluorescence lifetimes are concerned. Scattered light levels of 5% of the decay maximum are very much higher than those encountered in real experiments if any amount of care has been exercised.

Deconvolution of Biexponential Fluorescence Decay Curves Generated by  
the Addition of Real, Monoexponential Decays

In addition to using purely synthetic decay curves to model the biexponential decay of 2,2'-binaphthyl it is also desirable to simulate such two component decays with real decay data. The biexponential decay curve is produced by the addition of two, separate monoexponential curves, recorded under identical experimental conditions in separate groups of the multichannel analyzer (MCA). The compounds chosen were naphthalene and 1-cyanonaphthalene (1-naphthonitrile) since these are known to have monoexponential fluorescence decay kinetics<sup>229</sup> and lifetimes similar to the long and short components, respectively of the 2,2'-binaphthyl decay at 295K. These two solutes could be excited and monitored at common wavelengths ( $\lambda_A = 297.7$  nm;  $\lambda_F = 335.0$  nm) similar to those encountered in the 2,2'-binaphthyl decay studies.

Solutions of  $3.84 \times 10^{-3}$  M naphthalene in cyclohexane and  $4.0 \times 10^{-4}$  M 1-naphthonitrile in n-hexane were prepared in RotaFlo-sealed fluorescence cells and degassed by repeated freeze-pump-thaw cycles at a pressure of  $< 10^{-5}$  torr. Literature values of the fluorescence lifetimes of these solute/solvent pairs are available, with  $\tau = 110$  ns for naphthalene in cyclohexane (see Table 3.1) while values of  $1.83$ <sup>229</sup> and  $1.98$  ns<sup>230</sup> have been reported for 1-naphthonitrile in n-hexane at ambient temperatures.

With excitation at 297.7 nm ( $N_2$  lamp) and the fluorescence decay monitored at 335 nm the fluorescence decay of naphthalene was recorded in one group of 512 channels in the MCA until  $10^4$  counts had been acquired at the maximum of the decay curve. This sample was replaced by the 1-naphthonitrile solution and the fluorescence decay curve of this

solute was acquired in another memory group in the MCA until  $10^4$  counts had been obtained at the decay peak. The lamp temporal profile was collected in two halves into a third group of 512 channels, one half being collected before the recording of the naphthalene decay with the second half collected after completion of the 1-naphthonitrile acquisition period. The lamp profile was measured at the excitation wavelength, 297.7 nm.

By adding appropriate fractions of these two individually monoexponential decays a composite biexponential decay with variable ratios of the preexponential factors could be constructed in the remaining memory group of the MCA. This composite curve could then be deconvoluted in the normal manner and the values obtained for  $\alpha/\beta$ ,  $\tau_1$  and  $\tau_2$  compared with the "true" starting values. As an example, one might multiply the actual 1-NN (1-naphthonitrile) curve by .01, then add this to the full ( $10^4$  maximum) naphthalene decay curve; the multiplier re-normalizes the entire curve, so, in this case, the maximum of the .01x(1-NN) curve would have only 100 counts.

The results of two separate trials are shown in Tables II.2 and III.3. A number of features are apparent in these two tables. Even with the purely monoexponential curves for the 1-naphthonitrile and naphthalene decay, the collection of  $10^4$  counts at the maximum will sometimes be insufficient to give very good values of  $\chi^2_v$ . It is noted that these values are a little higher (ca. 1.3 - 1.5) than is desirable, although biexponential fitting of these curves revealed no systematic second component for either solute (both solutes were purified by reverse phase HPLC). For the composite curves the presence of the second

Table II.2  
Results of Deconvolution of Biexponential Decay Generated by Addition of  
Real, Monoexponential Fluorescence Decay Curves in MCA

Trial I

Multiplier of MCA Group x 100 <sup>a,b</sup>		Ratio of Preexponential Factors		$\tau_1$ (ns)	$\tau_2$ (ns)	$\chi^2_v$	Monoexponential Fit	
1-NN	Naphthalene	$\alpha/\beta$ (expected)	$\alpha/\beta$ (found)				$\tau$ (ns)	$\chi^2_v$
100	0						17.84	1.55
100	1	133.7	105.2	17.56	107.9	0.76	18.85	9.56
100	5	26.7	24.0	17.56	110.6	0.51	22.72	57.23
100	10	13.4	13.3	17.57	110.92	0.46	28.41	110.0
100	25	5.35	5.42	17.62	111.3	0.52	50.66	170.2
100	50	2.67	2.73	17.69	111.3	0.76	71.63	142.3
100	75	1.78	1.84	17.79	111.3	1.04	80.62	120.6
100	100	1.34	1.40	17.66	111.2	1.32	87.23	92.28
75	100	1.00	1.06	17.75	111.2	1.29	91.69	58.87
50	100	0.668	0.715	17.84	111.2	1.28	97.06	29.46
25	100	0.334	0.278	17.92	111.1	1.28	103.6	8.43
10	100	0.134	0.171	18.86	111.2	1.29	107.4	2.92
5	100	0.0668	0.101	20.68*	111.3	1.29	108.7	1.91
1	100	0.0503	0.0134	30.56	111.7	1.29	109.8	1.44
0	100						110.2	1.37

a 10<sup>4</sup> counts at max. for both measured decay curves.

b recorded at 0.6552 ns/channel.

Table II.3  
Results of Deconvolution of Biexponential Decay Generated by Addition of  
Real, Monoexponential Fluorescence Decay Curves in MCA

Trial II

1-NN	Multiplier of MCA Group x 100 <sup>a,b</sup>	Naphthalene	Ratio of Preexponential Factors		$\tau_1$ (ns)	$\tau_2$ (ns)	$\chi^2_v$	Monoexponential Fit	
			$\alpha/\beta$ (expected)	$\alpha/\beta$ (found)				$\tau$ (ns)	$\chi^2_v$
100	0							17.97	1.32
100	1		130.4	110.4	17.77	108.2	0.70	19.04	9.16
100	5		26.1	25.3	17.74	109.7	0.41	23.10	56.18
100	10		13.0	13.0	17.73	110.0	0.36	29.18	106.8
100	25		5.22	5.28	17.73	110.3	0.42	52.13	159.6
100	50		2.61	2.66	17.75	110.4	0.66	71.43	141.3
100	75		1.74	1.79	17.78	110.4	0.93	80.35	120.0
100	100		1.30	1.35	17.81	110.4	1.23	85.73	104.0
75	100		0.978	1.02	17.85	110.5	1.22	90.33	66.46
50	100		0.652	0.688	17.95	110.5	1.22	95.62	34.77
25	100		0.326	0.391	16.30	110.1	1.20	103.5	7.71
10	100		0.130	0.198	14.58	110.1	1.22	107.0	2.77
5	100		0.0652	0.142	12.30	110.1	1.22	108.4	1.75
1	100		0.0130	0.134	7.76	110.1	1.22	109.4	1.37
0	100							109.7	1.31

<sup>a</sup> 10<sup>4</sup> counts at max. for both measured decay curves.

<sup>b</sup> recorded at 0.6552 ns/channel.



decay was detectable at all the values of  $\alpha/\beta$  examined, from about 130 to .013. This corresponds to relative intensities,  $\alpha\tau_1/\beta\tau_2$ , of from 21 to  $2.1 \times 10^{-3}$ . Both lifetimes can be extracted with an accuracy of better than 2% over the range of relative intensities of 22:1 to about 1:18. In agreement with the conclusions for the synthetic data trials it would appear that a fairly accurate fluorescence lifetime can be determined for a minor component contributing only  $\sim 5\%$  to the total decay intensity. Not surprisingly, the ratio of preexponential factors is more difficult to estimate accurately. An accuracy of about  $\pm 10\%$  is possible for relative intensities in the ratio of 4.1:1 to about 1:9, with the accuracy improving as the relative intensities become more nearly equal. At very large or very small  $\alpha/\beta$ , the ratios obtained on deconvolution may be grossly in error.

The values of the reduced chi-squared shown in Tables II.2 and II.3 show a distinct "experimental" artifact. The abnormally small values of  $\chi^2_v \ll 1.0$  obtained for some of the biexponential fits are the product of the method used to generate the composite curves. Both curves initially contained  $10^4$  actual decay events at their respective maxima. Hence the true signal-to-noise specified by this maximum is  $10^4/\sqrt{10^4}$  or 100:1. Scaling down these curves by simple re-normalization of the entire curve does not change the actual Poisson distributed counting noise associated with this scaled curve. By way of example, consider the addition of two curves so the total in channel  $i$  of the composite curve is expressed as

$$y(i) = n_1 \times y_1(i) + n_2 \times y_2(i) \quad (II.7)$$

where  $n_1$  and  $n_2$  are the fractions of each recorded curve used in constructing the biexponential decay curve,  $y(i)$  ( $0 \leq n_1, n_2 \leq 1$ );  $y_1(i)$  and  $y_2(i)$  are the actual counts in channel  $i$  as recorded experimentally for the fluorescence decay of solute 1 and solute 2. Recalling that the reduced chi-squared is defined by Equation 2.30 as

$$\chi^2_v = \frac{S^2}{\bar{\sigma}_0(i)^2}$$

and that for Poisson distributed counting noise

$$\sigma(i)^2 = y(i)$$

it is apparent that the variance estimated for channel  $i$  of the composite curve in the deconvolution routine will be  $y(i)$ . The true variance of the curve,  $S^2$  is smaller than this however, being determined by the variances of the curves  $y_1(i)$  and  $y_2(i)$  prior to normalization (see also Equation 2.28). Briefly stated, the true counting error in the composite biexponential decay curves is smaller than the counting error estimated from the net curve, because of the downward scaling of one of the constituent curves. Hence  $S^2$  is substantially less than  $\bar{\sigma}_0(i)^2$  (Poisson) and so  $\chi^2_v \ll 1$ . In retrospect a more sound approach to reproducing the statistical counting noise of the true biexponential curve would be to first collect a known number of decay events for one solute, then, switching samples, record a known number of decay events for the second solute directly onto the decay histogram of the first solute, i.e., collect known fractional intensities of each into the same memory group of the MCA. For composite decay curves constructed in this manner the statistical counting error will be directly related to the  $y(i)$  of the composite, summed curve.

### Deconvolution of the Biexponential Fluorescence Decay of a Real, Binary Solution

The fluorescence decay kinetics of a cyclohexane solution containing two chemically distinct fluorophores, 9,10-diphenylanthracene (9,10-DPA) and 1,2-benzanthracene (1,2-BA) was studied at room temperature. Solutes were purified by reverse phase HPLC and the final concentrations were  $3.6 \times 10^{-5} \text{ M}$  for 9,10-DPA and  $8.5 \times 10^{-5} \text{ M}$  for the 1,2-BA. All solutions were thoroughly degassed by the freeze-pump-thaw technique. The fluorescence lifetimes of these two solutes are well characterized in cyclohexane at 295K, values of 7.9,<sup>163</sup> 7.6<sup>231</sup> and 7.58<sup>232</sup> being reported for 9,10-DPA and 44.1<sup>137</sup> and 42<sup>135</sup> ns for 1,2-BA. These are in good agreement with the average values found by deconvolution of the biexponential decay curve of the mixed fluorophores,  $7.72 \pm .27$  ns for 9,10-DPA and  $43.8 \pm 1.97$  ns for 1,2-BA. The results of deconvoluting as a biexponential fluorescence decay are shown in Table II.4. The emission wavelength is selected by a Schott KV380 cut-off filter while the excitation is varied within the net absorption envelope of the two species.

Table II.4 also gives the relative absorbances of 9,10-DPA and 1,2-BA in solution; this ratio of absorbances will also be the ratio of the fractions of the two solutes in their respective excited states. From the relation previously given as Equation 2.82

$$\gamma[\lambda_A, \lambda_F] = (\alpha/\beta)[\lambda_A, \lambda_F] = \frac{f_1[\lambda_A]F_1[\lambda_F]k_1}{f_2[\lambda_A]F_2[\lambda_F]k_2}$$

one can calculate the relative fluorescence intensities  $F_1[\lambda_F]/F_2[\lambda_F]$  since  $f_1[\lambda_A]/f_2[\lambda_A]$ ,  $\tau_1$ ,  $\tau_2$  and  $(\alpha/\beta)[\lambda_A, \lambda_F]$  are known by experiment.

Table II.4  
 Fluorescence Decay of a Cyclohexane Solution of 9,10-Diphenylanthracene and 1,2-Benzanthracene  
 at 295K as Fit to a Biexponential Decay Law<sup>a</sup>

$\lambda_A^b$ (nm)	$\frac{A(9,10-DPA)}{A(1,2-BA)}$ expt.	$\alpha/\beta$ expt.	$\tau_1$ (ns)	$\tau_2$ (ns)	$\chi^2_\nu$	$\frac{A(9,10-DPA)}{A(1,2-BA)}$ calc.	$\alpha/\beta$ calc.
357.7	0.66	16.4	7.76	46.26	0.98	0.84	13.0
355.0	0.82	18.2	7.70	44.23	1.06	0.93	16.1
350.0	1.03	20.2	7.66	43.89	1.10	1.03	20.2
345.0	0.45	7.4	7.21	42.60	1.13	0.39	8.8
337.1	0.36	6.9	8.27	44.90	1.08	0.35	7.1
330.0	0.29	4.2	7.71	43.54	1.10	0.22	5.7
320.0	0.25	5.0	7.61	38.76	1.10	0.26	4.91
313.6	0.19	1.4	8.00	44.11	0.98	0.07	3.73
310	0.17	1.2	7.64	44.89	1.19	0.06	3.24

Single solute lifetimes: 1,2-BA = 44.24 ns  
 9,10-DPA = 7.93 ns

<sup>a</sup> Emission filter = Schott KV380.

<sup>b</sup> N<sub>2</sub> lamp.

With  $\tau_1/\tau_2 = 7.72/43.8$  and normalizing at  $\lambda_A = 350.0$  nm where the absorbances are nearly equal one gets

$$\frac{F(9,10\text{-DPA})[\lambda_F = \text{KV380}]}{F(1,2\text{-BA})[\lambda_F = \text{KV380}]} = 3.46.$$

Application of this normalized value to the other excitation wavelengths allows calculation of the ratio of preexponential factors, or equivalently, the ratio of absorbances; these are compared with the experimental values in Table II.4. The agreement between these observed and calculated ratios is reasonably good at large  $\alpha/\beta$  but very poor where the contribution of the 9,10-DPA decay becomes small. While the Schott KV380 filter passes practically all of the 1,2-BA fluorescence, it blocks a significant portion of the 9,10-DPA emission. The calculated ratio of fluorescence intensities passed by the KV380 filter, 3.46, is a reasonable figure since the expected value if both total emissions were monitored would be just the ratio of the fluorescence quantum yields  $\phi_f(9,10\text{-DPA})/\phi_f(1,2\text{-BA}) = 5.3$  ( $\phi_f(9,10\text{-DPA}) = 1.0^{34}$  and  $\phi_f(1,2\text{-BA}) = 0.19$ ).<sup>137</sup> Since the KV380 blocks some of the 9,10-DPA emission while transmitting the entire 1,2-BA fluorescence, the actual ratio is found to be somewhat less than 5.3.

This suggests an interesting, if circuitous method for determining the relative fluorescence quantum yield for a pair of fluorophores without resorting to conventional steady-state fluorescence measurements. If the ratio of absorbances of the two components is known at some excitation wavelength and the total fluorescence emission of both species is monitored, then the ratio of fluorescence quantum yields is available from a fluorescence decay measurement of the binary mixture.

## APPENDIX III

### Fluorescence Decay Curves of 2,2'-Binaphthyl

The results of fitting the fluorescence decay profiles for  $10^{-4}$  M solutions of 2,2'-binaphthyl- $h_{14}$  in cyclohexane at 295K to mono- and biexponential decay laws are plotted in the figures overleaf. These are discussed in Section 5.3.3.

Figures III.1a,b

III.2a,b

III.3a,b

III.4a,b

Mono- and Biexponential Fitting of the  
Fluorescence Decay Curves for  $10^{-4}M$   
2,2'-Binaphthyl- $h_{14}$  in Cyclohexane at 295K  
at Various Excitation Wavelengths  $\lambda_F = 340$  nm.

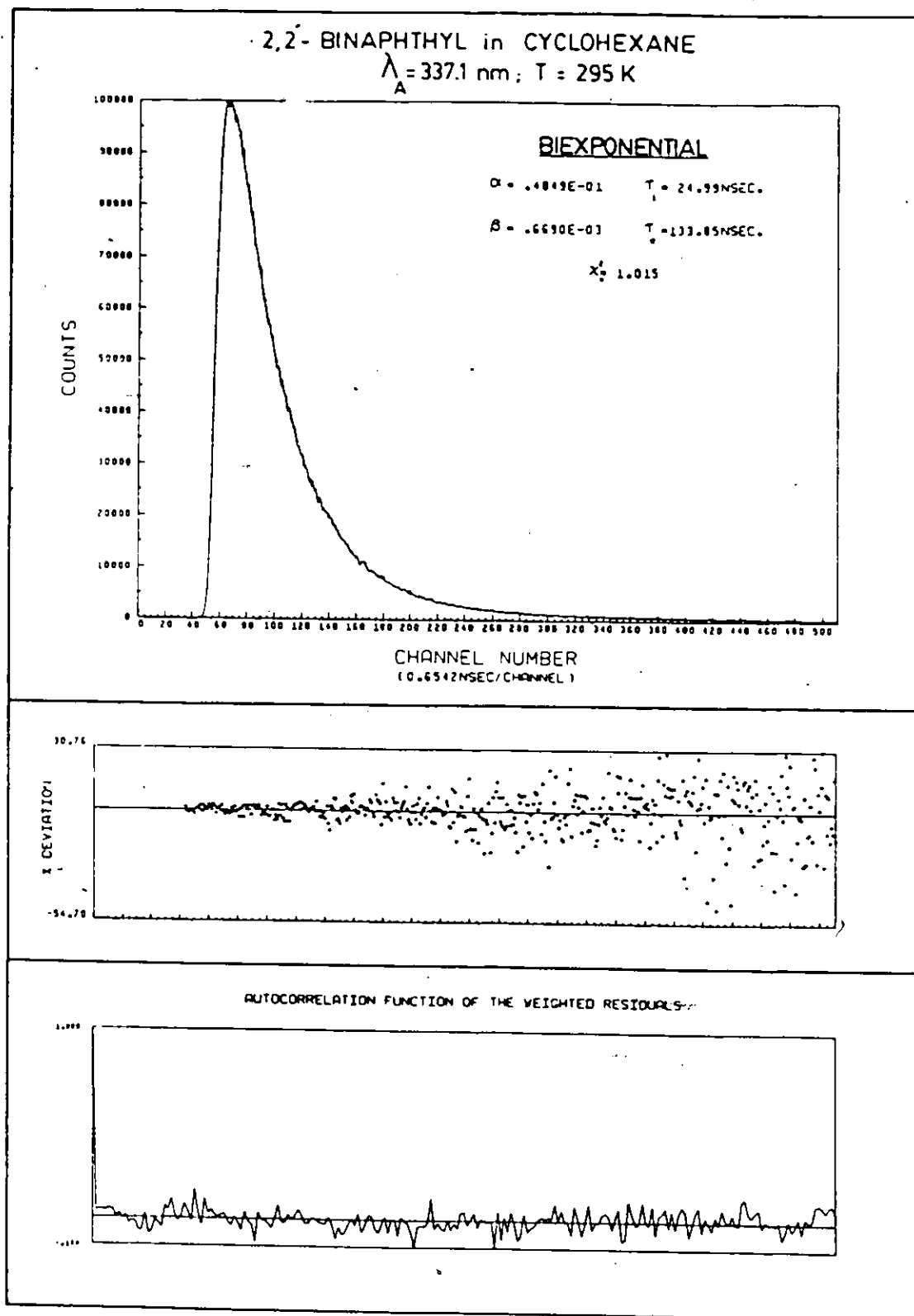


Figure III.1a



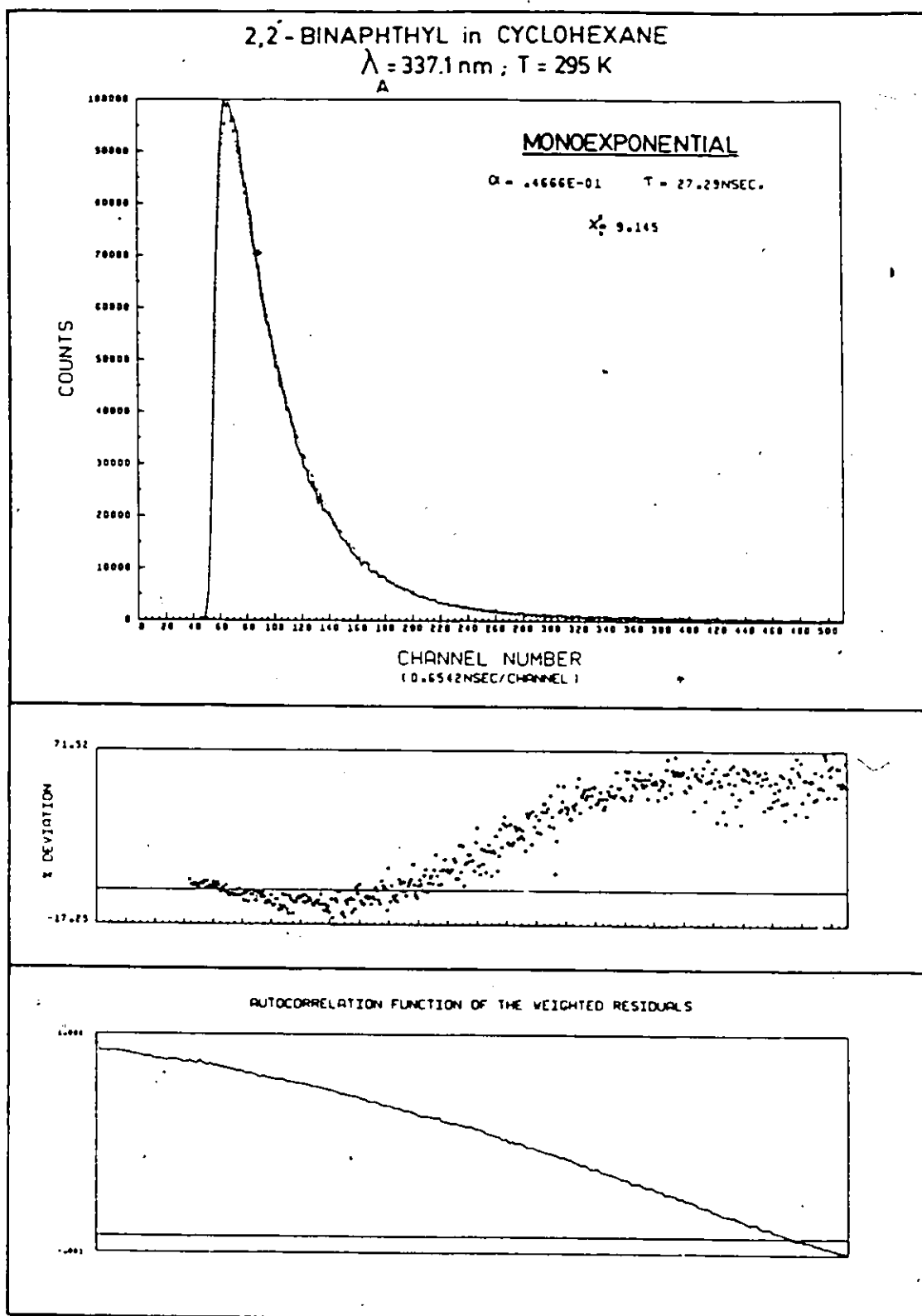


Figure III.1b

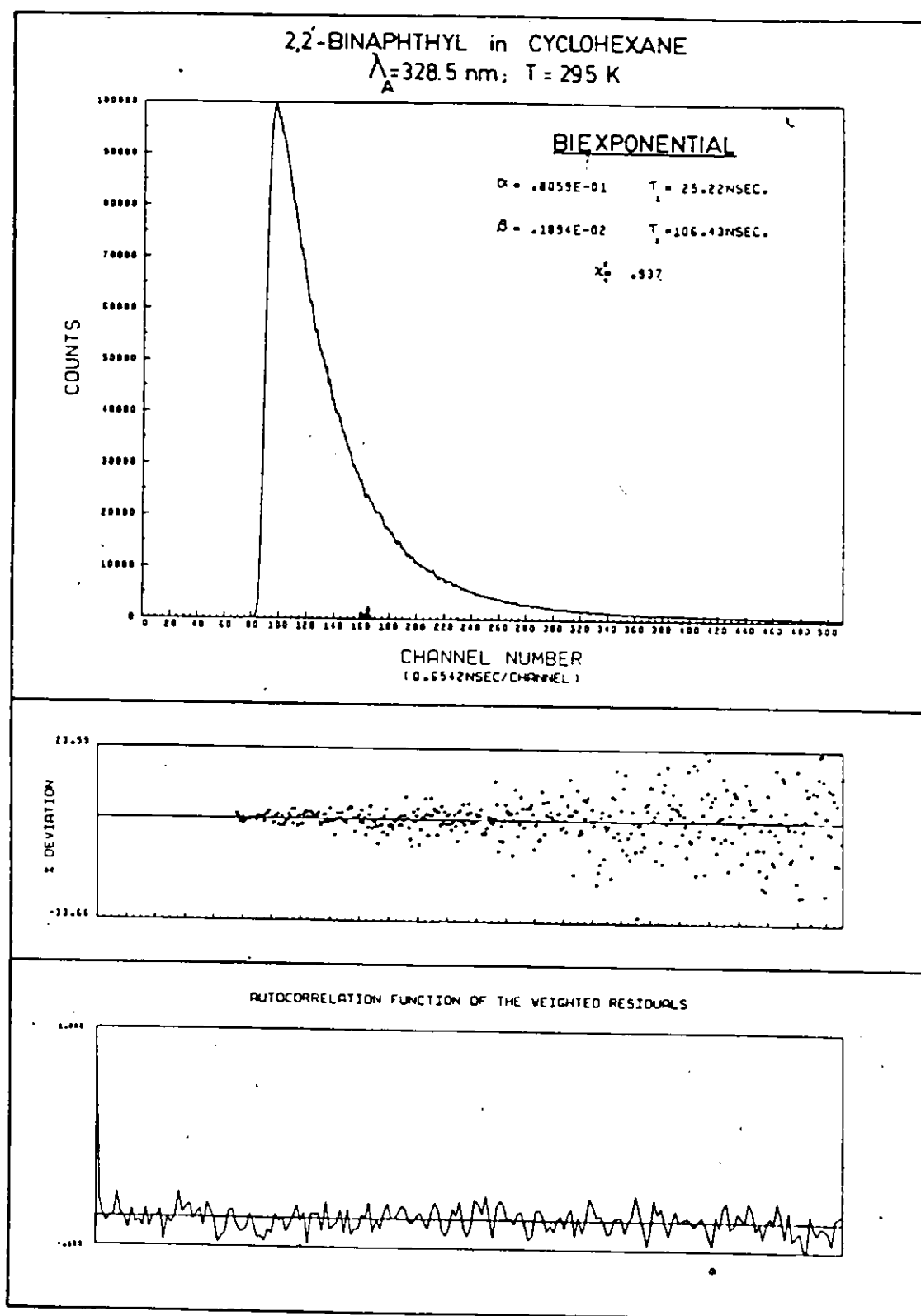


Figure III.2a

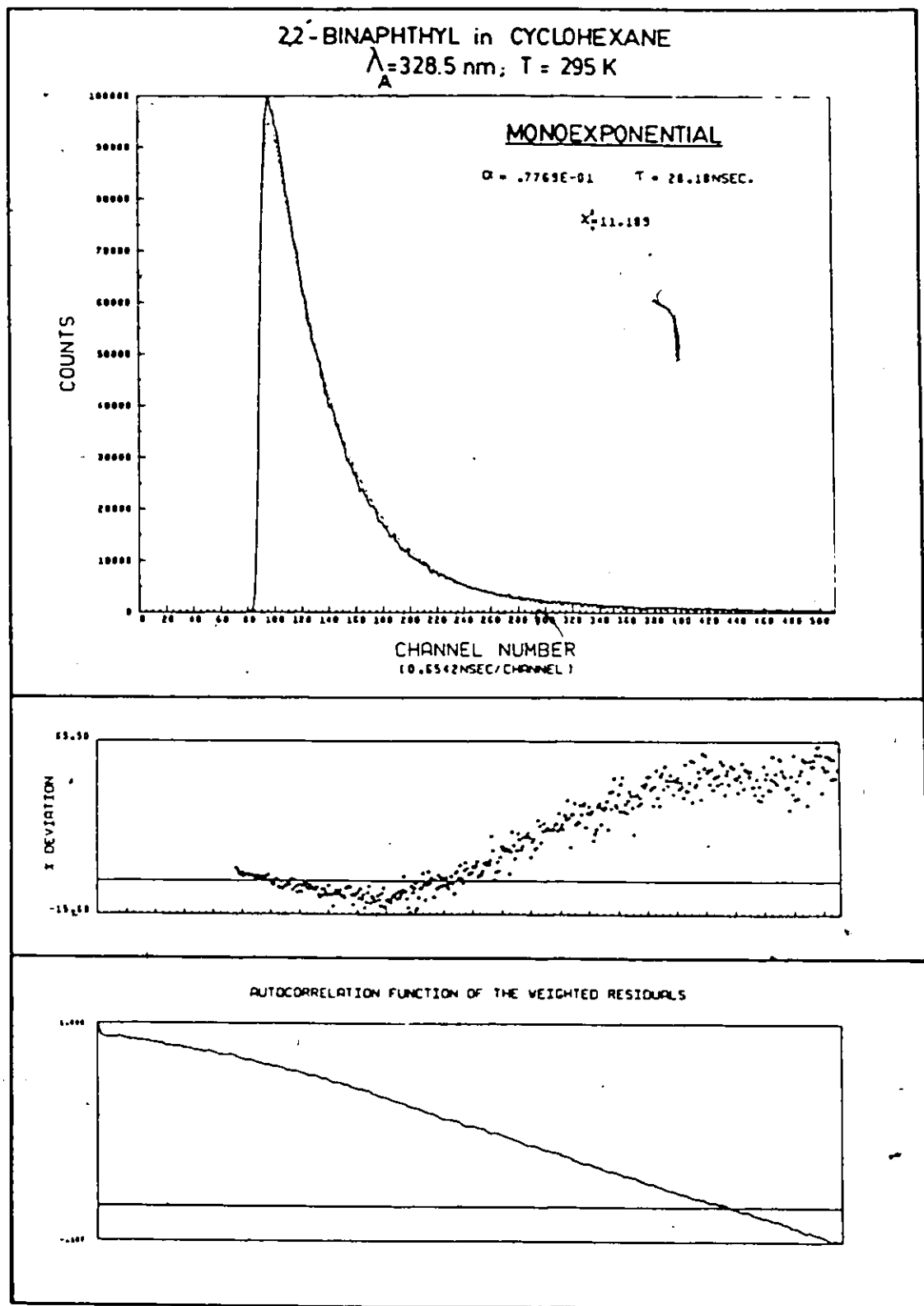


Figure III.2b

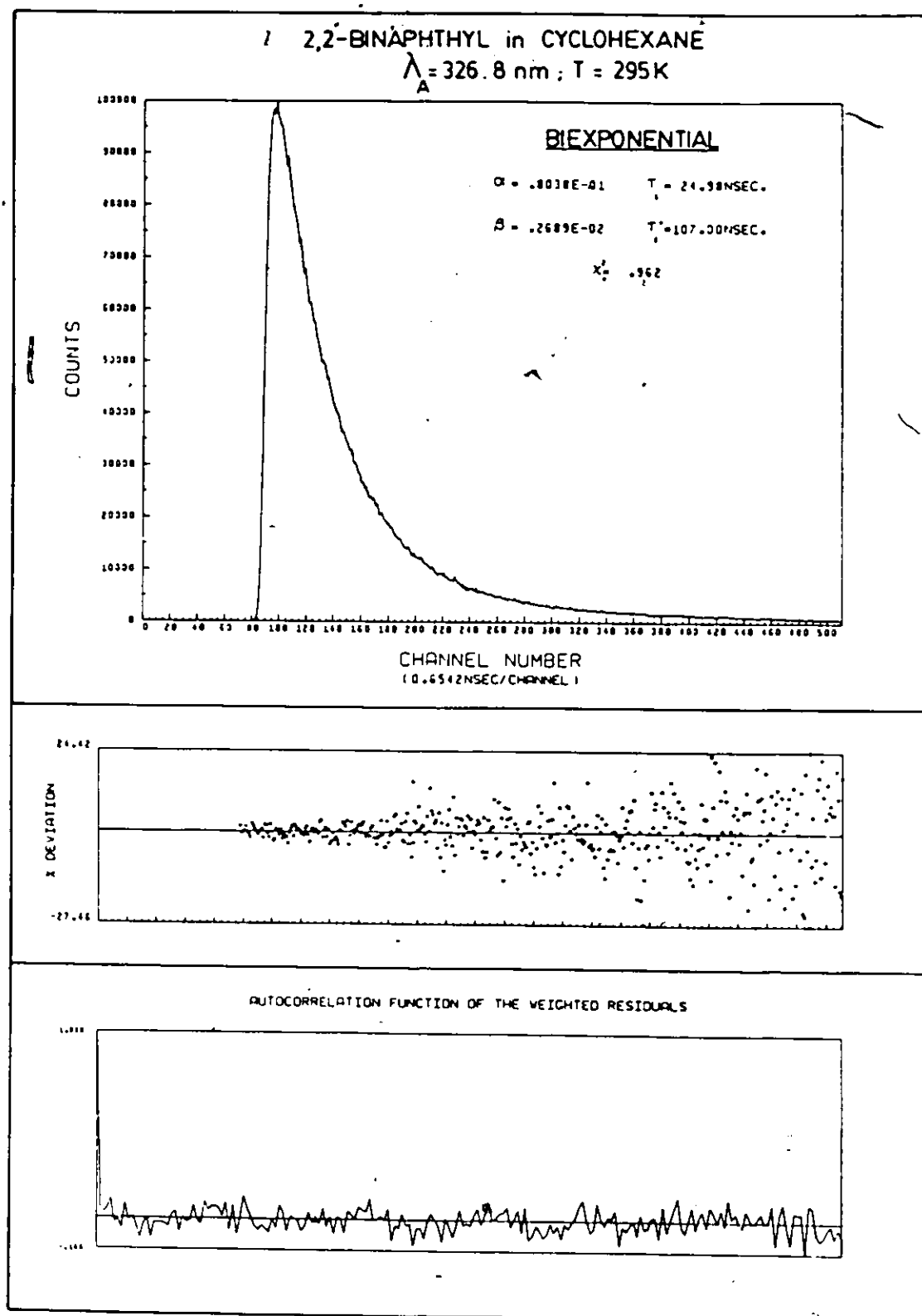


Figure III.3a

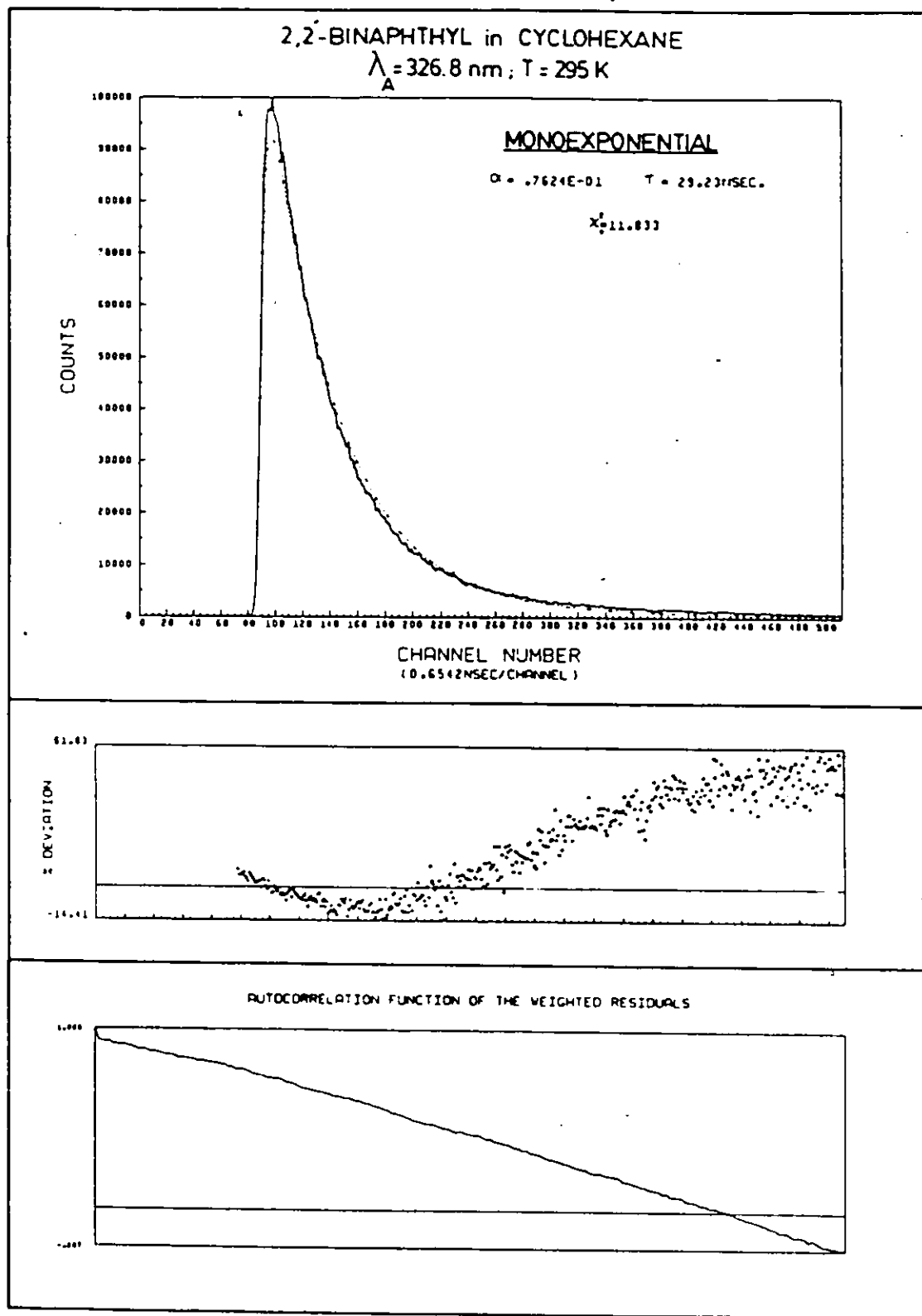


Figure III.3b

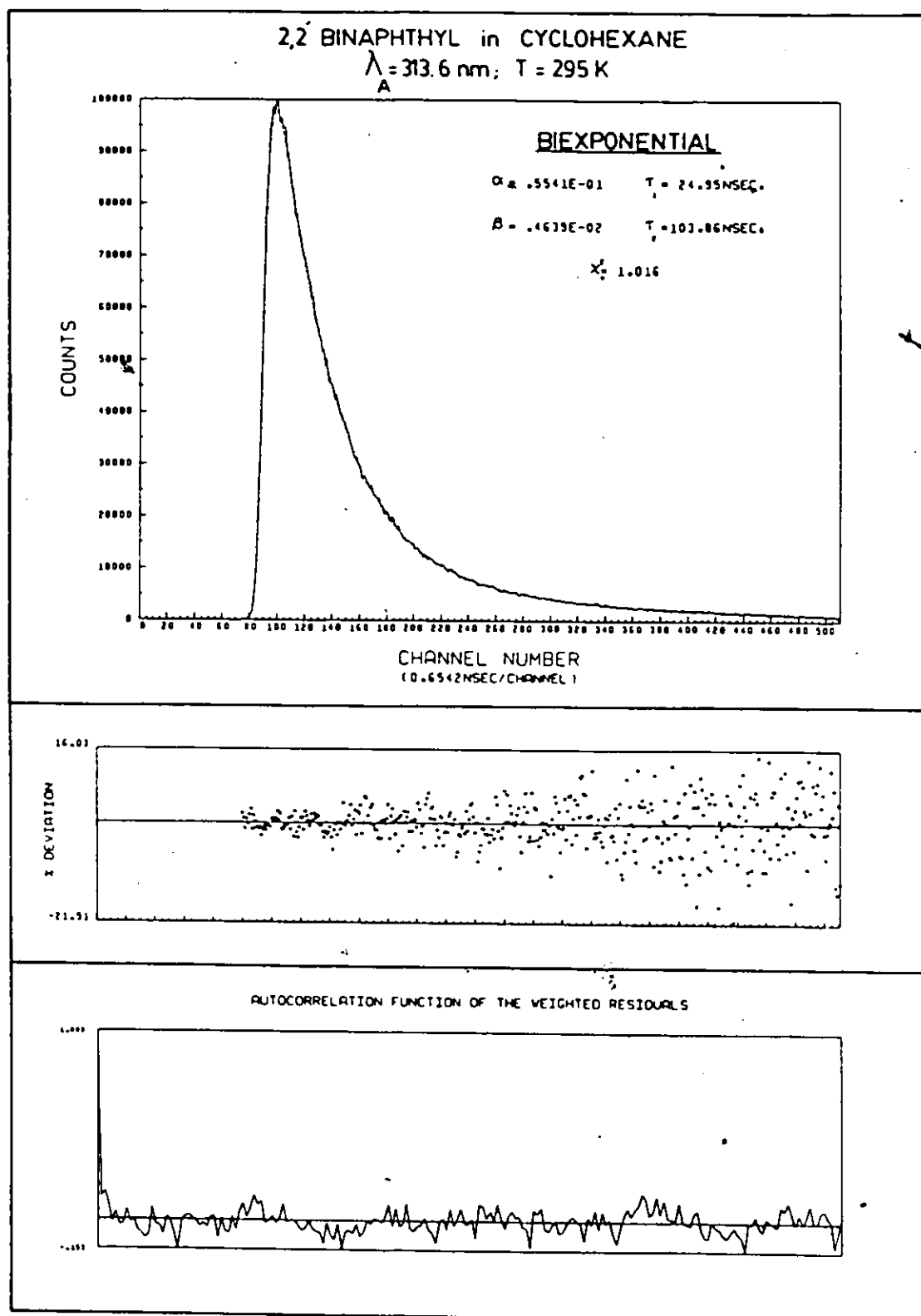


Figure III.4a

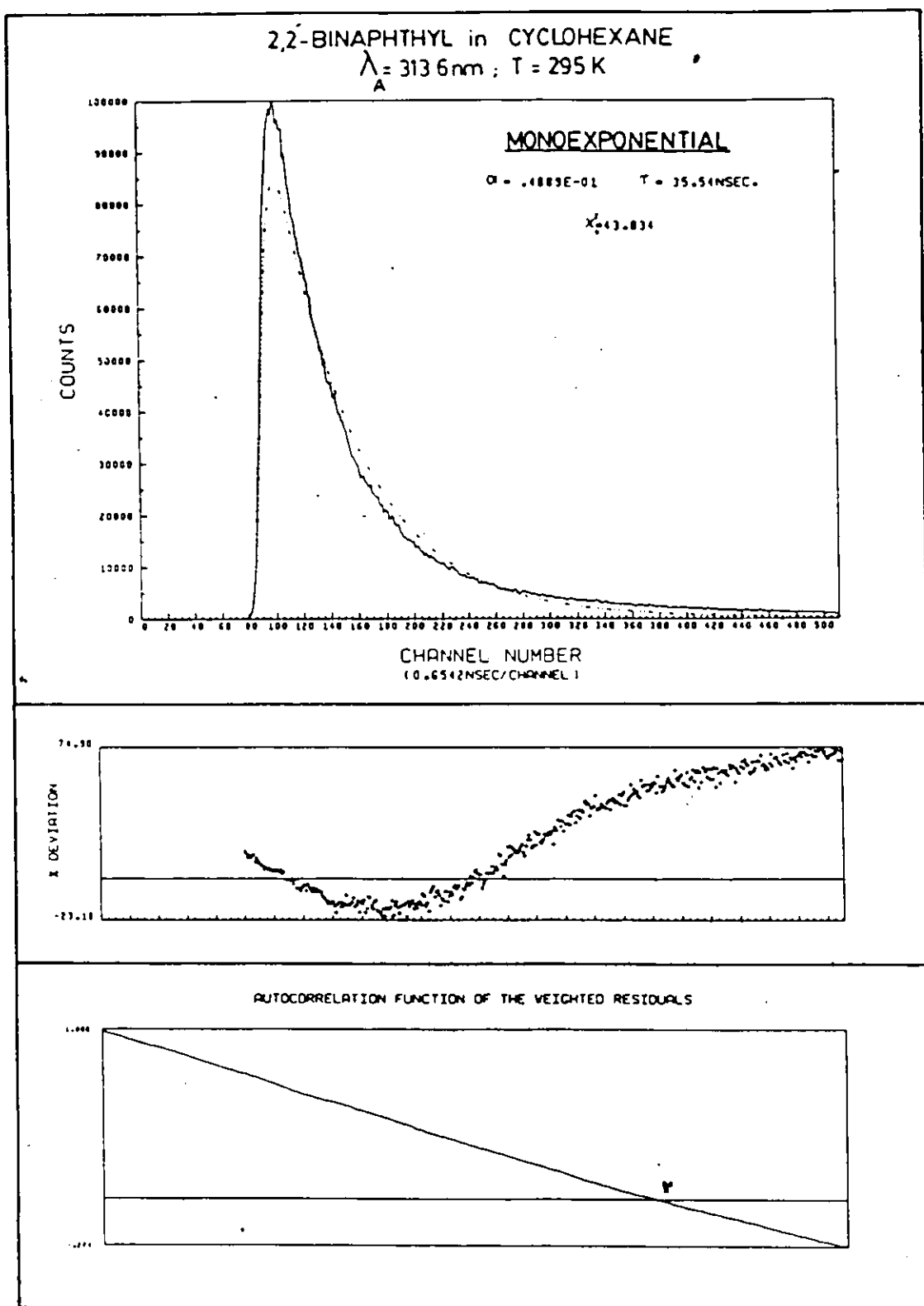


Figure III.4b

## APPENDIX IV

### Fluorescence Spectroscopy and Photophysics of 1,2,7,8-Dibenzofluorene

As mentioned in Section 5.3.1c the hydrocarbon 1,2,7,8-dibenzofluorene (1,2,7,8-DBF) was prepared as a model for the coplanar s-cis conformation of 2,2'-binaphthyl. Figure IV.1 shows the excitation and emission spectra for this material in fluid solution at room temperature, while Figure IV.2 illustrates the appearance of these spectra in alkane glasses at 77K. Apart from improved resolution of vibrational details the excitation and emission spectra were essentially unaffected by cooling. Polycrystalline matrices of n-pentane, cyclohexane and methylcyclohexane gave no better resolution at 77K than that of the glass-forming solvents. The apparent 0-0 bands in excitation and emission coincide at  $28\,030\text{ cm}^{-1}$  ( $356.8\text{ nm}$ ) at both 295K and 77K. 1,2,7,8-DBF exhibits a considerable mirror-image symmetry about this band in fluid and rigid solution. These foregoing observations are indicative of a planar or near-planar geometry in the ground and lowest excited singlet states. The lowest energy peak in the room temperature absorption spectrum of 1,2,7,8-DBF (Appendix I) was also coincident with this  $28\,030\text{ cm}^{-1}$  line.

The steady-state emission and excitation spectra of 1,2,7,8-DBF were independent of the excitation and emission wavelengths respectively (at 295K and 77K) while the fluorescence decay of this model compound was found to be monoexponential under a wide variety of experimental conditions (solvent,  $\lambda_A$ ,  $\lambda_F$  and temperature). The measured singlet



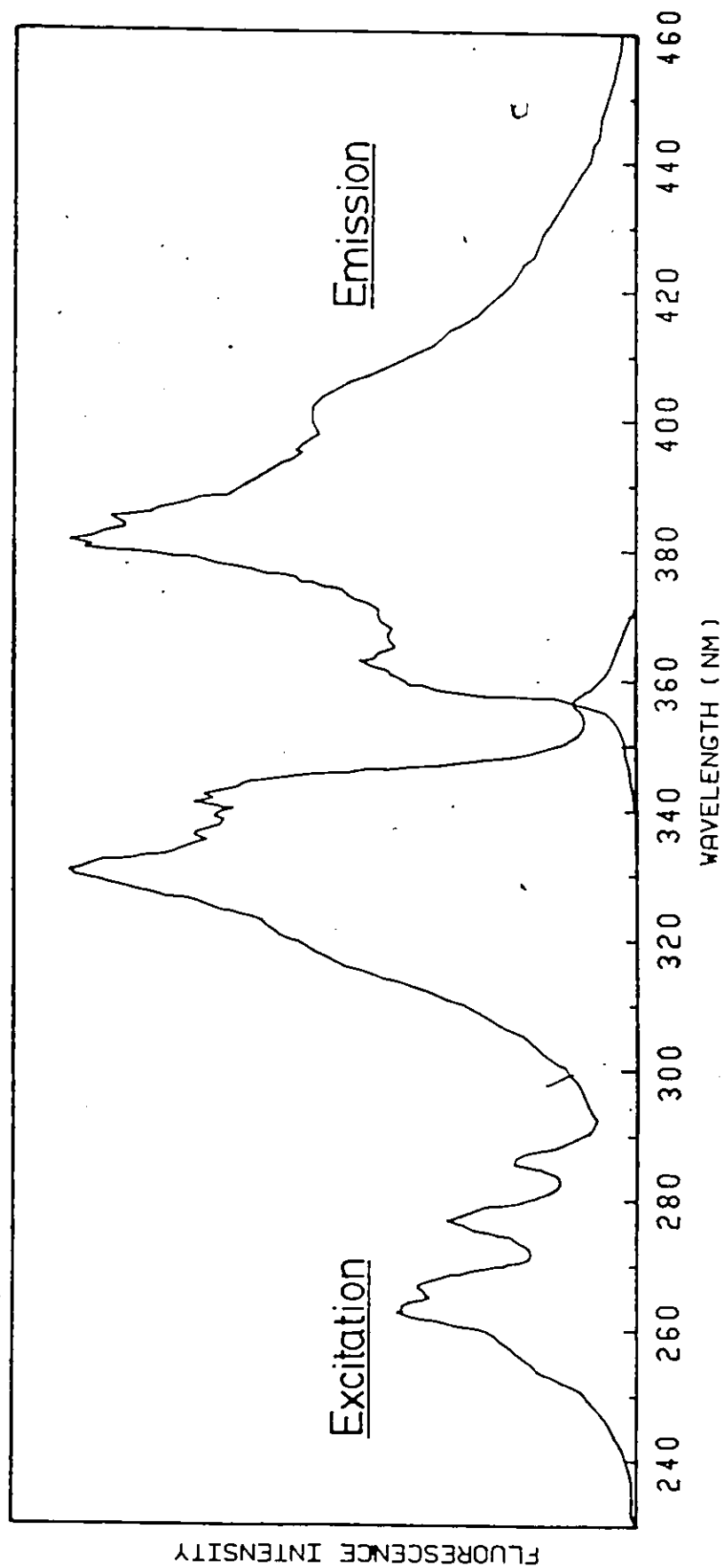


Figure IV.1

Fluorescence Emission and Excitation Spectra of  $10^{-5}M$  1,2,7,8-Dibenzofluorene in Alkane Solvents at 295K

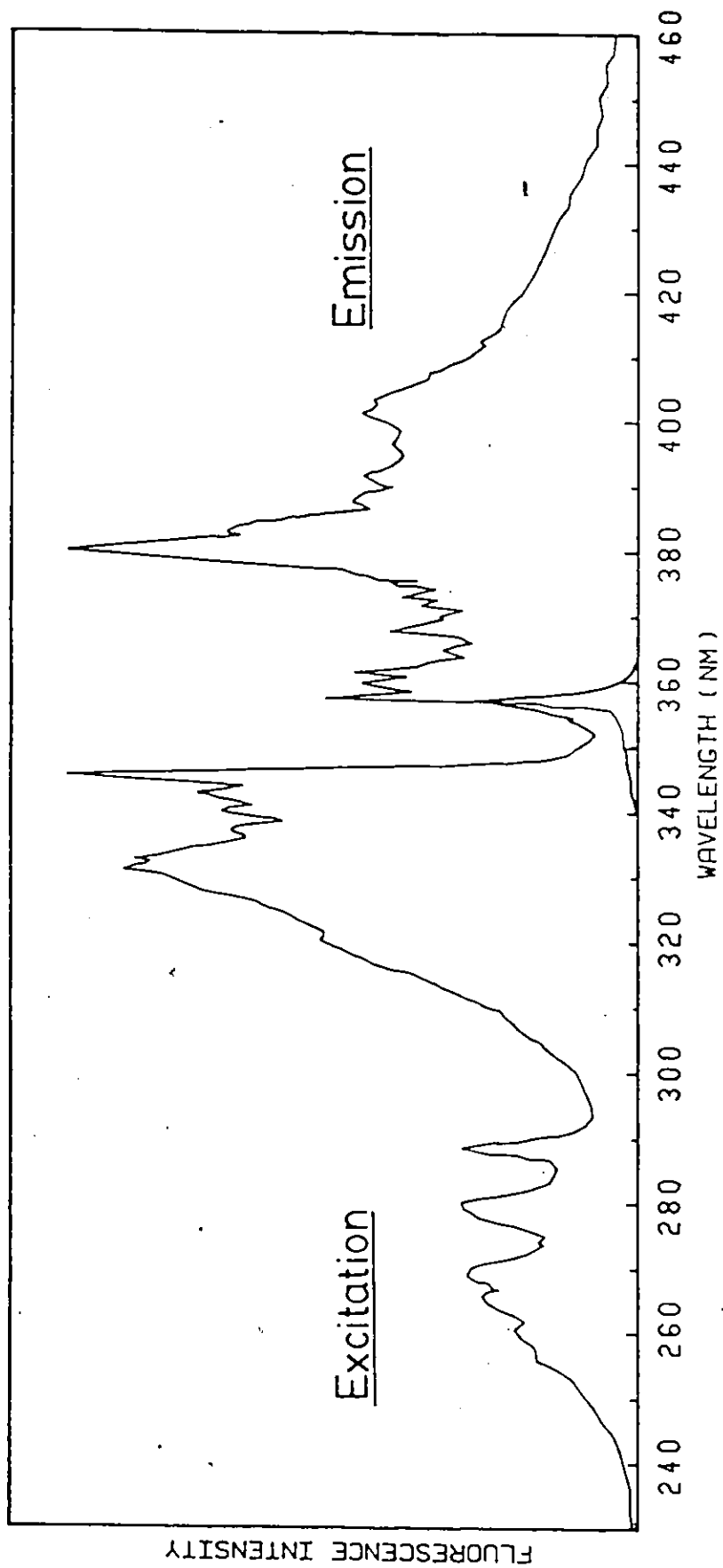


Figure IV.2

Fluorescence Emission and Excitation Spectra of  $10^{-5}$  M 1,2,7,8-Dibenzofluorene in Alkane Solvents at 77K

lifetime of  $10^{-5}$  M 1,2,7,8-DBF in cyclohexane or methylcyclohexane at 295K was  $22.4 \pm .2$  ns, increasing slightly in 3MP to  $25.1 \pm .1$  ns at this same temperature and concentration. Relative quantum yields of fluorescence at room temperature were essentially identical in 3MP and cyclohexane with  $\phi_f = 0.76 \pm 15\%$ . Unfortunately no literature values of  $\tau$  and  $\phi_f$  are available for comparison. The radiative lifetimes and rate constants calculated from these data are tabulated below.

Table IV.1

Radiative Lifetimes and Radiative and Nonradiative Rate Constants for First Excited Singlet State of 1,2,7,8-Dibenzofluorene at 295K

Solvent	$\tau_o = \tau/\phi_f$ (ns)	$k_f = 1/\tau_o$ (s <sup>-1</sup> )	$k_f^o = k_f/n^2$ (s <sup>-1</sup> )	$k_{nr}$ (s <sup>-1</sup> )
Cyclohexane	30	$3.4 \times 10^7$	$1.7 \times 10^7$	$1.1 \times 10^7$
3MP	33	$3.0 \times 10^7$	$1.6 \times 10^7$	$1.0 \times 10^7$

After application of an  $n^{-2}$  refractive index correction it is apparent that the radiative rate constant is independent of solvent, at least for this pair of hydrocarbons.

Upon cooling to 77K the fluorescence decay remained monoexponential but decreased to 18.5 ns in methylcyclohexane glass and 19.8 ns in 3MP glass. This decrease in observed lifetime is attributable to the increased refractive indices of those solvents at low temperature, while the quantum yield remains constant. This implies that for 1,2,7,8-DBF both  $k_f$  and  $k_{nr}$  are also independent of temperature.

BIBLIOGRAPHY

1. J. Stark, Z. Physik. 8, 91 (1907).
2. J. Stark and R. Meyer, Z. Physik. 8, 250 (1907).
3. R.S. Mulliken, J. Chem. Phys. 7, 121 (1939).
4. R.S. Mulliken, Rev. Mod. Phys. 14, 265 (1942).
5. A.S. Cherkasov, Dokl. Akad. Nauk. SSSR, 146, 852 (1962).
6. A.S. Cherkasov and K.G. Voldaikina, Buil. Acad. Sci. SSSR, Phys. Sev. 27, 630 (1963).
7. T.V. Veselova, L.A. Limareva, A.S. Cherkasov and V.I. Shirokov, Buil. Acad. Sci. SSSR, Phys. Sev. 29, 1345 (1965).
8. Y.T. Mazurenko, V.S. Udaltsov and A.S. Cherkasov, Opt and Spectrosc. (USSR) 46, 389 (1979).
9. M.V. Alfimov, Y.B. Sheck and N.P. Kovalenko, Chem. Phys. Lett. 43, 154 (1976).
10. Y.B. Sheck, N.P. Kovalenko and M.V. Alfimov, J. Luminescence 15, 157 (1977).
11. J.B. Birks, G. Bartocci, G.G. Aloisi, S. Dellonte and F. Barigelletti, Chem. Phys. 51, 113 (1980).
12. N.P. Kovalenko, A.T. Abdukadyrov, V.I. Gerko and M.V. Alfimov, J. Photochem. 12, 59 (1980).
13. K.P. Ghiggino, J. Photochem. 12, 173 (1980).
14. K.A. Maszkat and T. Wisnonski-Knittel, Chem. Phys. Lett. 83, 87 (1981).
15. E. Haas, G. Fischer and E. Fischer, J. Photochem. 9, 277 (1978).
16. E. Haas, G. Fischer and E. Fischer, J. Phys. Chem. 82, 1638 (1978).

17. E. Fischer, J. Phys. Chem. 84, 403 (1980).
18. G. Fischer and E. Fischer, J. Phys. Chem. 85, 2611 (1981).
19. G. Fischer and E. Fischer, J. Chem. Soc. Perkin II, 1264 (1981).
20. E. Fischer, J. Photochem. 17, 331 (1981).
21. G. Bartocci, F. Masetti, U. Mazzucato, S. Dellonte and G. Orlandi, Spectrochim. Acta 38A, 729 (1982).
22. G. Bartocci and U. Mazzucato, J. Luminescence 27, 163 (1982).
23. G. Marconi, G. Orlandi and G. Poggi, J. Photochem. 19, 329 (1982).
24. R.M. Hochstrasser, Can. J. Chem. 39, 459 (1961).
25. E. Hughes, J.H. Wharton and R.V. Nauman, J. Phys. Chem. 75, 3097 (1971).
26. H.E. Holloway, R.V. Nauman and J.H. Wharton, J. Phys. Chem. 72, 4468 (1968).
27. H.E. Holloway, R.V. Nauman and J.H. Wharton, J. Phys. Chem. 72, 4474 (1968).
28. D. Horrocks, Molecular Spectroscopy, An International Conference, p. 63, E.C. Lim, ed., W.A. Benjamin Inc., New York (1969).
29. R.N. Nurmukhametov, Usp. Khim. 28, 351 (1969).
30. E.W. Schlag, S. Schneider and S.F. Fischer, Ann. Rev. Phys. Chem. 22, 465 (1971).
31. E.C. Lim and J.D. Laposa, J. Chem. Phys. 41, 3257 (1964).
32. J.D. Laposa, E.C. Lim and R.E. Kellog, J. Chem. Phys. 42, 3025 (1965).
33. N. Khamuru, H.R. Bhattacharjee and E.C. Lim, Chem. Phys. Lett. 26, 174 (1974).
34. I. Berlman, Handbook of Fluorescence of Aromatic Molecules, 2nd ed.,

Academic Press, New York (1971).

35. M. Born and R. Oppenheimer, Ann. Physik. 87, 457 (1927).
36. G. Herzberg and E. Teller, Z. Physik. Chem. B 21, 410 (1933).
37. M.J. Robey, I.G. Ross, R.V. Southwood-Jones and S.J. Stricker, Chem. Phys. 23, 207 (1977).
38. R.M. Hochstrasser and G.J. Small, J. Chem. Phys. 45, 2270 (1966).
39. D.P. Craig and R.D. Gordon, Proc. Roy. Soc. A 288, 69 (1965).
40. G.R. Hunt and I.G. Ross, J. Mol. Spectrosc. 9, 50 (1962).
41. W. Siebrand and D.F. Williams, J. Chem. Phys. 46, 403 (1967).
42. W. Siebrand, J. Chem. Phys. 46, 440 (1967).
43. G.W. Robinson and R.P. Frosch, J. Chem. Phys. 37, 1962 (1962).
44. G.W. Robinson and R.P. Frosch, J. Chem. Phys. 38, 1187 (1963).
45. M.H. Hui, P. DeMayo, R. Suau and W.R. Ware, Chem. Phys. Lett. 31, 257 (1975).
46. M. Mahaney and J.R. Huber, Chem. Phys. 9, 371 (1975).
47. J.R. Huber and M. Mahaney, Chem. Phys. Lett. 30, 410 (1975).
48. T. Oka, A.R. Knight and R.P. Steer, J. Chem. Phys. 63, 2414 (1975).
49. D.J. Clouthier, A.R. Knight and R.P. Steer, Chem. Phys. Lett. 59, 62 (1978).
50. D.J. Clouthier, P.A. Hackett, A.R. Knight and R.P. Steer, J. Photochem. 17, 319 (1981).
51. J.N. Demas and G.A. Crosby, J. Chem. Phys. 75, 991 (1971).
52. C. Lewis, W.R. Ware, L.J. Doemeny and T.L. Nemzek, Rev. Sci. Instrum. 44, 107 (1973).
53. A.E.W. Knight and B.K. Selinger, Aust. J. Chem. 26, 1 (1973).
54. W.R. Ware, Creation and Detection of the Excited State, Vol. 1A,

- p. 213, A. Lamola, ed., Marcel Dekker, New York (1971).
55. L.J. Cline-Love and L.A. Shaver, Anal. Chem. 48, 364A (1976).
  56. C.M. Harris and B.K. Selinger, Aust. J. Chem. 32, 2111 (1979).
  57. A.E.W. Knight and B.K. Selinger, Spectrochim. Acta 27A, 1223 (1971).
  58. L.J. Cline-Love and L.A. Shaver, Anal. Chem. 52, 154 (1980).
  59. A.E. McKinnon, A.G. Szabo and D.R. Miller, J. Phys. Chem. 81, 1564 (1977).
  60. P.B. Coates, J. Sci. Instrum. 1, 878 (1968).
  61. D.E. Donahue and R.C. Stern, Rev. Sci. Instrum. 43, 791 (1972).
  62. C.C. Davis and T.A. King, Rev. Sci. Instrum. 41, 407 (1970).
  63. C.C. Davis and T.A. King, J. Phys. A, 3, 101 (1970).
  64. R. Schuyler and I. Isenberg, Rev. Sci. Instrum. 42, 813 (1971).
  65. J.B. Birks and I.H. Munro, Progress in Reaction Kinetics, Vol. 4, G. Porter, ed., Pergamon, Oxford (1967).
  66. I. Isenberg and R.D. Dyson, Biophys. J. 9, 1337 (1969).
  67. I. Isenberg, J. Chem. Phys. 59, 5696 (1973).
  68. E.W. Small and I. Isenberg, J. Chem. Phys. 66, 3347 (1977).
  69. I. Isenberg and E.W. Small, J. Chem. Phys. 77, 2799 (1982).
  70. A. Gafni, R.L. Modlin and L. Brand, Biophys. J. 15, 263 (1975).
  71. M. Almgren, Chemica Scripta 3, 145 (1973).
  72. W.R. Ware, L.J. Doemeny and T.L. Nemzek, J. Phys. Chem. 77, 2038 (1973).
  73. U.P. Wild, A.R. Holzwarth and H.P. Good, Rev. Sci. Instrum. 48, 1621 (1977).
  74. D.M. Rayner, A.E. McKinnon, A.G. Szabo and P.A. Hackett, Can. J. Chem. 54, 3246 (1976).

75. D.M. Rayner, A.E. McKinnon and A.G. Szabo, Rev. Sci. Instrum. 48, 1050 (1977).
76. M.R. Smith and S. Cohn-Sfeten, Nuclear Instrum. and Methods 114, 171 (1974).
77. A. Grinvald and I.Z. Steinberg, Anal. Biochem. 59, 583 (1974).
78. A.G. Szabo and D.M. Rayner, Biochem. and Biophys. Research Communications 94, 909 (1980).
79. A.G. Szabo and D.M. Rayner, J. Amer. Chem. Soc. 102, 554 (1980).
80. T.C. Werner and L.S. Forster, Photochem. and Photobiol. 29, 905 (1979).
81. A.C. Jones, K. Janecka-Styrzcz and J.O. Williams, J. Photochem. 19, 163 (1982).
82. M. Van der Auweraer, A. Gilbert and F.C. DeSchryver, J. Amer. Chem. Soc. 102, 4007 (1980).
83. B. Donzel, P. Gauduchon and P. Wahl, J. Amer. Chem. Soc. 96, 801 (1974).
84. M. Ameloot and H. Hendrickx, J. Chem. Phys. 76, 4419 (1982).
85. P.R. Bevington, Data Reduction and Error Analysis for the Physical Sciences, McGraw-Hill, Toronto (1969).
86. J.W. Lee, J. Chem. Phys. 77, 2806 (1982).
87. P. Hall and B. Selinger, J. Phys. Chem. 85, 2947 (1981).
88. J.B. Birks, D.J. Dyson and I.H. Munro, Proc. Roy. Soc. A 275, 575 (1963).
89. W.M. Vaughn and G. Weber, Biochemistry 9, 467 (1970).
90. M.H. Hui and W.R. Ware, J. Amer. Chem. Soc. 98, 4718 (1976).
91. T. Okada, M. Migita, N. Mataga, Y. Sakata and S. Misumi, J. Amer. Chem. Soc. 103, 4715 (1981).



92. G.E. Johnson, J. Chem. Phys. 61, 3002 (1974).
93. S.P. Van and G.S. Hammond, J. Amer. Chem. Soc. 100, 3895 (1978).
94. J.B. Birks, Photophysics of Aromatic Molecules, Wiley-Interscience, Toronto (1970).
95. E.V. Shpol'skii, A.A. Il'ina and L.A. Klimova, Dokl. Akad. Nauk. SSSR, 87, 935 (1952).
96. E.V. Shpol'skii and L.A. Klimova, Bull. Acad. Sci. SSSR, Phys. Ser. 18, 357 (1954).
97. J.J. Dekkers, G.P. Hoornweg, G. Visser, C. Maclean and N.H. Velthorst, Chem. Phys. Lett. 47, 357 (1977).
98. P. Baluk, A. Kowski and M. Kalas, Z. Naturforsch. 36A, 705 (1981).
99. M.N. Sokolov and L.M. Sverdlov, Opt. and Spectrosc. (USSR) 49, 104 (1980).
100. G.L. LeBel and J.D. Laposa, J. Mol. Spectrosc. 41, 249 (1972).
101. H. Singh and J.D. Laposa, J. Luminescence 5, 32 (1972).
102. R.A. Nalepa and J.D. Laposa, J. Luminescence 8, 429 (1974).
103. V.J. Morrison and J.D. Laposa, Spectrochim. Acta 32A, 443 (1976).
104. D.A. Condirston, Ph.D. Thesis, McMaster University (1979).
105. J.D. Spangler and H. Sponer, Spectrochim. Acta 19, 169 (1963).
106. D.R. Douslin and H.M. Huffman, J. Amer. Chem. Soc. 68, 173 (1946).
107. S.H. Hankin, O.S. Khalil and L. Goodman, Chem. Phys. Lett. 63, 11 (1979).
108. K. Palewska, Chem. Phys. 58, 21 (1981).
109. R.M. Barrett and D. Steele, J. Mol. Structure 11, 105 (1972).
110. G. Casalone, C. Mariani, A. Mugnoli and M. Simonetta, Mol. Phys. 15, 339 (1968).

111. E.C. Lim and Y.H. Li, J. Chem. Phys. 52, 6416 (1970).
112. C.S. Parmenter and J.D. Rau, J. Chem. Phys. 51, 2242 (1967).
113. K. Kawaoka, A.V. Khan and D.R. Kearns, J. Chem. Phys. 46, 1842 (1967).
114. B. Stevens and B.E. Algar, J. Phys. Chem. 72, 2582 (1968).
115. W.R. Ware, J. Phys. Chem. 66, 455 (1962).
116. N.H. Werstiuk and T. Kadai, Can. J. Chem. 51, 1485 (1973).
117. N.H. Werstiuk and G. Timmons, Can. J. Chem. 59, 3218 (1981).
118. A.E. Tschitschibabin and O.J. Magidson, J. Prakt. Chem. 90, 168 (1914).
119. J. Schmidlin and P. Massini, Berichte 42, 2377 (1909).
120. K. Mislow and R.A. McGinn, J. Amer. Chem. Soc. 80, 6036 (1958).
121. E.D. Bergmann, E. Fischer, Y. Hirshberg, D. Lavie, Y. Sprinak and J. Szmuszkovicz, Soc. Chim. Fr. 798 (1953).
122. A.I. Vogel, A Text-Book of Practical Organic Chemistry, p. 167, 3rd ed., Longmans, Green and Co. Ltd., London (1956).
123. M.E. Abu-Zeid, J.A. Moreno Bernal and J.R. Lopez, J. Photochem. 10, 221 (1979).
124. J.B. Birks, J. Research of the NBS 80A, 389 (1976).
125. Handbook of Chemistry and Physics, 49th ed., R.C. Weast, ed., The Chemical Rubber Company, Cleveland (1968).
126. J.L. Lauer, J. Chem. Phys. 16, 612 (1948).
127. J. Bendig, D. Kreysig and R. Schöneich, Opt. and Spectrosc. (USSR) 49, 29 (1980).
128. W.H. Melhuish, J. Phys. Chem. 65, 229 (1961).
129. G. Herzberg, Molecular Spectra and Molecular Structure, I. Spectra

- of Diatomic Molecules, 2nd ed., Van Nostrand, Toronto (1950).
130. R.W.B. Pearse and A.G. Gaydon, The Identification of Molecular Spectra, p. 169, 2nd ed., Chapman and Hall, London (1950).
  131. ORTEC, Inc., Operation Manual, Model 472 Constant Fraction Discriminator, Oak Ridge, Tenn. (1975).
  132. B. Leskovar, C.C. Lo, P.R. Hartig and K. Sauer, Rev. Sci. Instrum. 47, 1113 (1976).
  133. A. Nakajima, Bull. Chem. Soc. Japan 46, 2602 (1973).
  134. T.L. Nemzek, Ph.D. Thesis, University of Minnesota (1975).
  135. N. Mataga, M. Tomura and N. Nishimura, Mol. Phys. 9, 367 (1965).
  136. T.L. Nemzek and W.R. Ware, J. Chem. Phys. 62, 477 (1975).
  137. J.B. Birks, D.J. Dyson and T.A. King, Proc. Roy. Soc. 277A, 270 (1964).
  138. P.R. Hartig, K. Sauer, C.C. Lo and B. Leskovar, Rev. Sci. Instrum. 47, 1122 (1976).
  139. T. Takahashi, K. Kikuchi and H. Kokubun, J. Photochem. 14, 67 (1980).
  140. Y. Katsumura, S. Tagawa and Y. Tabata, J. Phys. Chem. 84, 833 (1980).
  141. P. Wahl, J.C. Auchet and B. Donzel, Rev. Sci. Instrum. 45, 28 (1974).
  142. M.G. Badea and S. Georghiou, Rev. Sci. Instrum. 47, 314 (1976).
  143. J.W. Eastman, Photochem. and Photobiol. 6, 55 (1967).
  144. D.K. Wong and A.M. Halpern, Photochem. and Photobiol. 24, 609 (1976).
  145. J.B. Gallivan, J. Phys. Chem. 73, 3070 (1969).

146. V.P. Lentz, H. Blume and D. Schulte-Frohlinde, Ber. Buns. Ges. 74, 484 (1970).
147. B. Amand and R. Bensasson, Chem. Phys. Lett. 34, 44 (1975).
148. J.R. Lombardi, J.W. Raymonda and A.C. Albrecht, J. Chem. Phys. 40, 1148 (1964).
149. A.C. Ling, J.E. Willard, J. Phys. Chem. 72, 1918 (1968).
150. C.L. Cheng, D.S.N. Murthy and G.L.D. Ritchie, Trans. Faraday, Soc. II 68, 1679 (1972).
151. E.D. Bergmann, M. Rabinovitz, M.J. Aroney, R.J.W. LeFèrre, L. Radom and G.L.D. Ritchie, J. Chem. Soc. B 1551 (1968).
152. B. Tinland, Theor. Chim. Acta 11, 385 (1968).
153. K. Gustav, U. Kempka and J. Sühnel, Chem. Phys. Lett. 71, 280 (1980).
154. H-J. Hofmann, Z. Chem. 15, 76 (1975).
155. K.R. Naqvi, J. Donätsch and U.P. Wild, Chem. Phys. Lett. 34, 285 (1975).
156. J. Kordas and M.A. El-Bayoumi, J. Amer. Chem. Soc. 96, 3043 (1974).
157. J.S. McCaskill and R.G. Gilbert, Chem. Phys. 44, 389 (1979).
158. B. Dellinger and M. Kasha, Chem. Phys. Lett. 38, 9 (1976).
159. B. Wilhelmi, Chem. Phys. 66, 351 (1982).
160. J.B. Birks, Z. Phys. Chem. 101, 91 (1976).
161. A.S. Cherkasov and V.I. Shirokov, Opt. and Spectrosc. (USSR) 49, 32 (1980).
162. R.B. Cundall and L.C. Pereira, Trans. Faraday Soc. 68, 1152 (1972).
163. J. Olmstead, Chem. Phys. Lett. 38, 287 (1976).
164. S.S. Kurtz, S. Amon and S. Sankin, Ind. and Eng. Chemistry 42, 174 (1950).

165. W.W. Mantulin and J.R. Huber, Photochem. and Photobiol. 17, 139 (1973).
166. H.E. Zimmerman, K.S. Kamm and D.P. Werthemann, J. Amer. Chem. Soc. 97, 3718 (1975).
167. K.J. Rosengren, Acta Chem. Scand. 16, 1421 (1962).
168. M. Sumitani, N. Nakashima, K. Yoshihara and S. Nagakura, Chem. Phys. Lett. 51, 183 (1977).
169. W.R. Dawson and J.L. Kropp, J. Phys. Chem. 73, 693 (1969).
170. J.L. Kropp, W.R. Dawson and M.W. Windsor, J. Phys. Chem. 73, 1747 (1969).
171. S.J. Strickler and R.A. Berg, J. Chem. Phys. 37, 814 (1962).
172. J. Birks and D.J. Dyson, Proc. Roy. Soc. A 275, 135 (1963).
173. R.G. Bennett and P.J. McCartin, J. Chem. Phys. 44, 1969 (1966).
174. J.S. Brinen and M.K. Orloff, J. Chem. Phys. 51, 527 (1969).
175. A. Gamba, E. Rusconi and M. Simonetta, Tetrahedron 26, 871 (1970).
176. E.V. Shpol'skii, L.A. Klimova, B.N. Nersesova and V.I. Glyadkovskii, Opt. and Spectrosc. (USSR) 24, 25 (1968).
177. G. Varsanyi, Vibrational Spectra of Benzene Derivatives, Academic Press, New York (1969).
178. J.E. Katon and E.R. Lippincott, Spectrochim. Acta 11, 627 (1959).
179. B. Pasquier, Mol. Cryst. and Liq. Cryst. 11, 25 (1970).
180. E.R. Lippincott and E.J. O'Reilly, J. Chem. Phys. 23, 238 (1955).
181. A.L. McClellan and G.C. Pimentel, J. Chem. Phys. 23, 245 (1955).
182. F.W. Westheimer, J. Chem. Phys. 15, 252 (1947).
183. H. Suzuki, Bull. Chem. Soc. Japan 32, 1340 (1959).
184. J. Trotter, Acta Cryst. 14, 1135 (1961).

185. A. Hargreaves and S.H. Rizvi, Acta Cryst. 15, 365 (1962).
186. M. Zander, Z. Naturforsch 32A, 339 (1977).
187. G. Orlandi and W. Siebrand, Chem. Phys. Lett. 30, 352 (1975).
188. D.J.S. Birch and J.B. Birks, Chem. Phys. Lett. 38, 432 (1976).
189. J.B. Birks, Chem. Phys. Lett. 54, 430 (1978).
190. M.J. Riley, A.R. Lacey, M.G. Sceats and R.G. Gilbert, Chem. Phys. 72, 83 (1982).
191. M.F.M. Post, J.K. Eweg, J. Langelaar and J.D.W. Van Voorst, Chem. Phys. 14, 165 (1976).
192. Y. Hara and M.F. Nicol, Bull. Chem. Soc. Japan 51, 1985 (1978).
193. M.F. Nicol, Y. Hara, J.M. Wiget and M. Anton, J. Mol. Structure 47, 371 (1978).
194. K. Gustav, J. Sühnel and U.P. Wild, Chem. Phys. 31, 59 (1978).
195. J. Sühnel and K. Gustav, Zeit. Chem. 17, 417 (1977).
196. R.W. Bigelow and R.W. Anderson, Chem. Phys. Lett. 58, 114 (1978).
197. R.E. Carter and T. Liljefors, Tetrahedron 32, 2915 (1976).
198. R.B. Kress, E.N. Dueslev, M.C. Etter, I.C. Paul and D.Y. Curtin, J. Amer. Chem. Soc. 102, 7709 (1980).
199. X.J. Luo, G.S. Beddard and G. Porter, J. Chem. Soc. Faraday I 78, 3488 (1982).
200. M.F.M. Post, J. Langelaar and J.D.W. Van Voorst, Chem. Phys. Lett. 32, 59 (1975).
201. R.A. Friedel, M. Orchin and L. Reggel, J. Amer. Chem. Soc. 70, 199 (1948).
202. M.M. Harris and A.S. Mellors, Chemistry and Industry 1082 (1961).
203. S.F. Mason, R.H. Seal and D.R. Roberts, Tetrahedron 30, 1671 (1974).

204. K.R. Wilson and R.E. Pincock, J. Amer. Chem. Soc. 97, 1474 (1975).
205. A.K. Goulter and L.M. Clemens, J. Phys. Chem. 68, 651 (1964).
206. R.E. Carter and L. Dahlgren, Acta Chem. Scand. 23, 504 (1969).
207. C.V. Shank, E.P. Ippen, O. Teschke and K.B. Eisenthal, J. Chem. Phys. 67, 5547 (1977).
208. Dr. J.J. McCullough, private communication.
209. O. Chalvet, R. Daudel, G. Evrard, J.P. Grivet, E. Heilbronner, P. Kottis, D. Lavalette, B. Muel, P.A. Straub and M. Van Meerssche, J. Mol. Structure 5, 111 (1970).
210. R.H. Fleming, F.H. Quina and G.S. Hammond, J. Amer. Chem. Soc. 96, 7738 (1974).
211. A. Zweig and J.B. Gallivan, J. Amer. Chem. Soc. 91, 260 (1969).
212. R.A. Friedel and M. Orchin, Ultraviolet Spectra of Aromatic Compounds, John Wiley and Sons, New York (1951).
213. H.H. Jaffé and M. Orchin, Theory and Applications of Ultraviolet Spectroscopy, John Wiley and Sons, New York (1962).
214. A.C. Ling and J.E. Willard, J. Phys. Chem. 72, 3349 (1968).
215. Dr. D.A. Condirston, private communication.
216. J.V. Morris, M.A. Mahaney and J.R. Huber, J. Phys. Chem. 80, 969 (1976).
217. D.R. Kearns, Chem. Rev. 71, 395 (1971).
218. T.V. Veselova, I.E. Obyknovennaya, A.S. Cherkasov and V.I. Shirokov, Opt. and Spectrosc. (USSR) 33, 488 (1972).
219. D.L. Horrocks and H.O. Wirth, J. Chem. Phys. 49, 2907 (1968).
220. D.L. Horrocks, J. Chem. Phys. 51, 5443 (1969).
221. L.K. Patterson, G. Porter and M.R. Topp, Chem. Phys. Lett. 7, 612 (1970).

222. W. Biebrand, Chem. Phys. Lett. 6, 192 (1970).
223. B. Sharf and R. Silbey, Chem. Phys. Lett. 5, 314 (1970).
224. P.M. Johnson and M.C. Studer, Chem. Phys. Lett. 18, 341 (1973).
225. R. Li and E.C. Lim, J. Chem. Phys. 57, 605 (1972).
226. R.S. Mulliken, J. Chem. Phys. 23, 1997 (1955).
227. J.R. Platt, J. Chem. Phys. 17, 484 (1949).
228. A.L. Hinde, B.K. Selinger and P.R. Nott, Aust. J. Chem. 30,  
2383 (1977).
229. R. Miller, Ph.D. Thesis, McMaster University (1978).
230. W.R. Ware, D. Watt and J.D. Holmes, J. Amer. Chem. Soc. 96, 7853  
(1974).
231. G. Heinrich, S. Schoof and H. Gusten, J. Photochem. 3, 315 (1974).
232. D.J.S. Birch and R.E. Imhof, Chem. Phys. Lett. 32, 56 (1975).